REPORT DOCUMENTATION PAGE

Form Approved
OMB No. 0704-0188

1. AGENCY USE ONLY *(Leave blank)*	2. REPORT DATE	3. REPORT TYPE AND DATES COVERED
	21 Apr 97	

4. TITLE AND SUBTITLE
PERFORMANCE OF CARBON FIBER REINFORCED POLYMER (CFRP) TENDONS AND THEIR USE FOR STRENGTHENING OF PRESTRESSED CONCRETE BEAMS

5. FUNDING NUMBERS

6. AUTHOR(S)
CARL VAN JERRETT

7. PERFORMING ORGANIZATION NAME(S) AND ADDRESS(ES)
NORTH CAROLINA STATE UNIVERSITY

8. PERFORMING ORGANIZATION REPORT NUMBER
97-007D

9. SPONSORING/MONITORING AGENCY NAME(S) AND ADDRESS(ES)
DEPARTMENT OF THE AIR FORCE
AFIT/CI
2950 P STREET
WRIGHT-PATTERSON AFB 45433-7765

10. SPONSORING/MONITORING AGENCY REPORT NUMBER

11. SUPPLEMENTARY NOTES

12a. DISTRIBUTION AVAILABILITY STATEMENT

12b. DISTRIBUTION CODE

13. ABSTRACT *(Maximum 200 words)*

14. SUBJECT TERMS

15. NUMBER OF PAGES
240

16. PRICE CODE

17. SECURITY CLASSIFICATION OF REPORT	18. SECURITY CLASSIFICATION OF THIS PAGE	19. SECURITY CLASSIFICATION OF ABSTRACT	20. LIMITATION OF ABSTRACT

CIVIL ENGINEERING RESEARCH

PERFORMANCE OF CARBON FIBER REINFORCED POLYMER (CFRP) TENDONS AND THEIR USE FOR STRENGTHENING OF PRESTRESSED CONCRETE BEAMS

DEPARTMENT OF CIVIL ENGINEERING
NORTH CAROLINA STATE UNIVERSITY

ABSTRACT

JERRETT, CARL VAN. Performance of Carbon Fiber Reinforced Polymer (CFRP) Tendons and their use for Strengthening of Prestressed Concrete Beams. (Under the direction of Shuaib Haroon Ahmad.)

The purpose of this study was to investigate the performance of Carbon Fiber Reinforced Polymer (CFRP) tendons and their use for strengthening of prestressed concrete beams. The study involved two phases. In the first phase, the performance and ultimate strength of CFRP tendons were investigated, with emphasis on the performance and ultimate strength of the tendon under combined axial load and harping. In the second phase, the performance of prestressed concrete beams strengthened by using exterior post-tensioned CFRP tendons was investigated. The second phase also included the development of an analytical model for predicting the behavior of strengthened beams and conducting a limited parametric study of prestressed concrete beams strengthened by exterior post-tensioned tendons.

The first phase of this study involved the testing of 0.32 in. (8 mm) diameter CFRP tendons subjected to uni-axial loading, combined axial loading and harping, bending-tension fatigue loading, and sustained loading under combined axial load and harping. Harping points consisted of curved plates with radii of 1 in. (25 mm), 5 in. (102 mm), and 20 in. (508 mm). Bending-tension fatigue tests were conducted up to 1 million cycles with axial loads ranging between 14.0 and 14.7 kips (62.3 and 65.4 kN) and bend angles between 4.5 and 5.5 degrees. Sustained loading tests were conducted over a duration of 120 days with tendons subjected to axial loads of about 12 kips (53 kN) and bend angles of 7.0 degrees. At the completion of all fatigue and sustained loading tests, residual strength tests were conducted under combined axial load and harping.

Test results of the first phase of the study indicated that increased strains associated with harping are confined to a region of about 6 in. (150 mm) on either side of the bend point of the tendon. Failure at the tendon harping point is associated with a maximum fiber strain of 0.0216, which greatly exceeds the largest reported uni-axial ultimate strain of 0.015. Based on the tendon strength tests, an analytical model was developed that accurately predicted the

conditions at failure for tendons subjected to combined axial load and harping.

The second phase of research included both experimental and analytical evaluation of steel prestressed concrete beams strengthened by exterior post-tensioned CFRP tendons. The experimental work included ultimate strength tests of six 8 x 16 x 216 in. (203 x 406 x 5490 mm) steel prestressed concrete beams. Two of the beams were tested to failure without exterior post-tensioning. The remaining four beams were first loaded to induce some damage and then were strengthened by use of two exterior post-tensioned CFRP tendons. The CFRP tendons were 0.32 in. (8 mm) in diameter and draped at two locations symmetric about the midspan of the beam. All beams were tested statically until failure. The analytical investigation included the development of an iterative computerized model for predicting the behavior of prestressed beams with exterior post-tensioned CFRP tendons. This analytical model was used to conduct a limited parametric study that investigated the influence of material and geometric properties on the performance of prestressed concrete beams with exterior post-tensioned CFRP tendons. Results of the experimental study indicated that CFRP tendons can be effectively used for external post-tensioning and that substantial increase in ultimate strength and stiffness of beams can be achieved by use of exterior post-tensioned CFRP tendons.

PERFORMANCE OF CARBON FIBER REINFORCED POLYMER (CFRP) TENDONS AND THEIR USE FOR STRENGTHENING OF PRESTRESSED CONCRETE BEAMS

by

CARL VAN JERRETT

A dissertation submitted to the Graduate Faculty of
North Carolina State University
in partial fulfillment of the
requirements for the Degree of
Doctor of Philosophy

Department of Civil Engineering

Raleigh

1996

APPROVED BY:

Chair of Advisory Committee

To My Parents

BIOGRAPHY

Carl Van Jerrett was born on April 30, 1963 in Havelock, North Carolina. He graduated from Havelock High School in 1981 and received a Bachelor of Science degree in Civil Engineering from North Carolina State University in 1985. Upon graduation, the author was commissioned as a 2nd Lieutenant in the United States Air Force.

In July 1985, the author entered his first active duty military assignment at Maxwell Air Force Base, Montgomery, Alabama. While there, he worked as an engineering contract planner and construction inspector, and before departing the base, he completed the Air Force Squadron Officers School.

In July 1988, the author was assigned to the University of Texas, Austin, where he completed a Masters of Science degree in Engineering. The title of his masters thesis was "Effects of Partial Composite Action on the Elastic Behavior of Wood Trusses." Upon leaving Texas in January 1990, he was assigned to the Headquarters, United States Air Forces, Europe, at Ramstein Air Base, Germany. While there, he completed a variety of projects including community planning initiatives, special military bed-down projects and program funding management.

In August 1993, the author returned to North Carolina State University to pursue a PhD in the area of Structural Engineering. In January 1995, the author married his wife, Justine. They were blessed with the birth of their son, Jacob, in February 1996. Upon completion of his doctoral program, the author is scheduled to become an instructor at the United States Air Force Academy, Colorado Springs, Colorado.

ACKNOWLEDGEMENTS

The author wishes to express his sincere gratitude to Professor Shuaib Ahmad, whose guidance, support, and encouragement were essential to the completion of this study. Also, appreciation is due to Drs. John M. Hanson, C. C. D. Tung, Paul Zia, and Harvey West for their constructive criticism and suggestions.

Special thanks are extended to the United States Air Force, for the opportunity to pursue this degree and for their support during completion of this degree. Thanks are also expressed to companies, including Mitsubishi Chemical Corporation, VSL International, Florida Wire and Cable, Ameristeel, and Ready Mix Concrete of Raleigh for providing materials for the experimental phase of the research study.

Appreciation is extended to the many friends that have assisted in this study. People that I would like to specifically acknowledge are Tatjana Blell, Tom Dismukes, Erdem Dogan, Bill Dunleavy, David Fedroff, Dan Fisher, Dena Guth, Art Illingsworth, Kim Sacket, B. Zeynep Savas, Luca Scotti, Jamal Shannag, Michael Smith, Frank Spagna, Greg Stillwell, Eggert Valmundsson, David Willers, and Brian Wood.

The author must give a very special thank you to two people: his wife, for her support and encouragement, and to his new son, Jacob, for being such a joy.

TABLE OF CONTENTS

LIST OF TABLES

LIST OF FIGURES

CHAPTER 1

INTRODUCTION

1.1 BACKGROUND

During the past several decades, the use of prestressed concrete has increased significantly. In general, these systems have shown to be a durable and effective structural system. However, today, many older prestressed concrete members require upgrading or replacement due to corroded reinforcement, damage due to vehicle impact, or greater load requirements. Damage to prestressed members, especially in bridge structures, is a significant problem. It was reported in 1980 that over 200 prestressed girders were damaged every year, with over 80% of the girders damaged due to over-height vehicles [Shanafelt and Horn, 1980]. Of the reported damage, severe and critical damages accounted for 20% of the damages. As a result, there is a need for effective and cost efficient repair and strengthening techniques for prestressed concrete members.

Currently, a number of repair and retrofit techniques are available for prestressed concrete girders. Such techniques include the use of internal splices for prestressing strand, the attachment of steel plates to the underside of girders, the addition of externally post-tensioned steel strands, and in the case of unbonded reinforcement, the selective replacement or addition of internal strands. Internal prestressing strand splices are effective at restoring prestressing forces, but they require significant demolition of the damaged area of the beam and the splices have a higher flexural stiffness than the existing strand. The stiffer splice contributes to cracking of the concrete and premature failure of the strand at the junction between the splice and strand [Shanafelt and Horn, 1985]. Attachment of steel plates to the underside of girders has not been shown to be consistently effective due to the stringent surface preparation requirements and failure of the concrete at the interface of the concrete and steel plate reinforcement. In addition, the reinforcement is generally not prestressed, thereby making the reinforcement only effective for supporting beam live loads. External

post-tensioning using steel strands requires little demolition of the beam, but the strands are susceptible to corrosion, especially if used in applications exposed to deicing salts. Limitations exist in the replacement or addition of strands in unbonded applications by the size of the internal ducts, the nature of the end anchorage, and the ease at which existing strands can be removed.

One relatively new approach for strengthening of prestressed concrete girders is to use exterior post-tensioned non-metallic tendons. The advantage of using the non-metallic tendons, such as Fiber Reinforced Polymer (FRP) tendons, is that these materials are non-corrodible. This eliminates the corrosion problems encountered with external steel tendons. These materials are also lightweight, with some Carbon Fiber Reinforced Polymer (CFRP) tendons having strength to weight ratios as much as five times that of prestressing steel strands. These materials generally have ultimate strengths equal or exceeding that of most prestressing steels. In addition, they have elastic moduli less than steel, which is beneficial in reducing the losses of post-tensioning forces.

Recent studies have investigated the use of externally post-tensioned FRP tendons for new construction and for repair/retrofit of non-prestressed (i.e. reinforced) concrete beams [Burgoyne, 1992; Mutsuyoshi and Machida, 1993, Saeki, et al., 1993]. Currently, there is no information available on the performance of steel prestressed concrete beams repaired or strengthened using external FRP tendons. The purpose of this study is to develop information on the performance of CFRP tendons and their use for strengthening of prestressed concrete beams. The study is limited to one type of CFRP tendon.

1.2 OBJECTIVES AND SCOPE

The objectives of the research are:

1. *To develop information on the mechanical properties of CFRP (Leadline) tendons as related to exterior post-tensioning requirements. This includes uni-axial tensile behavior, short-term behavior of tendons subjected to combined axial load and*

harping, behavior of harped tendons subjected to bending-tension fatigue, and the behavior of harped tendons subjected to sustained loads.

2. *To investigate the behavior of steel prestressed beams strengthened using exterior post-tensioned CFRP tendons. This includes testing of steel prestressed beams strengthened using exterior post-tensioned CFRP tendons, development of an analytical model, and conducting a limited parametric study.*

To meet the first objective, tests were conducted on CFRP tendons subjected to uni-axial loads, combined tensile and harping (i.e. bending) loads, bending-tension fatigue loads, and sustained combined tensile and harping loads. Limited uni-axial tension tests were conducted to determine the elastic modulus and the strength of the CFRP tendons. The vast majority of CFRP tendon testing was designed to understand the behavior of the tendons when subjected to combined axial load and harping. To develop this understanding, a series of tests were conducted that utilized a pivoting-end test frame that allowed the CFRP tendons to be stressed axially as well as harped about a curved plate. Test variables included three separate diameter harping plates, two loading paths, and various axial loads and bending angles of the tendons. The load paths for the static tests included (1) subjecting the tendons to simultaneous increases in axial load and bending angle until failure and (2) by leaving the tendon bend angle fixed and increasing the tendon axial load until failure. Bending-tension fatigue tests were conducted up to 1 million cycles and sustained loading tests were conducted up to a duration of 120 days. After completion of bending-tension fatigue tests and sustained combined tensile and harping tests, residual strength tests were conducted on the tendons. Results of the tendon tests under combined axial load and harping were used in developing analytical expressions that accurately predict the strain distribution and failure conditions of CFRP (Leadline) tendons subjected to combined axial load and harping.

The second objective was met by fabricating and testing two series of rectangular prestressed concrete beams. The two series of beams had different amounts of prestressing

steel. The beams were designed to obtain results for fully prestressed beams that could be strengthened externally by FRP tendons and for prestressed beams that have partially lost prestressing force due to corrosion of steel tendons and therefore need restoration of the design strength. The beams were tested under four-point static loading. They were initially loaded to induce cracking in them to simulate damage. Loads were then reduced prior to conducting the external post-tensioning procedure using CFRP tendons. The rehabilitated or strengthened beams were then loaded to failure. Changes in member deflections, strength and stiffness were observed and compared to unstrengthened "control" beams to verify behavioral changes due to the strengthening by external CFRP tendons.

The second objective included the development of an analytical model for predicting the behavior of steel prestressed concrete beams strengthened by exterior post-tensioned CFRP tendons. The predictions of the analytical model were compared with the experimental results to verify the predictive capability of the analytical model. The model was then used for conducting a limited parametric study of externally post-tensioned beams to understand the influence of various external post-tensioning parameters on the performance of the beam. Parameters of the study included initial external post-tensioning load, the location of external post-tensioning harping points, and the load-strain relationship of the external tendons.

1.3 THE STRUCTURE OF THE THESIS

The Thesis is presented in six chapters, with Chapter 1 as the introduction of the work. A literature review of related research is presented in Chapter 2. The investigation of CFRP tendon behavior is presented in Chapter 3. The experimental investigation of steel prestressed concrete beams externally post-tensioned with CFRP tendons and the development of an analytical model for predicting the behavior of steel prestressed concrete beams with exterior post-tensioned CFRP tendons is presented in Chapter 4. Chapter 5 presents the results of a limited parametric study of steel prestressed concrete beams with

exterior post-tensioned CFRP tendons. Summary and conclusion of the investigation is presented in Chapter 6. A list of the references cited in the dissertation is presented after Chapter 6. Tables and figures referred to in the text are shown at the end of each chapter. The algorithm and the listing of the analytical computer model developed in Chapter 4 is presented in Appendices A and B, respectively.

CHAPTER 2

LITERATURE REVIEW

2.1 INTRODUCTION

Exterior post-tensioning of structural members is a viable technique for new construction as well as for strengthening and retrofitting of existing structures. As early as 1936, an externally post-tensioned bridge was built in Aue, Germany. The bridge, designed by Franz Dischinger and built before the development of prestressing steel, is prestressed by bars of high strength steel with a yield stress of 73 ksi (500 MPa) [Virlogeux, 1990]. Despite some corrosion of the bars and prestress losses that required retensioning of the external bars, the bridge was still in service in 1990. In the early 1950's, externally post-tensioned bridges in Belgium (Sclayn bridge) and France (bridges at Villeneuve-Saint-Georges, Vaux-sur-Seine, Port à Binson, and Can Bia) were constructed. Several of these bridges suffered from corrosion of prestressing steel strands, but were otherwise mechanically sound [Virlogeux, 1990].

One of the earliest uses of external post-tensioning in the *strengthening* of concrete members was the strengthening of a 5-span, reinforced concrete T-beam bridge in Ontario, Canada in 1969 [Vernigora, et al., 1969]. In 1977, a prestressed concrete stringer bridge in the state of Washington was repaired with exterior post-tensioned tendons [University of Virginia, et al., 1980]. Since that repair, many other prestressed concrete systems have been repaired or strengthened using external post-tensioning.

Problems with corrosion of external tendons in early bridges resulted in very few externally post-tensioned structures being built in the 1960's and 1970's. However, developments in higher tensile capacity tendons, tendon protective systems, experience with prestressing/post-tensioning systems, and the need to repair existing prestressed members have encouraged a broader use of this type of structural system. With the progress in Fiber

Reinforced Polymer (FRP) tendon technology, the application of non-corrodible, high-strength FRP tendons in exterior post-tensioning systems has provided a new and promising approach to external prestressing systems.

The literature review that follows describes research and application of exterior post-tensioning, using either steel or FRP tendons, in the repair or strengthening of non-segmental concrete members. The review is divided into four main areas: 1) beams with exterior post-tensioned steel tendons, 2) analytical modelling of exterior post-tensioning, 3) behavior of FRP tendons, and 4) beams with exterior post-tensioned FRP tendons.

2.2 BEAMS WITH EXTERIOR POST-TENSIONED STEEL TENDONS

The results of a literature search on prestressed concrete beams with exterior post-tensioned steel tendons is described in this section. Each study is presented separately. At the end of the section, field applications are summarized.

2.2.1 University of Virginia, 1980

A model design for exterior post-tensioned repair of concrete beams is included in NCHRP Report 222 entitled "Bridges on Secondary Highways and Local Roads -- Rehabilitation and Replacement" [University of Virginia, et al., 1980]. The repair technique is based on the repair of a prestressed bridge girder in Washington State. The method is the only technique listed in the manual for strengthening the flexural behavior of prestressed concrete beams.

The post-tensioning tendons used in the repair are placed in straight post-tensioning ducts that are encased in concrete. The duct and concrete is placed on the top of the bottom flange on both sides of the beam. Shear keys are chipped into the existing beam flange and web at 18 in. (450 mm) spacing along the beam prior to placing the concrete. Through-web steel reinforcement is provided at 18 in. (450 mm) centers to tie the new concrete-encased

duct to the beam. Existing or new concrete diaphragms are used as reaction points for post-tensioning. After post-tensioning, the strands are grouted in place.

2.2.2 Shanafelt and Horn, 1985

In 1985, Shanafelt and Horn tested a 60 foot (18.3 m) span of an AASHTO Type III prestressed I-girder [Shanafelt and Horn, 1985]. The girder was made composite with a concrete deck 90 in. (2290 mm) in width and 6.5 in. (165 mm) thick that was cast 14 days after casting of the girder and 10 days after release of prestress. The girder was manufactured specifically for the research. Details of the test specimen are shown in **Figures 2.1** and **2.2**. Concrete strengths were 5 ksi (34 MPa) for the girder and 4 ksi (28 MPa) for the composite slab. Ten load tests involving two or three load cycles each were conducted on the girder. Loadings for each test were applied at midspan up to a load of 75% of the calculated ultimate load of the member under each of the ten test conditions. The ten tests were conducted in the following order: (1) as fabricated; (2) with external post-tensioning; (3) as fabricated but cracked; (4) with 4 strands out of a total of 16 internal prestressing strands severed; (5) with strands spliced with single strand internal splices; (6) with internal strand splices and exterior post-tensioning; (7) with strand splices removed and external post-tensioning removed; (8) with external post-tensioning; (9) with external post-tensioning removed, a total of 6 strands out of 16 strands severed, and with a metal sleeve splice installed; and (10) loading of the sleeve spliced girder to 100% of calculated ultimate moment capacity. Patching of broken concrete was completed prior to tests 5 and 8, and preloading of the girder was provided prior to patching for test 5. Additional testing of external post-tensioning corbel details was conducted in separate tests.

Of the ten tests conducted, the second test involved strengthening the girder by post-tensioning with two external 1-in. (25 mm) diameter, Grade 150 thread bars. The bars were post-tensioned to 84 kips (370 kN) each. The inside face of each corbel was 13 feet (3960 mm) from the centerline of the span. Each corbel had a length of 4 feet (1220 mm).

The centroid of each bar was 14.5 in. (370 mm) above the bottom of the girder. The calculated strength of the post-tensioned girder was 3,242 ft-kip (4,395 kN-m), compared to a calculated strength of 2,511 ft-kip (3,404 kN-m) for the unstrengthened girder. The test load for the strengthened girder was set at 75% of the calculated ultimate moment of 3,242 ft-kip (4,395 kN-m), for a total of 2,432 ft-kip (3,297 kN-m). Testing was halted, however, at 2,275 ft-kip (3,084 kN-m) because the midspan deflection exceeded the deflection found during testing of the original beam to a load of 75% of its predicted ultimate strength and the thread bar stress exceeded 90 percent of the bar expected yield stress. Both of these conditions were test limits imposed by the researchers. The test suggested that an increase in live load moment of 29% due to post-tensioning was possible. The researchers concluded that for the beam tested, however, an increase in live-load capacity of about 50% could be achieved with similar post-tensioning methods. No elaboration was provided by the researchers on the methods from which this larger increase in strength could be developed.

For test 6, the predicted behavior of the beam was the same as for test 2. The post-tensioning bar sizes and initial loads were the same as for test 2. The internal strand splices provided the prestress in the internal strands that existed prior to cutting the 4 internal strands. The test load moment of 2,255 ft-kip (3,057 kN-m) was approximately equivalent to the maximum load applied in test 2. Midspan deflections and external post-tensioning stresses were about the same as that for test 2.

For the test simulating repair using exterior post-tensioning, test number 8, four out of a total of 16, 1/2-in. (13 mm) strands were made ineffective at midspan. Each strand was initially stressed to approximately 28.9 kips (129 kN), with estimated effective load after losses of 22 kips (98 kN) per strand. Concrete in damaged areas was patched, but no preloading was applied prior to the patch. Post-tensioning was applied incrementally to a total of two, 1 in. (25 mm) diameter, Grade 150 thread bars. One bar was tensioned to 52.4 kips (233 kN); the second on the opposite side of the girder was tensioned to 89 kips (400 kN); and then the first bar was increased to 89 kips (400 kN). The external post-

tensioning load was approximately twice the load lost in the 4 internal strands cut. The higher post-tensioning load was necessary due to the location of the post-tensioning bars being closer to the centroid of the girder than were the strands that were cut.

The calculated flexural strength of the repaired girder with post-tensioning was 2,630 ft-kip (3,570 kN-m), and the undamaged girder strength was estimated at 2,511 ft-kip (3404 kN-m). The calculated ultimate moment of the damaged girder with 4 internal strands severed was 1,887 ft-kip (2,558 kN-m). At the ultimate test load of 89.7 kips (400 kN) (1,900 ft-kip maximum moment), the vertical midspan deflection caused by the test was 0.89 in. (23 mm). The vertical deflection for the undamaged/unstrengthened girder at the same load was 1.01 in. (26 mm). The decrease in the midspan displacement of the repaired beam was attributed to the higher prestress of the two post-tensioned bars (178 kips total) compared to the prestress provided by the four prestressing tendons cut (88 kips total).

The researchers recognized that the strength of the corbel used for developing the post-tensioning loads may be a limiting factor in the amount of post-tensioning that can be developed. To understand the strength and behavior of various corbels, the researchers tested three variations of corbel designs. The corbels were all 48 inches (1220 mm) in length and consisted of approximately 9 in. x 9 in. (230 x 230 mm) concrete cast along the top of the bottom flange of the girder. The corbels differed only by the method of attachment to the girder fillet. Corbel 1 was attached with twelve 1/2 in. (13 mm) diameter, round expansion bolts that penetrated the fillet 2.5 in. (64 mm). Corbel 2 was attached with twelve 1/2 in. (13 mm) diameter, round expansion bolts that were placed in 1.5 in. (38 mm) deep holes. Attachment of anchor bolts for Corbel 2 was augmented with epoxy resin. Corbel 3 was attached to the girder fillet by six Grade 60, No. 4 hairpin reinforcing bars which were inserted into 6 in. (150 mm) deep holes. Bars were affixed to the girder by epoxy. Corbel 3 was used in the post-tensioning of the test girder.

The corbels were not tested to failure, but instead specified design loads were applied to the corbels. The cracking pattern was observed and displacements were recorded. Based on the tests, Corbels 1 and 3 were considered to have sufficient strength to anchor a 1-in.

(25 mm) diameter 150 Grade thread bar. Corbel 2 was not considered adequate for anchoring. The researchers found that most of the load transfer from corbels to the girders occurs near the loaded face of the corbel. Increasing the length of corbels, therefore, may not lead to increased strength of the corbel.

2.2.3 Olson, 1992

Olson conducted tests on four, twenty-year-old prestressed bridge girders made available due to bridge realignment [Olson, 1991; and Olson, et al., 1992]. The girders were AASHTO Type 3 girders fabricated in 1967 and removed from service in 1984. The specimens were made composite with a 64 in. (1630 mm) by 6 in. (152 mm) top slab. Details of the test specimens are shown in **Figures 2.3** and **2.4**.

The first of the beams was tested as removed from the bridge as a control specimen. The remaining three girders were subjected to simulated impact damage of an over-height vehicle striking the side of the bridge. One girder was used to investigate the amount of damage the girder could sustain before repair became necessary. One girder was repaired using internal tendon splices, and the remaining girder was repaired using external post-tensioning. The repaired girders were evaluated under step-wise increasing fatigue loading, followed by a static load test to failure.

For the exterior post-tensioned beam, two 5/8 inch (16 mm) diameter, 157 ksi (1080 MPa), high-strength rods were post-tensioned straight along the top of the bottom flange of the concrete I-beam. The post-tensioning rods were placed on one side of the concrete girder (the side with cut strands) and attached to concrete corbels anchored by shear-friction to the bottom flange of the girder as shown in **Figure 2.4**. The clamping steel comprised of No. 4, Grade 60 hairpin steel affixed with epoxy into 4.25 in. (108 mm) deep holes in the girder. Each post-tensioning rod was individually tensioned to approximately 25 kips (111 kN).

During testing of the exterior post-tensioned girder, apparent fatigue failure of some

of the corbel hairpins caused a portion of one corbel to detach from the girder. The corbel detached from a flexural crack in the girder to its free-end bearing plate (beam support side of corbel). During ultimate loading, flexural cracks in the girder widened and intersected with some of the hairpin connectors, which allowed for pull-out of the hairpins and failure of the corbel. The peak load of the post-tensioned girder was 253 kips (1130 kN) with a deflection of approximately 7 in. (180 mm). The failure of the corbel took place at a midspan deflection of approximately 12 in. (300 mm). The overall strength of the post-tensioned girder was greater than the similarly damaged, unstrengthened beam of girder #2, which failed at a load of 209 kips (930 kN) at a midspan displacement of 25 in. (635 mm). The undamaged girder #1 failed at a load of 293 kips (1300 kN) at a midspan displacement of approximately 22 in. (560 mm).

The authors recommended that future repairs using similarly anchored corbels be anchored in locations that do not decompress during service loading. The use of through-bolts in anchoring of the corbel was also recommended.

2.2.4 Rao and Mathew, 1996

Rao and Mathew tested 4 internally bonded and 8 externally post-tensioned rectangular beams with steel strands [Rao and Mathew, 1996]. The beams were 6.9 x 14 x 157 in. (175 x 350 x 4000 mm) and were loaded at 1/3 points. The external steel tendons were harped at 1/3 points. All of the beams had additional non-prestressed longitudinal reinforcement. The percentage of non-prestressed reinforcement ranged from 0.164 to 0.985. The percentage of external post-tensioning steel ranged from 0.137 to 0.403. The total effective prestressing forces in the external strands ranged from 21.8 kips (97 kN) to 62.1 kips (276 kN). The beams were designed for a total assumed design service load of 18 kips (80.0 kN).

Loading was applied in two cycles. In the first cycle, the externally post-tensioned beam was loaded up to about 22 kips (100 kN) and released. The objective of the first loading cycle was to have the beam cracked, thereby representing a beam in service. In the

second cycle, the beams were reloaded to failure. In each cycle, loads were increased by increments of about 4.5 kips (20 kN) starting from zero. At each load stage, observations of deflection, strain in both prestressing and reinforcing steel, surface strain on concrete, crack width, and crack spacing were recorded.

The majority of results were reported as a ratio between the experimental results and analytical results. Comparisons between the beam ultimate moment, midspan deflection at various loading stages, and stresses in the prestressed and non-prestressed steel were compared with analytical results. The analytical procedure developed by Rao and Mathew and the comparison of results is discussed in Section 2.3.3.

2.2.5 Field Applications

Vernigora reported in 1969 the successful strengthening of a six-span, reinforced concrete (non-prestressed) bridge in Ontario, Canada [Vernigora, et al., 1969]. The bridge consisted of 5 girders for each span. The six simple spans were post-tensioned by means of draped tendons so as to make the repaired bridge continuous over the supports. The tendons were draped at the midspan of each span using a saddle running across the bottom of the beam. Post-tensioning was provided on each side of the girders by cable bundles consisting of either 8 or 9, 1/2 in. (13 mm) tendons, depending upon location. The maximum initial force was 454 kips (2020 kN) per girder. Additionally, transverse post-tensioning of the bridge was provided by either 7, 0.5 in (13 mm) diameter or 4, 0.5 in. (13 mm) diameter steel tendons. The tendons were placed in plastic tubes that were filled with grout to guard against corrosion. The repair allowed for the elimination of all but one of the bridge expansion joints.

Klaiber cited ten examples of field applications of exterior post-tensioning used for rehabilitation or strengthening of prestressed concrete beams [Klaiber, et al., 1987]. Of the ten examples cited, three were closely related to the research in this investigation. One repaired bridge included the bridge in Lewis County, Washington, discussed previously.

Two additional repair projects were completed in Europe. A three span, 280 foot, continuous prestressed concrete tee bridge in Netekanaal, Belgium utilized exterior post-tensioning to repair deterioration due to corrosion and to compensate for design deficiencies. A 116 foot span of a continuous prestressed concrete tee bridge in Wiesbaden-Hochheim, Germany used externally post-tensioned steel tendons to repair cracking and internal prestressing strand damage.

An extensive repair of a five story parking structure in San Fransico was completed using external post-tensioning with virtually no disruption in the parking structure operation [Aalami and Swanson, 1988]. The repair was necessary due to corrosion and failure of existing post-tensioning strands. The new strands consisted of 7/16 in. (11 mm) epoxy coated strands that were harped at the midpoint of each strengthened beam. The tendons were protected by a 2 in. (51 mm) corrugated PVC pipe encased in a 6.5 inch (165 mm) square precast concrete member that extended the length of the tendon.

2.3 ANALYTICAL MODELLING OF EXTERIOR POST-TENSIONING

A relatively large amount of research has been conducted to study the behavior of internal, unbonded post-tensioned concrete members. Study by Naaman and Alkhairi reviewed work of nine investigations of unbonded prestressed concrete beams totaling 143 tests carried out since 1960 [Naaman and Alkhairi, 1991]. The behavior of external post-tensioned members, however, differs from internal tendons because of the changes in prestressing eccentricity as the beam deflects. In this section, four proposed analysis procedures specifically for members with external tendons are reviewed.

2.3.1 Virlogeux, 1983

Virlogeux developed an analysis procedure for externally post-tensioned concrete [Virlogeux, 1983]. For service load stage analysis, the tendon length variation between two

deviators was obtained from the displacements of the deviators by assuming that the beam was uncracked and remained linearly elastic. At the ultimate load stage, he proposed a plastic hinge concept for predicting tendon elongation. A formula was used for the prediction of friction at the external tendon deviators.

2.3.2 Alkhairi and Naaman, 1993

Alkhairi and Naaman developed a numerical model for the analysis of beams prestressed with unbonded internal or external tendons throughout their range of behavior under load [Alkhairi and Naaman, 1993]. The proposed model involves calculating the average tendon elongation of unbonded tendons by performing a multilevel iterative nonlinear analysis at several locations throughout the beam. The model assumes: (1) plane sections remain plane; (2) symmetrical loading and tendon profile; (3) the post-cracking tensile capacity of concrete is neglected; (4) concrete within a cracked region of the beam is considered effective in resisting diagonal tensile stresses so far as the applied shear force is less than the cracked shear strength; and (5) the beam is assumed to be reinforced with a minimum amount of vertical stirrups necessary to resist shear stresses at all cracked sections along the beam.

The model offers a combination of features not found in other investigations, namely: (1) it assumes a most generalized case of reinforcement that includes non-prestressed reinforcement, prestressed bonded and unbonded steel, internal or external tendons, and non-prestressed compressive steel; (2) it accounts for the effect of member span-to-depth ratio using the truss mechanism; and (3) it incorporates the effects of eccentricity variations in beams prestressed with external tendons.

The general steps of the model are:

1. Determine the applied moment distribution on the beam. Using an assumed prestressing force, cracked and uncracked regions of the beam are determined based on comparisons between the applied moment and the theoretical cracking moment of longitudinal concrete segments.

2. Force and moment equilibrium analysis is accomplished for each longitudinal segment of the beam. For sections other than the midspan section, the moment equilibrium must satisfy the externally applied moments at the section plus any additional moments due to diagonal tensile cracking.

3. Beam deflections and elongations between post-tensioning anchors are then calculated by numerical integration. Increases in prestressing forces are added to assumed prestressing forces and additional loading iterations are conducted starting again at step 1. For unbonded reinforcement, an additional iteration is required during the same loading stage if the absolute value of the calculated to assumed stress increase in unbonded tendons is greater than a specified tolerance.

4. Eccentricity variations are incorporated in the model at each loading stage by first conducting an analysis with the initial tendon eccentricities. After convergence to a solution, revised internal moment of resistance and additional moments due to shear are calculated using the new eccentricity values. If the new values differ beyond a particular tolerance, the analysis is repeated with a different assumed unbonded prestressing force.

A parametric study conducted by the authors using the analytical model suggests that shear deformations may have a significant effect on the increase in the stress at ultimate in unbonded tendons for beams having span-to-depth ratios smaller than about 24, regardless of the unbonded tendon layout (whether internal or external) [Alkhairi and Naaman, 1993]. Neglecting the effect of shear deformations causes no significant change in tendon stresses at higher span-to-depth ratios.

The effects of eccentricity variations are most pronounced in beams having span-to-depth ratios greater than about 24. The analysis conducted in the research showed that midspan eccentricity variations can be safely neglected for span-to-depth ratios less than about 16. This is because for these span-to-depth ratios, the actual eccentricity at ultimate is predicted to be within 5 to 10% of the midspan eccentricity at the initial loading stage and because beams having low span-to-depth ratios are generally very stiff, thus producing very small vertical deflections. Since the actual eccentricity of the external tendon at any loading stage is a function of the vertical deflections, eccentricity variations for such beams will be very small.

2.3.3 Rao and Mathew, 1996

Rao and Mathew developed an analytical model to predict the behavior of externally post-tensioned reinforced concrete beams with multiple deviators [Rao and Mathew, 1996]. Assumptions made in the analysis include: (1) plane sections remain plane after bending; (2) the beam is symmetrical about its midspan; and (3) the tendon profile is of a general polygonal shape. The analysis includes frictional resistance at deviation points and accounts for changes in tendon eccentricity. Shear deformations and tension stiffening affects are not considered. Comparison of analytical results with Rao's experimental test results discussed in Section 2.2.4 show a good correlation for ultimate moment resistance and midspan deflections up to 36 kips (160 kN). Actual ultimate loads or moments were not given.

Rao also conducted a parametric study of a 98 ft. (30 m) span I-section with the following dimensions: height=73 in. (1850 mm); top flange width = 28 in. (700 mm); bottom flange width = 24 in. (600 mm); web width = 5.9 in. (150 mm); and flange thickness = 7.9 in. (200 mm). The beam was designed for an assumed live load of 1.37 kip/ft (20 kN/m). The effective prestressing force was 780 kip (3450 kN) with an area of prestressing steel of 4.86 sq.-in. (3136 mm^2). The external tendons were deviated at third points. Untensioned steels of area 1.40 sq.-in. (905 mm^2) and 2.50 sq.-in. (1610 mm^2) were provided at top and bottom flanges respectively. The properties of concrete assumed were f'_c = 6.53 ksi (45 MPa); f_{cr} = 0.42 ksi (2.8 MPa); and E_c = 4,930 ksi (34 GPa). The beam was analyzed by considering the following cases: (1) two deviators without friction; (2) two deviators with full fixity; (3) three deviators without friction; (4) three deviators with full fixity; and (5) internal unbonded tendons without friction.

The results of the Rao's parametric study were:

1. Friction at deviators reduces the deflection and increases the stress in prestressing steel.

2. An additional deviator at midspan increases moment-carrying capacity and ductility quite significantly. However, the paths of load verses deflection and stress in tendon do not change.

3. For this particular problem, the beam moment resistance is enhanced by 11 percent due to the introduction of a central deviator, and is further increased by 6 percent when the tendon is prevented from slipping at deviators.

2.3.4 Arduini, Tommaso and Giacani, 1996

Arduini, Tommaso and Giacani developed a modelling technique for externally prestressed concrete beams using FRP tendons [Arduini, et al., 1996]. These tests were compared with two beams tests conducted by the authors and described in Section 2.5.7. The analytical model uses a confined concrete constitutive relationship outlined in the CEB-FIP Model Code 90 [Model Code 90, 1993]. A bilinear elastic-plastic steel model was used for the steel reinforcement and a linear elastic model was used for the FRP tendons.

The authors state that the initial axial effect of the prestressing force is taken into account as a reduction of compressive strength and an increase of tensile strength without changing other mechanical properties. It is inferred by this author that what this approach does is to adjust the internal stresses in the beam cross section due to external loads by the appropriate change in stress due to the post-tensioning. With these adjustments, a moment-curvature relationship is developed for the section. For each step increase in applied load, an "effective moment" of the section is determined. The "effective moment" is defined as the externally applied moment minus the flexural effect of the eccentric post-tensioning force. After determining the "effective moment", segment curvatures can be determined based on the previously determined moment-curvature relationship. Segment curvatures are integrated over the beam span to determine axial and vertical displacements. Before increasing the value of the load, the program upgrades the value of the prestressing force and eccentricity for each segment.

2.4 BEHAVIOR OF FIBER REINFORCED POLYMER (FRP) TENDONS

There is a variety of fiber reinforced polymer (FRP) tendons available today due to the number of fiber materials (ex. glass, aramid, carbon), the variety of properties for each type of fiber material, the different binding matrix materials (ex. vinyl esters, thermoset epoxies, thermoplastic epoxies, etc.) and the form and size of the final product (ex. straight protruded, braided, etc.). With the great variety in properties of FRP products, specific conclusions about the use of these materials are dependent on the exact nature of the material tested. This review of FRP tendon behavior is therefore limited to research that is relatively comprehensive, related specifically to the material used in this research, or is otherwise noteworthy. Since the research in this study only concerns the mechanical behavior of the tendons, the review of research will focus primarily on the mechanical behavior of FRP tendons. Additional research on FRP tendon properties can be found in recent conference proceedings [Saadatmanesh and Ehsani, 1996; Taerwe, 1995; Nanni and Dolan, 1993; Neale and Labossiere, 1992].

2.4.1 Uomoto and Hodhod, 1993

Uomoto and Hodhod conducted tests on FRP tendons with three types of fiber: glass (GFRP), aramid (AFRP), and carbon (CFRP) [Uomoto and Hodhod, 1993]. The tendons were constructed with fiber volume fractions, V_f, of 0.45, 0.55, and 0.66. The tests indicated that the elastic modulus of the composite tendon can be accurately estimated using the "law of mixtures". This relationship is expressed as:

$$\mathbf{E_c = V_f E_f + E_m(1-V_f) \approx V_f E_f} \qquad \textbf{(2.1)}$$

where E_c = elastic moduli of the composite
V_f = volume fraction of fibers
E_f = elastic moduli of the fiber

E_m = elastic moduli of the matrix

The approximate value for the elastic modulus of the composite as calculated from Equation 2.1 neglects the matrix contribution, which is possible due to the relatively low elastic moduli of most matrix materials.

Uomoto found that a similar law of mixtures relationship for tendon strength does not predict the tensile strength of tendons. For the AFRP tendons, the strength of the tendons increased proportionally with the increase in fiber volume fraction, but was still below that predicted by the law of mixtures. For the GFRP and CFRP tendons, the anchorage or grip affects lowered the strengths of the tendons at higher loads, thereby reducing the observed strength of the tendons with higher fiber volume fraction. Tests on tendons with reduced cross section confirmed that the strengths of CFRP and higher fiber content GFRP tendons were reduced due to grip effects.

2.4.2 Uomoto, Nishimura and Ohga, 1995

Uomoto, Nishimura, and Ohga conducted a variety of tests on GFRP, AFRP, and CFRP rods [Uomoto, et al., 1995]. The rods were 0.24 in. (6 mm) in diameter and 16 in. (400 mm) in length. The fiber content of the tendons was 55% by volume. Vinyl ester resin was used as a binding material for the fibers, and split chucks were used to grip the tendons.

For the tensile tests, the researchers tested over 100 specimens of each type of rod. The mean values of the test failure loads were 216 ksi (152 kgf/mm^2) for GFRP, 240 ksi (169 kgf/mm^2) for AFRP, and 198 ksi (139 kgf/mm^2) for CFRP tendons. The tendons failed at the anchorage chucks due to apparent stress concentrations or due to failure of the interface between the fiber and matrix.

Sustained loading tests were conducted on ten specimens each of the GFRP, AFRP, and CFRP rods. The applied stress was between approximately 150 ksi (110 kgf/mm^2) and 210 ksi (150 kgf/mm^2). The sustained stresses were equivalent to 66.7 to 94.5% of the mean tensile strength for GFRP, 70 to 90% for AFRP, and 96.4 to 101.2% for CFRP. Based on

the test results, the authors derived the following expressions that relate the failure stress and sustained load time.

$$\sigma/\sigma_t = 79.2 - 8.29 \cdot \log T \quad \textbf{(for GFRP rods)} \quad \textbf{(2.2a)}$$
$$\sigma/\sigma_t = 79.8 - 5.67 \cdot \log T \quad \textbf{(for AFRP rods)} \quad \textbf{(2.2b)}$$
$$\sigma/\sigma_t = 102 - 1.91 \cdot \log T \quad \textbf{(for CFRP rods)} \quad \textbf{(2.2c)}$$

where, σ = applied stress
σ_t = mean static tensile failure stress for tendon
T = time in hours

Based on the above equations, for a 100 year service life, the critical applied stress for the tendons is 65 ksi (46 kgf/mm^2) or 30% σ_t for GFRP rods, 110 ksi (78 kgf/mm^2) or 46.1% σ_t for AFRP rods and 180 ksi (127 kgf/mm^2) or 91.1% σ_t for CFRP rods. The authors made no observations concerning relaxation characteristics of the rods.

Uomoto also conducted fatigue tests on the rods with the maximum tensile stress ranging from 20 to 100% of the static tensile strength of each rod. The stress range for the tests were set to 14, 28, 71, 114 and 142 ksi (10, 20, 50, 80 and 100 kgf/mm^2). The cyclic frequency ranged from 1 to 10 Hz. Up to 7 replicate specimens were tested for each case. For the GFRP tendons, the logarithm of the fatigue cycles to failure varied approximately linearly with the applied mean stress. The applied mean stress versus logarithm of cycles relationship was similar for each test amplitude, except that lower amplitude tests maintained a higher number of cycles (i.e. the mean stress versus logarithm of cycles relationships were parallel to other tests of different amplitude). The mean stress of AFRP tendons was also in proportion to the logarithm of fatigue cycles. However, the gradient of the mean stress versus fatigue cycles in logarithm for AFRP tendons with more than 71 ksi (50 kgf/mm^2) of amplitude was steeper than that with 14 and 28 ksi (10 and 20 kgf/mm^2) of amplitude. Fatigue strength of CFRP rods was higher than that of GFRP and AFRP rods. CFRP rods sustained more than four million fatigue cycles in the case that the maximum stress was less than 88% of the mean tensile strength, independent of the amplitude.

The authors concluded that for fatigue tests with a relatively high mean stress, creep rupture behavior may explain the relationships for AFRP tendons and, to a lesser extent, for GFRP tendons. In other words, for a fatigue test under a given mean stress, AFRP and GFRP tendons will fail after a set time, regardless of the number of loading cycles. The author concluded that CFRP tendons show virtually no degradation due to fatigue or sustained loading.

2.4.3 Hoshijima, Yagi, Tanaka and Ando, 1996

Short-term and sustained load tests on CFRP tendons were reported by Hoshijima, Yagi, Tanaka and Ando [Hoshijima, et al., 1996]. Tensile tests of the 0.31 in. (8 mm) diameter, indented tendons indicated a nominal ultimate tensile stress of 350 ksi (2400 MPa), a total tensile force of 27.0 kips (120 kN), an elastic modulus of 21,300 ksi (147 GPa), and an ultimate strain of 1.5%. These tests were carried out using a 4.75 in. (120 mm) long wedge anchoring system made by the manufacturer of the tendon. It should be noted that previous tensile strength data reported by the manufacturer indicated smaller ultimate strength and strain values of 23.4 kips (104 kN) and 1.3% respectively [Mitsubishi Kasei Corporation, 1993]. Hoshijima also conducted 200 hour and 1000 hour relaxation tests under an average stress of 192 ksi (1330 MPa). The authors observed virtually no relaxation characteristics (exact values were not reported). The researchers, however, recommend designers assume 2 to 3% relaxation.

2.4.4 Other Studies

Anigol and Khubchandani conducted separate short-term (48 hours) and long-term (1 year) uni-axial sustained load tests on GFRP and CFRP tendons [Anigol, 1991 and Khubchandani, 1992]. Sustained loads were set to 50% of the ultimate strength of the tendon. The tests indicated very little creep for both types of tendons. The elastic modulus and ultimate uni-axial tensile strength of the tendons after the creep tests did not indicate any

change.

Iyer and Khubchandani conducted a variety of tests on carbon fiber cables made from 7, 0.125 in. (3.2 mm) diameter carbon rods [Iyer and Khubchandani, 1992]. Short-term static strengths for the rods was found to be 318 ksi (2200 MPa). Static strength of the cables was not reported. Six-month sustained loading tests were conducted on three carbon cables with stress levels of 137 ksi (943 MPa), 143 ksi (989 MPa), and 155 ksi (1066 MPa). Results indicate very little drop in the strain values. Quantitative results were not reported.

Gerritse and Den Uijl conducted tests on AFRP strips measuring 0.8 in. x 0.06 in. (20 x 1.5 mm) subjected to sustained loadings and different environmental conditions [Gerritse and Den Uijl, 1995]. The uni-axial tensile strength of the strips was 6.7 kips (30 kN). Sustained loading tests were conducted on the strips in an alkaline environment (pH = 13) and with temperatures of 20 and 60 degrees Celsius. The loads for the tests was 60% and 80% of their short-term uni-axial strength. Failure of the specimens was generally initiated at the anchorage of the specimens. For the specimens tested at 20 degrees, the test results indicate a lower-bound 100 year failure load of 52% of the short-term strength. The time till stress-rupture was 10 to 15 times shorter at 60 degrees than at 20 degrees. After 1000 hours of sustained loading, the creep strain was estimated as 7% and appeared to be independent of the temperature of the test. Relaxation tests at similar loadings suggest relaxation in an alkaline liquid is about 40% more than in air.

Fatigue tests were performed in England on tendons made of 64 small diameter composite rods [Walton and Yeung, 1986]. Tests were performed on composite rods made of fiber and epoxy resin, anchored in a steel socket using an epoxy. These tests indicated that the fatigue strength of aramid and carbon fiber rods is superior to steel bars and that glass fiber rods are more susceptible to fatigue damage than steel bars.

In fatigue tests of up to 10 million cycles and at different stress ranges, Schwartz reported that carbon fiber epoxy composites have better fatigue strength than steel, while the fatigue strength of glass composites is lower than steel at low stress ratios [Schwartz, 1992].

In 1994, Gorty conducted fatigue tests on CFRP tendons for 2 million cycles [Gorty,

1994]. The maximum and minimum stress levels were 64% and 55% of the tendons short-term ultimate strength. No tendons failed during the test and the results showed that the modulus of elasticity of the tendons did not change after the fatigue test.

2.5 BEAMS WITH EXTERIOR POST-TENSIONED FRP TENDONS

The studies of beams with exterior post-tensioned FRP tendons deal with reinforced concrete beams. There is no information available on prestressed beams (with steel tendons) strengthened with exterior post-tensioned FRP tendons.

2.5.1 Burgoyne, 1992

Burgoyne constructed and tested a concrete beam externally prestressed with Aramid fiber tendons (Parafil) [Burgoyne, 1992]. Dimensions of the beam are shown in **Figure 2.5**. The beam had minimal non-prestressed steel reinforcement designed to resist the dead-weight moment of the beam. The beam used two, 132 kip (590 kN) tendons mounted externally to the concrete and deflected at saddles close to the loading points. The tendons were bent to an angle of 4.6 degrees at the saddles. At the concrete age of 10 days, the tendons were prestressed to 15 kips (67 kN) each. This initial prestressing was applied to guard against failure of the beam during relocation to test supports. At the concrete age of 33 days, the initial prestressing force of 70 kips (310 kN) per tendon was applied. The beam was simply supported close to its ends and loaded by two point loads applied through a spreader beam.

During post-tensioning, the load at the dead end of the external tendons was measured. The load readings indicated a loss of 5% of the tendon load due to friction between the fixed end and loading end of the tendon. A commonly used expression for calculating friction losses is:

$$P_x = P_o e^{-\mu\theta} \quad (2.3)$$

where P_x = tendon load at fixed end
P_o = tendon load at loaded end
μ = friction coefficient
θ = tendon bend angle

Using this relationship, the author computed a friction coefficient, μ, of 0.32. This value is slightly higher than would be expected with steel tendons. The author suggests that this friction coefficient could be brought down by a better selection of sheath and deflector materials.

Following post-tensioning to 70 kips (67 kN) per tendon, the first loading cycle was applied to the beam for 42 days. During this cycle, measurements were recorded to monitor the effects of creep and relaxation on the behavior of the beam. Loading during this stage was set such that a small tensile strain was observed in the bottom of the beam, but the beam remained uncracked. This load was set at 36 kips (160 kN).

At the end of the first cycle of loading lasting 42 days, the beam deflection due to the effects of shrinkage and creep of concrete was 59% of the instantaneous deflection. The author states that this increase in deflection was not affected by relaxation of the tendons. The relaxation of the tendons was, however, significant. After the initial prestress load of 15 kips (67 kN) per tendon, the tendon prestress losses were estimated at 13.5% at 23 days. After increasing the prestressing force to 70 kips (310 kN) per tendon, prestress losses were estimated at 11.5% of the 70 kip (310 kN) load after 42 days.

After the first load cycle, the beam was subjected to a number of load cycles, each at successively higher loads, until failure of the beam. Loading of the beams to successively higher loads and unloading produced expected results. The beams exhibited greatly reduced stiffness after cracking, but retained the original deflections upon unloading. Failure of the beam was characterized by large cracks opening in the tension face, with considerable deflection at virtually constant load. The final failure occurred by crushing of the top flange,

followed by compressive failure in the concrete down the web.

The AFRP tendons did not appear to be affected by the failure of the concrete. Upon completion of the beam test, the external AFRP tendons were removed and statically tested. The tendons failed at loads of 150 kips (670 kN) and 154 kips (685 kN), which is greater than the short term breaking load of the tendons of 135 kips (600 kN). This increase in strength is consistent with increases found by Chambers [Chambers, 1986]. The increase in strength is attributed to straightening of individual fibers of the tendon when subjected to sustained loads which allows for more uniform stress distribution across the tendon cross-section.

2.5.2 Sho-Bond Corporation and Fuji P. S. Corporation, 1993

Full scale tests on damaged prestressed concrete beams strengthened by external tendons was carried out by Sho-Bond Corporation and Fuji P.S. Corporation [FRP International, 1993]. The external tendons were heavy-duty prestressing steel, CFRP tendons (CFCC), and AFRP tendons (Parafil). Their research confirmed that external FRP tendons can be applied to retrofit old reinforced concrete and prestressed concrete bridges. After a thorough search, no additional details or references for the research were located by the author.

2.5.3 Mutsuyoshi and Machida, 1993

Mutsuyoshi and Machida tested six T-shaped reinforced concrete beams which were externally post-tensioned with three different tendons -- seven wire prestressing steel strand, AFRP tendon, and CFRP tendon [Mutsuyoshi and Machida, 1993]. The modulus of elasticity for the steel, aramid and carbon tendons was approximately 30500, 10900, and 17400 ksi (210, 75, 120 GPa) respectively. Tests included a total of six beams with tendon bend angles of 7.1 and 11.3 degrees. Changes in bend angles were accomplished by adjusting the harping saddle locations along the beam. Prestress forces were 15.4 kip

(68 kN) or 13.2 kip (59 kN) per tendon, which is less than 50% of the nominal tensile strength of each tendon. The load was applied monotonically to the beams except for one, which was tested under fatigue loading. A typical sketch of the beams is shown in **Figure 2.6**.

Deformed bars with a diameter of 0.39 in. (10 mm) and yield strength of 50 ksi (340 MPa) were used as longitudinal reinforcement and stirrups. The percentage of tensile reinforcement and shear reinforcement were 1.40% and 0.41%, respectively. The harping saddles had a radius of 7.9 in. (200 mm). One external tendon was placed on each side of the beam web.

The beams were loaded to cracking, unloaded, and subsequently tested to failure. The research indicated that before the ultimate state, the FRP post-tensioned beams exhibited a slightly lower secant stiffness than the steel post-tensioned beams. At a midspan displacement of 0.8 in. (20 mm), for example, the applied load on the steel, CFRP, and AFRP post-tensioned beams was approximately 45 kips (200 kN), 42 kips (185 kN), and 38 kips (170 kN), respectively. At ultimate, the steel and AFRP post-tensioned beams failed in compression failure of the concrete while the CFRP beams showed simultaneous compression failure of the concrete and rupturing of the CFRP tendon. The reason for the difference in failure modes of the beams was attributed to the fact that the tensile failure load of the CFRP tendon was less, 31.9 kips (140 kN), compared to the ultimate load of the steel, 36.0 kips (160 kN), and AFRP, 42.3 kips (188 kN). Despite having a lower rupture load, the tendons were all post-tensioned to the same initial load. It could also be reasoned that the stiffer CFRP tendon (as compared to the AFRP) developed a higher load for a given beam deflection than the AFRP tendon beam, thereby increasing the possibility of tendon rupture before concrete crushing. The breaking loads of the CFRP tendons, as measured by the load cells, were 24.6 kips (109 kN) for Beam 3 and 25.3 kips (113 kN) for Beam 4, which is 77% and 80% of the tendon uni-axial strength. The lower failure loads of the tendons were attributed to the influence of harping of the tendons at the saddles.

Mutsuyoshi and Machida concluded that the influence of the different tendon bending

angles (7.1 and 11.3 degrees) on the behavior of the beams was small. The beams tested with a higher tendon harping angle, however, used a smaller prestressing load, thereby making any conclusions about the bend angles suspect.

A proposed analysis procedure used by Mutsuyoshi and Machida assumes a bi-linear stress-strain relationship for the steel, a linear stress-strain relationship for the FRP reinforcement, and a Hognestad representation for the concrete. Since the increase in strain of the concrete at the level of the external tendon does not correspond with the increase in strain of the external tendon, the researchers used a factor, α, which represents the ratio of the increase in tendon strain to the increase in concrete strain at the level of the external tendon at ultimate. The strain in the external tendon was represented by the following equation.

$$\epsilon_{pu} = \epsilon_{ps} + \alpha \left(\epsilon_{cp} + \epsilon_u \frac{d-x}{x}\right) \tag{2.4}$$

where ϵ_{pu} = strain of the tendon at ultimate state
ϵ_{ps} = strain of the tendon at the effective prestressing state
ϵ_{cp} = strain of concrete at the level of the tendon at the effective prestressing state
ϵ_u = strain of the concrete at the ultimate state (0.0035)
d = distances from the top compression fiber to the tendon
x = distances from the top compression fiber to the neutral axis

To determine α, the researchers performed an iterative analysis that first assumed a value for α. With the assumed tendon strain at ultimate, a discrete element method analysis of the member was performed that provided curvatures at sections along the beam. By integrating these curvatures along the beam, the beam shape could be predicted. A comparison was then made between the tendon extension due to the calculated beam curvatures and the extension resulting from the assumed value of α. The value of α was adjusted until the difference in tendon extension between both methods was less than a given tolerance.

Using the above analysis, the researchers calculated appropriate values of α to be 0.35 for steel post-tensioned beams and 0.36 for both FRP tendon post-tensioned beams. Using these values of α, the calculated forces in the tendons at ultimate were higher (1.00% to 1.20%) than those found during experiments. The calculated flexural strengths, however, fell between 87% and 99% of the experimental strength values.

In Mutsuyoshi and Machida's testing, one CFRP reinforced beam was tested under fatigue loading. The beam was loaded to produce crack widths of 0.01 in. (0.3 mm) before installation and post-tensioning of CFRP tendons. The initial prestress was 41% of the nominal breaking load of the tendon. The loading was cycled between 2.5% and 40% of the ultimate strength of the beam. Loading was stopped at every 5×10^5 cycles so that static load tests could be applied to the beam. Load-displacement results after 10^7 cycles showed no changes in the tendon tension and only a very small softening of the beam stiffness. Mutsuyoshi and Machida concluded that fatigue was not a problem for concrete beams externally post-tensioned with CFRP tendons.

2.5.4 Saeki, Horiguchi, Inomata, Hata and Ikeda, 1993

Saeki, Horiguchi, Inomata, Hata and Ikeda conducted research concerning the use of a braided aramid fiber rope in the exterior post-tensioned strengthening of steel reinforced concrete members [Saeki, et al., 1993]. Static load tests were conducted on four externally post-tensioned beams, and fatigue tests were conducted on 6 externally post-tensioned beams. The beams had a rectangular cross-section with dimensions of 7.9 x 15.7 x 118 in. (200 x 400 x 3000 mm). The beam span was 98 in. (2.5 m). Beams included a reinforcement ratio for non-prestressed longitudinal steel of either 0.0055 (beam type A) or 0.0109 (beam type B). An equal number of each type of beam was tested for each test. External tendons were harped at a single location at midspan. Details of the specimens are shown in **Figures 2.7** and **2.8**.

The beam specimens were first loaded without post-tensioning until cracking, after

which they were unloaded and subsequently post-tensioned with the aramid fiber tendons. Some specimens utilized epoxy injection of cracks before post-tensioning. The beams were loaded under third-point loading across the 98 in (2.5 m) span.

Aramid fiber rope tendons were used for the post-tensioning in the research. The tendons consist of densely arranged parallel-filament aramid fibers, encased in a polyethylene sheathing. The material is not impregnated with resin, thereby giving it good flexibility and tensile properties in bending. The 0.53 in. (13.5 mm) diameter rope has an ultimate load of 23.2 kips (103 kN) with an elastic modulus of 18,700 ksi (129 GPa). The ultimate stress and elongation of the rope is 270 ksi (1870 MPa) and 1.5%. The target prestressing force for both ropes of the test beams was 15.4 kips (68.7 kN), which corresponds to 34% of the breaking strength of the rope.

Static test results indicate the load at cracking for each type of beam (A or B) roughly doubled, from 7.2 kips (32 kN) to 13.8 kips (61 kN), due to the post-tensioning. Increases in ultimate load due to post-tensioning were about 68% and 37% for beam types A and B, respectively. The ultimate loads for the post-tensioned beams averaged 37.7 kips (168 kN) for beam type A and 56.9 kips (253 kN) for beam type B.

Fatigue tests included three different loading ranges. Three beams of each type of non-prestressed reinforcement (beam type A or B) were tested with one of the following loading ranges: 2.2 kips (9.8 kN) to 11.0 kips (49 kN) , 2.2 kips (9.8 kN) to 15.4 kips (68.7 kN), and 2.2 kips (9.8 kN) to 19.8 kips (88.3 kN). Beam deformation, crack width, tension force in external tendons, and strains in non-prestressed reinforcement and concrete were measured after various numbers of cycles up to 2 million cycles. No beams had failed prior to reaching the 2 million loading cycles.

For the fatigue tests, Saeki compared the average beam rigidity, EI, at four different stages: prior to cracking and post-tensioning (EI_o); prior to post-tensioning but after 3 load cycles, resulting in a cracked beam (EI_{cr}); after post-tensioning but before more than three load cycles (EI_p); and after 2 million cycles (EI_{p200}). For type A beams ($\rho = 0.0055$), if results are normalized to EI_{cr} equal to 1, the value of EI_p varies from 1.2 to 1.3 and EI_{p200}

varies from 1.0 to 1.2. For type B beams (ρ = 0.0109), there is no significant difference between EI_{cr}, EI_p, and EI_{p200}.

Static tests of the fatigue specimens after 2 million loading cycles showed very little difference between the beams subjected to different loading ranges. The average ultimate loads for the beams were 39.9 kips (178 kN) and 60.6 kips (270 kN) for beam types A and B respectively. These results are about 6 percent higher than the purely static test results. The authors made no conclusions concerning the apparent higher strength.

2.5.5 Saeki, Horiguchi and Hata, 1995

Saeki, Horiguchi and Hata tested 6 T-shaped and 5 rectangular steel reinforced beams that were externally prestressed with Aramid rope [Saeki, et al., 1995]. The rectangular beams (R-type) and four of the T-shaped beams (T-type) were post-tensioned with a single drape point. The remaining two T-shaped beams (TT-type) had double drape points. The rectangular specimens were similar to those shown in **Figures 2.7** and **2.8**. The T-type and TT-type beams were set-up and post-tensioned similarly to that shown in **Figure 2.7**. The dimensions of the T-type beams were 118 in. (3 m) in length, 15.7 in. (400 mm) in height, and 2.0 in. (50 mm) in width. The TT-type beams were 98 in. (2.5 m) in length, 11.8 in. (300 mm) in height, and 2.0 in. (50 mm) in width. No details were provided about the flange dimensions or the distance between harping points for the TT-type beams. From diagrams provided by the authors, the flanges for both T-type and TT-type appear to be about 16 in. (400 mm) in width and 4 in.(100 mm) in thickness. Concrete strength was 5.7 ksi (39 MPa). The beams were tested in three point loading with span lengths of 98 in. (2.5 m) for R- and T-type beams and 83 in. (2.1 m) for TT-type beams. Reinforcing steel amounts varied, but all beams were predicted to fail in flexure without the post-tensioning.

The Aramid ropes were similar to those used in previous work by Saeki discussed in Section 2.5.4. For this research, however, the elastic modulus of the rope was listed as 11,300 ksi (77.7 GPa) and the average stress at rupture of the tendons was listed as 280 ksi

(1950 MPa). The ropes were prestressed to 91 ksi (630 MPa), which is about 33% of their ultimate strength found in uni-axial tests.

The ultimate strength and deformations observed in these tests were compared with estimations based on an analysis proposed by Pannell [Pannell, 1969]. Pannell's analysis calculates the ultimate strength and deflection of an unbonded prestress member given various beam properties, material properties, and the ratio of the plastic hinge length at ultimate to the depth of neutral axis at ultimate, which is represented by the symbol "ϕ". This analysis is based on empirical observations and is sensitive to the estimation of ϕ. Pannell recommended a value of $\phi = 10$ at ultimate for his research. Saeki found that estimations of ϕ based on test results for the beams in his research ranged between 13.5 to 44.7. An empirical equation was derived by Saeki to conservatively select ϕ for a given beam. Using the expression for ϕ, the ratio of ultimate load observed in experiments with the predicted load ranged from 1.07 to 1.42. The ratio of midspan deflections at ultimate observed in experiments with the predicted deflections ranged between 0.61 to 1.56. The variations in beam types did not appear to affect the accuracy of the analysis procedure. No conclusions were made between differences in performance of the different types of beams.

2.5.6 Horiguchi, Saeki and Hata, 1995

Research conducted by Horiguchi, Saeki and Hata investigated externally post-tensioned beams tested under low temperature (-20° C) and room temperature (+20° C) subject to both static and fatigue loadings [Horiguchi, et al., 1995]. One beam each (for low and room temperature conditions) were tested for the static load tests and four beams were tested in fatigue loading. These beam specimens were the same as the T-type beams used in their study discussed in Section 2.5.5. The AFRP external tendons were prestressed to 91 ksi (630 MPa), which is about 33% of their ultimate strength found in uni-axial tests.

The low-temperature static test resulted in about a 5% increase in resistance and about one half of the deflection at ultimate compared to the beam tested under room temperature

(+20° C). The failure of the low temperature beam resulted from tensile fracture of the steel reinforcement; where as the failure of the ordinary temperature tested beam was a combination of tensile failure of the steel reinforcement and crushing of the concrete. It is unclear what effects, if any, the low temperature had on the behavior of the Aramid rope.

Fatigue tests were conducted to 2 million cycles on each of the four beams. Each of the four beams were loaded to a different maximum load. The fatigue loading ranges were a minimum of 2.2 kips (9.8 kN) and a maximum of 11.0, 19.8, 28.7 and 37.5 kips (49, 88, 128 and 167 kN) for the four beams. Some of the tests were conducted under low temperatures (-20° C), but it is unclear from the authors what the temperature was for each test.

The author's experimental fatigue test results indicate a decrease in fatigue strength at the lower temperatures. The authors theorize that at lower temperatures, the concrete strength increases, which results in a greater bond between the reinforcing steel and concrete. The greater bond causes higher stress concentrations in the steel at cracks, which accelerates the fatigue failure. In these tests as well, the authors leave it unclear as to what effects, if any, the low temperature had on the behavior of the Aramid rope or the external prestressing system. The authors make no other comparisons between results for the different stress ranges.

2.5.7 Grace and Abdel-Sayed, 1996

Grace and Abdel-Sayed developed and are testing a double-T (DT) girder bridge that is reinforced with glass fiber reinforced plastic (GFRP) bars and prestressed internally and externally with carbon fiber reinforced plastic (CFRP) tendons [Grace and Abdel-Sayed, 1996]. The construction consists of precast, post-tensioned modified DT girders prestressed internally with CFRP tendons; cast-in-place deck slab reinforced with GFRP bars connected to the DT girders through shear connectors and an epoxy bonding agent; and externally-draped, post-tensioned CFRP tendons. The DT girders were cast with tendon deviators

extending to the depth of the girder, located approximately at the third points of the girder. These deviators served three purposes: allow for harping of the external draped CFRP tendons, allow for internal post-tensioning in the transverse direction, and improve transverse stiffness of the girder. The four DT bridge models constructed are being tested under static, dynamic, fatigue (up to 7 million cycles), and ultimate loading. Tendon stresses and girder behavior are monitored to understand the girder behavior throughout fabrication and post-tensioning. Results from the tests are currently unavailable.

2.5.8 Arduini, Tommaso and Giacani, 1996

Arduini, Tommaso and Giacani tested two reinforced concrete beams that were externally post-tensioned with two 0.37 in. (9.5 mm) diameter AFRP tendons [Arduini, et al., 1996]. The tests were conducted primarily to validate an analytical model developed that is discussed in Section 2.3.4. Details of the beams are shown in **Figure 2.9**. Steel deviators were covered with a 0.8 in. (20 mm) thick layer of rubber, resulting in an overall radius of 1.7 in. (45 mm). The beams were loaded at 1/3 points of the beam span.

Post-tensioning of the exterior tendons was accomplished on the uncracked concrete beam. The beams were then loaded in third-point loading until cracking followed by unloading to a load of 2.2 kips (9.8 kN). The beams were then subjected to loading and unloading cycles consisting of incrementally increasing load followed by unloading to about 2.2 kips (9.8 kN).

Failure of both beams was due to rupture of the external tendons at the deviators. Load-displacement curves from the tests suggest that the beam load was not significantly increasing at the time of the tendon failure. The rupture of the tendons was at a tendon load less than the uni-axial ultimate strength of the tendons. One of the two tendons for each beam failed with an axial load of 9.7 kips (43 kN) for Beam A and 7.6 kips (34 kN) for Beam B. The tendon failure loads were 54% and 43% of the uni-axial strength of the tendons.

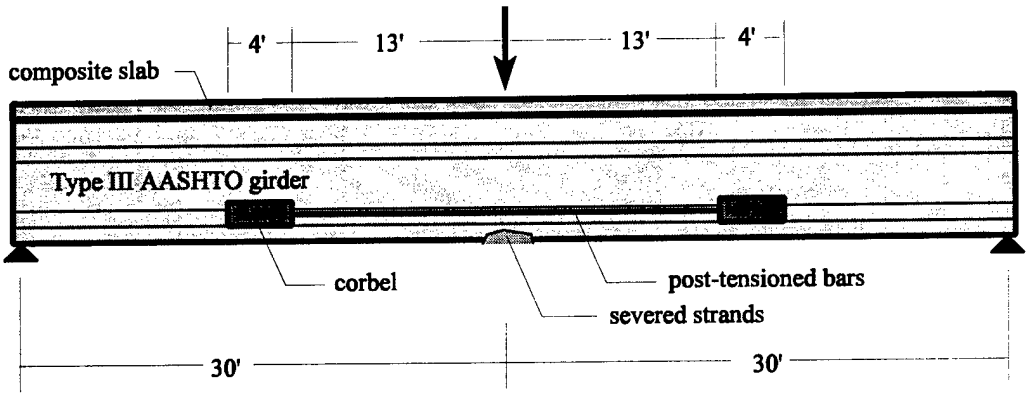

Figure 2.1 Girder test set-up [Shanafelt and Horn, 1985]

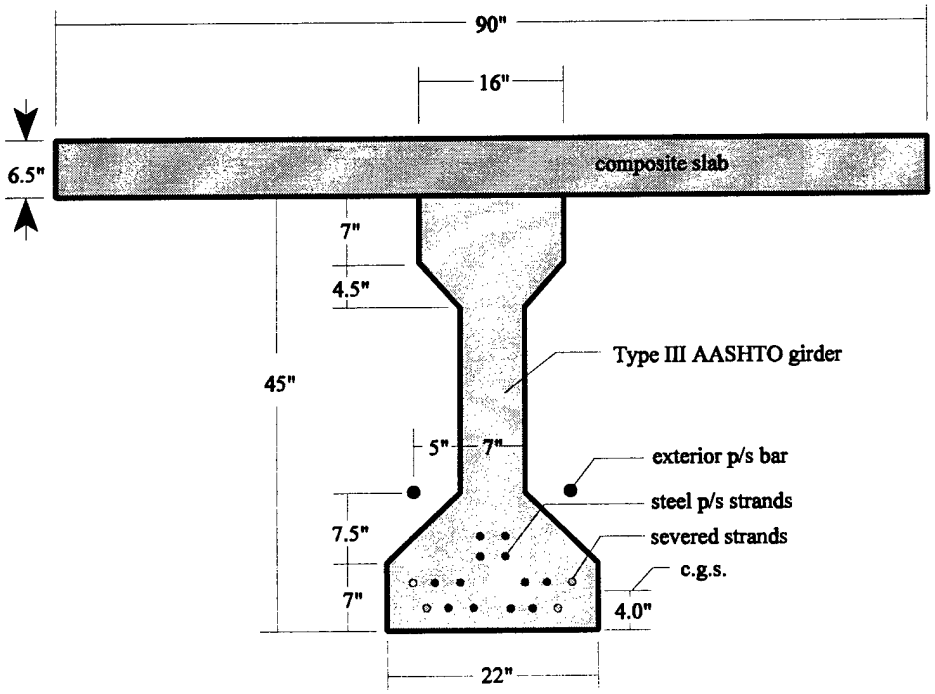

Figure 2.2 Composite girder detail at midspan [Shanafelt and Horn, 1985]

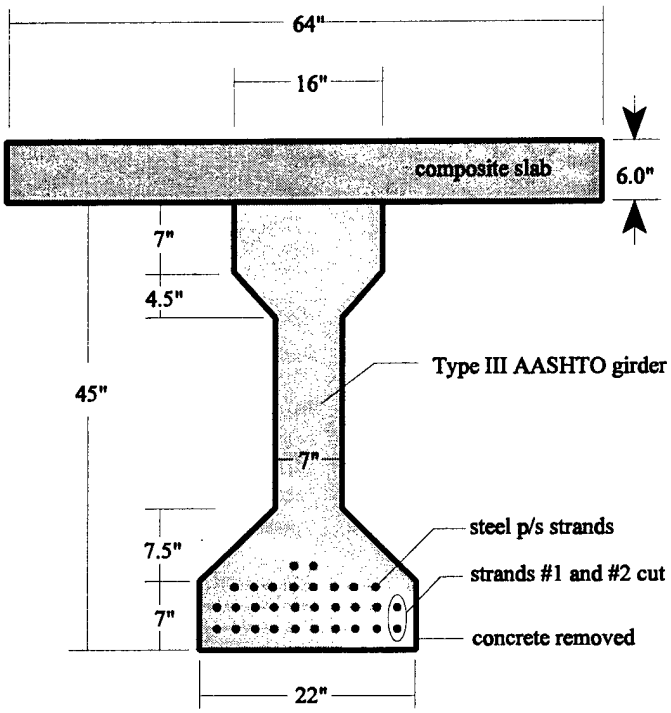

Figure 2.3 Composite girder detail at midspan [Olson, et al., 1992]

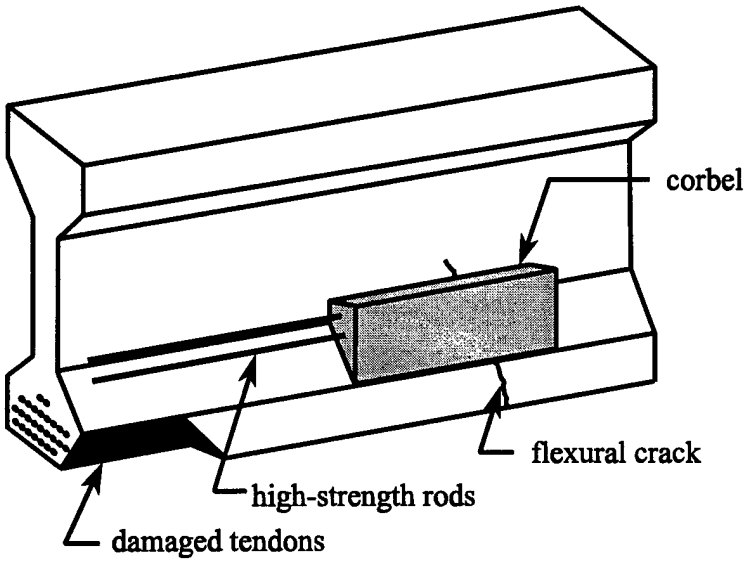

Figure 2.4 Post-tensioned repair detail [Olson, et al., 1992]

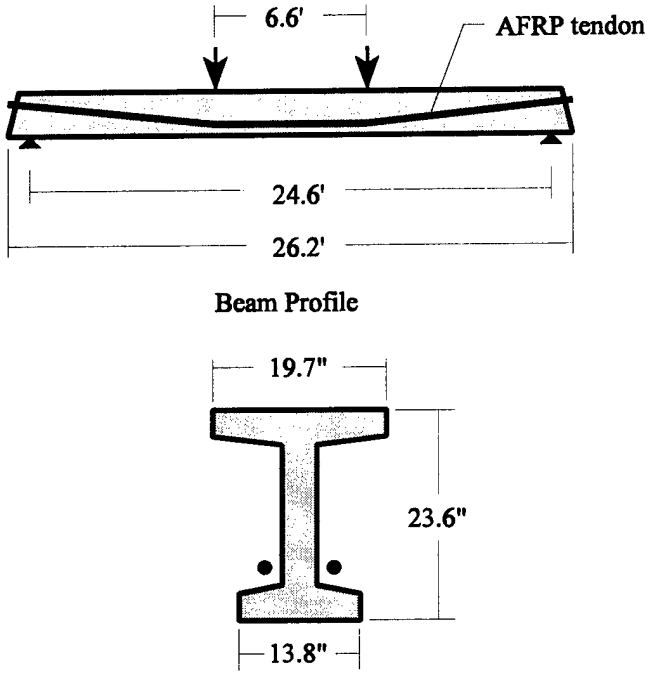

Figure 2.5 Beam specimen [Burgoyne, 1992]

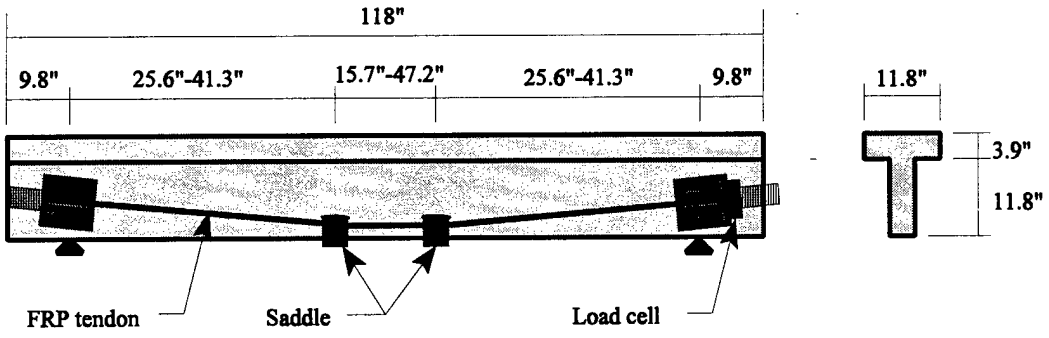

Figure 2.6 Beam specimen [Mutsuyoshi and Machida, 1993]

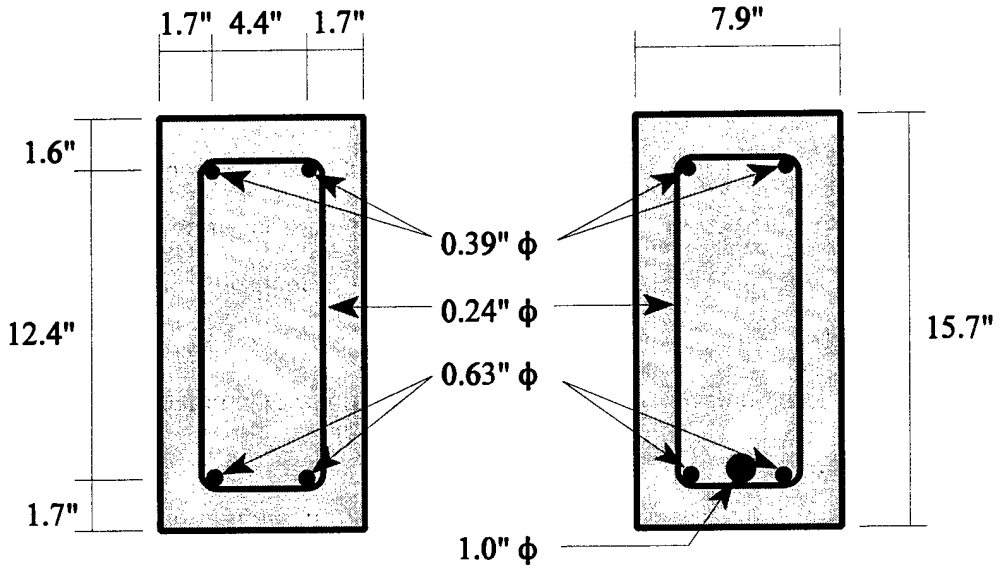

Figure 2.7 Cross-section of test specimens [Saeki, et al., 1993]

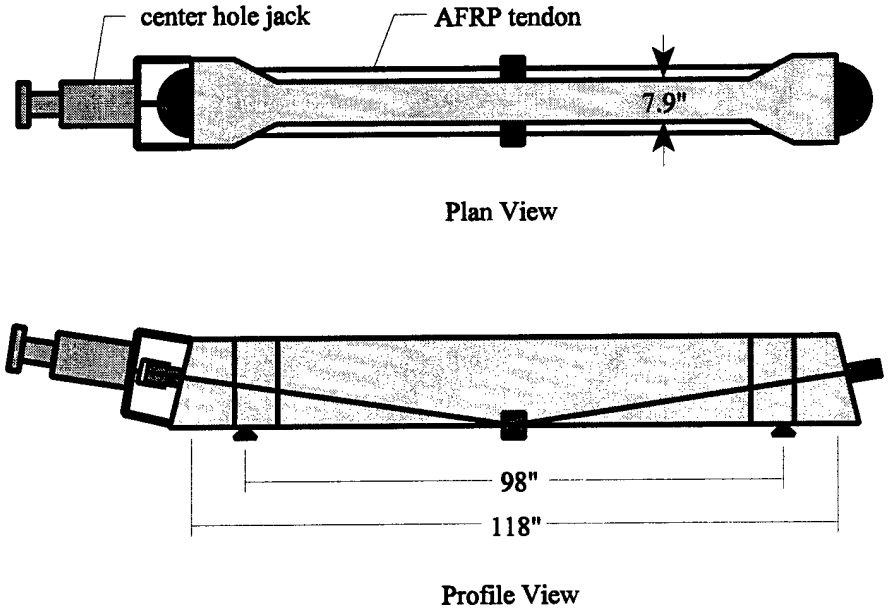

Figure 2.8 Beam specimen [Saeki, et al., 1993]

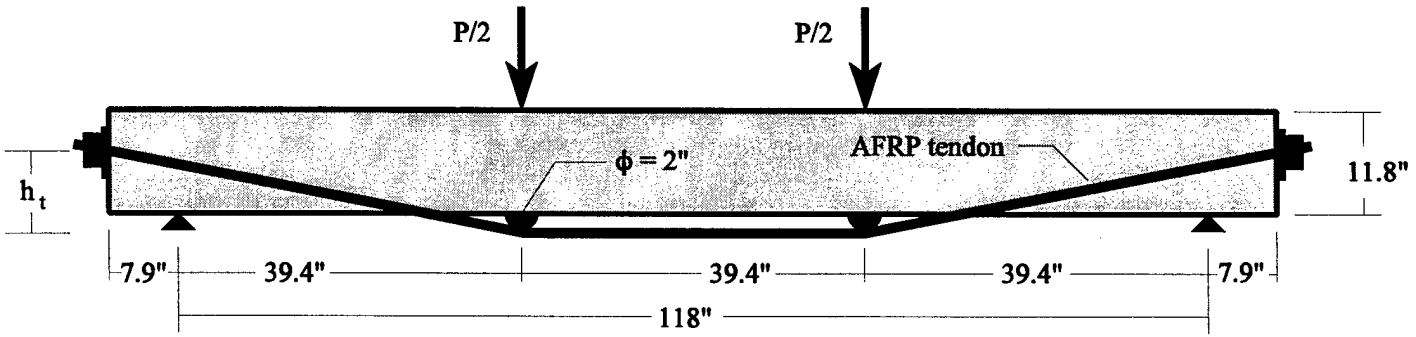

Beam A

h_t = 5.9 in.

steel reinforcement = 4 - 0.39 in. dia. bars

Beam B

h_t = 3.9 in.

steel reinforcement = 4 - 0.55 in. dia. bars

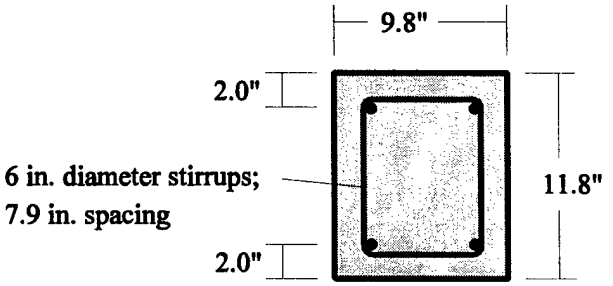

Beam cross-section

Figure 2.9 Beam specimen [Arduini, et al., 1996]

CHAPTER 3

BEHAVIOR OF CFRP TENDONS

3.1 INTRODUCTION

To maximize the benefit of prestressing in concrete members, tendons are frequently placed close to the beam centroid at sections which are anticipated to withstand smaller moments and towards the extreme tensile fibers of the beam at sections which are anticipated to withstand larger moments. This mode of placement requires that the tendons be bent or "harped". Previous research has shown, however, that Fiber Reinforced Polymer (FRP) tendons subjected to combined harping and axial load fail at axial loads less than their uni-axial strength [Arduini, et al., 1996; Mutsuyoshi and Machida, 1993].

Previous tests of straight Carbon Fiber Reinforced Polymer (CFRP) tendons subjected to fatigue or sustained axial loading have found no degradation in tendon performance; however, there is no information available of the effects of fatigue or sustained axial loads on harped tendons [Uomoto, et al., 1995; Hoshijima, et al., 1996]. Higher fiber strains exist at the extreme fibers of tendons subjected to harping. These strains can exceed the ultimate strains found in uni-axial tensile tests of the tendons and may influence the fatigue, relaxation, and creep-rupture performance of the tendons.

To understand the effect of combined axial loading and harping of CFRP tendons, a set of tests was conducted on CFRP tendons under a variety of loading and harping conditions. The experimental research studied the behavior of CFRP tendons when subjected to short-term uni-axial load, short-term combined axial load and harping, bending-tension fatigue loading with combined cyclic axial load and cyclic harping, and sustained axial loading under a harped condition. Following the bending-tension fatigue testing and sustained load testing, residual strength tests were conducted on the CFRP tendons to determine the effects of bending-tension fatigue and sustained loads on the residual tensile

strength of the harped tendons.

The CFRP tendons used in this study are manufactured under the name "Leadline" by Mitsubishi Chemical Corporation, Japan. The coal tar pitch carbon fibers used in the tendons are also manufactured by Mitsubishi Chemical Corporation under the name Dialead. The tendons consist of the continuous carbon fibers within an epoxy resin matrix having a 0.32 in. (8 mm) diameter. The tendons have a slightly deformed surface characterized by two helical indentations (approximately 0.08 in. wide and 0.002 in. in depth) running in opposite directions along the length of the tendon. Typical engineering properties of Leadline as reported by Hoshijima are shown in **Table 3.1** [Hoshijima, et al., 1996].

3.2 SHORT-TERM AXIAL STRENGTH

Research has shown that the short-term axial strength of CFRP tendons is greatly affected by the efficiency of the tendon anchorage devise [Erki and Rizkalla, 1993; Holt, et al., 1993; McKay and Erki, 1993]. The research reported in this thesis was not intended to investigate tendon anchorage devises, and consequently, no comprehensive uni-axial strength testing program was undertaken. Limited uni-axial strength tests were performed to determine the tendon uni-axial strength when anchored by the manufacturer-supplied anchorages. Due to difficulties associated with the removal of anchorages after testing, an alternative anchorage system was developed at North Carolina State University as a part of this investigation.

A total of six uni-axial strength tests were conducted with CFRP tendons. Of these six tests, two were conducted using the manufacturer-supplied "wedge" anchorage system shown in **Figures 3.1a** and **3.1b**. The remaining four tests were conducted using a steel plate grip fabricated at NCSU and shown in **Figures 3.2a** and **3.2b**. Uni-axial strength tests were also conducted during the development of the steel plate anchorage system, however, results of these preliminary tests during the development stage are not reported.

Two strain gages with a gage length of 0.125 in. (3.2 mm) were used to obtain strain

data for all tests. The gages were mounted on opposite sides of the tendon on a smooth surface located away from the helical indentations. The procedure for mounting the gages on to the tendons included cleaning the gage area with a degreasing solvent; sanding the area with 400 grit sand paper; cleaning the area with water; and after drying, using an epoxy to affix the gages to the tendons. The gages were taped to the FRP tendon prior to hardening of the epoxy. A foam pad was placed on top of the strain gage prior to taping to apply uniform pressure on the gage during curing of the epoxy. Gages were left in place for 24 hours before removal of tape and soldering of lead wires. Strain readings were recorded at specified loads using a Measurements Group P-3500 strain indicator.

The uni-axial tensile strength tests were conducted by using either a 120 kip MTS hydraulic compression/tension machine or by using a hydraulic ram in conjunction with a 25 kip load cell. The anchorages for the tendons were tied to the test frame by cables to avoid having the anchors "fly away" at failure of the test specimens. Tendon lengths varied between approximately 36 in. (914 mm) and 48 in. (1220 mm), depending upon the test set-up. Loading rates for all tests were approximately 6 kips/min (27 kN/min). Results from the six reported tensile tests are summarized in **Tables 3.2a** and **3.2b**.

The test results of the uni-axial tensile tests showed a linear stress-strain relationship up to failure. The stress-strain relationship for specimen 6 is typical of the tendons tested and is shown in **Figure 3.3**. The slight curvature of the stress-strain relationship at low load readings is likely due to end anchorage seating and straightening of the tendon. The average failure load found from the uni-axial tensile tests was 22.9 kips (102 kN), as reported in **Tables 3.2a** and **3.2b**. The average observed elastic modulus of the tendons was 21,800 ksi (150 GPa).

Failure mode for all tendons was consistent for all the specimens tested. When the load reached about 95% of the tendon ultimate load, random "popping" sounds were heard, indicating rupture of individual fibers. Rupture of the tendon was accompanied with a loud sound. Post-test inspection of the tendons generally showed a "brooming" of the tendon fibers at the failure location, which appeared to be at the face of one of the anchorages.

Generally, a large cross-section of fibers from one or both tendons appeared to be sheared from the face of the anchor. This was independent of the type anchor used. It is not clear as to whether the shearing at the anchors resulted from the high axial loads or if shearing occurred after failure of the tendon when the anchors were forced against the cables that tied the anchors to the test frame. A typical specimen after failure is shown in **Figure 3.4**.

In 1993, the failure load for CFRP tendons was reported to be 23.4 kips [Mitsubishi Kasei Corporation, 1993]. The test results of the present study indicate an average failure load of 22.9 kips, which is only 2% lower than the failure load reported by Mitsubishi [Mitsubishi Kasei Corporation, 1993]. Later in 1996, failure loads of 27.0 kips were reported [Hoshijima, et al., 1996]. The apparent increase in strength reported by Hoshijima in 1996 is most probably due to differences in anchorage systems. Hoshijima used a wedge-cone grip that had longer wedges than those used in the present study. The wedges were 4.75 in. (120 mm) long compared to 3.1 in. (80 mm) for the grips used in the present study. Also, the longer grips used by Hoshijima contained a thicker plastic membrane between the wedges and cone than did the shorter grips. All other details of the manufacturer's anchorage system were essentially the same. These longer grips are now the grips supplied by the manufacturer for the CFRP tendons.

3.3 BEHAVIOR OF TENDONS SUBJECTED TO COMBINED AXIAL LOAD AND HARPING

To develop experimental information on the behavior of tendons subjected to combined axial loading and harping, two test programs were conducted. The first part focused on the strain distribution along the span length of the tendons under combined axial loading and harping. The second part focused on the ultimate strength of tendons under combined axial loading and harping. Parameters of the tests included loading history (ex. static, sustained, or fatigue), loading path, harping angle of the tendon, and harping point geometry.

3.3.1 Strain Variation along Length of Harped Tendons

3.3.1.1 *Test program and test set-up*

Tables 3.3a and **3.3b** summarize the parameters of the test program for determining the strain variation along the length of harped CFRP tendons. The test set-up for harped tendon testing is shown in **Figures 3.5a** and **3.5b**. The test frame consisted of a structural steel frame supporting two hinged supports. One support consisted of a fixed "*saddle*", which allowed for rotation of the tendon end but did not allow for axial displacements of the tendon. The opposite support consisted of a saddle that allowed for rotation and axial displacements of the tendon anchorage. This support included a hydraulic ram for imparting axial loads and a 25 kip (111 kN) load cell. Axial displacements could be fixed by tightening nuts located behind the load cell support plate. Harping of the CFRP tendon was achieved by a 50 kip (222 kN) MTS actuator affixed with a special harping point apparatus. Harping of the tendon specimens was applied at the midpoint between the pin-hinge connectors, which was approximately the midpoint of the tendon test specimens.

The fixture used for harping the tendon extended downward from the 50 kip (222 kN) actuator and used a curved harping plate. Harping plates with a radius of 1 in. (25 mm), 5 in. (127 mm) and 20 in. (508 mm) were used for the tests. Each of the harping plates were curved longitudinally at a constant radius arch and contained a 0.32 inch (8 mm) diameter semi-circular groove along the arch to securely hold the tendons in place. Photographic views of the test set-up for harped tendons are shown in **Figures 3.6a**, **3.6b**, and **3.6c**.

To obtain the strain variation along the length of CFRP tendon, the tendon was affixed with nine strain gages as shown in **Figure 3.7**. Gage lengths for all gages was 0.125 in. (3.2 mm). Gage SG1 was located on the outside edge of the apex of the tendon at the bend. Gages SG8 and SG9 were located on opposite faces of the tendon approximately 18 in. (457 mm) away from the bend. The six remaining gages (SG2 through SG7) were located on the outside edge of the tendon at distances of 0.38, 0.75, 1.34, 3.0, 4.9, and 6.6 in. (9.7,

19, 34, 76, 124 and 168 mm) from the apex of the bend. All gages were affixed with the same procedure described in Section 3.2.

Data readings were recorded with an Optim Megadac 100 data acquisition system. Axial load readings were obtained using the 25 kip (111 kN) load cell. Transverse displacement of the CFRP tendons were recorded by a Linear Voltage Displacement Transducer (LVDT) within the MTS actuator.

3.3.1.2 *Test results and discussion*

For the test set-up shown in **Figures 3.5a** and **3.5b**, an increase in the tendon transverse displacement at midpoint caused an increase in the tendon axial load. This is due to the change in length of the tendon between the pin connections. This change in length is approximately equivalent to:

$$\Delta_L = L(1/\cos(\theta/2)-1) \qquad (3.1)$$

where Δ_L = the change in length between pin connections
L = the distance between the pin connections
$\theta/2$ = the angle the tendon makes with the horizontal line extending between the pin connections

The additional tendon axial strain due to transverse displacements at the harping point of the tendon is:

$$\Delta\epsilon_{axial} = \Delta_L/l \qquad (3.2)$$

where $\Delta\epsilon_{axial}$ = the additional tendon axial strain due to transverse displacements of the harping plate
l = original tendon length between anchorages with no harping

It was found during preliminary tests that axial strain readings observed at distances greater than approximately 6 in. (150 mm) on each side of the harping point of the tendon were not affected by the curvature produced due to harping of the tendon. Axial strain readings recorded approximately 18 in. (457 mm) away from the tendon bend by strain gages SG8 and SG9 (**Figure 3.7**) are sufficiently far from the tendon bend point that these readings can be considered to accurately represent the axial strains without the effect of harping.

Figures 3.8a through **3.11c** show the variation of flexural strain along the length of CFRP tendons for all test series. The flexural strain is defined as the difference between strain readings of the extreme fibers of a harped tendon and the average axial strain. For example, referring to **Figure 3.7**, the flexural strain at 3.0 in. (76 mm) from the harping point is calculated as the strain reading from strain gage SG5 minus the average strain reading of strain gages SG8 and SG9.

The flexural strain (**Figures 3.8a** through **3.11c**) is a maximum near the bend point and reduce drastically with increasing distance from the bend point. The magnitude of flexural strains beyond about 6 in. (152 mm) from the center of the tendon bend is zero. The 6 in. (152 mm) region along the tendon in which the flexural strains were non-zero appears to be independent of the tendon axial load, curvature of the bend point, and angle of the tendon bend. Results also indicate that larger bend angles resulted in larger flexural strains at the bend point.

Although it is recognized that the maximum flexural strain should occur directly under the bend point, due to slight relocation of the tendon with respect to the harping plate, strain gage SG2 sometimes measured a larger flexural strain value than strain gage SG1 (ex. **Figures 3.8b** and **3.8c**). For all future analysis, the maximum flexural strain recorded, whether from gage SG1 or SG2, is considered the flexural strain at the apex of the tendon bend.

3.3.1.3 *Model for prediction of flexural strain at harped point of CFRP tendon*

The test results indicate that for a given harping plate radius and initial axial load of the tendon, the maximum flexural strain at the harped location (termed as the flexural strain at harped point) increased linearly with the angle of the bend of the tendon (**Figure 3.12**). For a given average axial load, P, and harping plate radius, R, the ratio of flexural strain at harped point, ϵ_{fs}, to the bend angle of the tendon, θ, can be approximated by a constant. This constant is expressed as λ and is the slope of the line shown in **Figure 3.12**.

A total of 12 combinations of harping plate radii and initial axial load were used during testing. **Tables 3.4a** and **3.4b** summarize the twelve λ values calculated based on the results of these tests. Each λ value was calculated as the slope of the best fit line obtained by linear regression of the three bend angle values and corresponding flexural strains. The range of λ values calculated from the test results is shown in **Figure 3.13**. The magnitude of the flexural strain at harped point of the tendon is therefore defined as:

$$\epsilon_{fs} = \lambda\ \theta \qquad \textbf{(3.3)}$$

where ϵ_{fs} = the tendon flexural strain at harped point
λ = the ratio of flexural strain at harped point and bend angle of the tendon for a given tendon axial load and harping plate radius
θ = the bend angle of the tendon in degrees

It was observed that the values of λ appeared to vary linearly with increasing axial load of the tendon. Additionally, as the radius of the harping plate increased, flexural strains at harped point decreased. Based on the data presented in **Tables 3.4a** and **3.4b**, the equation that best represents λ as a function of axial load (P), and harping plate radius (R), was found to be:

$$\lambda = (845 + 44\ P)\ (1/R)^{0.123}\ (10^{-6}) \qquad \textbf{(3.4)}$$

where P = axial load of tendon in kips
R = radius of harping plate in inches

Conceptually, this equation appears reasonable. For very large values of R, the value of λ should approach zero, and for small values of R, λ should increase. Additionally, λ should not necessarily be zero if the axial load on the tendon, P, is zero.

By combining Equations 3.3 and 3.4, the expression for the flexural strain at harped point can be expressed as a function of axial load (P) in kips, radius of harping plate (R) in inches, and the bend angle of tendon (θ) in degrees. The equation can be written as:

$$\epsilon_{fs} = [(845 + 44\ P)\ (1/R)^{0.123}\ (10^{-6})][\ \theta\ ] \qquad (3.5)$$

Comparison of the predicted flexural strain at harped point from Equation 3.5 with the experimental values is shown in **Figure 3.14**, which shows a very good correlation between predicted and experimentally observed values.

It should be noted that the maximum curvature of the tendon at the bend point that can be achieved is limited to the maximum curvature allowed by the harping plate. In other words, no matter how large of an angle the tendon is bent, the tendon will not bend sharper than the maximum curvature allowed by the harping plate (**Figure 3.7**). Based on this observation, the theoretical maximum flexural strain at harped point that can be achieved can be written as:

$$\epsilon_{fs,max} = \frac{(Arch_{outside} - Arch_{centroid})}{(Arch_{centroid})} \qquad (3.6)$$

where $\epsilon_{fs,max}$ = the maximum flexural strain achievable at harped point for a given harping plate radius
$Arch_{outside}$ = the arch length of the outside face of the tendon at the bend
$Arch_{centroid}$ = the arch length of the centroid of the tendon at the bend

This expression can be formulated as:

$$\epsilon_{fs,max} = \frac{(R + r)\theta - R\theta}{R\theta} = \frac{r}{R} \quad (3.7)$$

where R = the harping plate radius
r = the cross-sectional radius of the tendon
θ = the bend angle of the tendon

For a CFRP tendon with a diameter of 0.314 in. (8 mm) and bent about the 20 in. (508 mm) radius harping plate, the theoretical maximum flexural strain at harped point as calculated using Equation 3.7 is (0.157 in.)/(20 in.), which equals 0.00787. As shown in **Figure 3.15**, the strains recorded in the testing of a tendon bent about a 20 in. (508 mm) harping plate approaches but does not exceed the strain of 0.00787. The "dip" in the strain value at a bend angle of about 8 degrees was due to the reduction in the axial load at that point which resulted in a slight relocation of strain gage SG1 relative to the center of the harping point. The axial load was reduced to make adjustments in the actuator position to obtain larger bend angles. If the load was not reduced, it is believed that the extreme fiber strain would have reached the maximum theoretical flexural strain at a bend angle of about 10 degrees, as shown by the dotted line in **Figure 3.15**.

Equating Equations 3.5 and 3.7 results in an equation for the bend angle beyond which there is no increase in the flexural strain at harped point with increase in the bend angle. This angle is the minimum bend angle corresponding to the maximum flexural strains achievable at harped point, $\epsilon_{fs,max}$, and is represented by the symbol, θ_{ss}. This angle, in degrees, can be expressed as:

$$\theta_{ss} = \frac{r \times 10^6}{(845 + 44P) R^{0.877}} \quad (3.8)$$

For example, for the harping plate with a radius of 20 in (508 mm) and an axial load of 4.4 kips (19.6 kN) (as recorded in the test shown in **Figure 3.15**), the calculated value for θ_{ss} is 11.0 degrees. As shown in **Figure 3.15**, this bend angle is very close to the minimum bend angle at which maximum flexural strains were recorded for this test.

3.3.2 Static Strength Tests of Harped Tendons

3.3.2.1 *Test program and test set-up*

The test matrices for the static strength of harped tendons are shown in **Tables 3.5a** and **3.5b**. For each series of tests, except series 1b, two replicate tendon specimens were tested. For series 1b, three replicate tendon specimens were tested. The test set-up was the same as that described in Section 3.3.1.1. The test set-up is shown in **Figures 3.5a** through **3.6c**.

The preparation of tendon test specimens was similar to the preparation procedure described in Section 3.3.1.1, except that for most cases, only three strain gages were affixed on the specimens. Gage SG1 was located directly under the center of the tendon bend, and gages SG8 and SG9 were located approximately 18 in. (457 mm) from the center of the bend (**Figure 3.7**).

Transverse displacements or axial loads were increased at a constant rate until failure of the tendons. For test series 1a, 2a, and 3a of **Tables 3.5a** and **3.5b**, the rate of increase of downward displacement of the harping point of the CFRP tendon was approximately 0.15 in./min. (3.8 mm/min.). For test series 1b, 2b, and 3b, the axial loading was increased at a rate of approximately 2.4 kips/min. (10.7 kN/min.).

3.3.2.2 *Test results and discussion*

When referring to harped tendons, failure is defined as the stage at which individual fibers of the tendon start to rupture. At about the time the individual fibers were breaking during tests, distinct sounds were heard and strain readings at the bend of the tendon showed

large strain changes or the strain gages became inactive and data recording ceased. This was identified as the point of failure for the tendons.

A summary of test results is shown in **Tables 3.6a** and **3.6b**. The results of these tests indicate that the harped tendons can withstand fiber strains far in excess of the average axial strains found from previous uni-axial tests. At failure, the average fiber strains recorded at the bend were approximately 0.02 (SG1 strains in **Tables 3.6a** and **3.6b**), compared to ultimate fiber strains of approximately 0.013 obtained from uni-axial strength tests. Failure for most of these tests was at an axial load below the failure load for the tendons found in the uni-axial strength tests. Failure loads for tests using the 20 in. (508 mm) radius harping plate are approximately equivalent to the failure loads found in uni-axial strength tests of 22.9 kips (102 kN). Therefore, it is possible that failure of tendons of test series 1a and 1b may have initiated at the anchorage of the tendons as opposed to fiber failure at the harping point.

Figure 3.16 shows the variation in average axial load at failure with the harping plate radius for test series 1a, 2a and 3a listed in **Tables 3.6a** and **3.6b**. **Figure 3.17** shows the variation in average tendon bend angle at failure with the harping plate radius for the same set of tests. The results indicate that tendons subjected to harping plates with smaller radii failed at a smaller transverse displacement which was associated with a smaller tendon bend angle and smaller tendon axial load. As shown in **Figures 3.16** and **3.17**, the relationship between the harping plate radius and the axial load or bend angle at failure appears to be linear. Tendon axial loads associated with the failure of the tendons for the 20 in. (508 mm), 5 in. (127 mm), and 1 in. (25 mm) harping plate radii averaged 103, 81, and 77 percent respectively of the failure load of the tendons found in the uni-axial strength tests, the average value of which was 22.9 kips (102 kN).

Figure 3.18 shows the average tendon axial load at failure versus the harping plate radius for test series 1b, 2b and 3b of **Tables 3.5a** and **3.5b**. The figure shows that failure of tendons bent about a harping plate with a smaller radius was at a lower axial load than those bent about a harping plate with a larger radius. The variation in failure loads with harping plate radius does not appear to be linear.

Comparison of results of series 1a, 2a and 3a and series 1b, 2b and 3b of **Tables 3.5a** and **3.5b** show that the effect of loading path on the failure loads of harped tendons with 1 in. (25 mm), 5 in. (127 mm) and 20 in. (510 mm) radius harping plates is insignificant (**Tables 3.6a** and **3.6b**).

3.3.3 Failure Prediction for Tendons Subjected to Combined Axial Load and Harping

Based on the results of the static tests described in Section 3.3.2, an analytical model which uses an ultimate strain failure criteria was developed for predicting the failure load for harped tendons subjected to axial loads. The strain at the harped point of tendons is the sum of the average axial strain and the flexural strain at harped point. Failure is predicted using the parameters of the tendon axial load (P), tendon bend angle (θ), and the harping plate radius (R).

3.3.3.1 *Development of failure model*

By summing the flexural strain at harped point computed using Equations 3.5 and 3.7 and the observed average axial strain, an equation for the maximum fiber strain at the harped point of the tendon can be written as:

$$\epsilon_{total} = \epsilon_{axial} + \epsilon_{fs} \qquad \textbf{(3.9)}$$

where ϵ_{total} = maximum fiber strain at harped point of the tendon
ϵ_{axial} = average axial strain of the tendon
= P/AE
P = axial load of the tendon
A = cross-sectional area of tendon
E = elastic modulus of tendon
ϵ_{fs} = flexural strain at harped point of the tendon (Equations 3.5 and 3.7)

Using the results from the static strength tests of harped tendons, the maximum fiber

strain at harped point of the tendon at failure was calculated for each test specimen of **Tables 3.5a** and **3.5b**. The resulting maximum fiber strains ranged from 0.0210 to 0.0225, with an average value of 0.0217. The average strain value of 0.0217 is close to the recorded strains at the harped point at failure shown in **Tables 3.6a** and **3.6b**.

By defining tendon failure as the point at which the maximum fiber strains reach a value of 0.0217, equations for predicting failure of the tendon were derived using Equations 3.5 and 3.7. The resulting equations for predicting the tendon axial load at failure, (P_f), are:

$$P_f = \frac{21700 - 845\,\theta\,R^{-.123}}{\left(\frac{1{,}000{,}000}{A\,E}\right) + 44\,\theta\,R^{-.123}} \qquad \text{(for } \theta < \theta_{ss}\text{)} \qquad \textbf{(3.10)}$$

$$P_f = \left(0.0217 - \frac{r}{R}\right) A\,E \qquad \text{(for } \theta \geq \theta_{ss}\text{)} \qquad \textbf{(3.11)}$$

where P_f = tendon axial load at failure (kips)
θ = tendon bend angle (degrees)
R = harping plate radius (in.)
A = cross-sectional area of tendon (sq.-in.)
E = elastic modulus of tendon (ksi)
r = radius of tendon cross-section (in.)
θ_{ss} = minimum bend angle corresponding to maximum flexural strains achievable at harped point computed by Eq. 3.8.

The actual axial load at failure will be the lesser of that obtained by the use of Equations 3.10 and 3.11 and the strength capacity of the end anchorage. The average strength of the end anchorages used in this study was 22.9 kips (102 kN).

From Equations 3.10 and 3.11, the expressions for the tendon bend angle at failure, (θ_f), can be written as:

$$\theta_f = \frac{21700 - \left(\frac{1{,}000{,}000}{A\,E}\right) P}{(845 + 44\,P)\,R^{-0.123}} \qquad \text{(for } \theta < \theta_{ss}\text{)} \qquad \textbf{(3.12)}$$

$$\theta_f = \textit{undefined} \qquad \text{(for } \theta \geq \theta_{ss}\text{)} \qquad \textbf{(3.13)}$$

where θ_f = bend angle at failure (degrees)
P = tendon axial load (kips)
A = cross-sectional area of tendon (sq.-in.)
E = elastic modulus of tendon (ksi)
R = harping plate radius (in.)

The strain value of 0.0217 is a more accurate measure of the tendons uni-axial ultimate strain capacity than that found in uni-axial strength tests. As discussed previously, during uni-axial strength tests the stress concentrations at the tendon anchorages leads to failure of the tendons at the anchorage before the full tendon uni-axial strength is developed. For an ultimate strain of 0.0217 and an elastic modulus found in this research of 21,800 ksi (150 GPa), the theoretical ultimate uni-axial stress is 473 ksi (3260 MPa). Research conducted in Canada on prestressed concrete beams using Leadline tendons estimated an average stress at rupture of the tendons to be 464 ksi (3200 MPa) [Abdelrahman and Rizkalla, 1995]. The theoretical ultimate uni-axial stress of 473 ksi (3260 MPa) is very close (within 2%) of the tendon stress at rupture found in the Canadian tests.

3.3.3.2 *Comparison of experimental and predicted failure loads*

Comparison of the predicted failure load values as computed by Equations 3.10 and 3.11 with experimental values is shown in **Figure 3.19**. The calculated values of the axial

load at failure of harped tendons corresponds well with the experimental data. The correlation coefficient, *r*, of the experimentally observed failure load data and the predicted failure load data for all tests that failed at the harping point (i.e. excluding tests using the 20 in. (508 mm) radius harping plate) is 0.82. The correlation coefficient, *r*, for all test data is 0.97. The square of the correlation coefficient, *r*-squared value, is 0.94.

Comparison of tendon bend angle at failure, (θ_f), as computed by Equation 3.12, with the experimental results is shown in **Figure 3.20**. Not included in the figure are tests of CFRP tendons that appear to have failed at the anchorage at axial loads of approximately 22.9 kips (102 kN). The experimental data is evenly dispersed about the predicted values of the bend angles at failure. The correlation coefficient of the experimentally observed bend angle at failure with the predicted bend angle at failure is -.45. The *r*-squared value is 0.20. The fact that the bend angles at failure were all within a small range, between 6.8 and 7.9 degrees, may have contributed to the apparently small *r*-squared value. The maximum variation between the predicted and observed values of bend angle at failure is only 0.55 degrees. The average difference between the predicted and the observed values of bend angle at failure is -0.11 degrees.

3.3.3.3 *Parametric study*

Figure 3.21 shows the predicted axial load at failure using Equations 3.10 and 3.11 versus the bend angle for various harping plate curvatures, (1/R). Note that for harping plates with curvatures less than about 0.05/in. (0.002/mm), there is no affect on the tendon failure load due to the bend angle. This assumes a uni-axial failure load of 23.4 kips (104 kN). The figure indicates that for harping plate curvatures of 0.07/in. (0.0028/mm) and 0.1/in. (0.0039/mm), the failure load becomes independent of the bend angle at bend angles greater than about 9 and 16 degrees, respectively.

The tendon bend angle at which simultaneous failures will occur at the harped point of the tendon and at the tendon anchorage is denoted as the tendon bend angle at balanced

failure, (θ_{bal}). The value of θ_{bal} is calculated using Equation 3.12 with the tendon axial load, (P), equal to the tendon capacity developable at the anchorage, (P_f). The expression for θ_{bal} can be written as:

$$\theta_{bal} = \frac{21700 - \left(\frac{1{,}000{,}000}{A\,E}\right) P_a}{(845 + 44\,P_a)\,R^{-0.123}} \qquad \text{(for } \theta < \theta_{ss}\text{)} \qquad \textbf{(3.14)}$$

$$\theta_{bal} = \textit{undefined} \qquad \text{(for } \theta \geq \theta_{ss}\text{)} \qquad \textbf{(3.15)}$$

where θ_{bal} = tendon bend angle at balanced failure (degrees)
P_a = tendon capacity developable at the anchorage (kips)
A = cross-sectional area of tendon (sq.-in.)
E = elastic modulus of tendon (ksi)
R = harping plate radius (in.)

Figure 3.22 shows the log of the harping plate curvature (1/R) versus the tendon bend angle at balanced failure, (θ_{bal}). The value of the tendon capacity developable at the anchorage, (P_a), was set to the reported capacity for the manufacturer supplied anchorage used in this study, which was 23.4 kips (104 kN). **Figure 3.22** shows that for small values of harping plate curvature (i.e. large values of harping plate radius), failure of the tendon at the harping point is not possible. Failure for tendons using these small harping plate curvatures will be at the tendon anchorage because the axial loads necessary for failure at the harping point cannot be generated at the anchorage. As the curvature of the harping plate becomes larger (i.e. as the harping plate radius decreases), the value of the tendon bend angle at balanced failure, (θ_{bal}), becomes smaller. A tendon anchorage capable of developing a higher tendon load would yield a similar relationship but with consistently smaller angles at balanced failure for the same harping plate radius, (R).

3.4 BEHAVIOR OF HARPED TENDONS SUBJECTED TO BENDING-TENSION FATIGUE LOADS

3.4.1 Test Program and Test Set-up

The test matrix for harped tendons subjected to bending-tension fatigue loads is shown in **Tables 3.7a** and **3.7b**. A schematic view of the minimum and maximum limits for the bending-tension fatigue testing is shown in **Figure 3.23**. The procedure for preparation of the test specimens was similar to the specimen preparation in Section 3.3.2.1. Strain gages identified as SG1, SG8 and SG9 in **Figure 3.7** were used during the testing.

Test specimens were placed in the test frame shown in **Figure 3.5a** and **3.5b** with the 1 in. (25 mm) radius harping plate. An Optim Megadac data acquisition system was used to record the test data. The use of data acquisition allowed the data to be recorded continuously, however, the strain readings corresponding to a tendon bend angle of 5.0 degrees are only reported.

Testing was initiated by applying a small seating axial load on the tendons in a straight configuration with no harping. The ram of the vertical 50 kip (222 kN) actuator was then extended until the harping plate just came in contact with the tendon. The displacement of the actuator at this point was defined as the displacement corresponding to 0 degree harping. The tendons were then vertically displaced or depressed at the harping point to a bend angle slightly greater than 5 degrees. Axial loads on the tendons were increased to 14.3 kips (64 kN). Nuts were tightened behind the adjustable plate supporting the axial load cell and loading end anchorage, thereby fixing the distance between anchorage points. Small adjustments were made in the alignment of the 50 kip (222 kN) actuator to ensure the center strain gage, SG1, was located directly under the center of the tendon harping point.

The controlling test parameter for the bending-tension fatigue tests was the harping plate displacement, which was set to cycle between a minimum of 1.73 in. (43.9 mm) and a maximum of 2.11 in. (53.6 mm) below the point associated with 0 degree harping

(**Figure 3.23**). These displacements resulted in a change of bend angles of the tendons between a minimum of 4.5 degrees and a maximum of 5.5 degrees, and the corresponding tendon axial loads at the minimum and maximum bend angles to be approximately 14.0 kips (62.3 kN) and 14.7 kips (65.4 kN), respectively. The rate of cycling was about 0.71 Hz for the first test and 0.88 Hz for the second and third tests. For 1 million cycles of bending-tension fatigue loadings, the duration of tests ranged between 13 and 16 days.

On completion of the 1 million cycles, the tendons were tested to failure. The initial conditions of the static strength test were that the tendons were harped at an angle of about 5 degrees and the initial axial load on the tendons was equal to the axial load at the completion of the fatigue test. The procedure for static strength tests was similar to the procedure for series 3a of **Tables 3.5a** and **3.5b**. Failure of the tendons was accomplished by increasing the harping plate displacement at a rate of approximately 0.15 in./min. (3.8 mm/min.).

3.4.2 Test Results and Discussion

Results of the bending-tension fatigue test for the three replicate specimens are shown in **Figures 3.24** through **3.26**. In these figures, the average axial strain is the average of strain gages SG8 and SG9 (**Figure 3.7**). The load cell strain is calculated as the axial load cell reading divided by the tendon cross-sectional area and modulus of elasticity. The flexural strain at harped point is the difference between strain readings of the extreme fibers at the harped point (strain gage SG1) and the average axial strain (average of strain gages SG8 and SG9) (**Figure 3.7**).

Figure 3.24 shows the results of test specimen F1. As illustrated in the figure, no significant changes were observed in the magnitude of flexural strain at harped point after 1 million cycles. Additionally, the average axial strain and load cell strain remained relatively constant after about 250,000 cycles, suggesting no relaxation in the tendons during this interval. The drop in axial strain within the first 250,000 cycles corresponds to a

reduction in length of approximately 0.014 in. (0.36 mm) between the tendon end anchorages. This reduction in length may be due to the movement of the test frame or slippage of the tendon at the face of the anchorage.

Figure 3.25 shows the results for specimen F2. Average axial strain and load cell strain values were relatively consistent over the duration of the test, and the results are similar to results for specimen F1. For specimen F2, the flexural strain at harped point readings were approximately 0.002 less than those found for specimen F1. Additionally, the flexural strain at harped point appears to increase from approximately 0.00615 to 0.00645 over the duration of the test. This could be attributed to the position of the strain gage relative to the harped point. The apparent increase in flexural strains at harped point found during testing is likely due to one of two factors. First, to ensure that the harping plate was centered over strain gage SG1, four turnbuckles attached to the actuator stabilizing cables were adjusted. In making minor adjustments prior to testing specimen F2, two of the turnbuckles attached to the actuator stabilizing cables were tightened to their maximum extent. By being tightened to their maximum extent, the turnbuckles did not allow for precise centering of the harping plate over the tendon center strain gage. At the start of testing, the small difference was not considered significant, but with the bending-tension fatigue, the effect became more pronounced. Secondly, the remaining two turnbuckles on the opposite side of the actuator were not sufficiently tightened. This may have allowed for the harping plate to migrate toward strain gage SG1 during the test. As shown in **Figure 3.10c**, flexural strains increase sharply as the location of the strain reading approaches the center of the tendon bend.

Figure 3.26 shows the results for specimen F3. The flexural strain increased by approximately 85 x 10^{-6} within the first 100,000 cycles, but remained approximately constant over the remainder of the test. Average axial strain and load cell strain values remain relatively unchanged after 1 million cycles.

The test results (**Figures 3.24** to **3.26**) indicate that the tendons remain stable with no apparent degradation in performance due to the fatigue loading. It is observed that the

bending-tension fatigue tests produced a relatively severe fatigue environment for the CFRP tendons. Median strains (average of maximum and minimum strains) at the apex of the tendon bend was approximately 0.016, and the strain range at the harped point during fatigue cycling was approximately 0.0022. This median strain is greater than the average axial rupture strain reported for uni-axial strength tests by Hoshijima of 0.015 [Hoshijima, et al., 1996] and is 19% higher than the average axial rupture strains of 0.013 found in uni-axial strength tests conducted as a part of this research and described in Section 3.2.

3.4.3 Residual Strength Test Results

After completing 1,000,000 fatigue cycles, the CFRP tendon specimens were tested to failure under combined axial load and harping. The axial load and bend angle at the start of the static tests averaged 14.1 kips (62.7 kN) and 5.0 degrees, respectively. Failure of the tendons was achieved by slowly increasing the downward displacement of the harping plate. The mode of failure was similar to failures observed during static strength tests under combined axial load and harping described in Section 3.3.2. Failure loads for the specimens were 16.1 kips (71.6 kN), 16.4 kips (72.9 kN) and 16.1 kips (71.6 kN) for F1, F2 and F3, respectively. The failure angles were 7.61, 7.85 and 6.99 degrees for specimens F1, F2 and F3, respectively (**Tables 3.8a** and **3.8b**).

The procedure for residual strength tests for specimens F1, F2 and F3 was similar to the procedure for strength tests of series 3a in **Tables 3.5a** and **3.5b**. However, the initial bend angle prior to initiating the strength tests of series 3a in **Tables 3.5a** and **3.5b** was 0 degrees, compared to about 5 degrees for the bending-tension fatigue test specimens. The average load at failure of the static strength tests was 17.6 kips (78.3 kN), compared to an average load at failure for the bending-tension fatigue specimens of 16.2 kips (72 kN). The average bend angle at failure of the static strength tests was 6.81 degrees, compared to an average bend angle at failure of the fatigue specimens of 7.48 degrees. The average post-fatigue load at failure and average bend angle at failure for the fatigue specimens was 92%

and 110% of the static strength test results, respectively. The differences in load and bend angles at failure are likely due to the differences in the bend angle at the start of the strength tests.

Figure 3.27 show the results of residual strength tests of the tests specimens F1, F2 and F3, versus the failure load predicted by Equation 3.10. **Figure 3.28** show the results of static strength tests of the tests specimens F1, F2 and F3, versus the predicted angle at failure predicted by Equation 3.12. It is evident from both of these figures that the failure of tendon specimens subjected to bending-tension fatigue with the variables used in this study are reasonably well predicted using the failure prediction equations developed based on the static strength tests (Eqs. 3.10 and 3.12). It is concluded, therefore, that the results of the residual strength tests of the bending-tension fatigue specimens show no degradation in performance for the range of variables conducted in this investigation.

3.5 BEHAVIOR OF HARPED TENDONS SUBJECTED TO SUSTAINED LOAD

3.5.1 Test Program and Test Set-up

The test matrix for harped tendons subjected to sustained load is shown in **Tables 3.9a** and **3.9b**. The test frame used for the tests is shown in **Figure 3.29**. Strain gages with a gage length of 0.125 in. (3.2 mm) were affixed to the tendons by the same process as described in Section 3.2. **Figure 3.30** shows the location of strain gages used during testing. Strain gages SG2 and SG3 were located on the loading side of the test frame. For test specimens S2 and S3, strain gages SG4 and SG5 were not used.

Wedge anchors supplied by the tendon manufacturer were used for anchoring of tendons. Load cells were placed on one end of each tendon (**Figure 3.29**). The tendons were bent about a curved harping plate with a 1 in. (25 mm) radius. These plates were similar to the harping plates described in Section 3.3.1.1. The harping plates were greased prior to

loading. The tendons were bent to an angle of 7 degrees and axially loaded to approximately 12 kips (53 kN). Loading of the tendons was accomplished using a 60 kip (267 kN) hydraulic ram acting against a U-shaped steel "chair" at the load-cell end of the frame. **Figures 3.31a** and **3.31b** are photographic views of the test set-up.

Data readings were recorded by an Optim Megadac data acquisition system. Readings were taken at 5 minute intervals over several hours at selected times over the duration of the sustained load tests. The total test duration was 120 days. The eight strain gages for tendons 1 and 2 were connected to the data acquisition system by soldering the gage cables into a 37-pin electrical connector that attached directly to the data acquisition system. The remaining 3 strain gages for test specimen S3 and the 3 load cell connections were made with electrical "quick-connects" to the computer card for the data acquisition system.

At the end of 120 days of sustained loading, each of the tendons were statically tested to failure under combined axial load and harping. The procedure for residual strength tests was the same as the procedure used for test series 3b of **Tables 3.5a** and **3.5b**. The axial load on the tendons was increased at a rate of approximately 2.4 kips/min. (10.7 kN/min.) until failure. The initial conditions of the residual strength tests were the conditions on the tendons at the completion of 120 days of sustained loading.

3.5.2 Test Results and Discussion

Flexural strain values over the duration of the test for all three test specimens are shown in **Figures 3.32** through **3.34**. All tests show a decrease in flexural strain at harped point over the duration of the test. Strain gage SG1 for test specimen S1 did not appear to provide valid results and ceased to work after 46 days (**Figure 3.32**). The strain gage at harped point for specimen S2 ceased to work after 89 days (**Figure 3.33**). The apparent flexural strain reduction for specimen S3 was 64 x 10^{-6}. The reduction of the flexural strain could be a localized phenomenon occurring at the strain gage location.

After application of initial tendon loads, tendon anchorage wedges appeared to continue to "sink-in". Unequal anchorage losses should cause minor lateral movement of the tendon

within the test frame. The resulting relative movement of strain gage SG1 relative to the apex of the tendon bend would cause changes in the flexural strain readings. The movement of the tendons would therefore make it not possible to determine what fraction of the observed flexural strain change is due to material behavior and what is due to lateral movement of strain gage SG1 relative to the apex of the tendon bend.

Intuitively, if flexural strains at the apex of the tendon bend changes, the change would likely be an increase in flexural strain due to relaxation at the higher strain areas of the bend. The high strain areas at the bend of the tendon would likely result in higher relaxation in these areas compared to the straight portions of the tendon. The drop in load associated with relaxation in these areas would require increased strains in these areas to maintain force equilibrium along the tendon. Results shown in **Figures 3.32** through **3.34** do not show any increase in flexural strains. It is concluded, therefore, that these tests results do not indicate any significant relaxation of the tendon fibers at the harping point of the tendons.

Figure 3.35 shows the variation in the difference between the equivalent load cell strain and the average axial strain for specimens S1, S2 and S3. The load cell strain is calculated by dividing the tendon load readings taken from the load cell located at the end of the tendon by the product of the tendon cross-sectional area and elastic modulus. The figure shows that the results are similar for test specimens S1 and S2. The difference in strains for these test specimens after 120 days of sustained loading was approximately zero. For specimen S3, the difference in load cell strain and average axial strain was -83×10^{-6} after 120 days of sustained loading. The large variations observed during the test for all specimens, however, suggest that any small differences at the end of the test are insignificant.

The difference between load cell strain and average axial strain for specimen S3 results in a relaxation value equivalent to 1.2% of the tendon load after 120 days. The average relaxation for all specimens was approximately 0.6%, which is insignificant.

The load drop across the harping plate for test specimen S1 was measured to better understand the friction existing at the harping plate during tensioning of the tendon. The tendon loads on each side of the harping plate were calculated based on average strain

readings from strain gages SG2 and SG3 on the loading side and SG4 and SG5 on the fixed side of the test frame (**Figure 3.30**). At the maximum axial load during prestressing of test specimen S1, the average axial strain on the tendon was 0.00769 on the loading end of the tendon and 0.00758 on the fixed end of the tendon. The average strain difference of 110×10^{-6} is associated with a load drop across the harping plate of 0.19 kips (0.85 kN). Using the expression for reduction in axial load at a bend due to friction, an estimate of the friction coefficient was calculated. The expression for load loss due to friction is:

$$P_x = P_o e^{-\mu\theta} \tag{3.16}$$

where P_x = tendon load at fixed end
P_o = tendon load at loading end
μ = friction coefficient between harping plate and tendon
θ = bend angle in radians

Based on the average strain readings at the loading and fixed ends of the tendon, the following conditions were placed on the tendon: $P_o = 13.06$ kips (58.09 kN), $P_x = 12.87$ kips (57.26 kN), and $\theta = 7.0$ degrees (0.122 rad.). The resulting value of the friction coefficient, μ, calculated from Equation 3.16 is 0.12. The estimated friction coefficients for unbonded steel tendons listed in ACI 318-95 range between 0.05 and 0.15 [ACI Committee 318, 1995]. The value of friction coefficient found in this test for a CFRP tendon appears to be consistent with the friction coefficients listed for unbonded tendons in ACI 318-95.

3.5.3 Residual Strength Test Results

Testing of the tendons to failure was accomplished after 120 days of sustained loading. The initial conditions of the test were the conditions that existed on the tendons at the end of the sustained loading. For specimens S1 and S2, strain gage SG1 was not working during the residual strength tests and estimates of initial rupture of fibers was based on audible and visual indications of fiber rupture. The axial load at failure for specimen S3 was determined based on changes in the tendon flexural strain readings as well as audible and visual

indications of fiber rupture.

The procedure for the residual strength tests of specimens S1, S2 and S3 was similar to the procedure used for strength tests of specimens in series 3b in **Tables 3.5a** and **3.5b**. Failure loads for the harped tendons were 18.5 kips (82.3 kN), 18.4 kips (81.8 kN) and 18.0 kips (80.1 kN) for specimens S1, S2 and S3, respectively (**Tables 3.10a** and **3.10b**). The average failure loads of the specimens was 18.3 kips (81.4 kN), compared to an average failure load of 18.5 kips (82.3 kN) for specimens in series 3b in **Tables 3.5a** and **3.5b**. The average load at failure of the sustained loading specimens was 99% of the load at failure observed during the static strength tests.

Figure 3.36 shows the comparison between the failure loads of specimens S1, S2 and S3 with the predicted failure loads calculated from Equation 3.10. It is evident from the figure that Equation 3.10 can reasonably predict the failure load of harped tendons subjected to sustained loading for the range of variables in this test. It is therefore concluded that sustained loading of harped CFRP tendons does not degrade the strength of the tendons for the range of variables conducted in this investigation.

3.6 SUMMARY AND CONCLUSIONS

Tests were conducted on 0.32 in. (8.0 mm) diameter CFRP tendons subjected to uni-axial load, short-term combined axial load and harping, bending-tension fatigue loading, and sustained axial loading under a harped condition. Following the bending-tension fatigue testing and sustained load testing, residual strength tests were conducted on the CFRP tendons to determine the effects of bending-tension fatigue and sustained loads on the residual tensile strength of the harped tendons. A failure prediction model was developed in this study that accurately predicts the conditions associated with failure of the tendons at harping points.

Based on the results of the study, the following conclusions are made:

1. Flexural strains, defined as the difference in extreme fiber strains of a harped tendon and the average axial strain of the tendon, are a maximum at the apex of the tendon bend and are approximately zero beyond 6 in. (152 mm) on either side of the bend point. The maximum value of the flexural strains increase with increases in the tendon bend angle, decreases in the harping plate radius, and increases in the average axial load of the tendon.

2. Failure of CFRP tendons at harping points is generally at an axial load less than the uni-axial rupture strength of the tendon. The failure load of harped tendons decreases with increases in the tendon bend angle and with decreases in the harping plate radius.

3. Failure of tendons at the bend point or harping point appears to be associated with an extreme fiber strain of about 0.0217, which is 145% of the maximum reported uni-axial failure strain of 0.015. Based on a fiber strain of 0.0217 and a modulus of 21,800 ksi (150 GPa), the estimated uni-axial failure stress of the tendon is calculated to be 473 ksi (3260 MPa).

4. For the CFRP tendons tested in this study, failure conditions of the tendons at a harped point can be predicted based on an ultimate fiber strain model. The resulting equations (Equations 3.10, 3.11, 3.12 and 3.13) for predicting the axial load and bend angle at failure are shown to have good predictive capability.

5. CFRP tendons subjected to severe bending-tension fatigue loading show no degradation in performance through 1 million fatigue cycles. Residual strength tests show that bending-tension fatigue does not degrade the strength of the tendons.

6. CFRP tendons subjected to sustained axial loads of 12 kips (53 kN) while harped at an angle of 7 degrees using a 1 in. (25 mm) radius harping plate for a duration of 120 days show no significant relaxation. Residual strength tests show that sustained loading of harped CFRP tendons does not degrade the strength of the tendons.

Table 3.1 Typical engineering properties of Leadline

Item	Specification
Carbon Fiber Content	65%
Ultimate Tensile Strength	27.0 kips (120 kN)
Ultimate Tensile Stress	350 ksi (2400 MPa)
Elastic Modulus	21,300 ksi (147 GPa)
Extension at Failure	0.015
Weight	0.05 lb/ft (77 g/m)
Relaxation Ratio	2-3% (at 20° C)

Table 3.2a Test results for short-term axial strength of tendons, US customary units

Specimen, no.	Failure load, kips	Failure stress, ksi	Strain at failure, %	Elastic modulus, ksi	Type of end anchorage
1	20.0	257	1.19	21,600	wedge-cone
2	22.4	288	1.39	20,700	wedge-cone
3	24.3	312	1.38	22,600	NCSU -plate grips
4	21.5	276	1.24	22,300	NCSU -plate grips
5	25.9	332	1.51	22,000	NCSU -plate grips
6	23.1	297	1.36	21,800	NCSU -plate grips
average	**22.9**	**294**	**1.35**	**21,800**	

Table 3.2b Test results for short-term axial strength of tendons, SI Units

Specimen, no.	Failure load, kN	Failure stress, MPa	Strain at failure, %	Elastic modulus, GPa	Type of end anchorage
1	89	1770	1.19	149	wedge-cone
2	99.6	1990	1.39	143	wedge-cone
3	108	2150	1.38	156	NCSU -plate grips
4	95.6	1900	1.24	154	NCSU -plate grips
5	115	2290	1.51	152	NCSU -plate grips
6	103	2050	1.36	150	NCSU -plate grips
average	**102**	**2030**	**1.35**	**150**	

Table 3.3a Test matrix for behavior of tendon subjected to combined axial load and harping, US customary units

Test series	Harping plate radius, (R), in.	Initial axial load, kips	Axial load at reading, (P), kips	Bend angle, (θ), degrees	Total number of test readings	Procedure
1	20	4	---	2.3; 4.7; 7.0	3	application of axial load and then increment of bend angle
		8	---	2.3; 4.7; 7.0	3	
		12	---	2.3; 4.7; 7.0	3	
2	5	4	---	2.3; 4.7; 7.0	3	application of axial load and then increment of bend angle
		8	---	2.3; 4.7; 7.0	3	
		12	---	2.3; 4.7; 7.0	3	
3	1	4	---	2.3; 4.7; 7.0	3	application of axial load and then increment of bend angle
		8	---	2.3; 4.7; 7.0	3	
		12	---	2.3; 4.7; 7.0	3	
4	20	---	8	2.3; 4.7; 7.0	3	application of bend angle and then adjust axial load
	5	---	8	2.3; 4.7; 7.0	3	
	1	---	8	2.3; 4.7; 7.0	3	

Table 3.3b Test matrix for behavior of tendon subjected to combined axial load and harping, SI units

Test series	Harping plate radius, (R), mm	Initial axial load, kN	Axial load at reading, (P), kN	Bend angle, (θ), degrees	Total number of test readings	Procedure
1	508	17.8	---	2.3; 4.7; 7.0	3	application of axial load and then increment of bend angle
		35.6	---	2.3; 4.7; 7.0	3	
		53.4	---	2.3; 4.7; 7.0	3	
2	127	17.8	---	2.3; 4.7; 7.0	3	application of axial load and then increment of bend angle
		35.6	---	2.3; 4.7; 7.0	3	
		53.4	---	2.3; 4.7; 7.0	3	
3	25	17.8	---	2.3; 4.7; 7.0	3	application of axial load and then increment of bend angle
		35.6	---	2.3; 4.7; 7.0	3	
		53.4	---	2.3; 4.7; 7.0	3	
4	508	---	35.6	2.3; 4.7; 7.0	3	application of bend angle and then adjust axial load
	127	---	35.6	2.3; 4.7; 7.0	3	
	25	---	35.6	2.3; 4.7; 7.0	3	

Table 3.4a Summary of linear regression analysis of test results for tendon subjected to combined axial load and harping, US customary units

Test series	Harping plate radius, (R), in.	Axial load, (P), kips			Average load for all (θ), kips	λ, με/deg.
		θ = 2.3 deg.	θ = 4.7 deg.	θ = 7.0 deg.		
1	20	4.2	4.9	6.0	5.03	730
		8.3	9.3	11.0	9.52	881
		12.4	13.3	14.9	13.6	948
2	5	4.3	5.2	6.6	5.33	878
		8.4	9.3	10.9	9.55	1088
		12.2	13.1	14.8	13.4	1198
3	1	4.3	5.2	6.8	5.43	1058
		8.3	9.2	10.6	9.37	1349
		12.3	13.3	15.0	13.6	1452
4	20	8.0	8.0	8.0	8.00	807
	5	8.0	8.0	8.0	8.00	1032
	1	8.0	8.0	8.0	8.00	1179

Table 3.4b Summary of linear regression analysis of test results for tendon subjected to combined axial load and harping, SI units

Test series	Harping plate radius, (R), mm	Axial load, (P), kN			Average load for all (θ), kN	λ, με/deg.
		θ = 2.3 deg.	θ = 4.7 deg.	θ = 7.0 deg.		
1	508	19	22	27	22.4	730
		37	41	49	42.3	881
		55	59	67	60.5	948
2	127	19	23	29	23.7	878
		37	42	49	42.5	1088
		54	58	66	59.6	1198
3	25	19	23	30	24.2	1058
		37	41	47	41.7	1349
		55	59	67	60.5	1452
4	508	36	36	36	35.6	807
	127	36	36	36	35.6	1032
	25	36	36	36	35.6	1179

Table 3.5a Test matrix for static strength of harped tendons, US customary units

Test series	Initial axial stress, ksi	Bend angle, (θ), degrees	Harping plate radius, (R), in.	Number of replicate specimens	Procedure
1a	180	---	20	2	application of axial load and then increment of bend angle until failure
1b	0	7	20	3	application of bend angle and then increment of axial load until failure
2a	180	---	5	2	application of axial load and then increment of bend angle until failure
2b	0	7	5	2	application of bend angle and then increment of axial load until failure
3a	180	---	1	2	application of axial load and then increment of bend angle until failure
3b	0	7	1	2	application of bend angle and then increment of axial load until failure

Table 3.5b Test matrix for static strength of harped tendons, SI units

Test series	Initial axial stress, MPa	Bend angle, (θ), degrees	Harping plate radius, (R), mm	Number of replicate specimens	Procedure
1a	1240	---	508	2	application of axial load and then increment of bend angle until failure
1b	0	7	508	3	application of bend angle and then increment of axial load until failure
2a	1240	---	127	2	application of axial load and then increment of bend angle until failure
2b	0	7	127	2	application of bend angle and then increment of axial load until failure
3a	1240	---	25	2	application of axial load and then increment of bend angle until failure
3b	0	7	25	2	application of bend angle and then increment of axial load until failure

Table 3.6a Test results for static strength of harped tendons, US customary units

Test series	Harping plate radius, (R), in.	Axial load at failure, (P), kips	Bend angle at failure, (θ), degrees	Recorded SG1 strain, $x10^{-6*}$	Flexural strain, $x10^{-6**}$
1a	20	23.58	12.03	19162	5279
	20	23.63	12.12	19658	5746
average	**20**	**23.61**	**12.08**	**19410**	**5513**
1b	20	22.25	7.00	---	----
	20	23.25	7.00	---	---
	20	22.75	7.00	---	---
average	**20**	**22.75**	**7.00**	**---**	**---**
2a	5	18.44	7.75	19844	8987
	5	18.82	7.93	21607	10524
average	**5**	**18.63**	**7.84**	**20726**	**9756**
2b	5	20.76	7.12	21416	10593
	5	19.48	7.15	19970	8498
average	**5**	**20.12**	**7.14**	**20693**	**9546**
3a	1	17.49	6.79	17502	7205
	1	17.63	6.82	21433	11050
average	**1**	**17.56**	**6.81**	**19468**	**9128**
3b	1	18.54	6.99	16970	6053
	1	18.43	7.00	17052	6198
average	**1**	**18.49**	**7.00**	**17011**	**6126**

* SG1 is the strain gage located initially directly under the harping point

** Flexural strain is the strain reading from SG1 minus the average axial strain from SG8 and SG9
(Location of SG1, SG8 and SG9 are shown in Figure 3.7)

Table 3.6b Test results for static strength of harped tendons, SI units

Test series	Harping plate radius, (R), mm	Axial load at failure, (P), kN	Bend angle at failure, (θ), degrees	Recorded SG1 strain, $x10^{-6*}$	Flexural strain, $x10^{-6**}$
1a	508	104.9	12.03	19162	5279
	508	105.1	12.12	19658	5746
average	**508**	**105.0**	**12.08**	**19410**	**5513**
1b	508	98.97	7.00	---	----
	508	103.4	7.00	---	---
	508	101.2	7.00	---	---
average	**508**	**101.2**	**7.00**	**---**	**---**
2a	127	82.01	7.75	19844	8987
	127	83.72	7.93	21607	10524
average	**127**	**82.87**	**7.84**	**20726**	**9756**
2b	127	92.34	7.12	21416	10593
	127	86.66	7.15	19970	8498
average	**127**	**89.50**	**7.14**	**20693**	**9546**
3a	25	77.78	6.79	17502	7205
	25	78.43	6.82	21433	11050
average	**25**	**78.11**	**6.81**	**19468**	**9128**
3b	25	82.47	6.99	16970	6053
	25	81.99	7.00	17052	6198
average	**25**	**82.23**	**7.00**	**17011**	**6126**

* SG1 is the strain gage located initially directly under the harping point

** Flexural strain is the strain reading from SG1 minus the average axial strain from SG8 and SG9
(Location of SG1, SG8 and SG9 are shown in Figure 3.7)

Table 3.7a Test matrix for bending-tension fatigue behavior of harped tendons, US customary units

Specimen number	Harping plate radius, (R), in.	P_{min}, kips; θ_{min}, deg.	P_{max}, kips; θ_{max}, deg.	Frequency, Hz	No. of cycles	Procedure
F1	1	14.0; 4.5	14.7; 5.5	0.71	1×10^6	apply 14.3 kip tendon load, then cycle tendon bend angle between θ_{min} and θ_{max} by vertical actuator displacement
F2	1	14.0; 4.5	14.7; 5.5	0.88	1×10^6	
F3	1	14.0; 4.5	14.7; 5.5	0.88	1×10^6	

Table 3.7b Test matrix for bending-tension fatigue behavior of harped tendons, SI units

Specimen number	Harping plate radius, (R), mm	P_{min}, kN; θ_{min}, deg.	P_{max}, kN; θ_{max}, deg.	Frequency, Hz	No. of cycles	Procedure
F1	25	62.3; 4.5	65.4; 5.5	0.71	1×10^6	apply 14.3 kip tendon load, then cycle tendon bend angle between θ_{min} and θ_{max} by vertical actuator displacement
F2	25	62.3; 4.5	65.4; 5.5	0.88	1×10^6	
F3	25	62.3; 4.5	65.4; 5.5	0.88	1×10^6	

Table 3.8a Test results for residual strength after bending-tension fatigue tests of harped tendons, US customary units

Specimen number	Harping plate radius, (R), in.	Initial tendon load/angle, kips/degrees	Tendon load at failure, (P), kips	Bend angle at failure, (θ), degrees	Procedure
F1	1	13.7/4.69	16.1	7.61	starting at initial conditions, increment bend angle until failure
F2	1	13.9/4.26	16.4	7.85	
F3	1	14.2/4.64	16.1	6.99	
Average	1	13.9/4.53	16.2	7.48	

Table 3.8b Test results for residual strength after bending-tension fatigue tests of harped tendons, SI units

Specimen number	Harping plate radius, (R), mm	Initial tendon load/angle, kN/degrees	Tendon load at failure, (P), kN	Bend angle at failure, (θ), degrees	Procedure
F1	25	60.9/4.69	71.6	7.61	starting at initial conditions, increment bend angle until failure
F2	25	61.8/4.26	72.9	7.85	
F3	25	63.2/4.64	71.6	6.99	
Average	25	62.0/4.53	72.1	7.48	

Table 3.9a Test matrix for sustained loading behavior of harped tendons, US customary units

Specimen number	Harping plate radius, (R), in.	Initial load, kips	Bend angle, (θ), degrees	Strain gage location*	Duration of test, days	Procedure
S1	1	12	7	SG1 thru SG5	120	configure tendon to bend angle and then apply axial load; maintain for duration of test
S2	1	12	7	SG1 thru SG3	120	
S3	1	12	7	SG1 thru SG3	120	

* refer to **Figure 3.7**.

Table 3.9b Test matrix for sustained loading behavior of harped tendons, SI units

Specimen number	Harping plate radius, (R), mm	Initial load, kN	Bend angle, (θ), degrees	Strain gage location*	Duration of test, days	Procedure
S1	25	53	7	SG1 thru SG5	120	configure tendon to bend angle and then apply axial load; maintain for duration of test
S2	25	53	7	SG1 thru SG3	120	
S3	25	53	7	SG1 thru SG3	120	

* refer to **Figure 3.7**.

Table 3.10a Test results for residual strength after sustained loading tests of harped tendons, US customary units

Specimen number	Harping plate radius, (R), in.	Bend angle, (θ), degrees	Initial tendon load, kips	Tendon load at failure, (P), kips	Procedure
S1	1	7.0	11.7	18.5	starting at initial conditions, increment tendon load until failure
S2	1	7.0	10.9	18.4	
S3	1	7.0	11.6	18.0	
Average	1	7.0	11.4	18.3	

Table 3.10b Test results for residual strength after sustained loading tests of harped tendons, SI units

Specimen number	Harping plate radius, (R), mm	Bend angle, (θ), degrees	Initial tendon load, kN	Tendon load at failure, (P), kN	Procedure
S1	25	7.0	52.0	82.3	starting at initial conditions, increment tendon load until failure
S2	25	7.0	48.5	81.8	
S3	25	7.0	51.6	80.1	
Average	25	7.0	50.7	81.4	

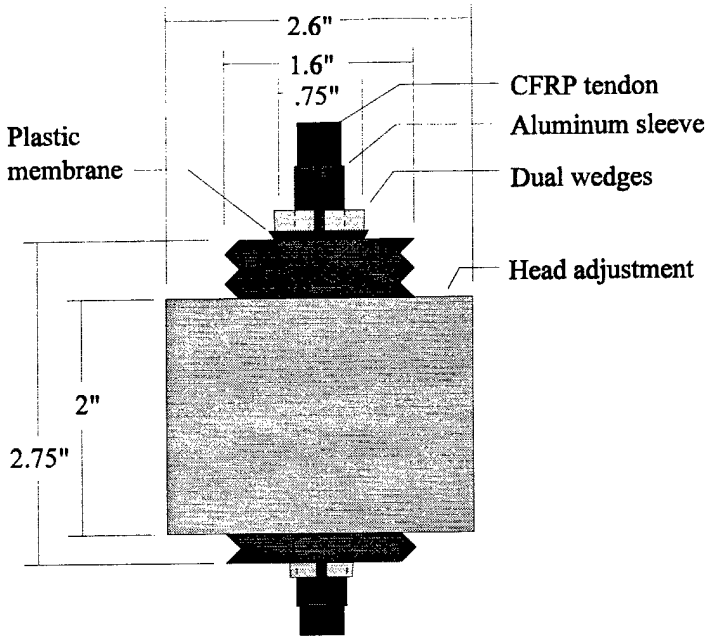

Figure 3.1a Wedge-type anchorage system for Leadline tendon

Figure 3.1b Photographic view of wedge-type anchorage system

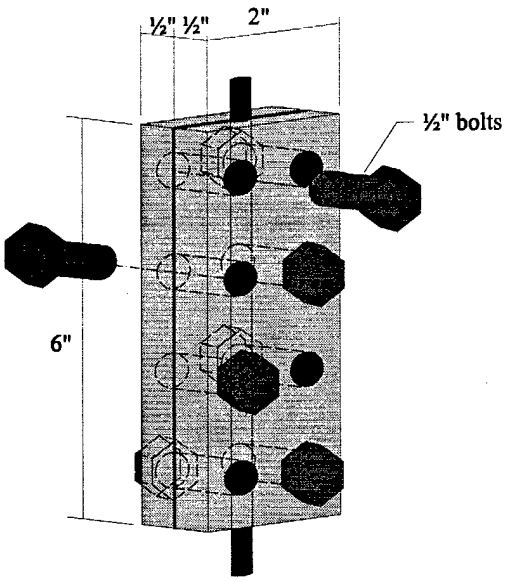

Figure 3.2a Steel plate anchorage system developed at NCSU

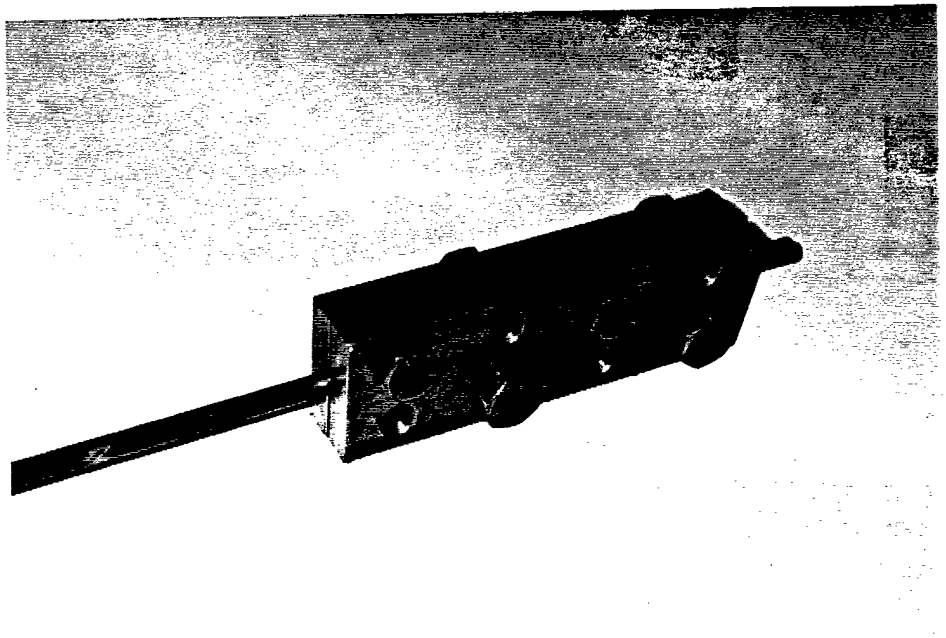

Figure 3.2b Photographic view of steel plate anchorage system

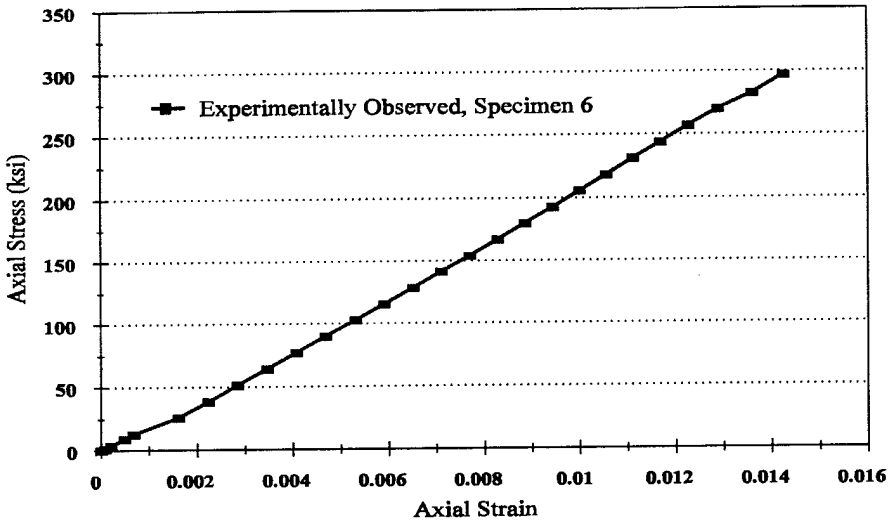

Figure 3.3 Typical stress-strain diagram of Leadline

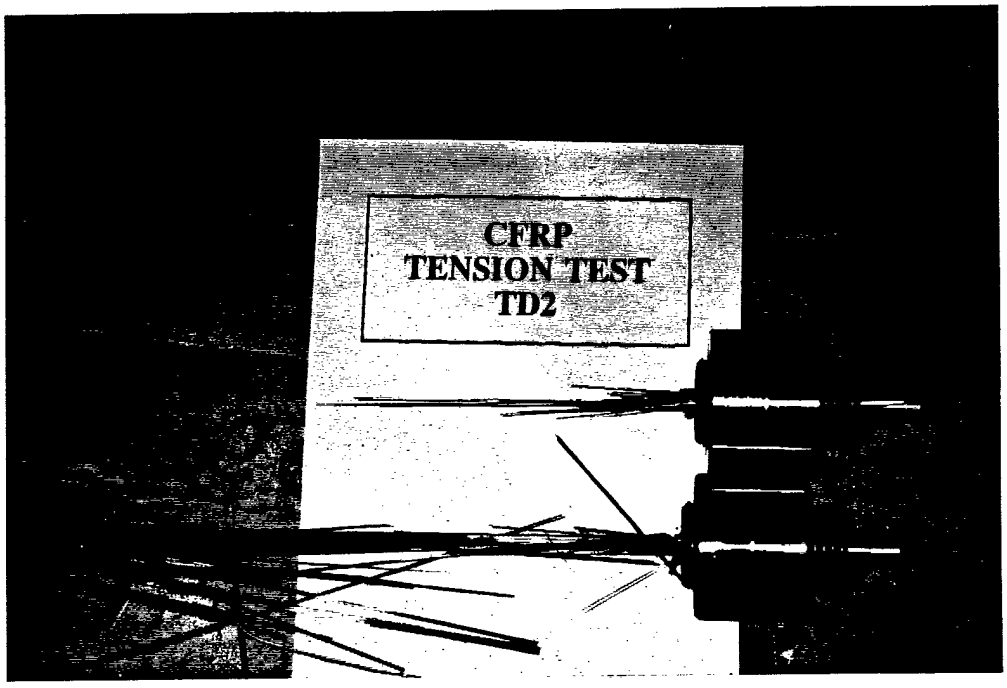

Figure 3.4 Photograhic view of failure of CFRP tendon subjected to uni-axial load

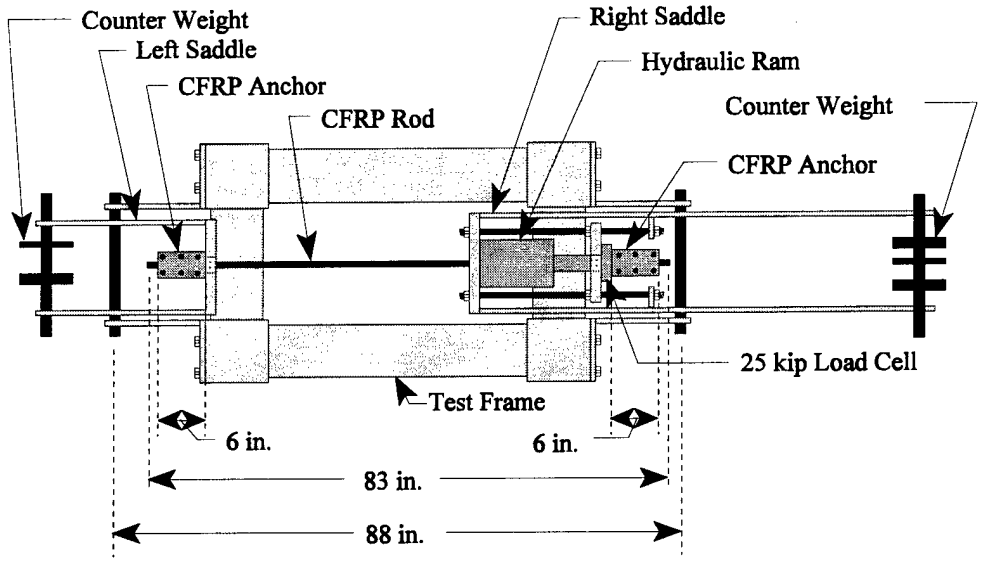

Figure 3.5a Top view of test set-up for harped tendons

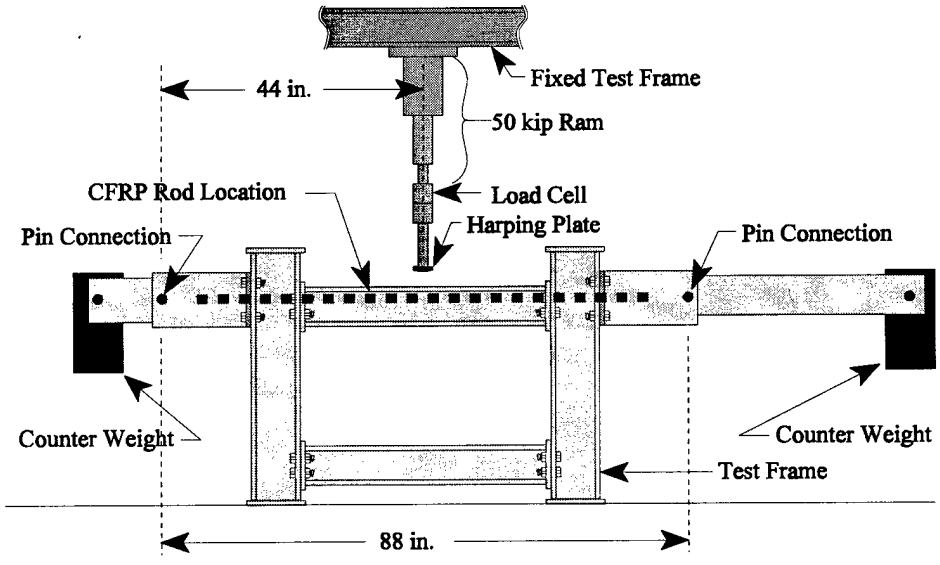

Figure 3.5b Side view of test set-up for harped tendons

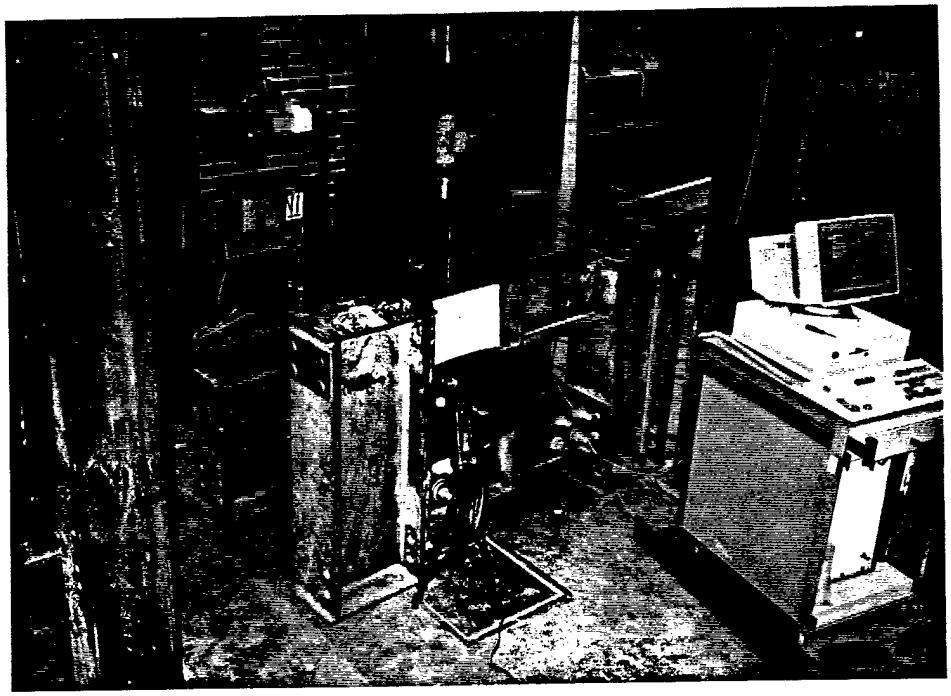

Figure 3.6a Photographic profile view of the test set-up for harped tendons

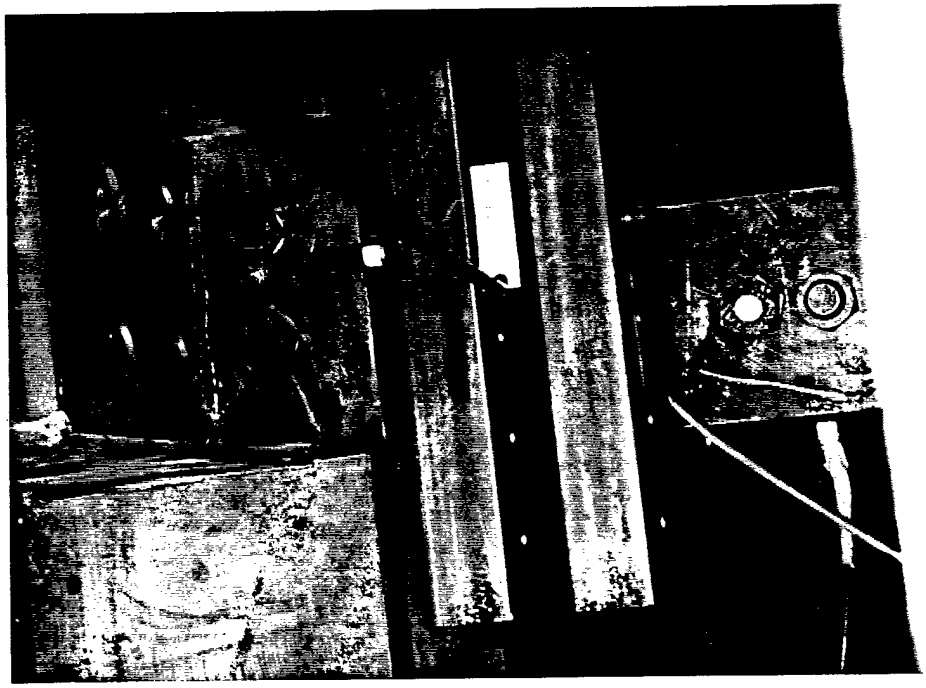

Figure 3.6b Photographic view of the bottom of the harping plate for the test set-up for harped tendons

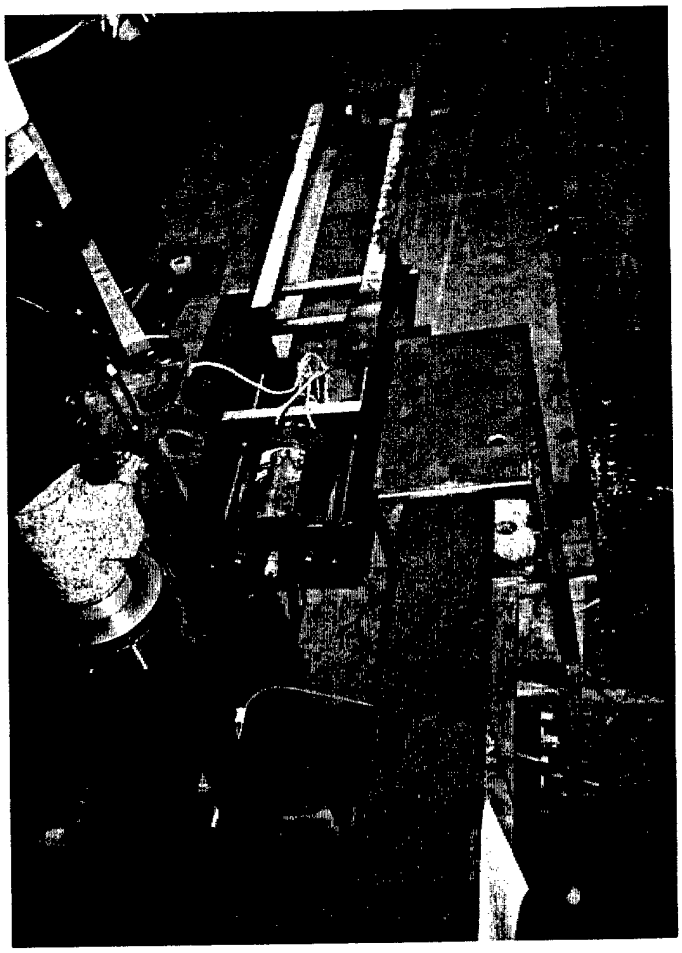

Figure 3.6c Photographic view of the loading end of the test set-up for harped tendons

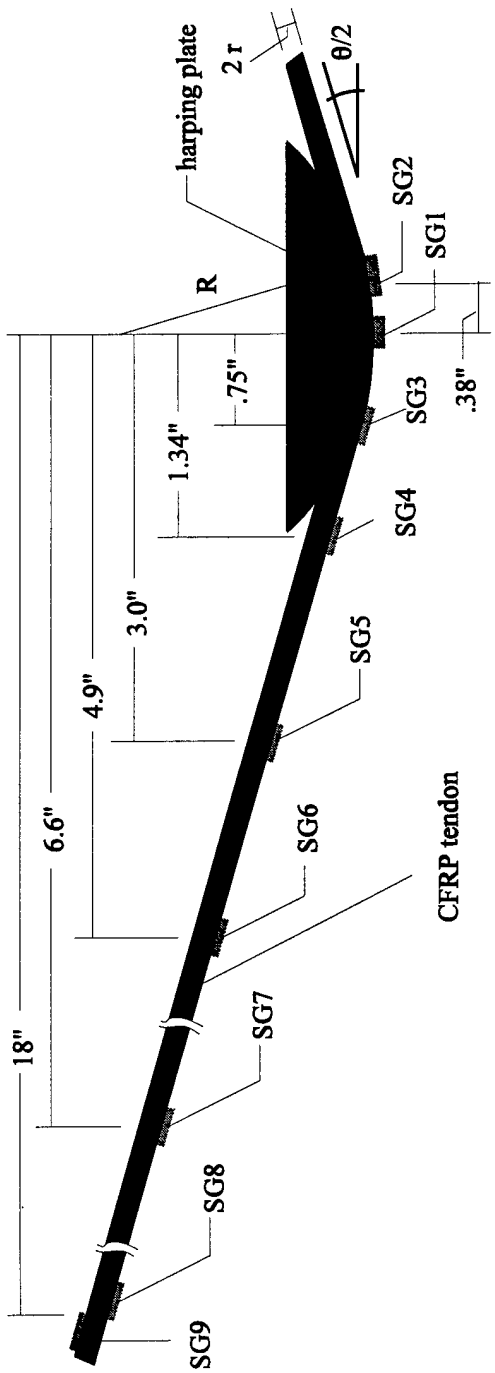

Figure 3.7 Location of strain gages on harped CFRP tendon

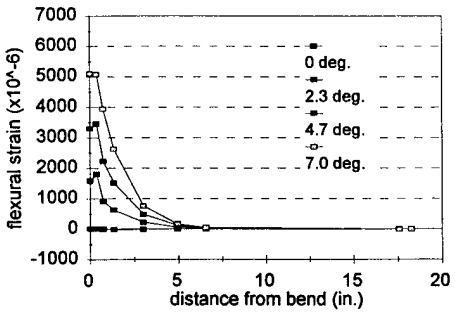

(a) Initial load is 4 kips

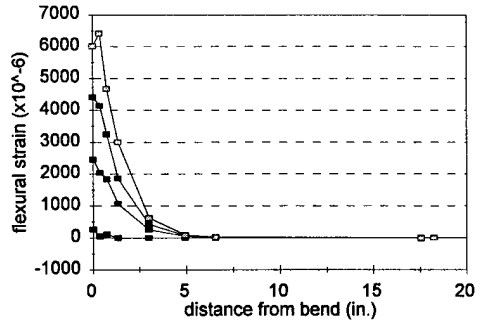

(b) Initial load is 8 kips

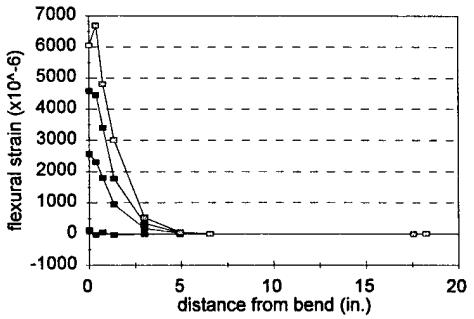

(c) Initial load is 12 kips

Figure 3.8 Series 1 test results

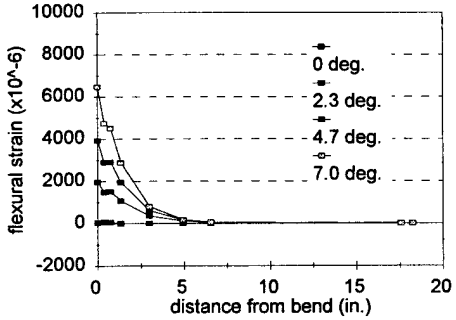

(a) Initial load is 4 kips

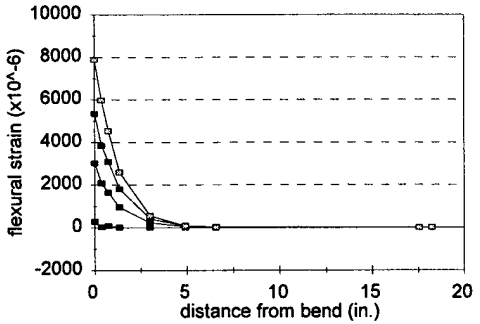

(b) Initial load is 8 kips

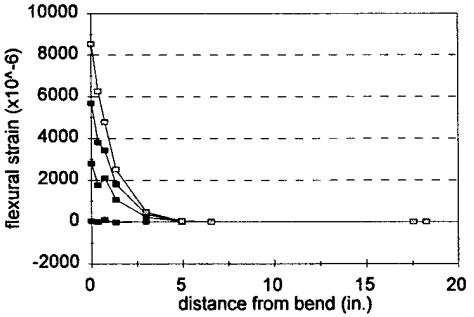

(c) Initial load is 12 kips

Figure 3.9 Series 2 test results

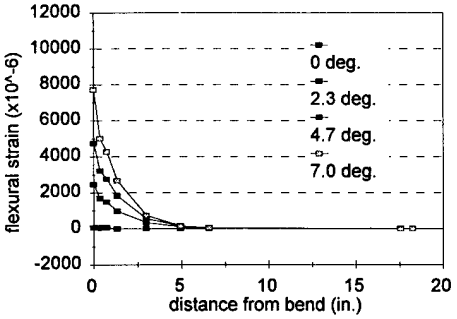

(a) Initial load is 4 kips

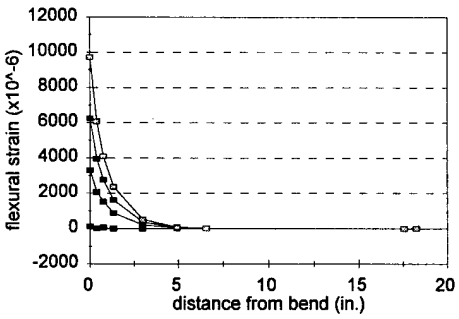

(b) Initial load is 8 kips

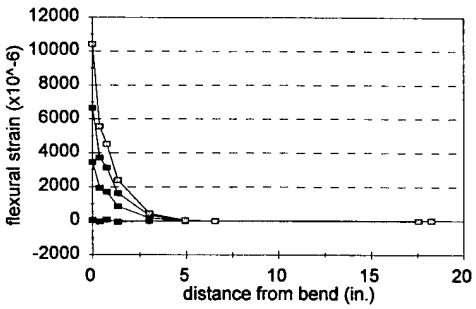

(c) Initial load is 12 kips

Figure 3.10 Series 3 test results

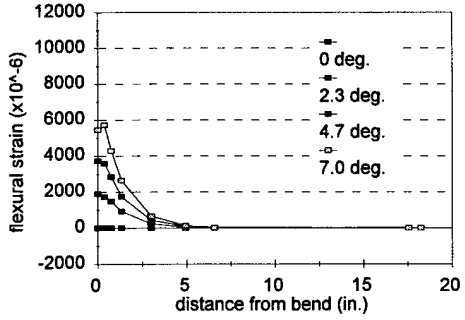

(a) Harping plate radius = 20 in.

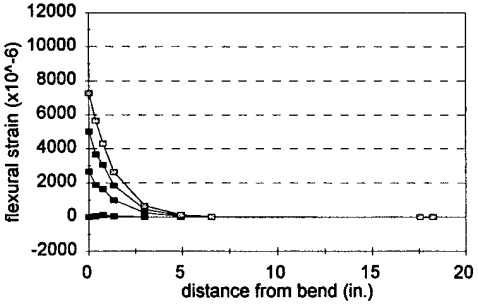

(b) Harping plate radius = 5 in.

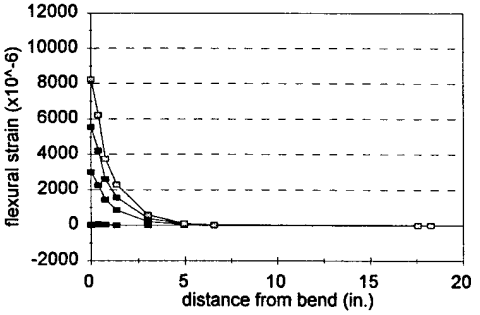

(c) Harping plate radius = 1 in.

Figure 3.11 Series 4 test results

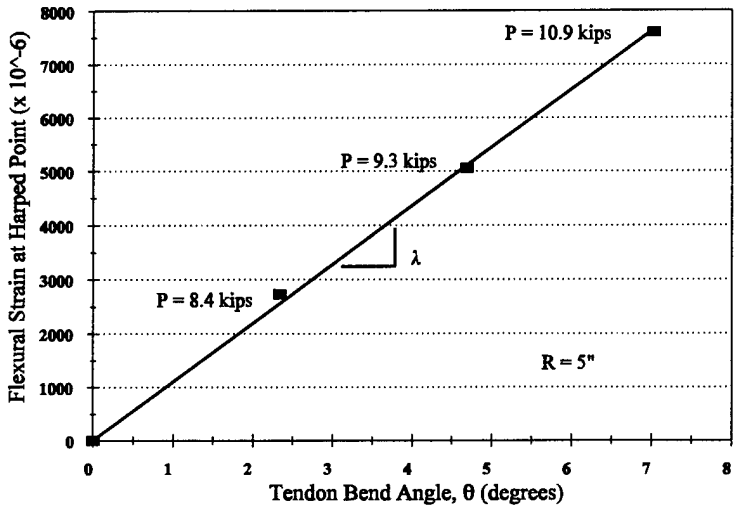

Figure 3.12 Variation of flexural strain at harped point with bend angle for test series 2 with initial axial load of 8 kips

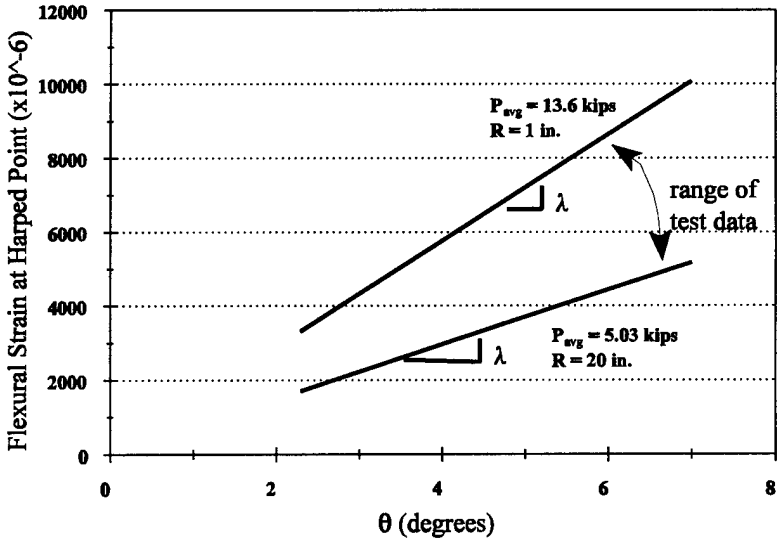

Figure 3.13 Range of λ values for all tests of Tables 3.4a and 3.4b

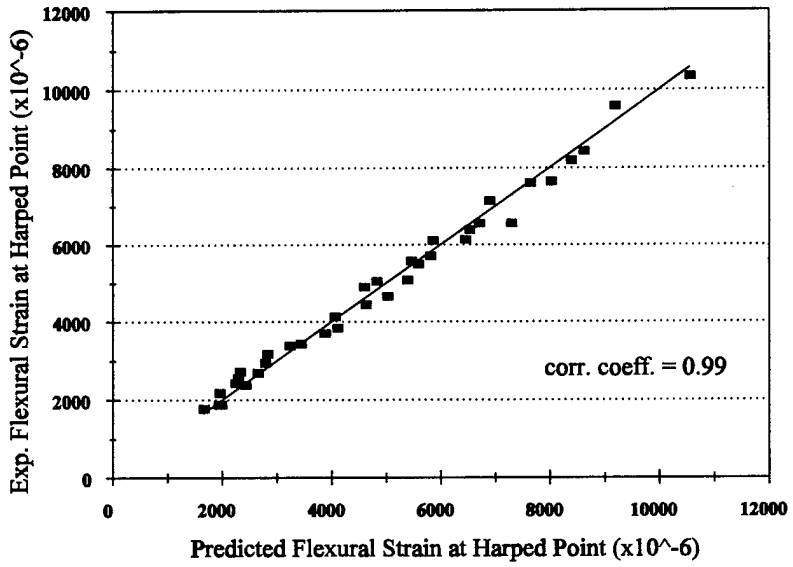

Figure 3.14 Comparison of experimental versus predicted flexural strain at harped point

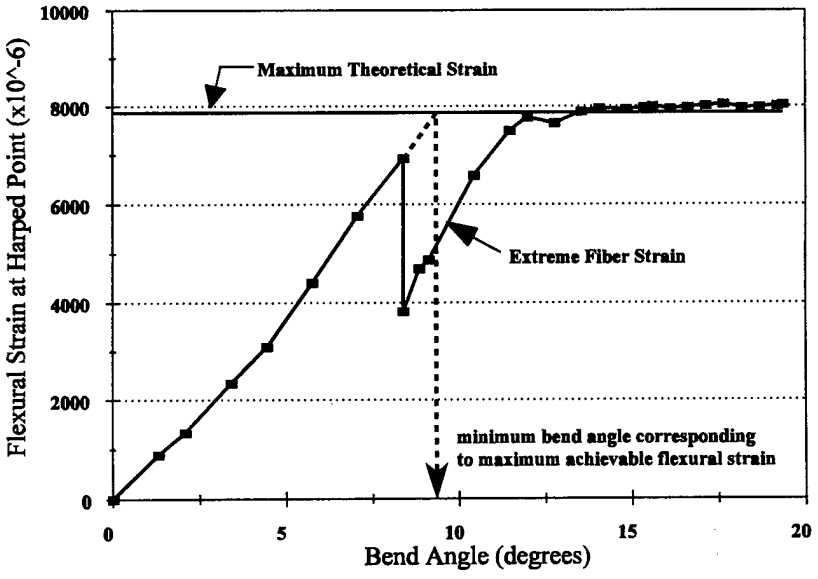

Figure 3.15 Flexural strain readings for 20 inch radius harping plate

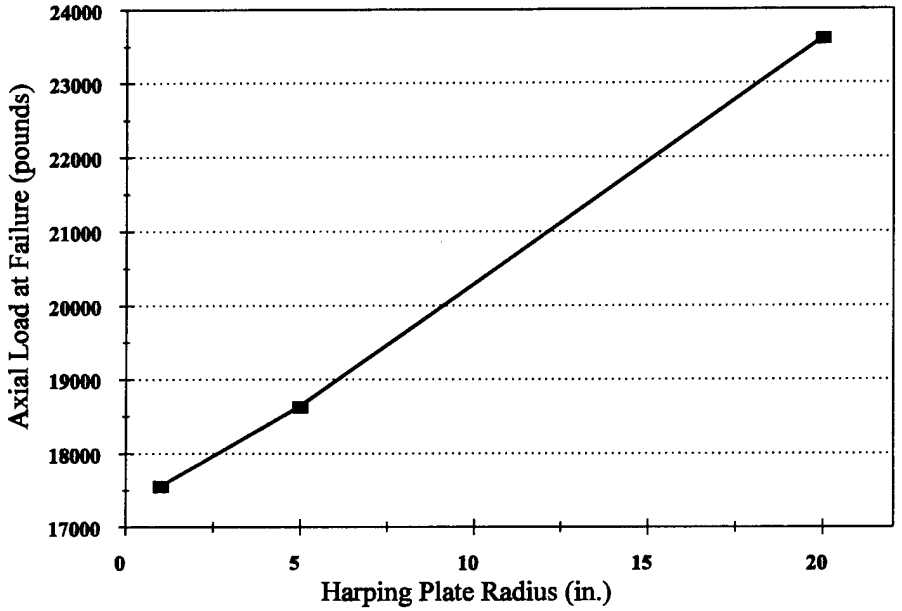

Figure 3.16 Variation in average axial load at failure with harping plate radius for test series 1a, 2a and 3a

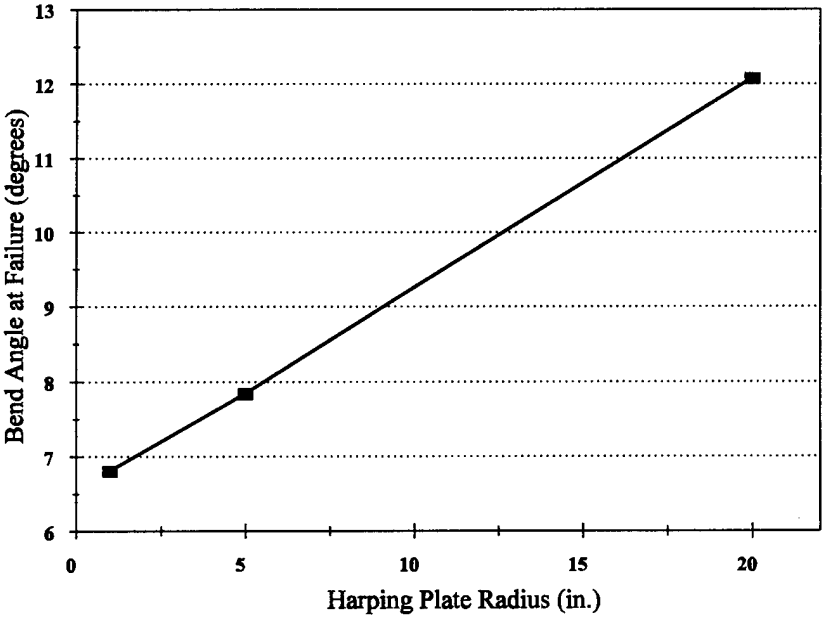

Figure 3.17 Variation in average bend angle at failure with harping plate radius for test series 1a, 2a and 3a

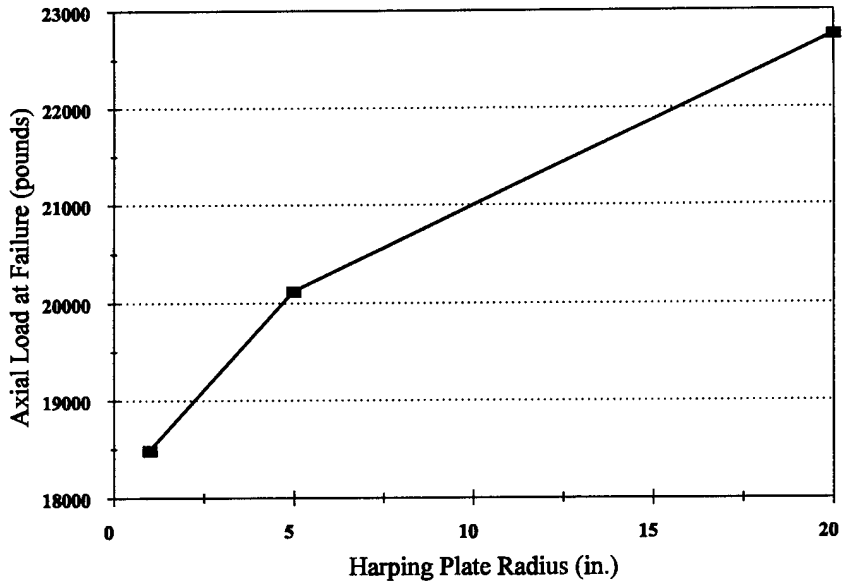

Figure 3.18 Variation in average axial load at failure with harping plate radius for test series 1b, 2b and 3b

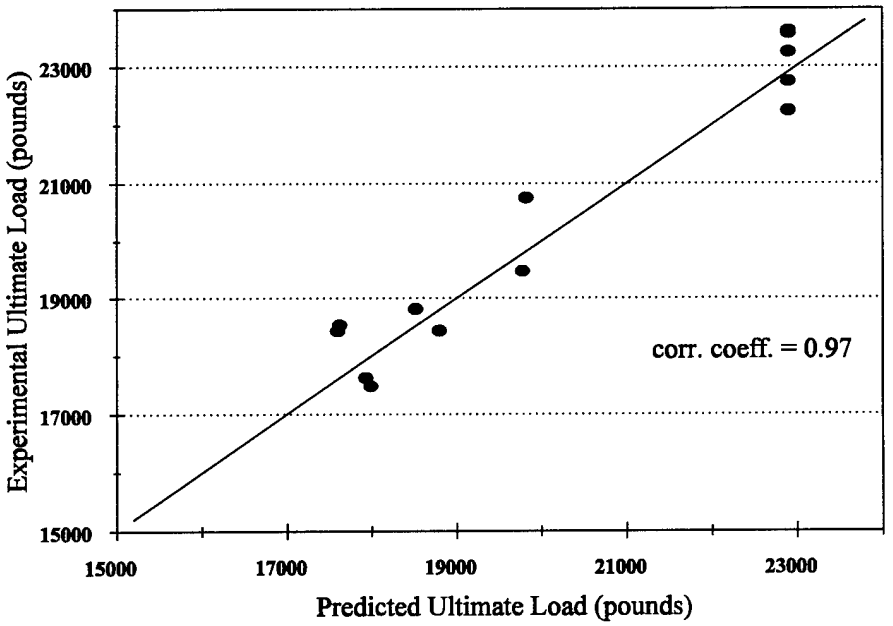

Figure 3.19 Comparison of experimental versus predicted failure loads for harped tendons subjected to axial load

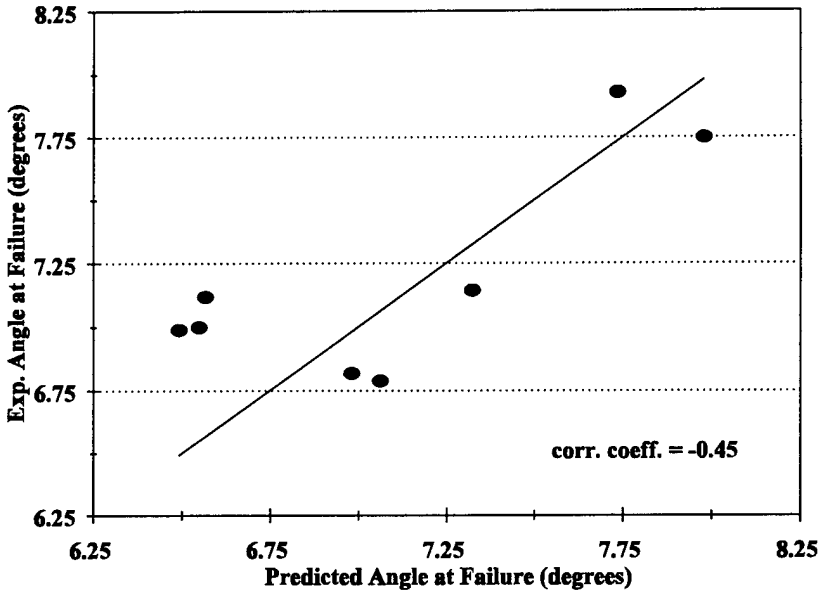

Figure 3.20 Comparison of experimental versus predicted angle at failure for harped tendons subjected to axial load

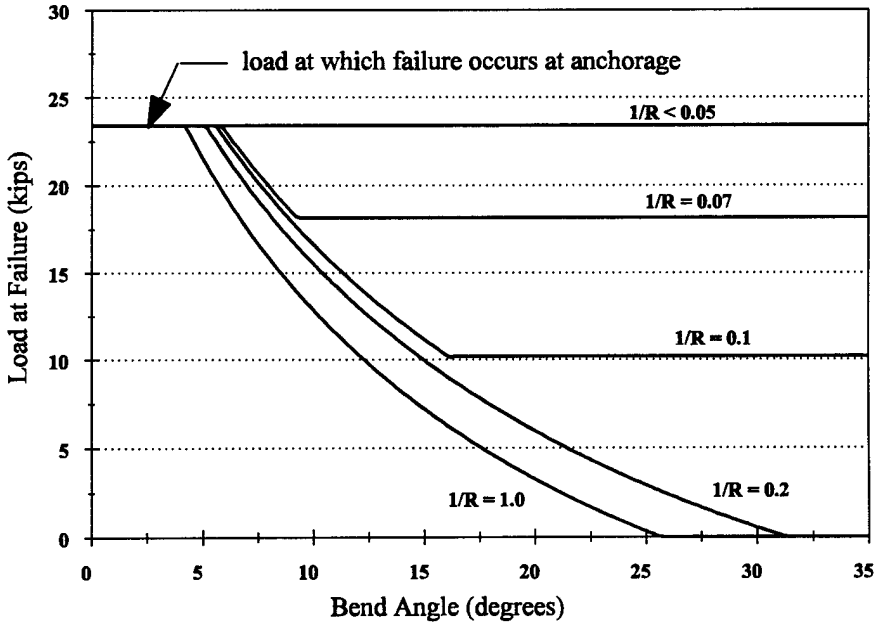

Figure 3.21 Predicted failure load for varying bend angles with various harping plate curvatures

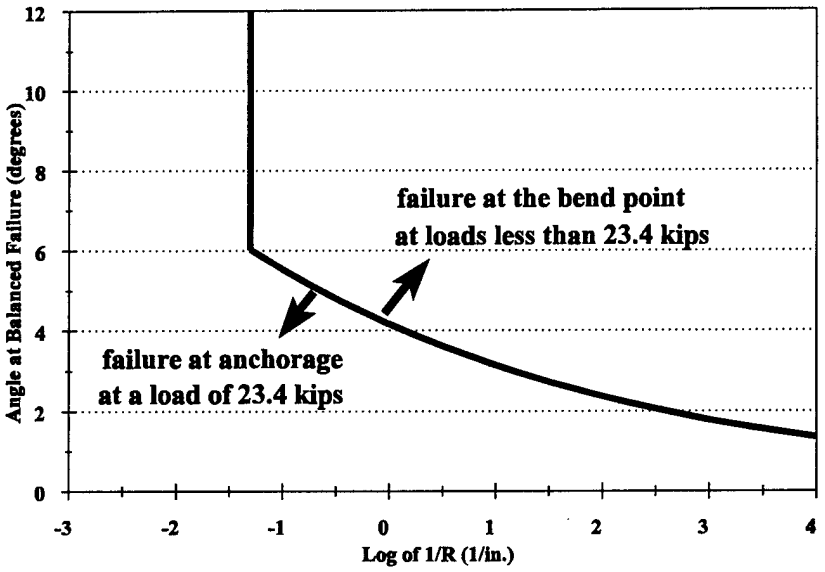

Figure 3.22 Balanced failure angle for various harping plate curvatures

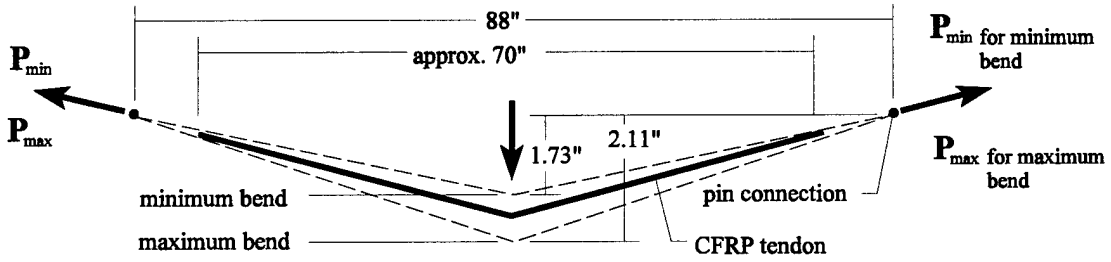

Figure 3.23 Schematic view of the minimum and maximum limits for bending-tension fatigue test

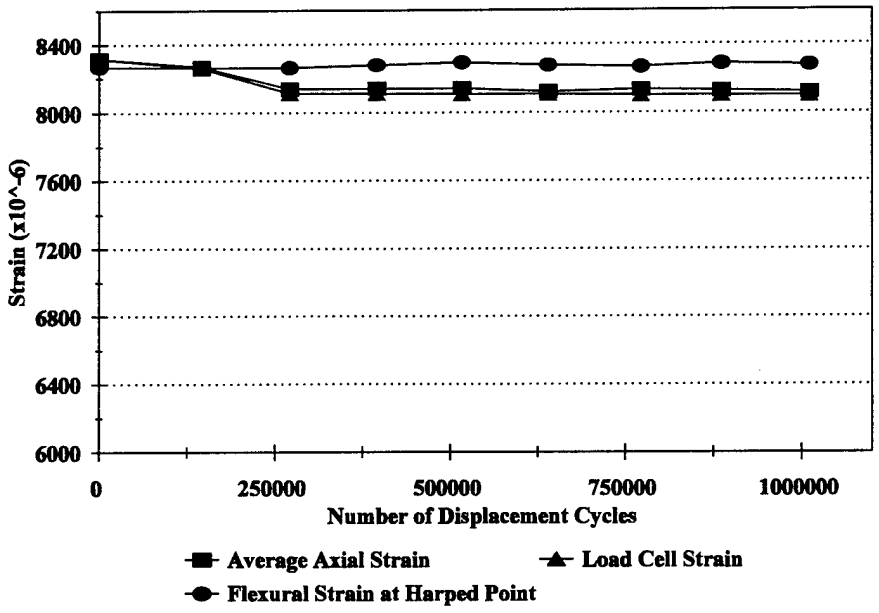

Figure 3.24 Fatigue test results for tendon F1

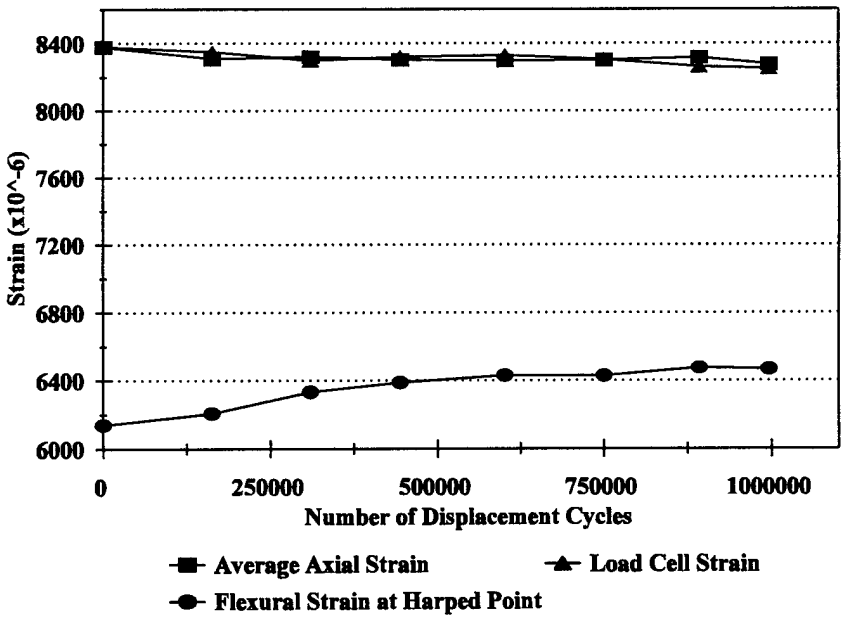

Figure 3.25 Fatigue test results for tendon F2

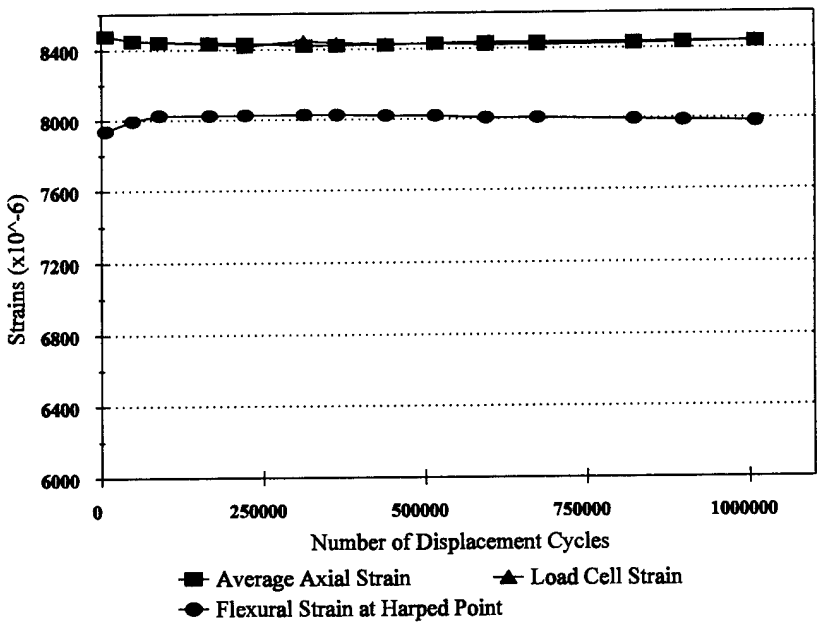

Figure 3.26 Fatigue test results for tendon F3

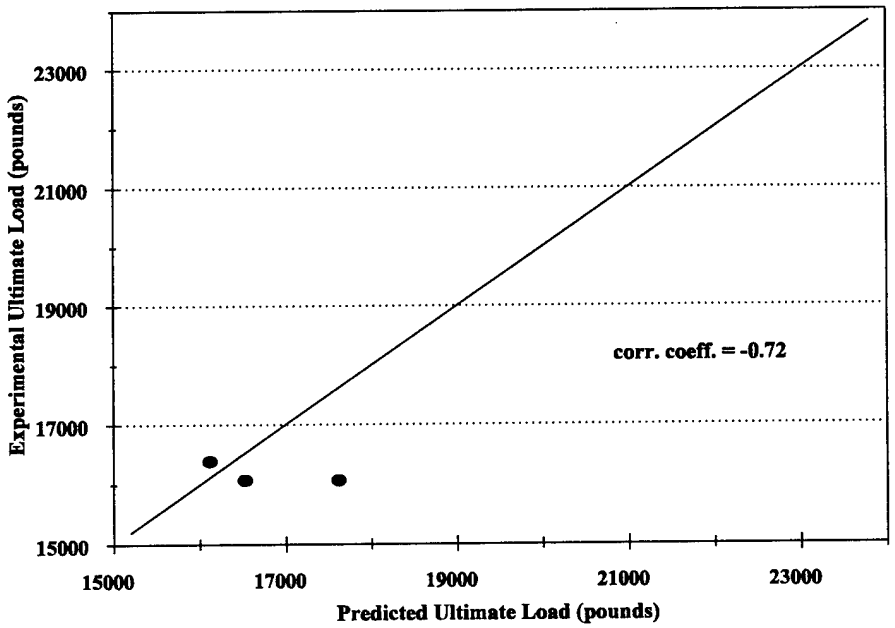

Figure 3.27 Comparison of experimental versus predicted failure loads for residual strength of tendons subjected to bending-tension fatigue

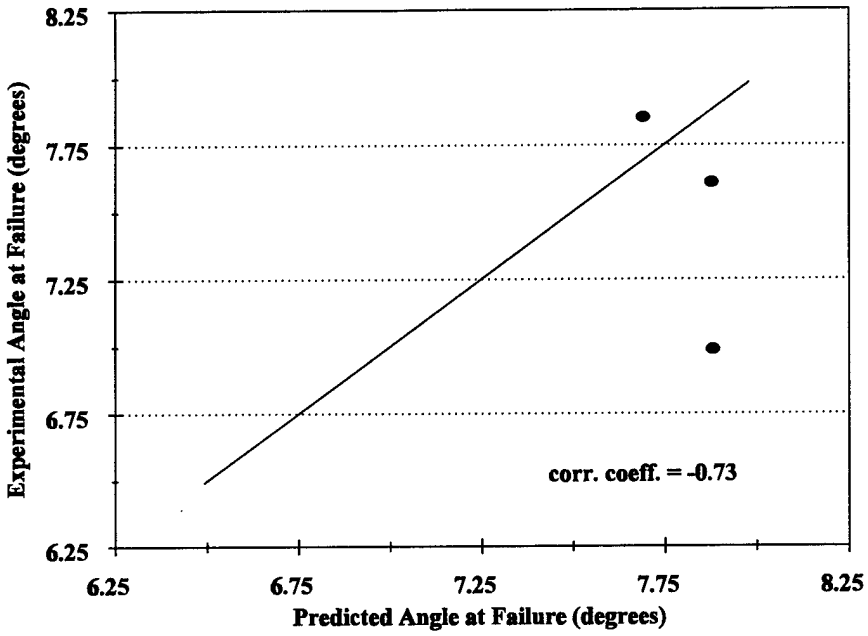

Figure 3.28 Comparison of experimental versus predicted bend angle at failure for residual strength of tendons subjected to bending-tension fatigue

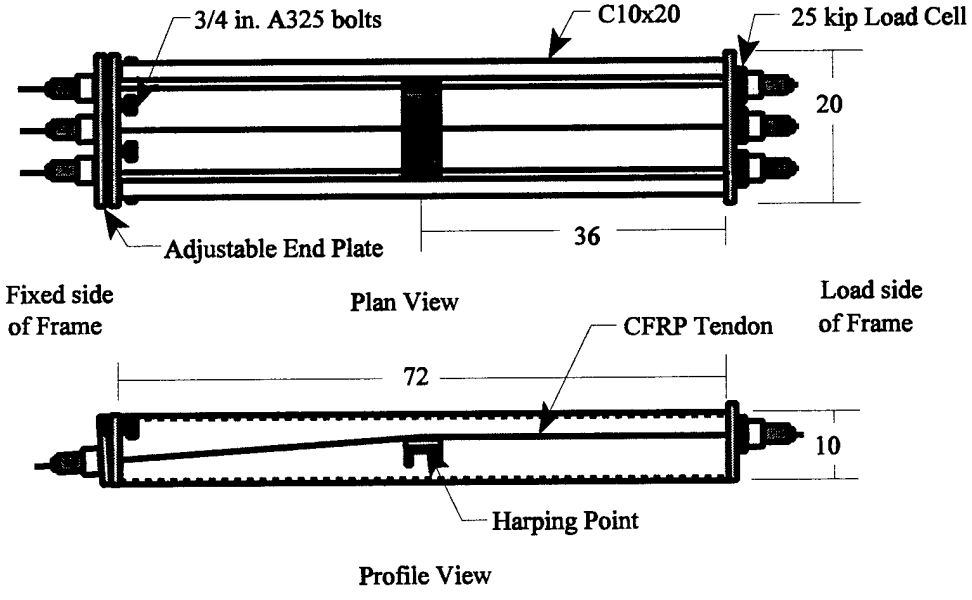

Figure 3.29 Test set-up for harped tendons subjected to sustained loading

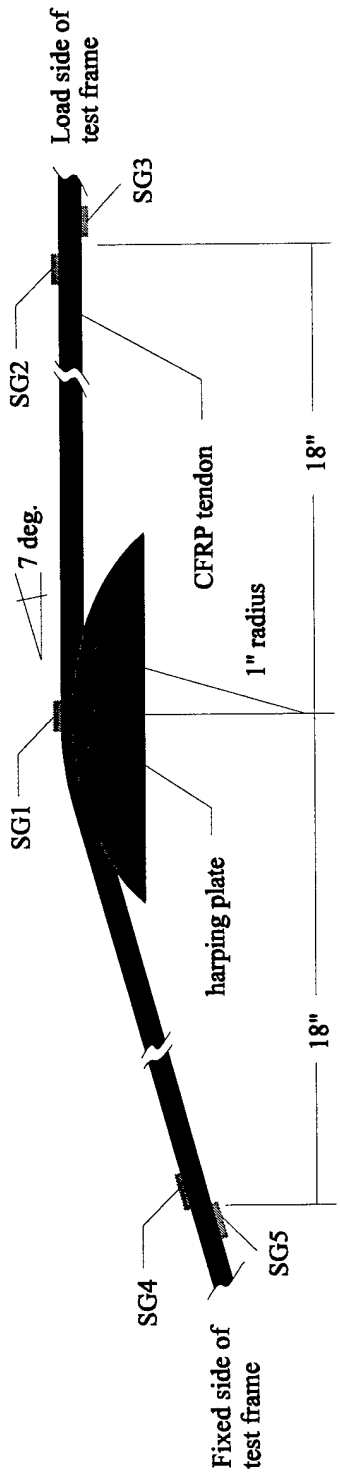

Figure 3.30 Location of strain gages for harped tendons subjected to sustained load

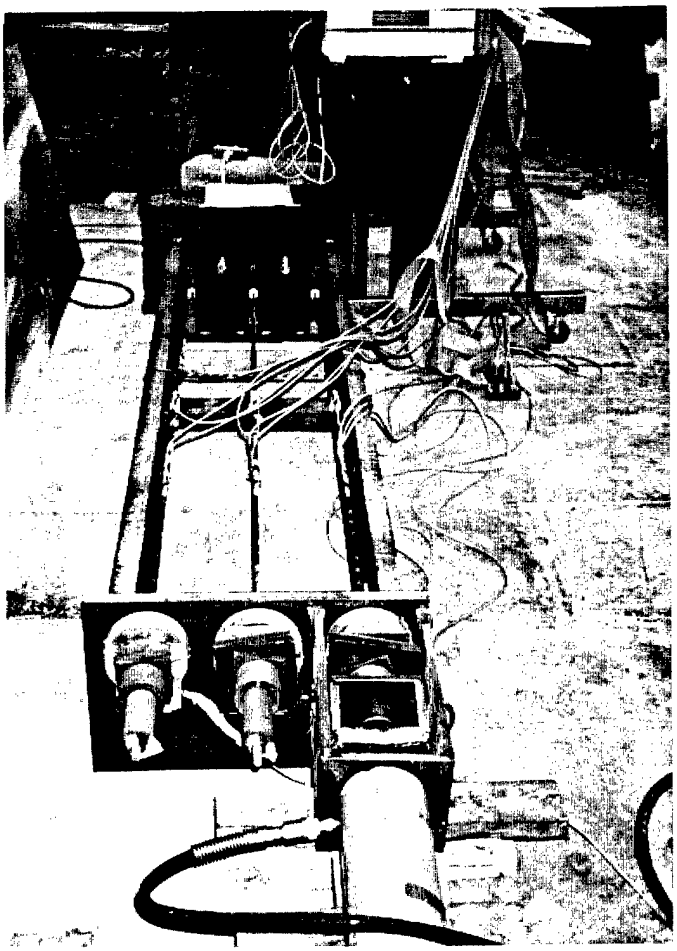

Figure 3.31a Photographic view of the test set-up for harped tendon subjected to sustained loading

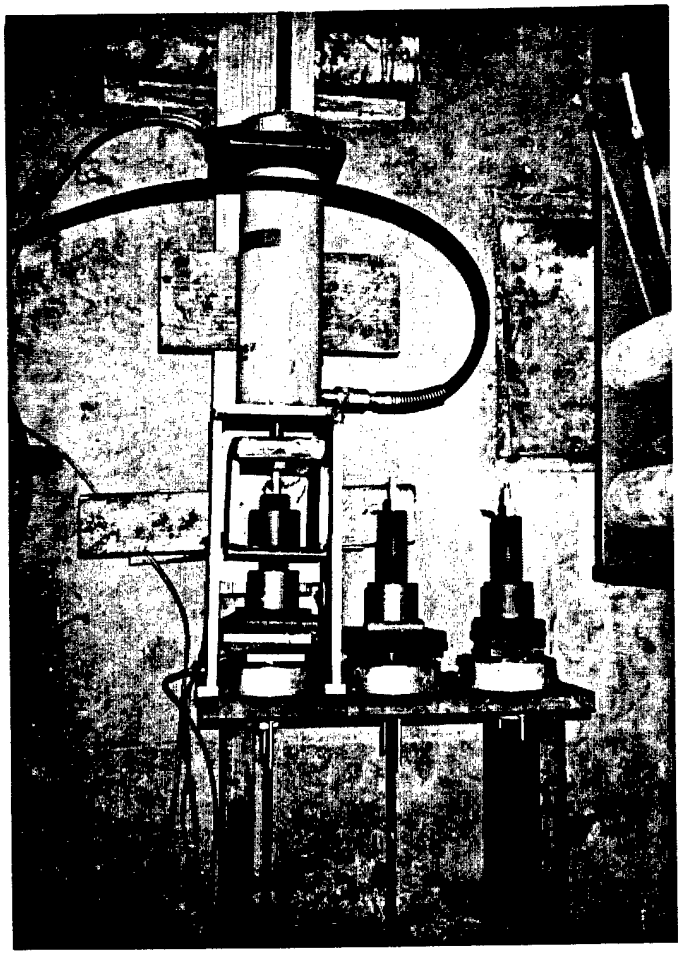

Figure 3.31b Photographic view of the test set-up of harped tendons subjected to sustained loading during tendon loading

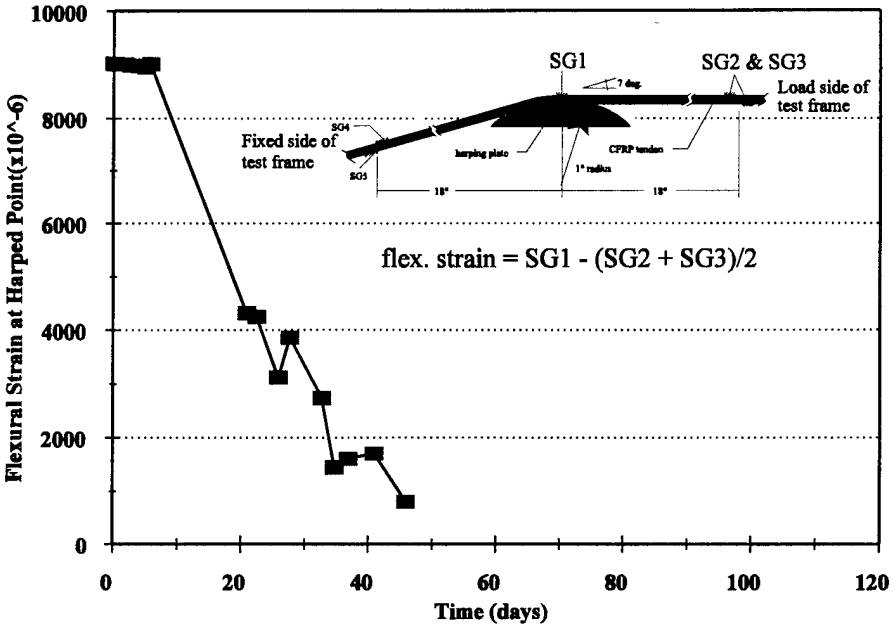

Figure 3.32 Variation of flexural strain at harped point for tendon S1

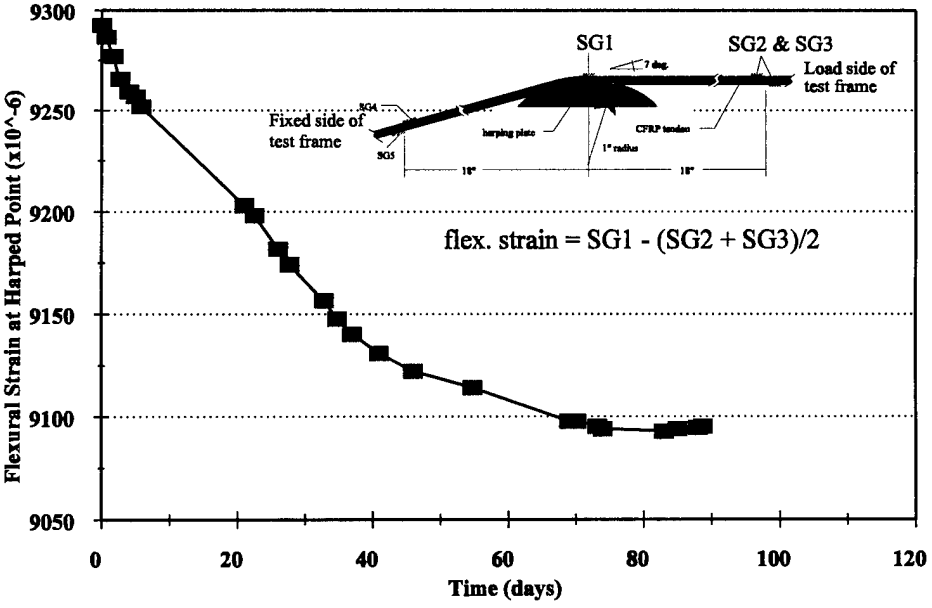

Figure 3.33 Variation of flexural strain at harped point for tendon S2

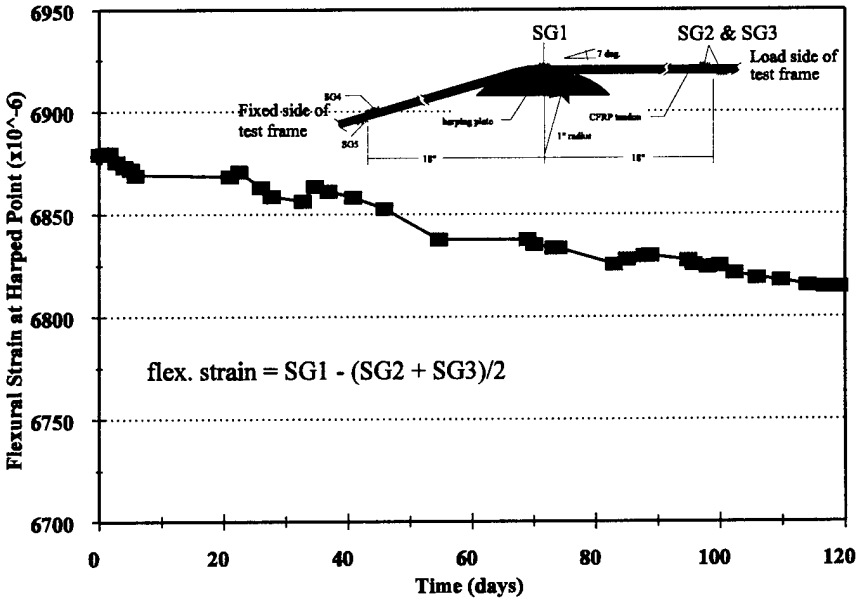

Figure 3.34 Variation of flexural strain at harped point for tendon S3

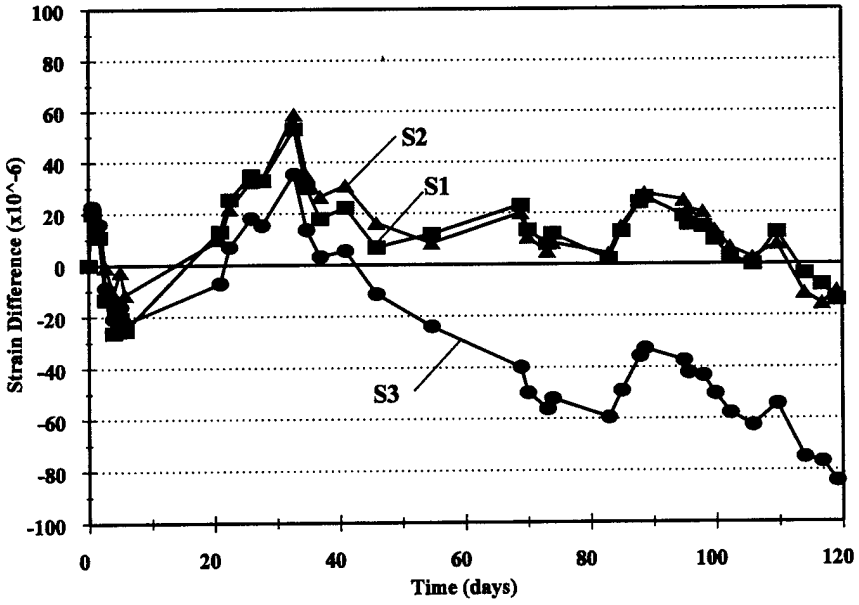

Figure 3.35 Variation in the difference between equivalent load cell strain and average axial strain for tendons S1, S2 and S3

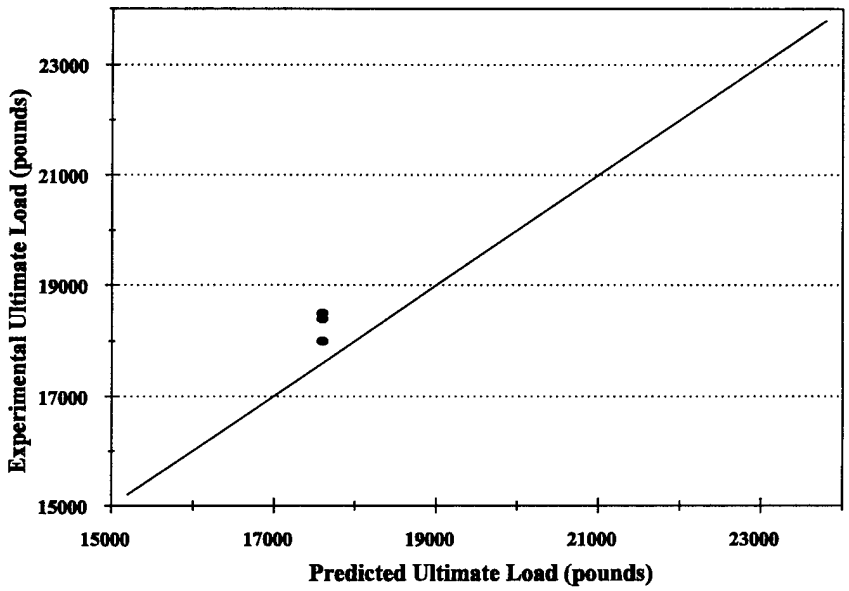

Figure 3.36 Comparison of experimental versus predicted failure loads for residual strength of harped tendons subjected to sustained axial load

CHAPTER 4

STEEL PRESTRESSED CONCRETE BEAMS STRENGTHENED WITH EXTERIOR POST-TENSIONED CFRP TENDONS

4.1 INTRODUCTION

The second objective of the research conducted in this study was to investigate the behavior of steel prestressed beams strengthened using exterior post-tensioned CFRP tendons. As partial fulfillment of that objective, this chapter discusses the laboratory testing of steel prestressed concrete beams that were strengthened using exterior post-tensioned CFRP tendons and development of an analytical model used in predicting the behavior of externally post-tensioned beams. Comparisons of laboratory test results with the predictions of the analytical model is also presented in this chapter.

The steel prestressed concrete beams that were externally post-tensioned using CFRP tendons were tested for three main purposes: to understand the strength and stiffness increases due to the CFRP tendon post-tensioning, to evaluate the ability of CFRP tendons to act as exterior post-tensioning tendons, and to provide experimental results for comparisons with predictions of an analytical model developed in this study.

Two sets of beams were fabricated and tested under the same conditions, except that one set of beams had twice the prestressing steel area and twice the effective prestress as compared to the other set of beams. The test program was designed to obtain results for fully prestressed beams that are externally strengthened by CFRP tendons and for prestressed beams that have partially lost prestressing force due to corrosion of steel tendons and therefore need restoration of the design strength.

The analytical model that was developed as a part of this study was included in a

computer program. The program, named EXPOST, is valid for rectangular, I-section and T-section beams which are simply supported and symmetrically loaded with two point loads. The program can incorporate reinforced and internally prestressed beams, both with or without compression reinforcement. Comparison between EXPOST results and the experimental results of this study show that EXPOST has good predictive capability. Comparisons between EXPOST results and experimental results of other researchers show that EXPOST is also capable of predicting behavior of reinforced concrete beams strengthened by exterior CFRP tendons.

4.2 EXPERIMENTAL RESULTS

This section describes the test specimen fabrication, describes the testing procedure, and presents the results of tests on six steel prestressed concrete beams. Of the six beams, four were externally post-tensioned with CFRP tendons and two were tested as control specimens without the externally post-tensioned CFRP tendons.

4.2.1 Specimen Fabrication

The target design parameters of the test specimens are shown in **Tables 4.1a** and **4.1b**. The cross-sectional details of the test beams prior to addition of external tendons are shown in **Figure 4.1**. A profile of the test specimens with the CFRP exterior tendons is shown in **Figure 4.2**. Each set of beams with three replicate beam specimens was fabricated from the same batch of concrete. The beams were fabricated within a 21 by 4 ft. (6.4 x 1.2 m) prestressing bed.

Prestressing tendons consisted of commercially available 1/2 in. (13 mm) diameter, seven wire steel prestressing strand with a nominal ultimate strength of 270 ksi (1860 MPa). Prior to stressing the steel tendons, two 0.125 in. (3.2 mm) gage strain gages were placed on each steel prestressing tendon at the midspan of the beams. Preparation of the gages included cleaning the strand with a degreasing solvent; sanding the steel with 400 grit sand paper; wet

abrading the wire with 400 grit sand paper and a mild acid conditioner; and cleaning the gage area with a neutralizer solution. Gages were affixed with an epoxy resin. After curing of the epoxy, electrical connections were soldered; exposed gage and wires were coated with polyurethane; and gages were covered with a malleable rubber-like material to ensure water-tightness.

Stressing of steel tendons was accomplished approximately 24 hours before casting of concrete. The tendons were stressed in parallel, for a total of three separate strands (B series beams) or six separate strands (C series beams). Strain gage readings were recorded using an Optim Megadac data acquisition system during stressing of the steel tendons. Data from these readings were eventually used to obtain a load-strain reading relationship for each tendon. The initial prestressing forces are listed in **Tables 4.2a** and **4.2b**.

Steel stirrups of #2 wires were provided as reinforcement in the shear span of the beams. Stirrups were placed at 8 in. (200 mm) spacing, excluding the center 36 in. (910 mm) of the beams. The stirrups were tied to the prestressing steel at the bottom of the stirrup and to two longitudinally placed #2 wires at the top of the stirrup. The longitudinally placed #2 wires provided minimal compression reinforcement and were neglected in analytical analysis.

Concrete was supplied by a commercial ready-mix company. The mix proportions are as listed in **Table 4.3**. After casting and finishing of beams, the beams were continuously wet and covered in plastic for seven days. The B series beams also included wet burlap under the plastic. After seven days, plastic and burlap were removed from the beams and the beams were left to air dry.

Five or six days after casting, DEMEC points were attached to one side of each beam at their midspan region. **Figure 4.2** shows the location of the DEMEC points. Four aluminum DEMEC points were placed 2.75 in. (70 mm) from the top of the beam and another four were placed 2.75 in. (70 mm) from the bottom of the beam. These locations corresponded to the location of the top #2 wires and the bottom prestressing steel. The points were spaced approximately 8 in. (200 mm) apart along the length of the beam and

were symmetric about the midspan of the beam. The DEMEC points were attached by a silicone adhesive for B series beams and by "super glue" for the C series beams. Initial DEMEC points readings were recorded prior to release of the prestressing tendons.

Seven days after casting, two 4 x 8 in. (102 x 203 mm) concrete cylinders were tested under uni-axial compression for strength. Since the results confirmed sufficient concrete strength for release of tendon forces, the steel prestressing tendons were released. Prestress release was accomplished by individually stressing the tendons in order to remove slotted shim plates located behind the tendon anchors. Removal of one or two shim plates released all force. After the release of force, the tendons were cut to within 1 in. (25 mm) of the concrete beam end.

DEMEC strain readings were taken immediately after the release of the tendons. DEMEC strain readings were also taken just prior to testing of each beam when the beam was simply supported at its ends. Compressive strains observed between these last DEMEC readings and those taken just prior to release of the prestressing tendons were strains associated with prestressing losses. Prestress losses at the time of testing were assumed to equal the stress losses associated with the observed strains from the DEMEC readings and estimated relaxation losses of the steel strand. Steel relaxation losses were based on the following formula [Lin and Burns, 1981]:

$$\frac{f_p}{f_{pi}} = 1 - \frac{\log t}{10}\left(\frac{f_{pi}}{f_{py}} - 0.55\right) \qquad (4.1)$$

where f_p = stress in tendons after relaxation
f_{pi} = initial stress in tendon prior to casting concrete
t = time after initial stressing in hours
f_{py} = yield stress of tendons

The effective prestressing force at the time of testing was calculated by subtracting the total prestress losses from steel relaxation and that recorded using the DEMEC points from

the initial prestress force. The initial prestress in the steel tendons, the prestress losses recorded using DEMEC points, the steel relaxation losses estimated using Equation 4.1, and the estimated effective prestressing for the steel tendons at the time of testing for each beam is listed in **Tables 4.2a** and **4.2b**.

For prestressed beams strengthened by external CFRP tendons, one CFRP tendon was placed on each side of the beam. Attachment of the CFRP tendons to the ends of the concrete beam was accomplished using a steel "saddle" as shown in **Figures 4.3a** and **4.3b**. The U-shaped saddles were made of 0.5 in. (13 mm) steel plates that fit across the ends of the concrete beam and were held in place by 0.5 in. (13 mm) diameter threaded rods. The threaded rods were at mid-height of the concrete beam, approximately 5 in. (127 mm) from the beam ends. Nuts were tightened on each end of the rods to secure the saddles. The U-shaped saddles had flanges extending outward from the sides of the beam from which the CFRP tendon anchorages were supported. The CFRP anchorages reacted against an unattached plate (Plate B, **Figure 4.3a**). The angle of the unattached plate was adjusted to ensure it was perpendicular with the post-tensioned CFRP tendon. A picture of the saddle and CFRP anchorage is shown in **Figure 4.3b**.

Harping of each of the CFRP tendons at the midspan of the beams was provided at two locations. The harping was provided using two 2 in. (51 mm) by 4 in. (102 mm) tubes extending along the bottom of the beam spaced 28 in. (710 mm) apart and symmetric about the midspan of the beam. Attached to the tubes were steel frames holding curved tendon harping plates. The harping plate attachment is shown in **Figure 4.4a**. A photographic view of the harping plate hardware is shown in **Figure 4.4b**. The harping plates were similar to harping plates used in the testing of CFRP tendons subjected to combined axial loads and harping (Chapter 3). The harping plates were manufactured from 0.75 in. (19 mm) thick aluminum plates, with a longitudinal radius of curvature of 20 in. (510 mm) and a 0.315 in. (8.0 mm) diameter semicircular groove along the longitudinal arch. The initial harping angle of the tendon at each harping point was 4.8 degrees.

4.2.2 Testing Procedure

Figure 4.2 shows a schematic diagram of the test set-up. For testing, the beams were centered under a 50 kip (220 kN) actuator that applied the vertical loads. Beam ends were supported on 8 in. (200 mm) wide pin and roller supports centered 6 in. (150 mm) from the beam ends. The resulting beam span was 204 in. (5180 mm). Pin and roller supports were also placed on top of the beam at the loading supports. Loading points were spaced 28 in. (710 mm) apart and were symmetric about the midpoint of the concrete beam. These top pin and roller supports supported a spreader beam that was loaded at its midpoint by the 50 kip (220 kN) actuator.

The beams had a shear span of 88 in. (2240 mm) and a constant moment region of 28 in. (710 mm). Curvature at the midspan of the beams was computed from readings of two Linear Voltage Displacement Transducers (LVDT), each attached to an aluminum frame. **Figures 4.5a** and **4.5b** illustrate the use of the aluminum frame and LVDTs. The use of the LVDTs allowed for measurement of longitudinal displacements between two points spaced 14 in. (360 mm) apart along the top and bottom of the beam. The beam curvature was calculated as the sum of the average top and bottom strains divided by the vertical distance between the two LVDTs. Average concrete strain of the midspan region was also determined using the readings from the two LVDTs.

Vertical deflections of the concrete beams were measured at two locations: midspan of the beams and at one of the two loading points (**Figure 4.5b**). Vertical displacements were measured using LVDT's reacting against aluminum angles attached along one side of the beams. The LVDT's had a capacity of 2 in. (51 mm) extension. As the limit of the vertical displacement LVDT's was reached, the testing was temporarily halted to reposition the LVDT's for recording additional displacements.

Figure 4.6 shows the location of strain gages which were mounted on the CFRP tendons. Strains of the CFRP exterior tendons were measured at the midspan by two 0.125 in. (3.2 mm) strain gages and along the sloped portion of the tendon by one 0.125 in. (3.2 mm) strain gage affixed to each tendon. Strains gages at midspan were spaced

approximately 6 in. (150 mm) apart. Strain gages on sloped portions were approximately midway between the tendon anchorage and the harping point on the post-tensioning end of the beam. Beam load readings were recorded as output from a load cell attached to the 50 kip (220 kN) actuator. Load, strain, and LVDT readings were recorded continuously throughout the test using an Optim Megadac data acquisition system.

Prior to post-tensioning of the CFRP tendons, the tendon harping points were greased. Post-tensioning was provided by temporarily anchoring the tendons to a spreader beam as shown in **Figures 4.7a** and **4.7b**. With the opposite end of the tendon anchored against the steel saddle, the spreader beam was jacked away from the beam by a 60 kip (270 kN) hydraulic ram. Axial forces on the tendons were measured by 25 kip (110 kN) load cells placed between the spreader beam and the temporary CFRP tendon anchorages. After loading the tendons to the appropriate post-tensioning force, separate anchors were tightened at the face of the steel end saddle. After the tendons were secured, the jacking force in the hydraulic ram was released. The post-tensioning hardware remained on the tendons throughout the testing of the beams.

Prior to testing, the magnitude of self-weight of the beam was obtained by placing a 25 kip (110 kN) load cell under one beam support. The resulting dead load was approximately 2300 pounds (10 kN) per beam, or 128 pounds per foot (1.87 kN/m). This corresponds to a unit weight of 144 pounds per cubic foot (22.6 kN/m^3). The weight of the steel loading supports and spreader beam was approximately 300 pounds (1.3 kN).

All tests were conducted under displacement control. Displacements were applied at a rate of approximately 0.2 in./min. (5 mm/min.). For each set of three beams, the first beam was not strengthened with CFRP. This beam was termed as the "control" beam. To simulate damaged beams in service, all beams were initially loaded to just beyond their cracking load and then unloaded to 4.3 kips (19 kN). This initial limit load for the beams was 8.3 kips (37 kN) and 14.3 kips (64 kN) for the B series beams and C series beams, respectively. For the control beams, after reducing the load to 4.3 kips (19 kN), the beam load was increased until crushing of the top concrete. For the strengthened beams, after reducing the load to

4.3 kips (19 kN), the CFRP tendons were post-tensioned. The deflection associated with the 4.3 kip (19 kN) load was maintained on the beam throughout the post-tensioning process. At the completion of post-tensioning, the vertical load on the beam increased due to the camber affect induced by post-tensioning. The load on the beam was again reduced to 4.3 kips (19 kN) before loading the beam to failure.

Concrete strength for the beam tests was estimated based on the compression strength of 4 x 8 in. (102 x 204 mm) concrete cylinders. For the B series beams, 3 companion cylinders were tested on the same day of the first beam test, which was 42 days after concrete casting. Another set of 3 concrete cylinders were tested three days after the last beam test, which was 56 days after casting. The average concrete strength for each set of 3 cylinders was 6.26 ksi (43.2 MPa) at 42 days after casting and 6.34 ksi (43.7 MPa) at 56 days after casting. Estimations of concrete strength at test age of the beam between 42 and 56 days was done by linearly interpolating between the average cylinder strengths at 42 and 56 days. The estimated concrete strength for B series beams are shown in **Tables 4.2a** and **4.2b**.

For the C series beams, 3 concrete cylinders were tested one day before the first beam test, which was 26 days after concrete casting. Another set of 3 concrete cylinders were tested one day after the last beam test, which was 40 days after casting. The average concrete strength for each set of 3 cylinders was 6.46 ksi (44.5 MPa) at 26 days after casting and 6.60 ksi (45.5 MPa) at 40 days after casting. Estimations of concrete strength at test age of the beam between 26 and 40 days was done by linearly interpolating between the average cylinder strengths at 26 and 40 days. The estimated concrete strength for C series beams are shown in **Tables 4.2a** and **4.2b**.

4.2.3 Test Results

This section provides a summary of the beam test results. Beams B-0 and C-0 were not post-tensioned and were tested as control specimens. Beams B-1, B-2, C-1 and C-2 were all similarly post-tensioned with external CFRP tendons. A summary of the test results for

the beam tests is presented in **Tables 4.4a** and **4.4b**. The test results include cracking load, ultimate load and corresponding midspan deflection, and the initial and final external tendon forces. Load-midspan deflection curves for the beam tests are shown in **Figures 4.8** and **4.9**. **Figures 4.10a** through **4.11c** show the midspan region of each beam after failure. Load values reported do not include the dead load due to beam weight, but do include the weight of the top roller supports and spreader beam. Zero deflection corresponds to the condition of the beam simply supported with a 0.3 kip (1.3 kN) load. The initial 0.3 kip (1.3 kN) load corresponds to the load due to the top roller supports and spreader beam. Additional details about specific beam behavior and beam component behavior are provided next.

4.2.3.1 Beam B-0

Beam B-0 was tested 42 days after casting. The average concrete strength was 6.3 ksi (43 MPa). The measured load-midspan deflection response of the beam is shown in **Figure 4.8**. Cracking of the beam initiated at a single crack at the midspan of the beam at a load of approximately 8.0 kips (36 kN). A second crack under one of the point loads was visible at a load of 8.3 kips (37 kN). The measured crack lengths were 10 in. (250 mm) at midspan and 4 in. (100 mm) under the point load. The cracks closed upon reduction of the beam load to 4.3 kips (19 kN). Upon reloading, the beam showed significantly lower stiffness after about 8 kips (35 kN). One additional crack appeared under the second point load at a load of about 9 kips (40 kN). The average crack spacing for the three cracks was about 14 in. (360 mm).

After a load of approximately 10 kips (44 kN), the midspan deflection of the beam increased rapidly with very little increase in load. Increase in midspan deflection appeared to result from widening of three cracks, with the midspan crack producing the largest width. At failure, the midspan crack width was estimated to be between 0.5 in. (13 mm) and 1 in. (25 mm). Failure of the beam was associated with crushing of concrete in the region above the crack near one of the load points. The average concrete strain at failure for the midspan

was found to be 0.00307. Failure of the beam was at a load of 11.5 kips (51.2 kN).

The reinforcing index for the beam section is defined by the following equation.

$$\omega_p = \frac{(A_{ps}\, f_{ps}) + T_{ps}}{b\, d\, f_c} \qquad (4.2)$$

where ω_p = reinforcing index
A_{ps} = cross-sectional area of prestressing steel
f_{ps} = the stress in prestressing steel at ultimate capacity of the section
T_{ps} = total force in external tendons at ultimate capacity of the section
b = width of compression face of member
d = depth of prestressing steel
f_c = concrete compressive strength

At failure, the prestressing steel strain was 0.030, which corresponds to a stress of 277 ksi (1910 MPa). For the control beams (B-0 and C-0), the value for T_{ps} is zero. The corresponding value of the beam section reinforcing index for beam B-0 was calculated based on Equation 4.2 to be 0.063.

4.2.3.2 *Beam B-1*

Testing of beam B-1 was accomplished at 45 days after casting. The average concrete strength was 6.3 ksi (43 MPa). The measured load-midspan deflection response of the beam is shown in **Figure 4.8**. At the initial limit load of 8.3 kips (37 kN), cracking was limited to a single midspan crack. The measured crack length was 10 in. (25 mm) from the bottom of the beam. Upon unloading, the crack in the beam closed.

Post-tensioning of the beam was accomplished in about 30 minutes. During post-tensioning (i.e. prior to securing tendon anchorages), the average force on the tendons were estimated as 15.29 kips (68.01 kN) for the sloped portion of the tendons and 15.05 kips (66.94 kN) for the midspan regions of the tendons. The forces in the tendons at the completion of post-tensioning were 13.7 and 12.7 kips (60.9 and 56.5 kN). These forces were computed from the measured strain readings obtained from strain gages on the tendons.

Because midspan deflection was held constant during the post-tensioning process, the load on beam B-1 was 3.4 kips (15 kN) higher after post-tensioning than the initial load of 4.3 kips (19 kN) at the start of post-tensioning. Reduction of the load to 4.3 kips (19 kN) resulted in a midspan deflection of -0.05 in. (1.2 mm). This reduction in midspan deflection accounted for 68% of the initial deflection of the beam. During the external post-tensioning of the CFRP tendons, the strains in the prestressing steel tendons reduced an average of 290 microstrain. After the reduction in load to 4.3 kips (19 kN), the increased camber of the beam reduced tendon forces by an average of 75 pounds (0.33 kN). The initial force for the external tendons reported in **Table 4.4a** and **4.4b** are those corresponding to a load of 4.3 kips (19 kN) on the beam.

Opening of existing cracks for beam B-1 did not take place until the beam loads were approximately 14 kips (62 kN). Two additional cracks appeared along the outside edge of the harping point supports (i.e. opposite side from the midspan) at about 15 kips (67 kN). Additional deflection of the beam resulted largely due to widening of the three cracks in the beam, with the original midspan crack maintaining a larger width than the other two cracks. At a load of about 20 kips (89 kN), two additional cracks appeared approximately 28 in. (710 mm) on each side of the midspan of the beam. Cracks were spaced an average distance of 14 in. (360 mm).

Figure 4.12 shows the variation of the force in the external CFRP tendon #1 with increase in the beam load. The response of tendon #2 for beam B-1 was similar. Increases in CFRP tendon forces were similar whether the sloped or midspan regions of the tendons were considered. The increase in CFRP tendon force was approximately linear between beam loads of 4.3 and 13 kips (19 and 58 kN). After a beam load of about 13 kips (58 kN), the CFRP tendon force increased at an increasing rate until failure of the beam.

Figure 4.13 shows the variation in tendon forces with the midspan deflection of the beam. Increases in tendon forces were proportional to increases in midspan deflection. It is unclear why the force for tendon #2 dropped at a midspan deflection of about 2 in. (51 mm). This may be an indication of slippage of the tendon at the grips, however, no

slippage was observed during testing. The slight non-linearity in CFRP tendon force increase at the midspan deflection of about 2.8 in. (71 mm) is likely the result of the crushing of the concrete at failure, resulting in an overall shortening of the concrete beam.

Failure of beam B-1 took place after the center crack extended to within 2 in. (51 mm) from the top of the concrete. Crushing of concrete in the region above this crack defined failure for the beam. The average concrete strain at failure of the externally post-tensioned prestressed concrete beam was measured to be 0.00255. At the ultimate load of the beam, CFRP tendon forces were 19.7 and 18.4 kips (87.6 and 81.8 kN) for tendons #1 and #2, respectively. The increase in tendon forces was 11.7 kips (52.0 kN), which was an increase of 44% from the initial force in the CFRP tendon (**Tables 4.4a** and **4.4b**).

At failure, the prestressing steel strain was 0.0246, which corresponds to a stress of 276 ksi (1900 MPa). The value of T_{ps} was 38.1 kips (169 kN) (**Tables 4.4a** and **4.4b**). The corresponding value of the beam section reinforcing index for beam B-1 was calculated based on Equation 4.2 to be 0.12.

4.2.3.3 *Beam B-2*

Testing of beam B-2 was accomplished at 53 days after casting. The average concrete strength was 6.3 ksi (43 MPa). The measured load-midspan deflection response of the beam is shown in **Figure 4.8**. Initial behavior of the beam prior to strengthening with CFRP tendons was similar to the behavior of beam B-1. At the initial limit load of 8.3 kips (37 kN), cracking was limited to a single crack at midspan. The measured crack length was 8 in. (200 mm). Upon unloading, the crack in the beam closed.

Post-tensioning of the beam was accomplished in about 30 minutes. During post-tensioning, the average force on the tendons were estimated as 15.10 kips (67.16 kN) for the sloped portion of the tendons and 14.62 kips (65.03 kN) for the midspan regions of the tendons. The forces in the tendons at the completion of post-tensioning were 14.6 and 14.0 kips (64.9 and 62.3 kN). These forces were computed from the measured strain

readings obtained from strain gages on the tendons.

Because midspan deflection was held constant during the post-tensioning process, the load on beam B-2 was 4.2 kips (19 kN) higher after post-tensioning than the initial load of 4.3 kips (19 kN) at the start of post-tensioning. Reduction of the load to 4.3 kips (19 kN) resulted in a midspan deflection of -.06 in. (1.5 mm). This reduction in midspan deflection accounted for 89% of the initial deflection of the beam. During the external post-tensioning of the CFRP tendons, the strains in the prestressing steel tendons reduced an average of 279 microstrain. After the reduction in loads to 4.3 kips (19 kN), the increased camber of the beam reduced tendon forces by an average of 110 pounds (0.49 kN). The initial force for the external tendons reported in **Table 4.4a** and **4.4b** are those corresponding to a load of 4.3 kips (19 kN) on the beam.

Opening of existing cracks for beam B-2 did not take place until beam loads were approximately 14 kips (62 kN). Two additional cracks appeared along the outside edge of the harping point supports at about 15 kips (67 kN). Additional deflection of the beam resulted largely due to widening of the three cracks in the beam, with the original midspan crack maintaining a larger width than the other two cracks. At failure, a total of six cracks were visible on the beam. The cracks were spaced an average distance of 13 in. (330 mm).

The response of the exterior CFRP tendons was similar to the response observed for beam B-1. Increases in CFRP tendon forces were similar whether the sloped or midspan regions of the tendons were considered. The increase in CFRP tendon force was approximately linear between beam loads of 4.3 and 13 kips (19 and 58 kN). After a beam load of about 13 kips (58 kN), the CFRP tendon force increased at an increasing rate until failure of the beam. Increases in tendon forces was proportional to increase in midspan deflection.

Failure of beam B-2 took place after the center crack extended to within about 2 in. (51 mm) from the top of the concrete. Crushing of concrete in the region above this crack defined failure for the beam. The average concrete strain at failure for the midspan was found to be 0.00311. At the ultimate load of the beam, CFRP tendon forces were 20.4 and

19.8 kips (90.7 and 88.1 kN) for tendon #1 and #2, respectively. The increase in tendon forces was 11.6 kips (51.6 kN), which was an increase of 41% from the initial force in the CFRP tendon (**Tables 4.4a** and **4.4b**).

At failure, the prestressing steel strain was 0.0220, which corresponds to a stress of 275 ksi (1900 MPa). The value of T_{ps} was 40.2 kips (179 kN) (**Tables 4.4a** and **4.4b**). The corresponding value of the beam section reinforcing index for beam B-2 was calculated based on Equation 4.2 to be 0.12.

4.2.3.4 *Beam C-0*

Beam C-0 was tested 27 days after casting. The average concrete strength was 6.5 ksi (45 MPa). The measured load-midspan deflection response of the beam is shown in **Figure 4.9**. Cracking of the beam initiated at a single crack at the midspan of the beam at a beam load of approximately 12.5 kips (56 kN). At a beam load of 14.3 kips (64 kN), three cracks were visible at an average distance of 14.5 in. (370 mm). The measured crack lengths were 10 in. (250 mm) at midspan and 5.5 in. (140 mm) for the outer cracks. The cracks closed upon reduction of the beam load to 4.3 kips (19 kN). Upon reloading, the beam showed significantly lower stiffness after about 15 kips (67 kN). At failure, a total of seven flexural cracks were visible. The average crack spacing for the cracks was 12.5 in. (318 mm).

After a load of approximately 15 kips (67 kN), the midspan deflection of the beam increased rapidly with very little increase in load. At failure, the midspan crack and one adjacent crack had significantly larger widths than all other cracks. Increase in midspan deflection appeared to result mostly from widening of these two cracks. Failure of the beam was associated with crushing of the concrete in the region above the crack near on of the load points. The average concrete strain at failure for the midspan was found to be 0.00339. Failure of the beam was at a load of 22.2 kips (98.7 kN).

At failure, the prestressing steel strain was approximately 0.02, which corresponds to

a stress of 274 ksi (1890 MPa). Since there was no external tendons, the value of T_{ps} was zero. The corresponding value of the beam section reinforcing index for beam C-0 was calculated based on Equation 4.2 to be 0.12.

4.2.3.5 *Beam C-1*

Testing of beam C-1 was accomplished at 33 days after casting. The average concrete strength was 6.5 ksi (45 MPa). The measured load-midspan deflection response of the beam is shown in **Figure 4.9**. At the initial limit load of 14.3 kips (63.6 kN), cracking was limited to three cracks at midspan. The crack spacing averaged 15 in. (380 mm). The measured crack lengths were 9 in. (230 mm) at midspan and 3.5 in. (89 mm) for the outer cracks. Again, upon unloading, the crack in the beam closed.

Post-tensioning of the beam was accomplished in about 30 minutes. During post-tensioning, the average force on the tendons were estimated as 15.56 kips (69.21 kN) for the sloped portion of the tendons and 14.94 kips (66.45 kN) for the midspan regions of the tendons. The forces in the tendons at the completion of post-tensioning were 14.6 and 14.3 kips (64.9 and 63.6 kN). These forces were computed from the measured strain readings obtained from strain gages on the tendons.

Because midspan deflection was held constant during the post-tensioning process, the load on beam C-1 was 4.5 kips (20 kN) higher after post-tensioning than the initial load of 4.3 kips (19 kN) at the start of post-tensioning. Reduction of the load to 4.3 kips (19 kN) resulted in a midspan deflection of -0.06 in. (1.5 mm). This reduction in midspan deflection accounted for 75% of the initial deflection of the beam. During the external post-tensioning of the CFRP tendons, the strains in the prestressing steel tendons reduced an average of 214 microstrain. After the reduction in load to 4.3 kips (19 kN), the increased camber of the beam reduced tendon forces by an average of 150 pounds (0.67 kN). The initial force for the external tendons reported in **Table 4.4a** and **4.4b** are those corresponding to a load of 4.3 kips (19 kN) on the beam.

Opening of existing cracks for beam C-1 did not take place until the beam load was approximately 18 kips (80 kN). Additional deflection of the beam resulted largely due to widening of the three cracks in the beam, with the crack at midspan maintaining the largest width. At beam loads above about 20 kips (89 kN), additional cracks started to appear. At failure, 7 flexural cracks were evident. The cracks were spaced approximately 15 in. (380 mm) for the three cracks at midspan and 8.5 in. (220 mm) for the remaining outer cracks.

Figure 4.14 shows the variation of the force in the external CFRP tendon #1 with the increase in the beam load. The response of tendon #2 for beam C-1 was similar. Increases in CFRP tendon forces were similar whether the sloped or midspan regions of the tendons were considered. The increase in CFRP tendon force increased was approximately linear between beam loads of 4.3 and 22 kips (19 and 98 kN). After a beam load of about 22 kips (98 kN), the CFRP tendon forces increased at a faster rate until failure of the beam.

Figure 4.15 shows the variation in tendon forces with the midspan deflection. The increases in tendon forces was proportional to the increase in midspan deflection.

Failure of beam C-1 took place after the center crack extended to within 2 in. (51 mm) from the top of the concrete. Crushing of concrete in the region above this crack defined failure for the beam. The average concrete strain at failure for the midspan was found to be 0.00321. At the ultimate load of the beam, CFRP tendon forces were 18.5 and 18.4 kips (82.3 and 81.8 kN) for tendons #1 and #2, respectively. The increase in tendon force was 8.1 kips (36 kN), which was an increase of 28% from the initial force in the CFRP tendon (**Tables 4.4a** and **4.4b**).

At failure, the prestressing steel strain was approximately 0.013, which corresponds to a stress of 271 ksi (1870 MPa). The value of T_{ps} was 36.9 kips (164 kN) (**Tables 4.4a** and **4.4b**). The corresponding value of the beam section reinforcing index for beam C-1 was calculated based on Equation 4.2 to be 0.17.

4.2.3.6 *Beam C-2*

Testing of beam C-2 was accomplished at 39 days after casting. The average concrete strength was 6.6 ksi (46 MPa). The measured load-midspan deflection response of the beam is shown in **Figure 4.9**. Initial behavior of the beam prior to strengthening with CFRP tendons was similar to the behavior of beam C-1. At the initial limit load of 14.3 kips (63.6 kN), cracking was limited to three cracks at midspan. The crack spacing averaged 18 in. (460 mm). The measured crack lengths were 8 in. (200 mm) at midspan and 3.5 in. (89 mm) for the outer cracks. Upon unloading, the cracks in the beam closed.

Post-tensioning of the beam was accomplished in about 30 minutes. During post-tensioning, the average forces on the tendons were estimated as 15.08 kips (67.08 kN) for the sloped portion of the tendons and 14.78 kips (65.74 kN) for the midspan regions of the tendons. The forces in the tendons at the completion of post-tensioning were 14.0 and 13.8 kips (62.3 and 61.4 kN). These forces were computed from the measured strain readings obtained from strain gages on the tendons.

Because midspan deflection was held constant during the post-tensioning process, the load on beam C-2 was 4.0 kips (18 kN) higher after post-tensioning than the initial load of 4.3 kips (19 kN) at the start of post-tensioning. Reduction of the load to 4.3 kips (19 kN) resulted in a midspan deflection of -0.05 in. (1.4 mm). This reduction in midspan deflection accounted for 71% of the initial deflection of the beam. During the external post-tensioning of the CFRP tendons, the strains in the prestressing steel tendons reduced an average of 181 microstrain. After the reduction in load to 4.3 kips (19 kN), the increased camber of the beam reduced tendon forces by an average of 110 pounds (0.49 kN). The initial force for the external tendons reported in **Table 4.4a** and **4.4b** are those corresponding to a load of 4.3 kips (19 kN) on the beam.

Opening of existing cracks for beam C-2 did not take place until loads were approximately 18 kips (80 kN). Additional deflection of the beam resulted largely due to widening of the three cracks in the beam, with the original midspan crack maintaining a

larger width than the other two cracks. At a load of about 20 kips (89 kN), additional cracks started to appear. At failure, 8 flexural cracks were evident. The cracks were spaced approximately 14 in. (360 mm) for the three cracks at midspan and 9 in. (230 mm) for the remaining outer cracks.

The response of the exterior CFRP tendons was similar to the response observed for beam C-1. Increases in CFRP tendon forces were similar whether the sloped or midspan regions of the tendons were considered. The increase in CFRP tendon force was approximately linear between beam loads of 4.3 and 22 kips (19 and 98 kN). After a beam load of about 22 kips (98 kN), the CFRP tendon force increased at an increasing rate until failure of the beam. Increases in tendon forces was proportional to increases in midspan deflection.

Failure of beam C-2 took place after the center crack extended to within about 2 in. (50 mm) from the top of the concrete. Crushing of concrete in the region above this crack defined failure for the beam. The average concrete strain at failure for the midspan was found to be 0.00322. At the ultimate load of the beam, CFRP tendon forces were 18.0 and 18.3 kips (80.1 and 81.4 kN) for tendon #1 and #2, respectively. The increase in tendon forces was 8.5 kips (37.8 kN), which was an increase of 31% from the initial force in the CFRP tendon.

At failure, the prestressing steel strain was approximately 0.013, which corresponds to a stress of 271 ksi (1870 MPa). The value of T_{ps} was 36.3 kips (161 kN) (**Tables 4.4a** and **4.4b**). The corresponding value of the beam section reinforcing index for beam C-2 was calculated based on Equation 4.2 to be 0.17.

4.2.4 Discussion of Test Results

4.2.4.1 *Friction at Harping Points*

During post-tensioning, at the maximum tensioning load, the ratio of the CFRP tendon force at midspan versus the CFRP tendon force at the sloped portion was estimated based on tendon strain readings. These ratios were calculated to be: 0.980, 0.988, 0.981, 0.950, 0.966, 0.954, 0.981 and 0.981. Using the equation for friction losses across a harping point stated in Chapter 3 (Eq. 3.9), the value of the friction coefficient, μ, for each of these force ratios was calculated to be 0.24, 0.14, 0.23, 0.61, 0.42, 0.57, 0.23, and 0.23. These friction coefficients were calculated with a bend angle, θ, equal to 0.084 radians (4.8 degrees). The average value of μ is 0.33. The median value of μ is 0.235. It is observed that both the average and median values of μ are greater than that recommended by the ACI 318-95 code for unbonded steel tendons [ACI Committee 318, 1995]. This code suggest friction coefficients for unbonded steel tendons to be between 0.05 and 0.15.

4.2.4.2 *Beam Stiffness and Load Deflection Response*

For the B series beams, the unstrengthened beam stiffness was 60 kips/in. (11 kN/mm) between the beam loads of 4 and 7 kips (18 and 31 kN). During unloading, the stiffness averaged 36 kips/in. (6.3 kN/mm). Upon reloading, the stiffness of B-0 between a load of 4 and 7 kips (18 and 31 kN) was 31 kips/in. (5.4 kN/mm) and the average for B-1 and B-2 was 86 kips/in. (15 kN/mm). Between beam loads of 4 and 7 kips (18 and 31 kN), the externally CFRP post-tensioned beams exhibited an increase in beam stiffness of 43% over the original uncracked beam stiffness and 177% over the cracked beam stiffness.

For the C series beams, the unstrengthened beam stiffness was 65 kips/in. (11 kN/mm) between the beam loads of 4 and 8 kips (18 and 36 kN). During unloading, the stiffness averaged 46 kips/in. (8.1 kN/mm). Upon reloading, the stiffness of C-0 between a load of 4 and 8 kips (18 and 36 kN) was 63 kips/in. (11 kN/mm) and the average for C-1 and C-2

was 80 kips/in. (25 kN/mm). Between beam loads of 4 and 8 kips (18 and 36 kN), the externally CFRP post-tensioned beams exhibited an increase in beam stiffness of 23% over the original uncracked beam stiffness and 27% over the cracked beam stiffness.

All of the externally post-tensioned beams maintained a positive tangential stiffness up to failure. This behavior is unlike that found for beam B-0, and to a lesser extent beam C-0, which showed virtually a horizontal load-midspan deflection response prior to failure. **Tables 4.5a** and **4.5b** summarize information concerning beam stiffness at failure. Over the increase in load of about 0.5 kips (2.2 kN) prior to failure, the tangential stiffness of the exterior post-tensioned beams averaged 682 lbs/in. (0.119 kN/mm) greater than the companion unstrengthened beams.

Figure 4.16a shows a schematic diagram of the beams tested in this study with the external CFRP tendons replaced with their associated forces. The total force acting upward at the harping points of the external CFRP tendons was calculated as:

$$\mathbf{P_{hp} = 2\ T_{FRP}\ \sin(\theta)} \qquad \mathbf{(4.3)}$$

where P_{hp} = total force acting upward at the harping points of the external CFRP tendons
T_{FRP} = force in both CFRP tendons
θ = $\tan^{-1}\{(\delta_o + \delta_{hp})/(l_{slope})\}$
δ_o = initial vertical displacement of CFRP tendon at midspan (7.3 in.)
δ_{hp} = harping point displacement due to beam deflection
l_{slope} = horizontal length of sloped portion of tendon (88 in.)

Figure 4.16b shows a schematic diagram of the beams tested in this study with the external CFRP tendons replaced with their associated forces but with the upward acting forces at the harping points subtracted from the beam point loads. The value of the total point loads applied to the beams minus the total upward acting forces at the harping points is defined as P_r.

In **Figures 4.17** and **4.18**, the load-midspan deflection response of beams B-0 and B-1

and of beams C-0 and C-1 are shown, respectively. The response for beams B-1 and C-1 with the beam load, (P), replaced by the load P_r is also shown in **Figures 4.17** and **4.18**, respectively. It is evident from **Figures 4.17** and **4.18** that at failure, the positive tangential stiffness observed for beams B-1 and C-1 is due to the force acting upward at the harping points due to the external CFRP tendons.

The predicted tangential stiffness of the beams due only to the upward force at harping points at failure averaged 720 lbs/in. (0.13 kN/mm) for beams B-1, B-2, C-1 and C-2. This stiffness is the ratio of the increase in upward acting forces at the harping points, computed using Equation 4.3, and the increase in midspan deflection at failure. The predicted value of 720 lbs/in. (0.13 kN/mm) is close to the average increase in stiffness of 682 lbs/in. (0.119 kN/mm) observed in the tests for the strengthened beams at failure compared to companion unstrengthened beams at failure.

4.2.4.3 *Ultimate Load and Midspan Deflection*

The ultimate load of the strengthened beams was 209% and 149% of the companion unstrengthened control beams for B series and C series beams, respectively (**Tables 4.4a** and **4.4b**). The absolute increases in ultimate loads averaged 12.5 and 10.9 kips (56.0 and 48.5 kN) for B series and C series beams, respectively (**Tables 4.4a** and **4.4b**). The larger percentage increase for B series beams is due in a large part to the relatively lower strength of control beam B-0. The greater quantitative increase in strength of the B series beams is likely due to the larger deflection at failure for the B series beams compared to the C series beams. The larger deflection at failure allowed for a larger contribution to strength by the external tendons due to the associated larger load increase in the external tendons and the larger increase in the harping angle of the external tendons.

Average midspan deflection at ultimate load for the strengthened beams was smaller than the deflection for the companion unstrengthened control beams (**Tables 4.4a** and **4.4b**). The average midspan deflection at ultimate load for the strengthened beams were 63% and 65% of the deflection of the companion unstrengthened beams for B series and C series

beams, respectively (**Tables 4.4a** and **4.4b**).

4.3 ANALYTICAL MODEL

An analytical model was developed to predict the behavior of the prestressed beams strengthened by external post-tensioned tendons. The model was included in a computer program called EXPOST. The program was written with Fortran77 format. An algorithm for the computer program EXPOST is presented in Appendix A. Details concerning the analysis can be found in the review of the computer program statements listed in Appendix B. The computer program is valid for rectangular, I-section and T-section beams simply supported and symmetrically loaded with two point loads. The program assumes plane sections remain plane and strain compatibility between concrete and steel. The program can incorporate reinforced and internally prestressed beams, both with or without compression reinforcement. The following sections describe the material, beam sectional, and beam member modelling used in computer program EXPOST.

4.3.1 Material Modelling

The computer program EXPOST requires stress-strain relationships for four materials: concrete, non-prestressed steel reinforcement, prestressing steel tendons, and FRP tendons. A schematic stress-strain curve of the concrete used in program EXPOST is shown in **Figure 4.19**. Schematic stress-strain curves of the CFRP tendon, prestressing steel, and non-prestressed steel reinforcement used in program EXPOST is shown in **Figure 4.20**.

For the concrete relationship, a constitutive model developed by Ahmad is used [Ahmad, 1986]. For the concrete used in this research, the concrete compressive strength, based on compression tests of 4 in. (102 mm) by 8 in. (203 mm) cylinders, was 6.3 to 6.6 ksi (43 to 46 MPa). The tensile rupture stress is defined to be equivalent to $7.5\sqrt{f_c'}$ (f_c' in psi). The ultimate concrete strain used was the ultimate concrete strain found from beam tests of this study. This strain was found to average 0.0032.

The non-prestressed reinforcing steel stress-strain relationship was modelled as a bi-linear relationship. The model calculates the steel yield strain as the steel yield stress divided by the steel elastic modulus. For strains below the steel yield strain, the stress in the steel is assumed to equal the steel elastic modulus times the steel strain. The steel elastic modulus and yield stress are read into the program as inputs.

The prestressing steel properties were modelled using the steel strand information provided by the strand supplier. The stress-strain relationship for the steel is modelled linearly up to yielding of the steel and linearly during strain hardening prior to failure. A forth order polynomial expression was developed to represent yielding. The ultimate strength of the steel tendons was listed by the manufacturer as 289 ksi (1990 MPa).

The CFRP tendons are considered as perfectly elastic. Axial forces in the CFRP tendons are assumed to be uniform along the entire length of the tendons (i.e. no friction at the harping points).

4.3.2 Beam Sectional Modeling

The influence of external tendons on the behavior of the concrete beam is treated separately from the behavior of the other beam constituents. The curvatures and deflections of the beam are determined based on the effective moment and curvature on the steel reinforced or prestressed beam only. The effective moment is therefore the moment existing on the beam minus the moment due to upward forces at the external tendon harping points. The segment curvatures do incorporate the effect of the increased axial load placed on the concrete member due to the external tendons.

Beam segment cross-section stress and strain distributions are determined by first discritizing the cross-section into a prescribed number of layers. Stresses and strains for each layer are combined to represent the entire cross-section behavior. Initial, non-post-tensioned beam stresses and strains are calculated based on the effective steel stress and the material properties. It is recognized that since cross-section geometry and reinforcement, excluding

the external FRP tendons, do not change along the beam, the moment-curvature relationship of the concrete-steel cross-section is unchanged among segments with the same crack condition (i.e. cracked or not cracked) and externally applied axial force from the FRP tendons. To minimize computational effort, a new moment-curvature relationship is calculated only when cracking conditions or external axial forces change.

The effective moment-curvature relationship is determined by first assuming a concrete strain at the top fiber of the beam equivalent to the concrete tensile rupture strain. The neutral axis for the beam is then adjusted such that the sum of the axial forces due to concrete stresses, steel stresses, and external FRP tendons are zero. For this neutral axis and strain distribution, the required sectional moment is calculated at the height of the exterior post-tensioning anchorage. This process is repeated for incrementally increasing concrete strains at the top fiber of the beam until the ultimate concrete strain is reached. The curvature associated with ultimate concrete strain is the maximum allowable curvature.

Once the sectional moment-curvature relationship is determined, the average segment curvature for any given effective moment on the segment can be interpolated from the moment-curvature relationship. If the effective moment on the beam exceeds the maximum moment found for the moment-curvature relationship, the curvature of the segment is set equivalent to the maximum allowable curvature.

When developing the beam cross-section moment-curvature relationship, two separate analyses are possible. A flag for the analysis type desired is read as part of the user input. The flag T0 performs analysis which assumes no tensile stresses in the concrete after cracking within the concrete segment. Cracking within the segment exists when concrete strains at the bottom of the beam exceed the concrete tensile rupture strain. The tensile rupture strain was defined as the concrete tensile rupture stress divided by the initial elastic modulus of concrete. Once cracking has occurred within a concrete segment, no tensile stresses exist for the concrete, regardless of the concrete strains.

For the second analysis, TS analysis, contributions to beam stiffness due to the presence of concrete tensile stresses between cracks was included. This contribution to stiffness,

referred to as tension stiffening, was accounted for by using a smeared tensile stress model when developing curvature relationships. The smeared tensile stress does not have any physical meaning for the cross-section, but is intended to provide the correct average curvature of a cracked concrete segment. The value of the smeared concrete tensile stress for strains greater than the concrete tensile rupture strain is expressed as [Collins and Mitchell, 1991]:

$$f_c = \frac{\alpha_1 \alpha_2 f_{cr}}{1 + \sqrt{500 \epsilon_{cf}}} \tag{4.4}$$

where f_c = smeared concrete tensile stress
α_1 = 0.7 for plain bars, wires, or bonded strands
α_2 = 0.7 for sustained and/or repeated loads
f_{cr} = concrete modulus of rupture
ϵ_{cf} = extreme fiber tensile strain

For concrete tensile strains less than the tensile rupture strain but within a cracked section, the following expression was used:

$$f_c = \alpha_1 \alpha_2 f_{ct} \tag{4.5}$$

where f_{ct} = concrete tensile stress using the initial uncracked elastic modulus of the concrete

4.3.3 Beam Member Modeling

The beam member behavior is modelled as a steel reinforced or steel prestressed concrete beam subjected to four types of load: dead load, symmetrically applied dual point loads, upward forces at the harping points of the tendons due to the external post-tensioning, and additional axial forces placed at the level of the FRP end anchorage. The behavior of

the beam is initially determined with an assumed external FRP force. Expected FRP forces based on beam deflection are then compared to assumed FRP forces. The analysis is repeated until assumed and expected FRP forces are within a set tolerance. When this tolerance is met, the maximum effective moment on the beam is compared to the maximum nominal effective moment that can be carried by the beam. The computation of the maximum nominal effective moment is completed after convergence to the appropriate exterior tendon force and incorporates no tension stiffening affects.

The analytical model effectively divides the beam into segments of various lengths. Segment lengths are chosen such that point loads and harping points are located at the junction of segments. Harping of exterior tendons must be at midspan or at two variable locations symmetrically spaced about the midspan of the beam. The model assumes no friction between FRP tendons and harping deviators. The analysis is conducted over one-half of the symmetric beam, starting with the segment closest to the midspan.

The program is designed to determine the beam behavior at prescribed loading increments and with a specific loading history. The loading history involves increasing loads from zero to a prescribed "high load" with or without exterior post-tensioning affects. The load is then decreased to a predetermined "low load" where two analyses are conducted: one with the initial post-tensioning (if any) and the second with a new effective exterior post-tensioning force. The loads are then increased incrementally from this point with the analysis including the exterior post-tensioning effects until projected failure of the beam. The loading history is important to accurately reflect the extent of cracking in the beam prior to post-tensioning and to accurately predict the beam deflection corresponding to the effective prestressing force of the exterior tendons.

For each increment of load, segment curvatures are integrated along the beam to determine the overall beam deflection. When exterior post-tensioning is provided, the analysis assumes a post-tensioning force, TFTRY, and applies the associated axial and transverse loads at the anchorage and harping locations, respectively. The effective moments on each beam segment is determined by summing the moments due to beam weight, the

applied point loads, and the upward action of the tendons at the harping points. After determination of beam deflection and axial elongation at the height of the FRP anchorage, the actual tendon force, TFDISP, is calculated.

The value of TFDISP is determined using the initial effective tendon force plus an additional force due to elongation of the exterior tendons. The elongation of the exterior tendons is due to harping point vertical displacement and FRP anchorage horizontal displacement. The additional length is divided by the original tendon length to obtain the additional tendon strain and subsequently, the additional tendon force. If TFTRY and TFDISP are not equal, the analysis is repeated with a new value for TFTRY until TFTRY and TFDISP are within a set tolerance.

4.4 COMPARISON BETWEEN ANALYTICAL RESULTS AND EXPERIMENTAL RESULTS

For the analytical predictions of the test beams used in this study, the beams were divided into approximately 30 segments with 160 equal layers dividing the cross-section. The preset "high" and "low" loads defining the limits for the non-post-tensioned and post-tensioned loading histories were 8.3 and 4.3 kips (37 and 19 kN) for B series beams and 14.3 and 4.3 kips (64 and 19 kN) for C series beams. These loads reflect the loading history of the test beams.

4.4.1 Predictions Prior to Ultimate

The comparison of the load-midspan deflection relationships predicted analytically with those observed experimentally for the test beams are shown in **Figures 4.21** through **4.24**. The analytical predictions from the computer program EXPOST for load-midspan deflection relationships are shown for analysis including tensile stiffening affects (TS) and analysis without tensile stiffening (T0). For clarity purposes, the figures do not show beam response prior to external post-tensioning.

Figures 4.21 through **4.24** show that the response of the non-post-tensioned beams, B-0 and C-0, are accurately predicted by the results of the T0 analysis from EXPOST. It is evident in the figures that the results of EXPOST when tension stiffening is included (TS analysis) more closely match the response of the beams at early loading stages. As the loadings approach ultimate, the predictions as per the T0 analysis of EXPOST agree more closely with observed response of the test beams.

Figures 4.25 through **4.30** show the moment-curvature relationships for all beam test specimens. The results of EXPOST using the TS analysis and results using the T0 analysis bracket the measured response of the test beams at low moments. The results of TS analysis do not show the large rotations that exist as the moment approaches ultimate. At ultimate stage of the beams, the results of the T0 analysis generally show a very good comparison with the measured moment-curvature response. It should be noted that the longitudinal segment over which average beam curvatures were measured in the laboratory was 14 in. (360 mm). This segment distance is close to the crack spacing at midspan observed in the tests, which ranged from 13 in. (330 mm) to 15 in. (380 mm). The average curvature measured in the laboratory should therefore be a relatively accurate measure of the average curvature of the cracked midspan region of the beams.

Figures 4.31 and **4.32** show the relationship between the total force in CFRP tendons versus the beam midspan deflection. The analytical results shown are for the analysis neglecting tensile stiffening (T0), but the results of TS analysis are very close to the results shown. It is evident from the figures that for a given beam midspan deflection, the analytical approach used in EXPOST has a good capability of predicting the total force in the external CFRP tendons. The comparison are so close that the results for beams B-2 and C-1 are virtually indistinguishable from the experimental results. Any differences between the analytical and experimentally observed CFRP tendon forces for a given beam load are therefore likely related to differences in the predictions of beam deflections.

4.4.2 Predictions at Ultimate

Comparison between experimental and analytical results of ultimate load, midspan deflection at ultimate load, and CFRP tendon force at ultimate beam load are shown in **Tables 4.6a** and **4.6b**. Analytical results are shown for analysis including tensile stiffening affects (TS) and analysis without tensile stiffening (T0).

As shown in **Tables 4.6a** and **4.6b**, the results of program EXPOST provided accurate predictions of the measured beam ultimate load, and the predicted ultimate beam loads were conservative as compared to measured ultimate loads for the test beams. The ratio of predicted ultimate loads to experimental ultimate loads ranged from 0.88 to 1.00 for TS analysis and ranged from 0.95 to 1.00 for T0 analysis. For non-externally post-tensioned beams, the difference in the TS and T0 analysis only affects the beam curvature and deflection. Consequently, the predicted ultimate load for B-0 and C-0 are independent of the type of analysis.

For all of the results listed in **Tables 4.6a** and **4.6b**, analytical results that neglect tensile stiffening more accurately predict the measured beam response than analytical results that include tensile stiffening. This is especially true for predictions of midspan deflection. Since predictions of CFRP tendon forces are based mainly on the deflection of the beam, the results of analysis including tensile stiffening underestimated the CFRP tendon force at ultimate.

4.5 COMPARISON BETWEEN ANALYTICAL RESULTS AND EXPERIMENTAL RESULTS FROM OTHER RESEARCHERS

No research results were found for *steel prestressed* concrete members strengthened using external post-tensioning. Limited research results are available for *steel reinforced* concrete members strengthened by external post-tensioning. Results from research by Saeki, Horiguchi, Inomata, Hata and Ikeda [Saeki, et al., 1993] and by Arduini, DiTommaso and Giacani [Arduini, et al., 1996] were used to compare with the analytical predictions from

computerized model -- EXPOST. These two research studies were reviewed in Chapter 2.

4.5.1 Saeki, et al., 1993

Research conducted by Saeki involved testing of exterior post-tensioned, steel reinforced beams using Parafil (AFRP) rope as the external tendons [Saeki, et al., 1993]. The nature and results of the research have previously been discussed in Chapter 2. Cross-sections of the beams are shown in **Figure 2.7**. The profile of the beam as tested in shown in **Figure 2.8**. Properties of the test beams are shown in **Tables 4.7a** and **4.7b**. Results from tests that include fatigue loading or repair of cracks by epoxy injection are not included in the comparison.

Selected parameters of the tests conducted by Saeki, results of the tests, and results from EXPOST are shown in **Tables 4.8a** and **4.8b**. Predicted ultimate loads were the same for the T0 and TS analysis. The predictions of ultimate load using EXPOST compare reasonably well with the results found by Saeki. For two of the four specimens compared, predicted ultimate load values from EXPOST are within 5% of the values observed in the experiments conducted by Saeki and are closer to the experimental results than the predictions made by Saeki. For the remaining two specimens, the predicted ultimate load from EXPOST under estimates the experimental results by 12% and 20%.

Midspan deflection recorded by Saeki was reported for test specimens RC1 and PRC1 for load values of up to about 70% of the respective beam ultimate load. Comparison of deflections at loads of 70% of the experimentally observed failure loads are shown in **Tables 4.8a** and **4.8b** for test specimens RC1 and PRC1. Deflections predicted by EXPOST neglecting tension stiffening are 100 and 81 percent of the deflections observed experimentally for RC1 and PRC1, respectively. Predictions of deflections including tension stiffening affects are 77 and 69 percent of the experimental values for RC1 and PRC1, respectively.

4.5.2 Arduini, et al., 1996

The research conducted by Arduini included the testing of two steel reinforced concrete beams strengthened with two 0.37 in. (9.5 mm) diameter Aramid fiber tendons [Arduini, et al., 1996]. The nature and results of the research have previously been discussed in Chapter 2. Properties of the materials used in tests by Arduini are shown in **Tables 4.9a** and **4.9b**. Beam specimen details are shown in **Figure 2.9**.

Failure of both beams tested by Arduini was due to rupture of the external tendons. Load-deflection curves from the tests suggest that the beam load was not significantly increasing at the time of the tendon failure. The beam loads at tendon failure are therefore reported as the ultimate beam load. The results of program EXPOST do not consider failure of the external tendons.

Tables 4.10a and **4.10b** summaries the experimental results of the beams tested by Arduini and the predictions of EXPOST. The results show that EXPOST provided reasonably accurate predictions of the beam ultimate load and tendon force at ultimate deflection. Ultimate load predictions ranged from 89 to 102 percent of the respective experimental beam results. Estimates of the tendon forces by use of EXPOST ranged from 96 to 100 percent of the respective experimental results. The TS analysis provided slightly better estimation of tendon forces, but was less accurate than the T0 analysis in predicting the ultimate beam load.

4.6 SUMMARY AND CONCLUSIONS

Tests were conducted on four steel prestressed concrete beams externally strengthened with externally post-tensioned CFRP tendons. Beam behavior and component behavior was observed during static testing up to failure. Results were used for comparing the predictions by an analytical model developed in this study to predict the behavior of beams externally post-tensioned with FRP tendons. The computerized analytical model -- EXPOST is presented in Appendix B. Results from EXPOST are also compared with the experimental

results from other researchers.

Based on the results of the experimental beam tests, the following conclusions are made:

1. The addition of external post-tensioning can provide significant increases in strength and reductions in ultimate deflection of prestressed concrete beams. Average strength increases of 109% and 49% were observed for the beams tested in this study. Quantitative increases in strength were about the same for beams with different amounts of prestressing steel. Midspan deflections of the externally post-tensioned beams at ultimate averaged 64% of the companion unstrengthened beams.

2. For the CFRP tendons and harping plates used in this study, the average value of the friction coefficient between the tendons and the greased harping plates was 0.33. This value is approximately twice the friction coefficient recommended in the ACI 318-95 code for unbonded steel tendons.

3. Beams strengthened by external post-tensioned CFRP tendons demonstrated a higher tangential stiffness at failure than did the companion unstrengthened beams. This increase in stiffness was equivalent to the stiffness associated with the increased upward forces at the external tendon harping points at failure.

4. Tests conducted in this study verify that CFRP tendons can be effectively used as external post-tensioning tendons under short-term loading conditions.

Based on the results of the comparisons of the predictions using the computerized model -- EXPOST developed in this study and the experimental results, the following conclusions are made:

1. The computerized model -- EXPOST provides accurate predictions for the response of the prestressed beams strengthened by external post-tensioned CFRP tendons and subjected to short-term loads.

2. Analysis that neglects the contribution of concrete tensile stresses in cracked regions of the externally post-tensioned beams provides accurate predictions of the beam's ultimate load, midspan deflection, and external tendon force at failure.

Table 4.1a Design parameters of beam test program, US customary units

Beam No.	Concrete target strength, ksi	Effective prestress in steel strands, ksi	No. of steel strands	Area of prestressing steel strands, in^2	Effective prestress in CFRP tendons, ksi
B-0	6.5	160	1	0.153	no external tendons
B-1	6.5	160	1	0.153	180
B-2	6.5	160	1	0.153	180
C-0	6.5	160	2	0.306	no external tendons
C-1	6.5	160	2	0.306	180
C-2	6.5	160	2	0.306	180

Table 4.1b Design parameters of beam test program, SI units

Beam No.	Concrete target strength, MPa	Effective prestress in steel strands, MPa	No. of steel strands	Area of prestressing steel strands, mm^2	Effective prestress in CFRP tendons, MPa
B-0	45	1100	1	99	no external tendons
B-1	45	1100	1	99	1240
B-2	45	1100	1	99	1240
C-0	45	1100	2	197	no external tendons
C-1	45	1100	2	197	1240
C-2	45	1100	2	197	1240

Table 4.2a Beam properties at testing, US customary units

Beam No.	Concrete strength, ksi	Specimen age at testing, days	Initial prestress in steel tendons, ksi	DEMEC recorded prestress losses, ksi	Estimated prestress losses due to relaxation (Eq. 4.1), ksi	Total prestress loss in steel tendons, ksi	Effective prestress in steel tendons, ksi
B-0	6.3	42	183	17.2	8.9	26.1	157
B-1	6.3	45	182	21.7	8.7	30.4	152
B-2	6.3	53	183	21.8	9.2	31	152
C-0	6.5	27	181	14.2	7.9	22.1	159
C-1	6.5	33	181	15.2	8.1	23.3	158
C-2	6.6	39	179	16.0	7.8	23.8	155

Table 4.2b Beam properties at testing, SI units

Beam No.	Concrete strength, MPa	Specimen age at testing, days	Initial prestress in steel tendons, MPa	DEMEC recorded prestress losses, MPa	Estimated prestress losses due to relaxation (Eq. 4.1), MPa	Total prestress loss in steel tendons, MPa	Effective prestress in steel tendons, MPa
B-0	43	42	1260	119	61	180	1080
B-1	43	45	1250	150	60	210	1040
B-2	43	53	1260	150	63	213	1050
C-0	45	27	1250	98	54	152	1100
C-1	45	33	1250	105	56	161	1090
C-2	46	39	1230	110	54	164	1070

Table 4.3 Concrete mix proportions

Material	Quantity
Type I Cement	650 lbs (295 kg)
Sand (surface dry)	1126 lbs (512 kg)
Stone (surface dry)	1180 lbs (536 kg)
Water	270 lbs (123 kg)
Water Reducer	39 oz. (1.15 ltr)
Superplasticizer	104 oz. (3.98 ltr)

Table 4.4a Test results from beam tests, US customary units

Beam No.	Cracking load, kips	Ultimate load, kips	Midspan deflection at ultimate load, in.	Total force of external CFRP tendons, kips	
				Initial	At ultimate load
B-0	8	11.5	4.4	---	---
B-1	8.3	23.7	2.8	26.4	38.1
B-2	8.3	24.3	2.7	28.6	40.2
C-0	12.5	22.2	3.1	---	---
C-1	13.3	33	2.0	28.8	36.9
C-2	14.1	33.1	2.0	27.8	36.3

Table 4.4b Test results from beam tests, SI units

Beam No.	Cracking load, kN	Ultimate load, kN	Midspan deflection at ultimate load, mm	Total force of external CFRP tendons, kN	
				Initial	At ultimate load
B-0	36	51.2	113	---	---
B-1	36	105	71	117	169
B-2	37	108	69	127	179
C-0	56	98.7	78	---	---
C-1	59	147	51	128	164
C-2	63	147	51	124	161

Table 4.5a Beam stiffness at failure, US customary units

Beam No.	Midspan deflection at ultimate load, in. (1)	Selected incremental change in load at failure, lbs (2)	Incremental midspan deflection, in. (3)	Incremental point load disp./ incremental midspan defl. (4)=(3)/(2)	Incremental beam stiffness, lbs/in. (5)	Increased stiffness of post-tensioned beams, lbs/in. (6)
B-0	4.4	497	1.12	0.91	442	---
B-1	2.8	486	.324	0.87	1500	1060
B-2	2.7	542	.396	0.96	1370	929
C-0	3.1	566	.301	0.90	1880	---
C-1	2.0	513	.239	0.98	2150	268
C-2	2.0	511	.217	0.94	2360	476
Avg.*	2.4	513	.294	0.94	---	682

* Average of B-1, B-2, C-1 and C-2 only.

Table 4.5b Beam stiffness at failure, SI units

Beam No.	Midspan deflection at ult. load, mm (1)	Selected incremental change in load at failure, kN (2)	Incremental midspan deflection, mm (3)	Incremental point load disp./ incremental midspan defl. (4)=(3)/(2)	Incremental beam stiffness, N/mm (5)	Increased stiffness of post-tensioned beams, N/mm (6)
B-0	112	2.21	28.4	0.91	77.4	---
B-1	71	2.16	8.23	0.87	262	185
B-2	69	2.41	10.1	0.96	240	163
C-0	79	2.52	7.65	0.90	329	---
C-1	51	2.28	6.07	0.98	376	46.9
C-2	51	2.27	5.51	0.94	413	83.4
Avg.*	61	2.28	7.47	0.94	---	119

* Average of B-1, B-2, C-1 and C-2 only.

Table 4.6a Summary of experimental and analytical beam test results, US customary units

Beam No.	Ultimate load, kips			Midspan deflection at ultimate load, in.			Total force of external CFRP tendons at ultimate, kips		
	Exp.	Analytical		Exp.	Analytical		Exp.	Analytical	
		TS*	T0*		TS*	T0*		TS*	T0*
B-0	11.5	11.1 (0.97)	11.1 (0.97)	4.44	.972 (0.22)	3.81 (0.86)	--	--	--
B-1	23.7	20.7 (0.87)	22.7 (0.96)	2.81	1.05 (0.37)	2.43 (0.86)	38.1	30.9 (0.81)	36.9 (0.97)
B-2	24.3	21.5 (0.88)	23.2 (0.95)	2.71	1.07 (0.39)	2.28 (0.84)	40.2	33.3 (0.83)	38.5 (0.96)
C-0	22.2	22.3 (1.00)	22.3 (1.00)	3.09	1.38 (0.45)	2.68 (0.87)	--	--	--
C-1	33.0	32.3 (0.98)	33.1 (1.00)	1.99	1.34 (0.67)	1.97 (0.99)	36.9	34.4 (0.93)	36.8. (1.00)
C-2	33.1	32.1 (0.97)	32.7 (0.99)	1.99	1.38 (0.69)	1.95 (0.98)	36.3	33.5 (0 .92)	35.6 (0.98)

* TS = analysis accounting for tension stiffening affects
* T0 = analysis assuming no tensile stiffening affects
( ) numbers in parenthesis indicate the percent (%) of experimental value

Table 4.6b Summary of experimental and analytical beam test results, SI units

Beam No.	Ultimate load, kN			Midspan deflection at ultimate load, mm			Total force of external CFRP tendons at ultimate, kN		
	Exp.	Analytical		Exp.	Analytical		Exp.	Analytical	
		TS*	T0*		TS*	T0*		TS*	T0*
B-0	51.2	49.4 (0.97)	49.4 (0.97)	113	24.7 (0.22)	96.8 (0.86)	--	--	--
B-1	105	92.1 (0.87)	101 (0.96)	71.4	26.7 (0.37)	61.7 (0.86)	169	137 (0.81)	164 (0.97)
B-2	108	95.6 (0.88)	103 (0.95)	68.8	27.2 (0.39)	57.9 (0.84)	179	148 (0.83)	171 (0.96)
C-0	98.7	99.2 (1.00)	99.2 (1.00)	78.5	35.1 (0.45)	68.1 (0.87)	--	--	--
C-1	147	144 (0.98)	147 (1.00)	50.5	34.0 (0.67)	50.0 (0.99)	164	153 (0.93)	164 (1.00)
C-2	147	143 (0.97)	145 (0.99)	50.5	35.1 (0.69)	49.5 (0.98)	161	149 (0.92)	158 (0.98)

* TS = analysis accounting for tension stiffening affects
* T0 = analysis assuming no tensile stiffening affects
( ) numbers in parenthesis indicate the percent (%) of experimental value

Table 4.7a Properties of test specimens, US customary units [Saeki, et al., 1993]

Material	Dimensions, in.	Elastic modulus, ksi	f_c, ksi	f_y, ksi	f_t, ksi	Ultimate tensile load, kips
Concrete RC1 PRC1 RC2 PRC2	7.9 x 15.7	---	 4.48 4.32 5.96 5.18	---	0.42	---
Steel RC1 PRC1	0.24 sq.-in. top 0.62 sq.-in. bot	29,000 (assumed)	---	60 (assumed)	---	---
RC2 PRC2	0.24 sq.-in. top 1.38 sq.-in. bot					
AFRP	0.083 sq.-in.	18800	---	---	270	23.2

Table 4.7b Properties of test specimens, SI units [Saeki, et al., 1993]

Material	Dimensions, mm	Elastic modulus, GPa	f_c, MPa	f_y, MPa	f_t, MPa	Ultimate tensile load, kN
Concrete RC1 PRC1 RC2 PRC2	200 x 400	---	 30.9 29.8 41.1 35.7	---	2.9	---
Steel RC1 PRC1	155 sq.-mm top 400 sq.-mm bot	200 (assumed)	---	414 (assumed)	---	---
RC2 PRC2	155 sq.-mm top 890 sq.-mm bot					
AFRP	54 sq.-mm	130	---	---	1860	103

Table 4.8a Summary of experimental and analytical results, US customary units [Saeki, et al., 1993]

Beam No.	Type of cross-section (see Figure 2.4)	Initial post-tensioning force, kips	Ultimate beam load, kips*				Deflections at 70% of experimental ultimate load, in.*		
			Exp.	Prediction - Saeki	EXPOST - T0**	EXPOST - TS***	Exp.	EXPOST - T0**	EXPOST - TS***
RC1	A	---	22.5	20.7 (0.92)	19.9 (0.88)	19.9 (0.88)	0.13	0.13 (1.00)	0.10 (0.77)
PRC1	A	15.2	37.7	37.0 (0.98)	30.3 (0.80)	30.3 (0.80)	0.16	0.13 (0.81)	0.11 (0.69)
RC2	B	---	41.5	34.4 (0.83)	43.7 (1.05)	43.7 (1.05)	---	0.12	0.11
PRC2	B	15.2	52.9	51.2 (0.97)	53.5 (1.01)	53.5 (1.01)	---	0.12	0.11

* numbers in parentheses, '( )', are the ratio of experimental results to analytical results

** EXPOST - T0 = analysis using computer program EXPOST with tension stiffening affects neglected

*** EXPOST - TS = analysis using computer program EXPOST with tension stiffening affects included

Table 4.8b Summary of experimental and analytical results, SI units [Saeki, et al., 1993]

Beam No.	Type of cross section (see Figure 2.4)	Initial post-tensioning force, kN	Ultimate beam load, kN*				Deflections at 70% of experimental ultimate load, mm*		
			Exp.	Prediction - Saeki	EXPOST - T0**	EXPOST - TS***	Exp.	EXPOST - T0**	EXPOST - TS***
RC1	A	---	100	92.1 (0.92)	88.5 (0.88)	88.5 (0.88)	3.3	3.3 (1.00)	2.5 (0.77)
PRC1	A	68	168	165 (0.98)	135 (0.80)	135 (0.80)	4.1	3.3 (0.81)	2.8 (0.69)
RC2	B	---	185	153 (0.83)	194 (1.05)	194 (1.05)	---	3.0	2.8
PRC2	B	68	235	228 (0.97)	238 (1.01)	238 (1.01)	---	3.0	2.8

* numbers in parentheses, '( )', are the ratio of experimental results to analytical results

** EXPOST - T0 = analysis using computer program EXPOST with tension stiffening affects neglected

*** EXPOST - TS = analysis using computer program EXPOST with tension stiffening affects included

Table 4.9a Properties of test specimens, US customary units [Arduini, et al., 1996]

Material	Dimensions, in.	Elastic modulus, ksi	f_c, ksi	f_y, ksi	f_t, ksi	Ultimate tensile load, kips
Concrete	9.8 x 11.8	4400	6.8	---	0.42	---
Steel	0.39 dia. (beam A) 0.55 dia. (beam B)	29700	---	94	112	---
AFRP	0.1 sq.-in.	6400	---	---	180	18.0

Table 4.9b Properties of test specimens, SI units [Arduini, et al., 1996]

Material	Dimensions, mm	Elastic modulus, GPa	f_c, MPa	f_y, MPa	f_t, MPa	Ultimate tensile load, kN
Concrete	250 x 300	30	47	---	2.9	---
Steel	10 dia. (beam A) 14 dia. (beam B)	205	---	650	770	---
AFRP	65 sq.-mm	44	---	---	1240	80

Table 4.10a Summary of experimental and analytical results, US customary units [Arduini, et al., 1996]

Beam no.	Initial post-tensioning load per cable, kips	Beam load at ultimate, kips*				Tendon load at ultimate deflection observed in experiments, kips*			
		Exp.	Prediction - Arduini	EXPOST - T0**	EXPOST - TS***	Exp.	Prediction - Arduini	EXPOST - T0**	EXPOST - TS***
A	7.9	25	25 (1.00)	25.6 (1.02)	23.5 (0.94)	9.7	9.7 (1.00)	9.4 (0.97)	9.6 (0.99)
B	5.8	30.8	29 (0.94)	28.5 (0.93)	27.5 (0.89)	7.6	8.1 (1.07)	7.3 (0.96)	7.6 (1.00)

* numbers in parentheses, '( )', are the ratio of experimental results to analytical results

** EXPOST - T0 = analysis using computer program EXPOST with tension stiffening affects neglected

*** EXPOST - TS = analysis using computer program EXPOST with tension stiffening affects included

Table 4.10b Summary of experimental and analytical results, SI units [Arduini, et al., 1996]

Beam no.	Initial post-tensioning load per cable, kN	Predicted load at ultimate, kN*				Tendon load at ultimate deflection observed in experiments, kN*			
		Exp.	Prediction - Arduini	EXPOST - T0**	EXPOST - TS***	Exp.	Prediction - Arduini	EXPOST - T0**	EXPOST - TS***
A	35	111	111 (1.00)	114 (1.02)	105 (0.94)	43	43 (1.00)	42 (0.97)	43 (1.00)
B	26	137	129 (0.94)	127 (0.93)	122 (0.89)	34	36 (1.07)	32 (0.96)	34 (1.00)

* numbers in parentheses, '( )', are the ratio of experimental results to analytical results

** EXPOST - T0 = analysis using computer program EXPOST with tension stiffening affects neglected

*** EXPOST - TS = analysis using computer program EXPOST with tension stiffening affects included

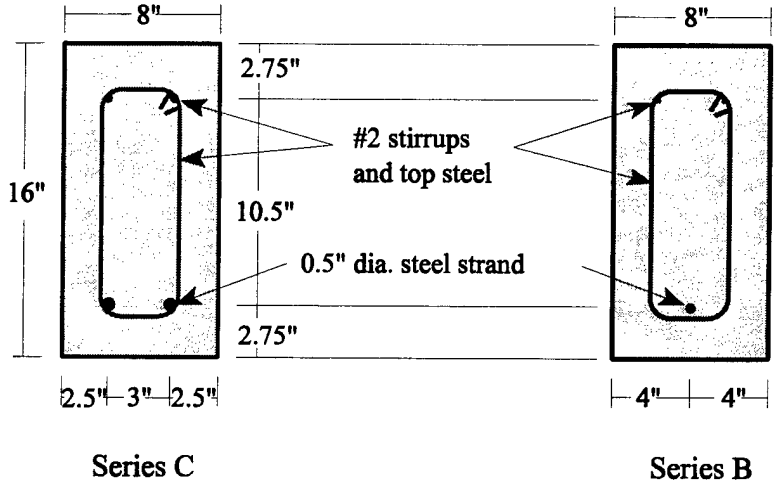

Figure 4.1 Cross-section of beam specimens

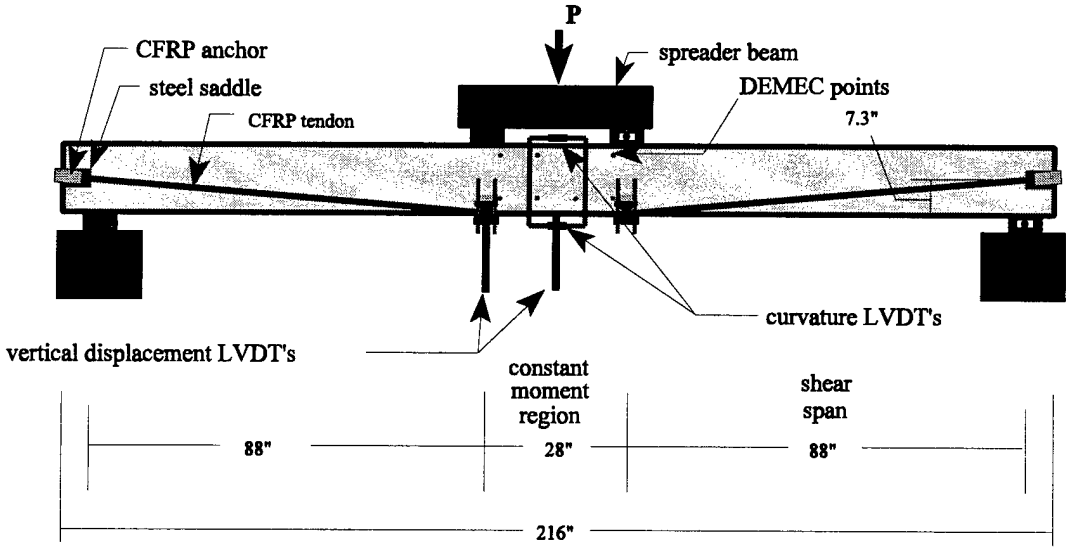

Figure 4.2 Schematic diagram of the prestressed beams strengthened by external CFRP tendons

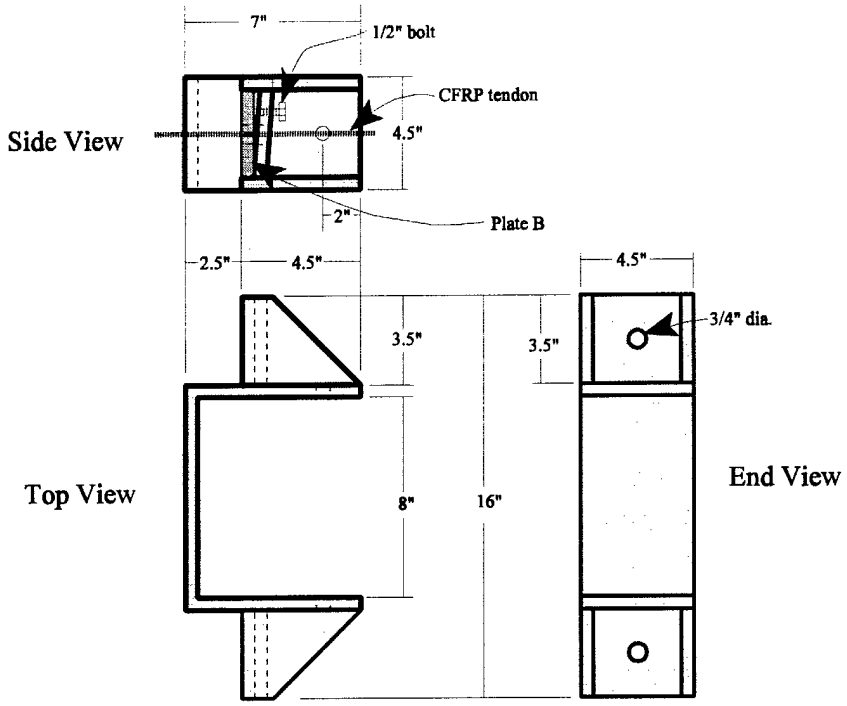

Figure 4.3a Beam saddle for mounting external CFRP tendons to prestressed beams

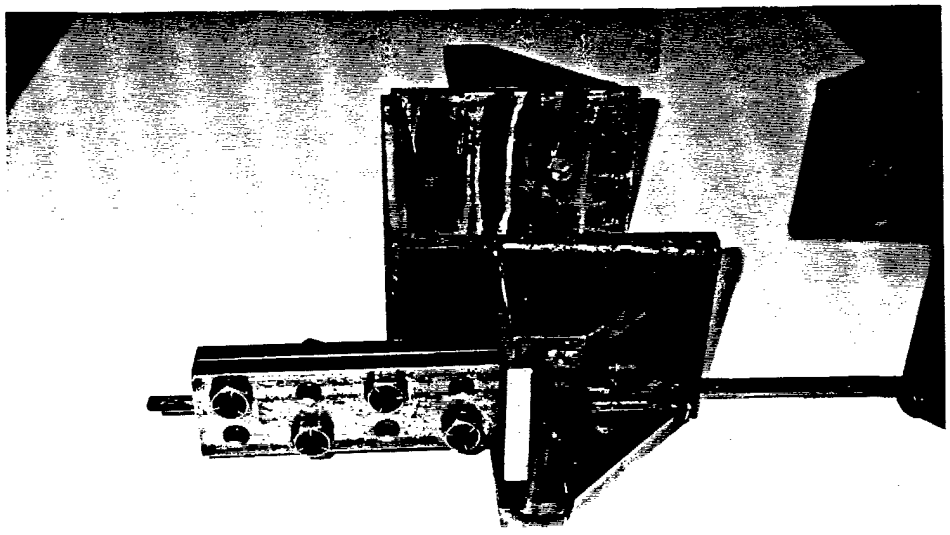

Figure 4.3b Photographic view of beam saddle and anchorage for CFRP tendons

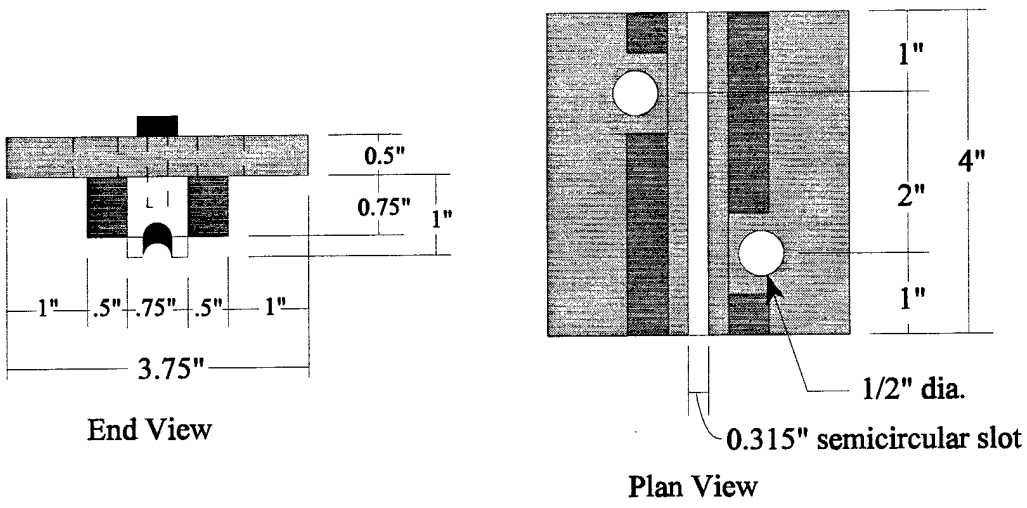

Figure 4.4a Schematic diagram of harping hardware for CFRP tendons

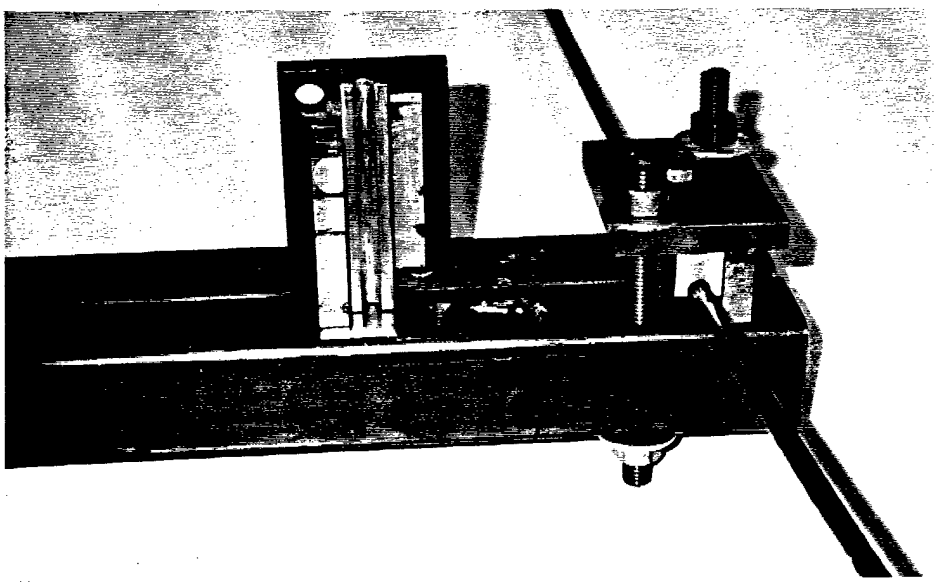

Figure 4.4b Photographic view of harping hardware for CFRP tendons

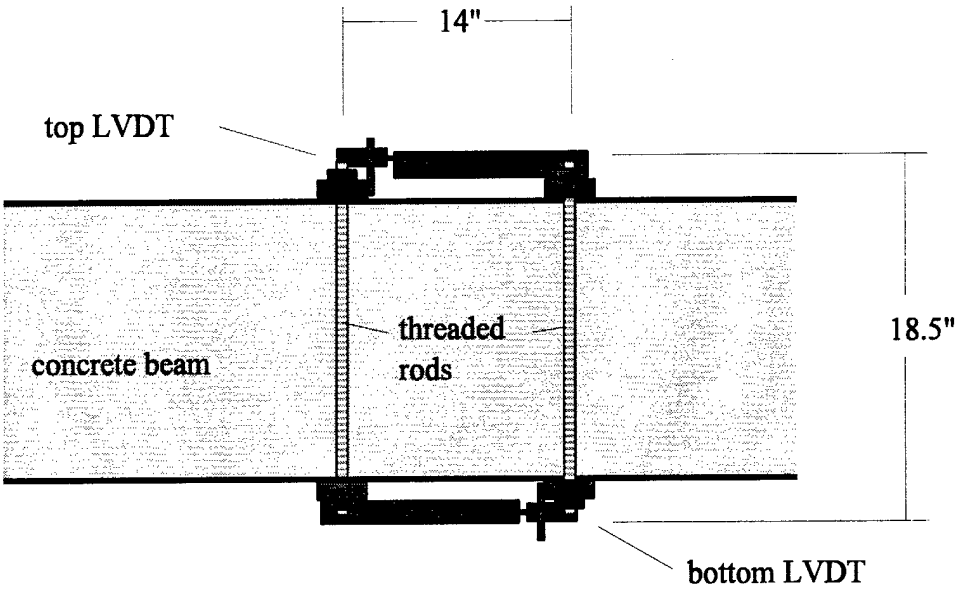

Figure 4.5a Schematic diagram of hardware and set-up for recording curvatures

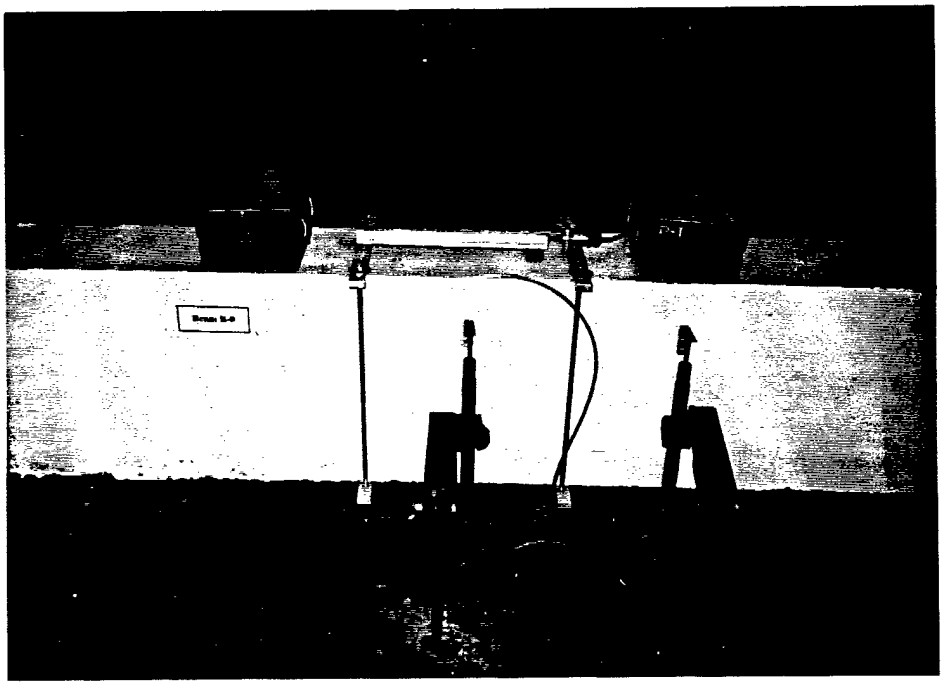

Figure 4.5b Photographic view of hardware and set-up for recording curvatures and vertical displacements

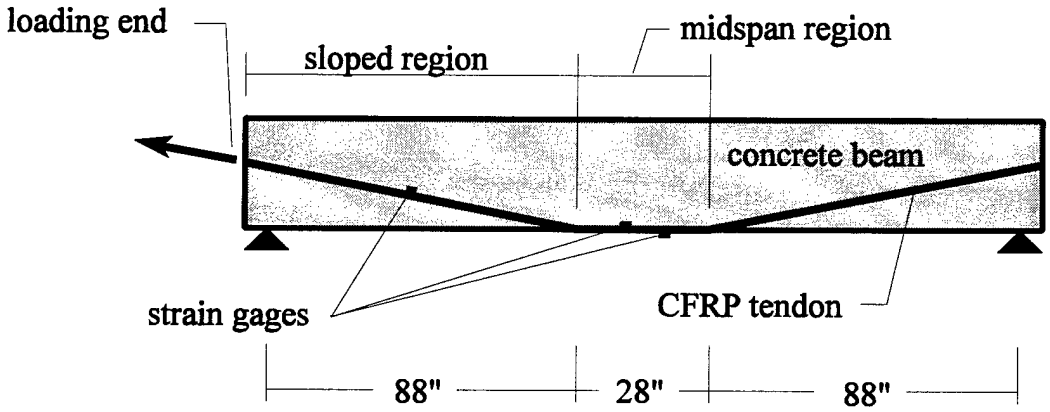

Figure 4.6 Locations of the strain gages on external CFRP tendons

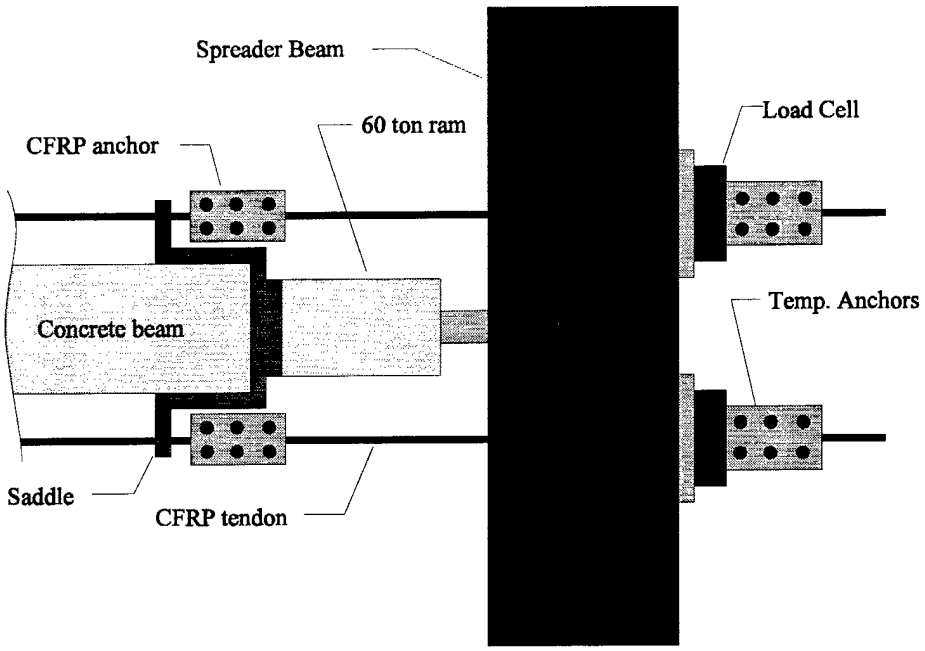

Figure 4.7a Post-tensioning hardware set-up

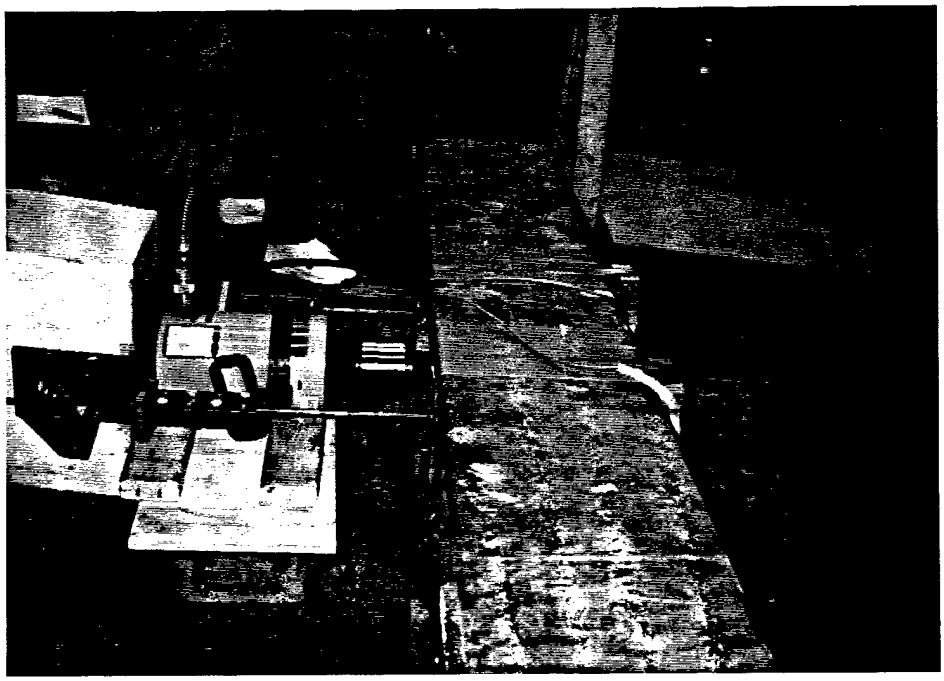

Figure 4.7b Photographic view of post-tensioning hardware set-up

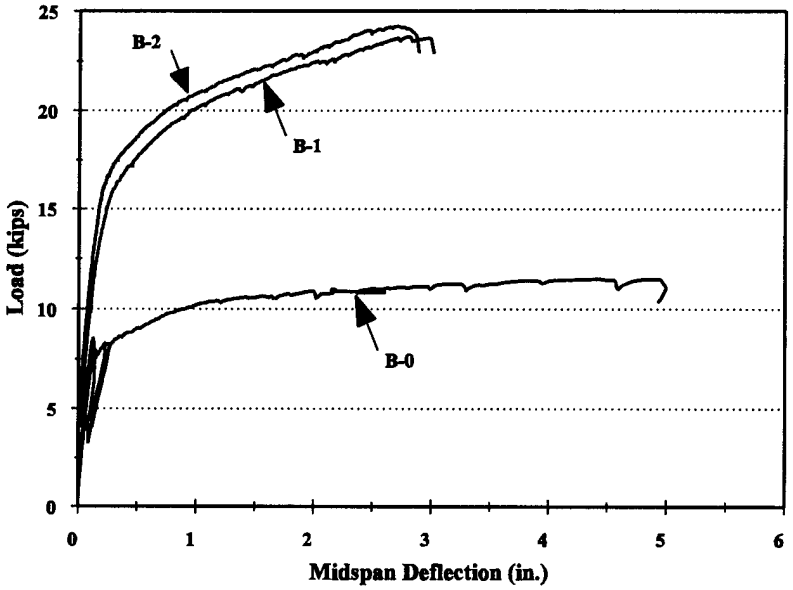

Figure 4.8 Load - midspan deflection for B series beams

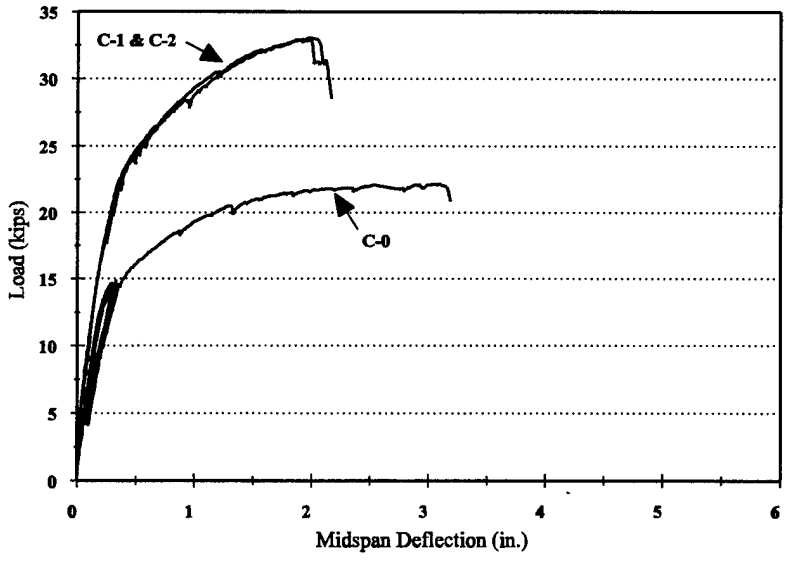

Figure 4.9 Load - midspan deflection for C series beams

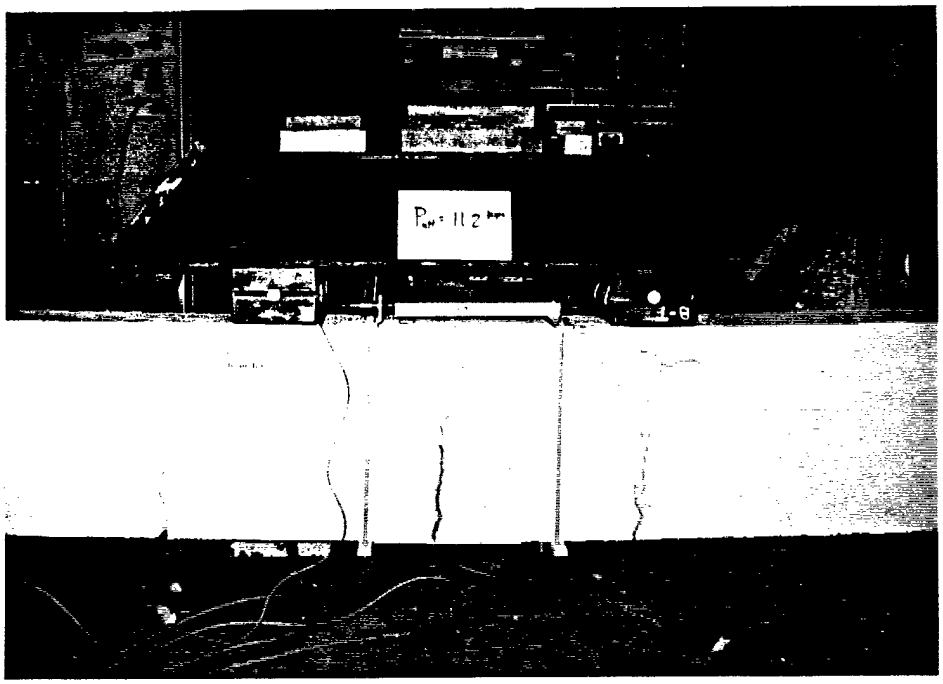

Figure 4.10a Photographic view of midspan region of beam B-0 after failure

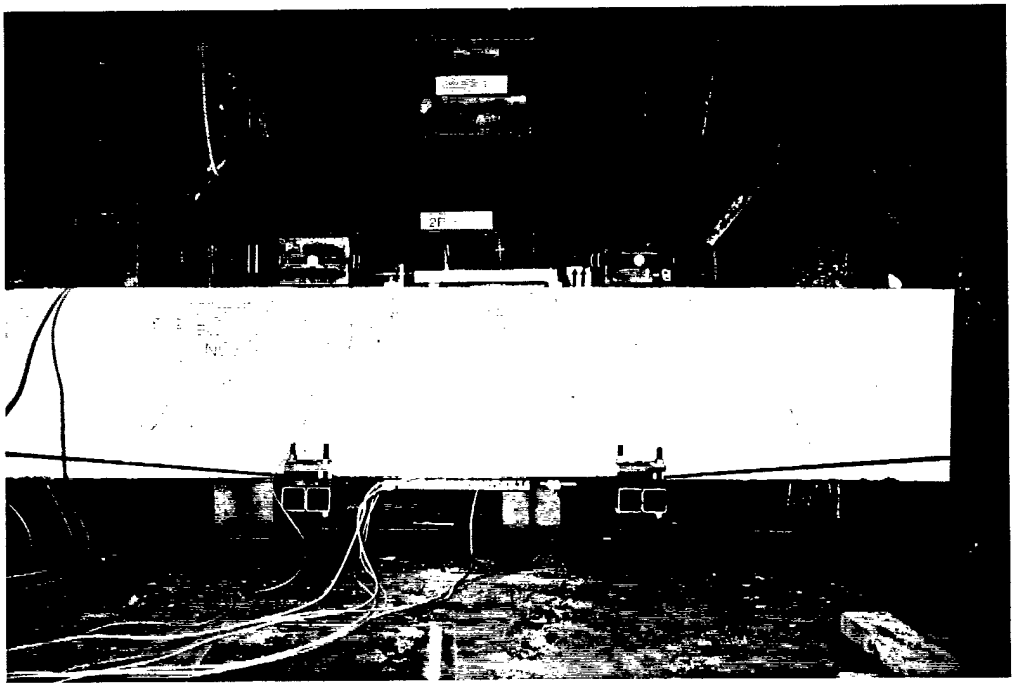

Figure 4.10b Photographic view of midspan region of beam B-1 after failure

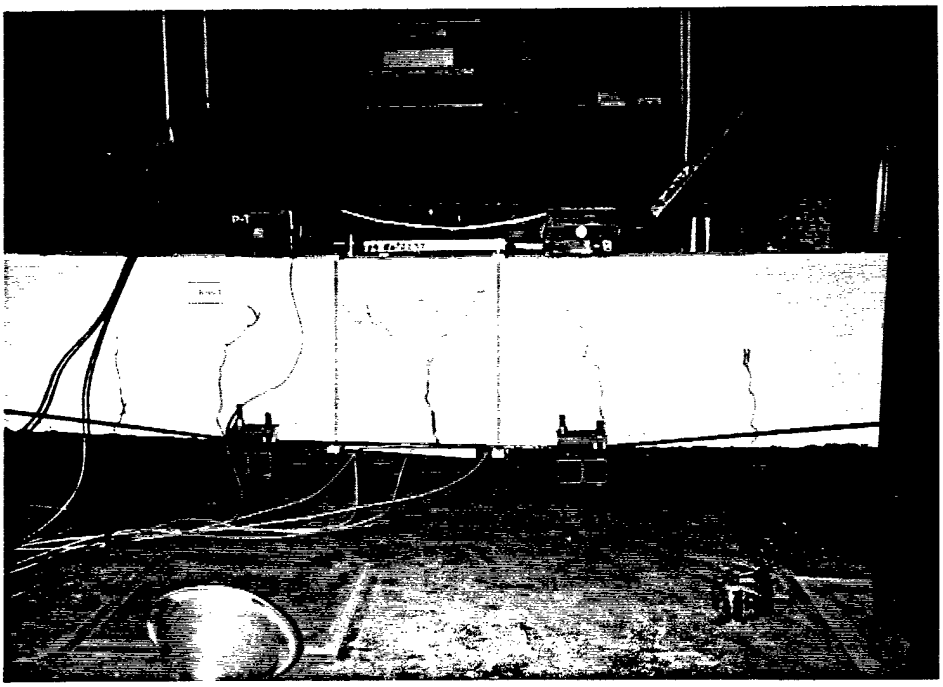

Figure 4.10c Photographic view of midspan region of beam B-2 after failure

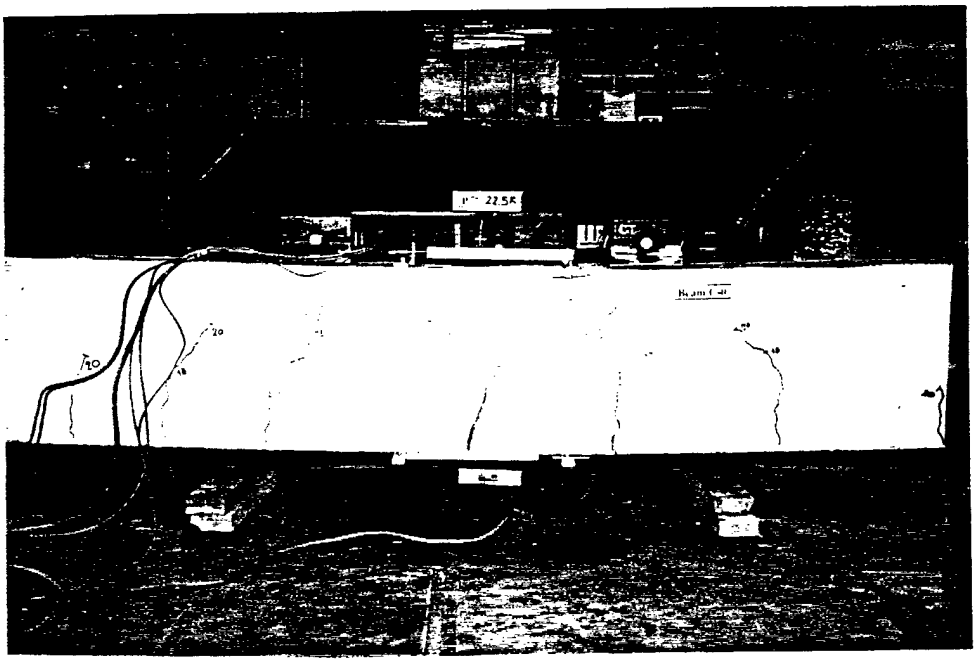

Figure 4.11a Photographic view of midspan region of beam C-0 after failure

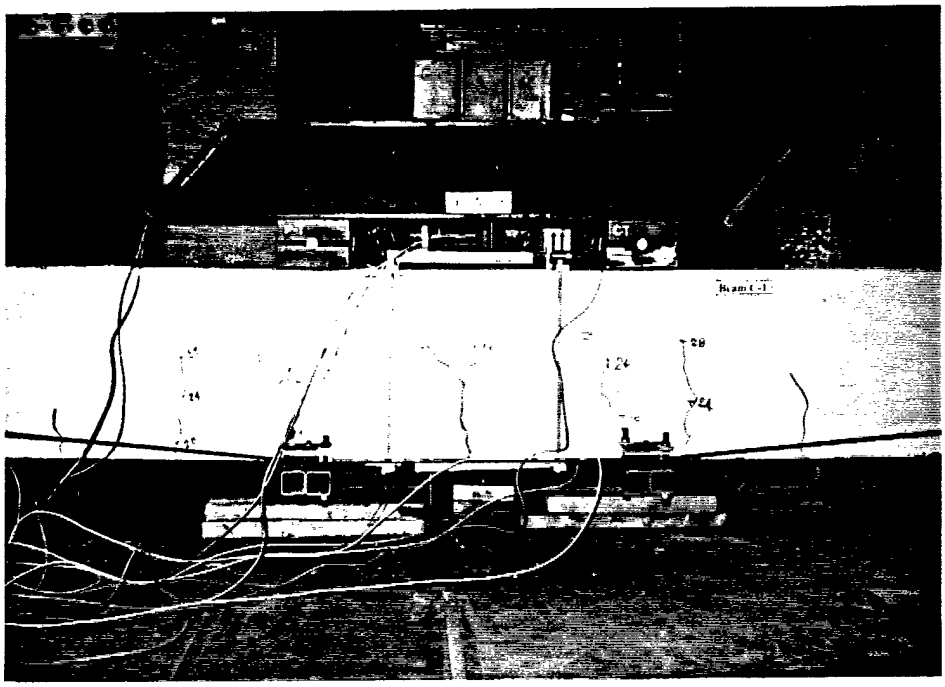

Figure 4.11b Photographic view of midspan region of beam C-1 after failure

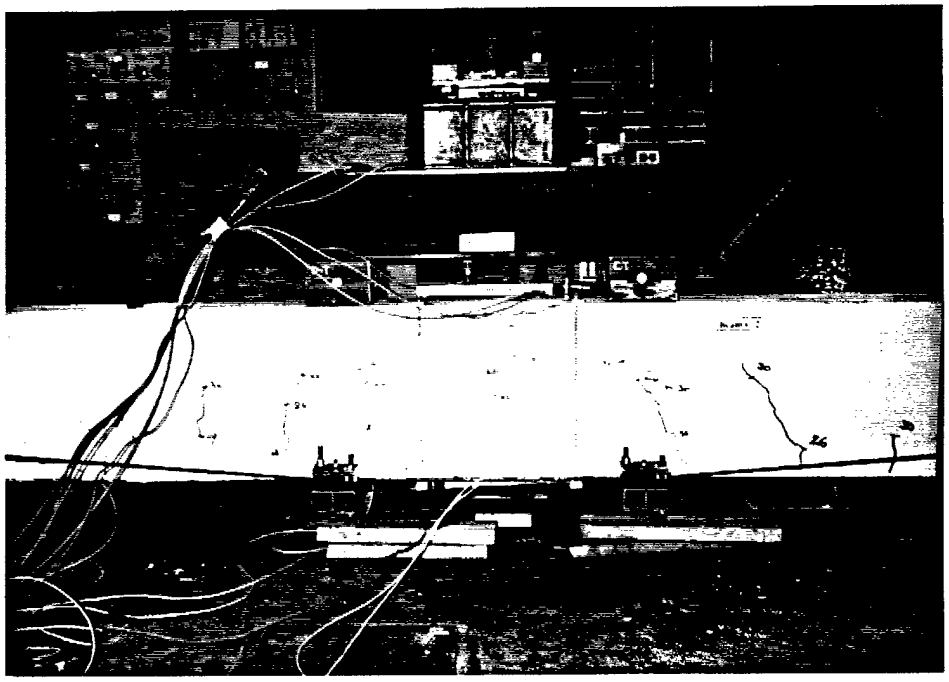

Figure 4.11c Photographic view of midspan region of beam C-2 after failure

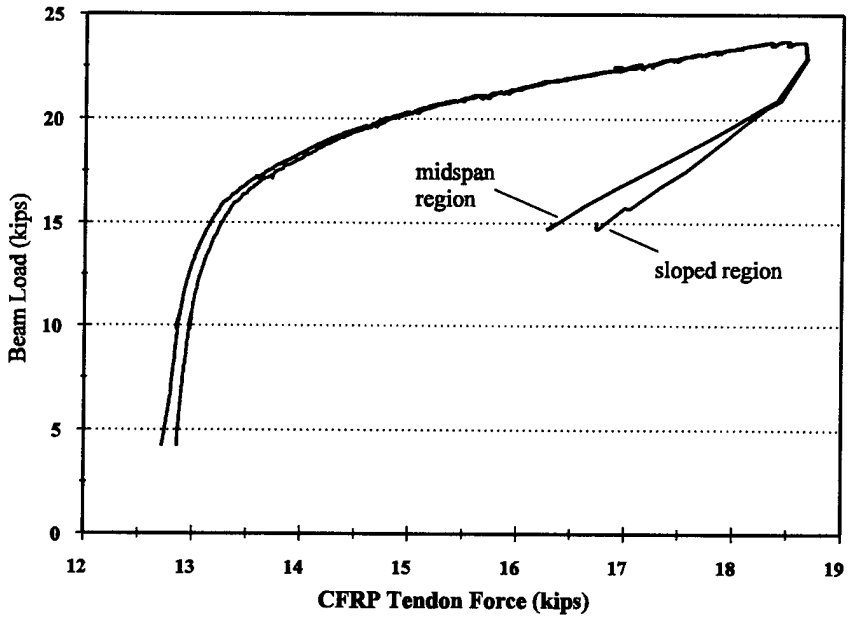

Figure 4.12 Beam load versus CFRP tendon force for tendon #1, beam B-1

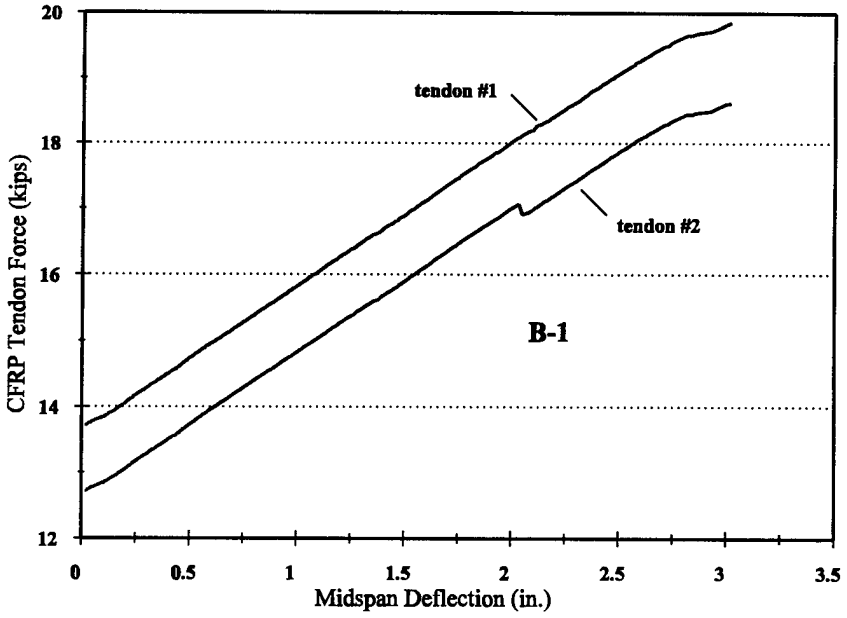

Figure 4.13 CFRP tendon force versus beam midspan deflection, beam B-1

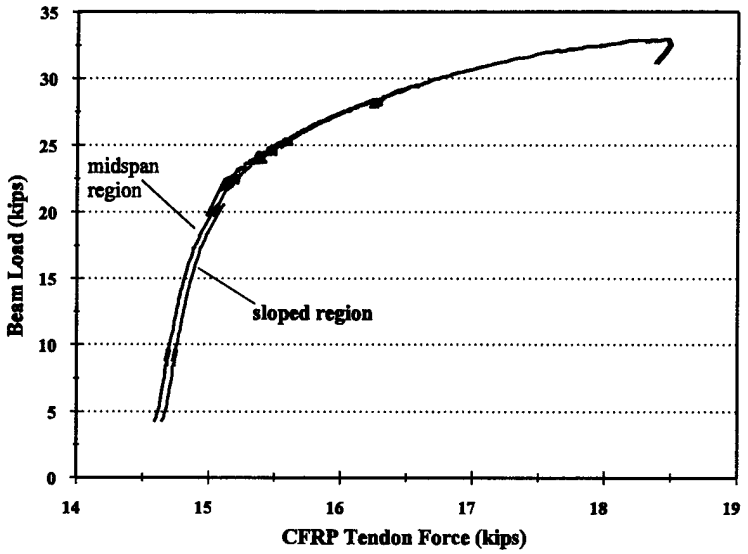

Figure 4.14 Beam load versus CFRP tendon force for tendon #1, beam C-1

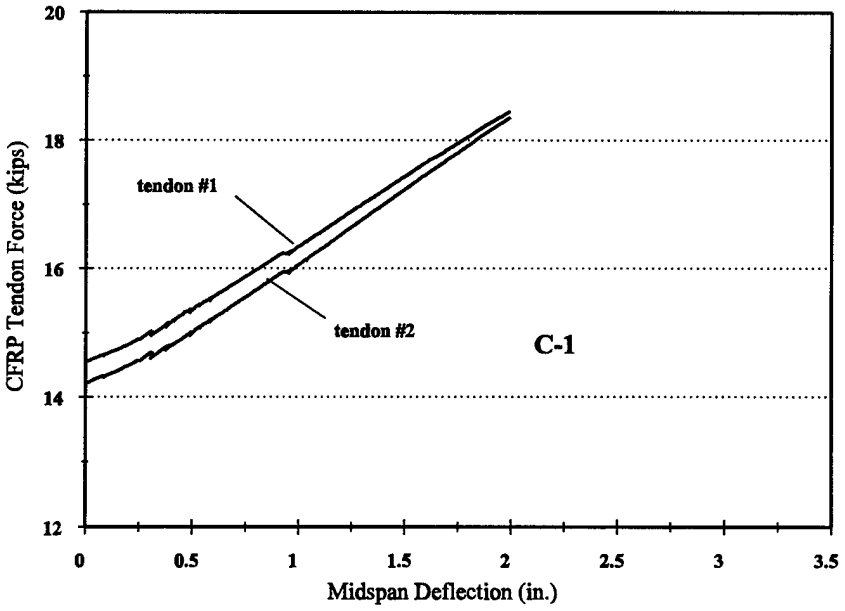

Figure 4.15 CFRP tendon force versus beam midspan deflection, beam C-1

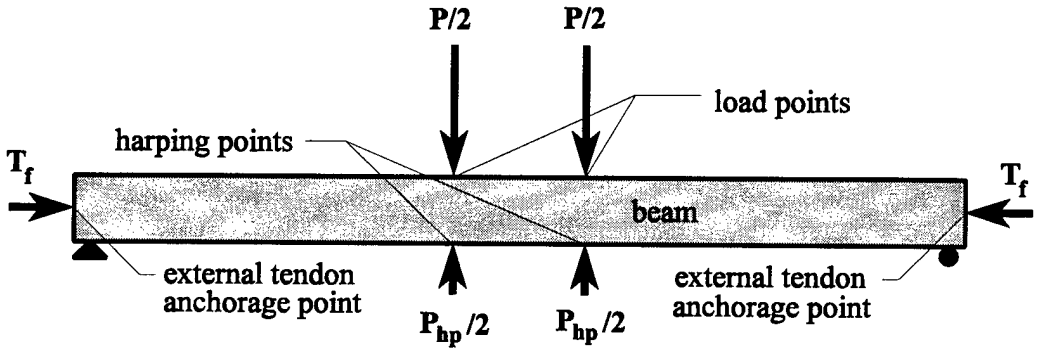

P = total point load on beam
T_f = total force in external tendons
P_{hp} = upward acting force at harping points

Figure 4.16a Schematic view of beam with point loads, axial load due to external tendons, and upward acting forces at harping points

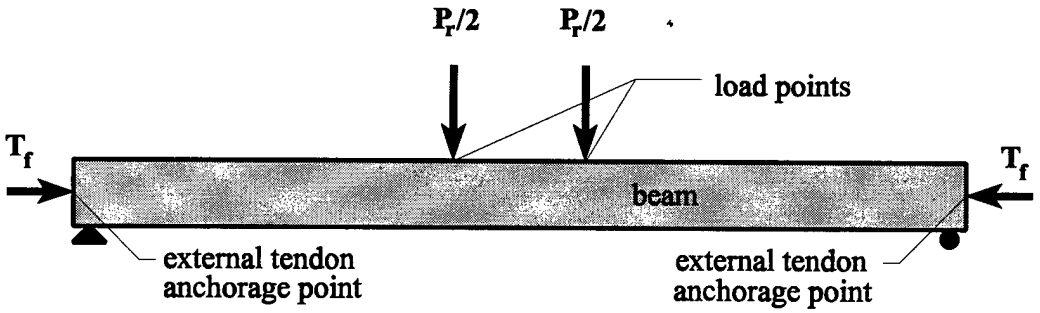

$P_r = P - P_{hp}$
P = total point load on beam
T_f = total force in external tendons
P_{hp} = upward acting force at harping points

Figure 4.16b Schematic view of beam with load P_r and axial load due to external tendons

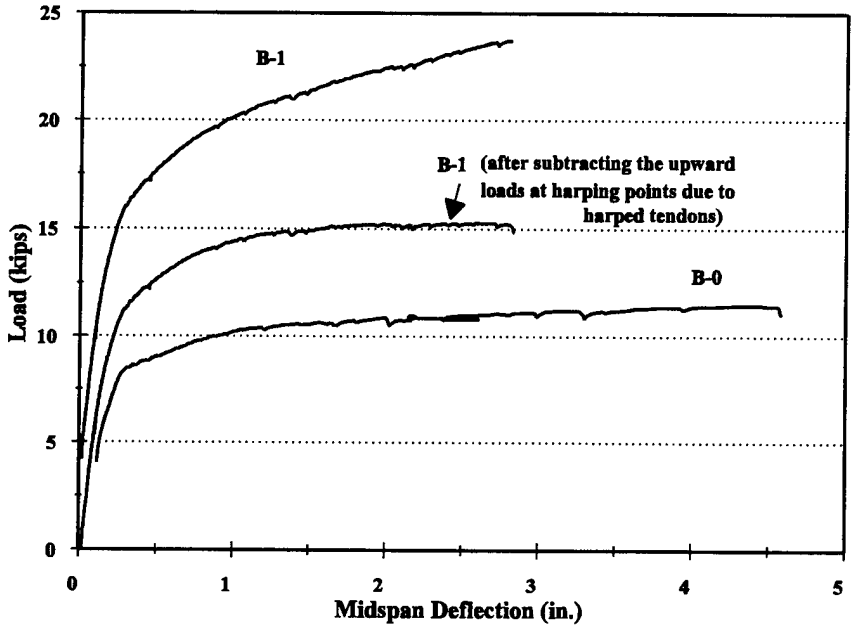

Figure 4.17 Effect of upward harping forces on the load-midspan deflection, Beam B-1

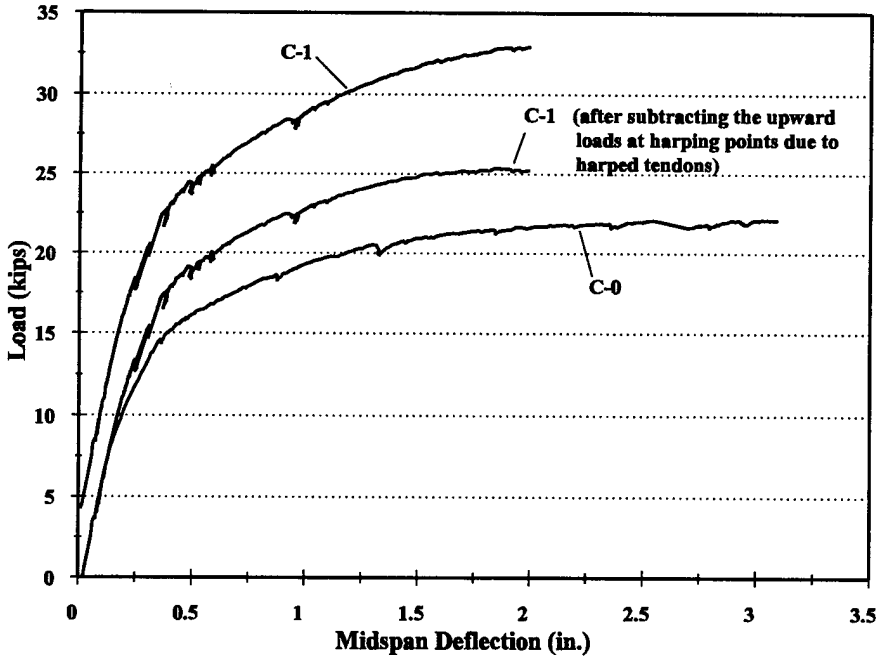

Figure 4.18 Effect of upward harping forces on the load-midspan deflection, Beam C-1

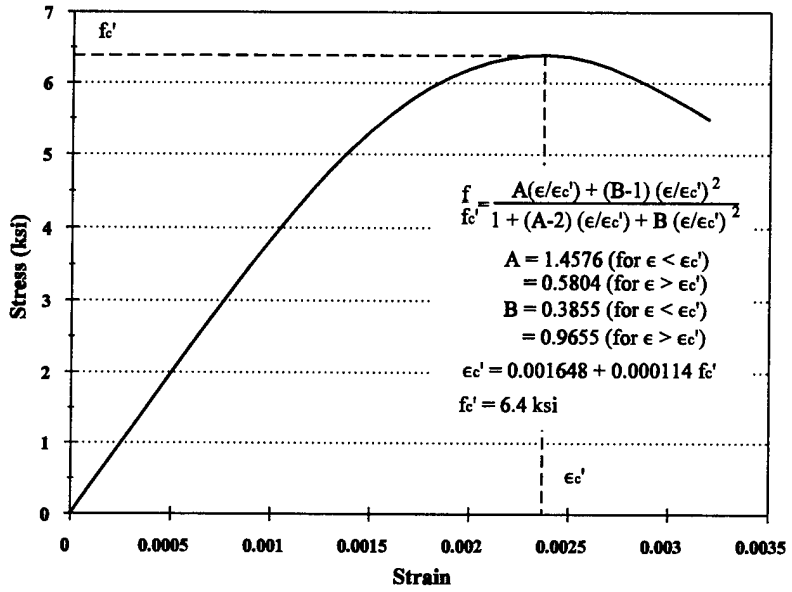

Figure 4.19 Schematic stress-strain curve of concrete used in program EXPOST

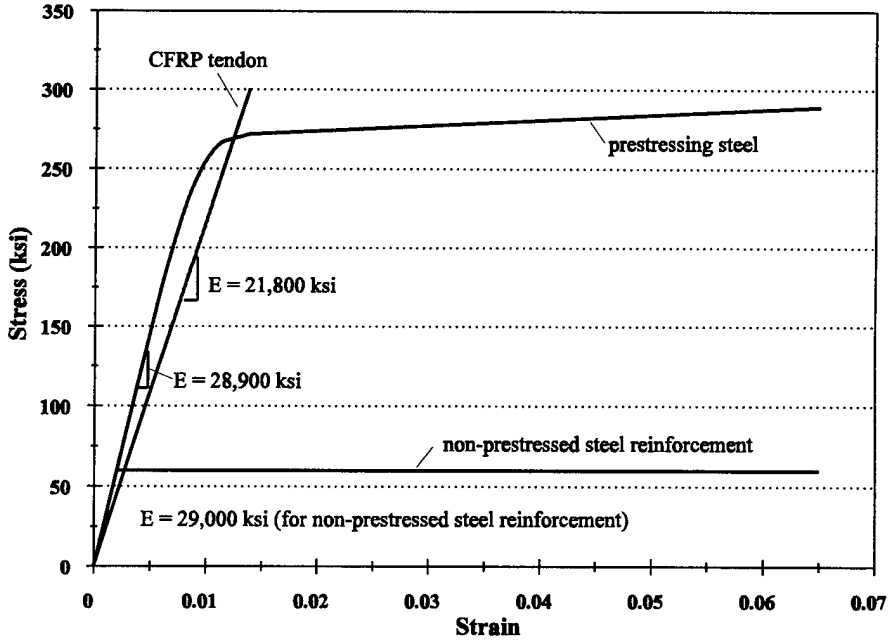

Figure 4.20 Schematic stress-strain curve of CFRP tendon, prestressing steel, and non-prestressed steel reinforcement used in program EXPOST

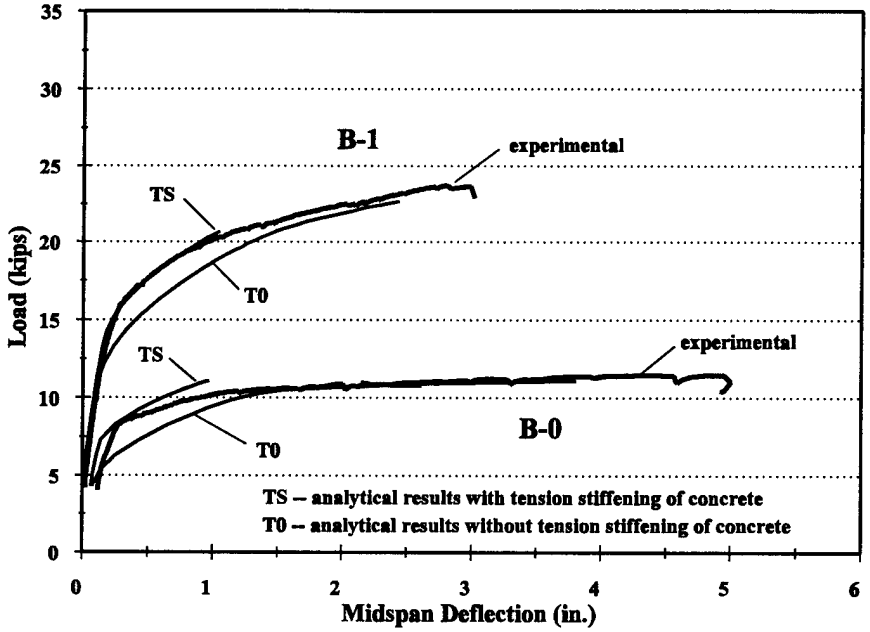

Figure 4.21 Experimentally observed and predicted load-midspan deflection for B-0 and B-1

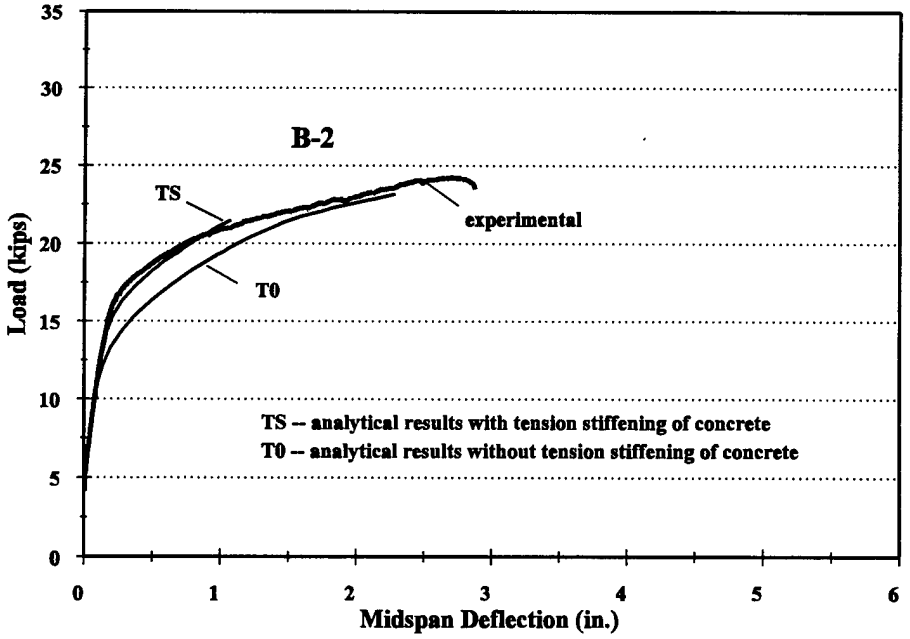

Figure 4.22 Experimentally observed and predicted load-midspan deflection for B-2

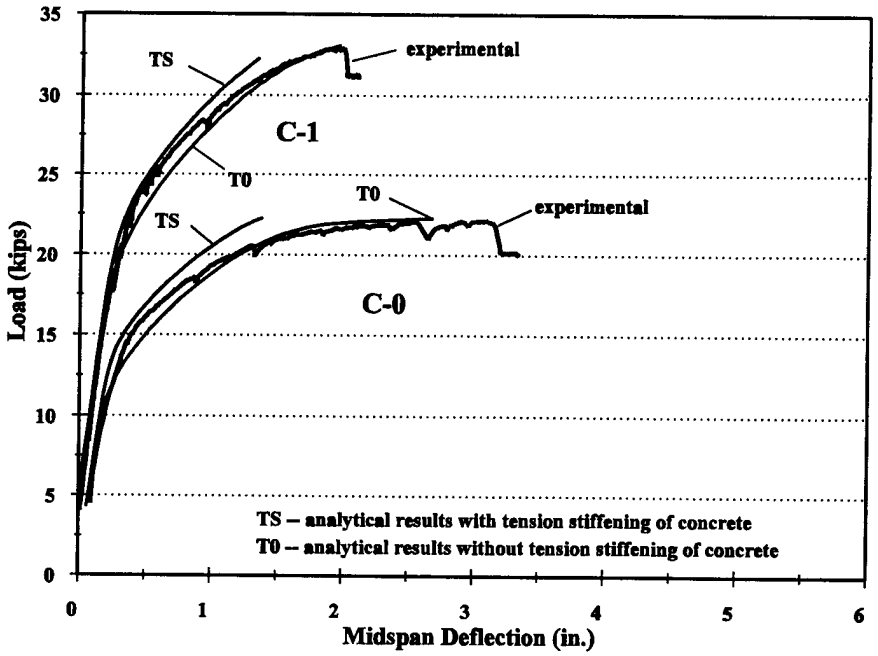

Figure 4.23 Experimentally observed and predicted load-midspan deflection for C-0 and C-1

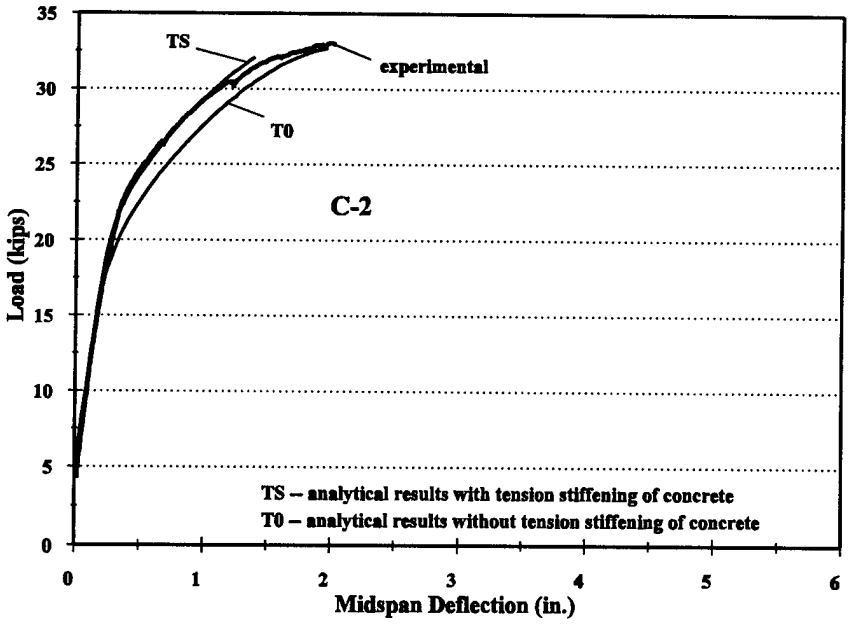

Figure 4.24 Experimentally observed and predicted load-midspan deflection for C-2

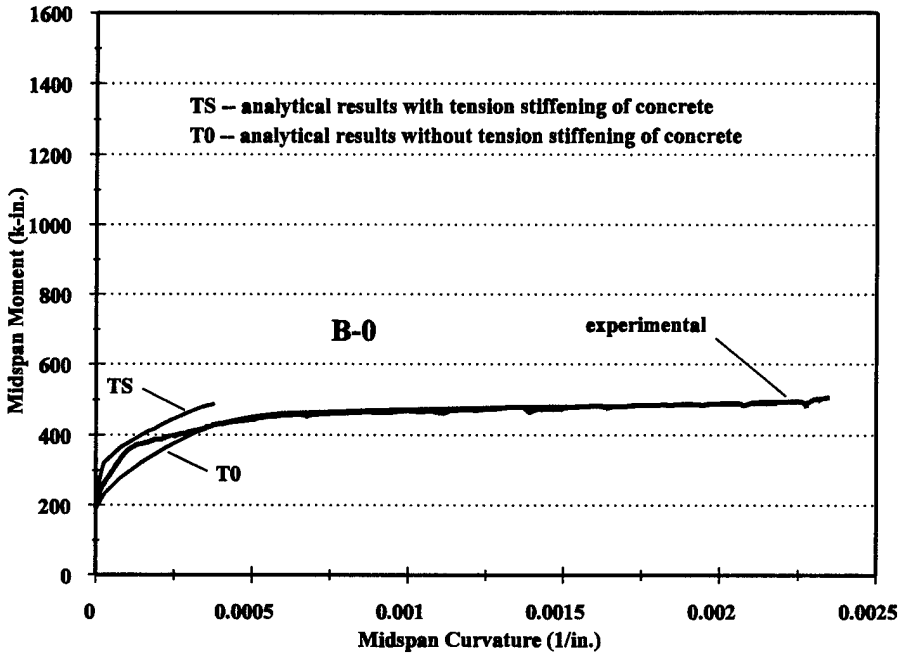

Figure 4.25 Midspan moment-curvature relationship for B-0

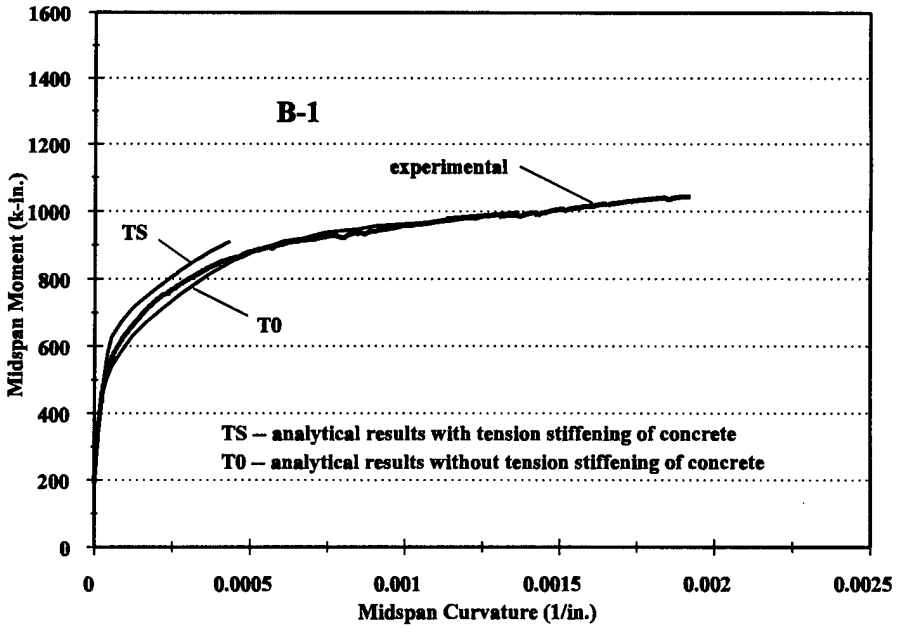

Figure 4.26 Midspan moment-curvature relationship for B-1

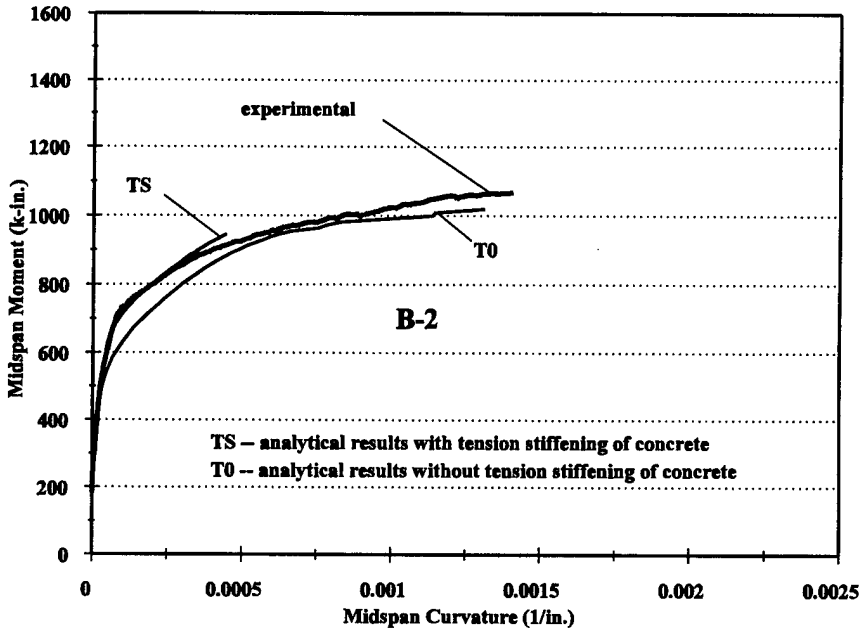

Figure 4.27 Midspan moment-curvature relationship for B-2

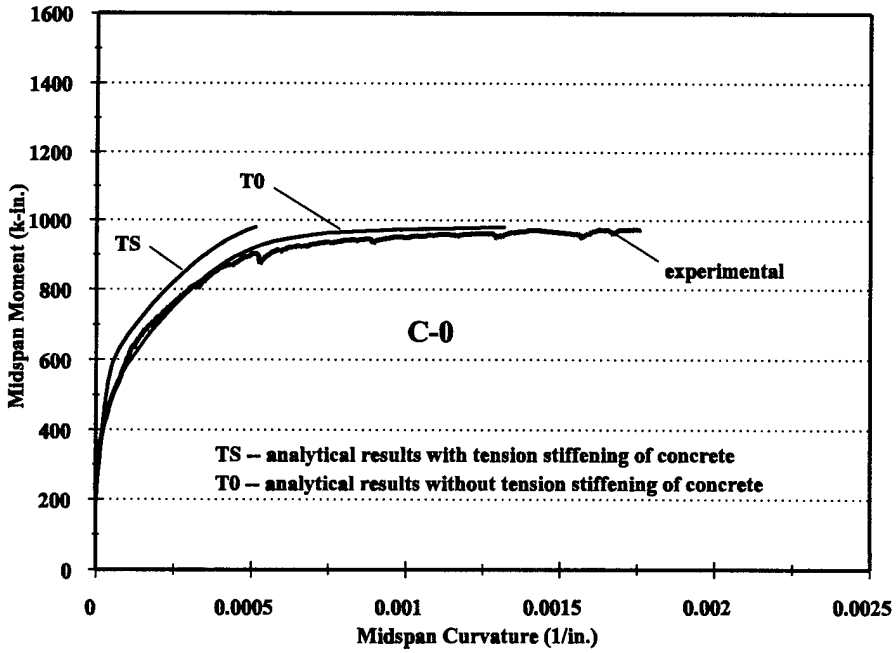

Fiugre 4.28 Midspan moment-curvature relationship for C-0

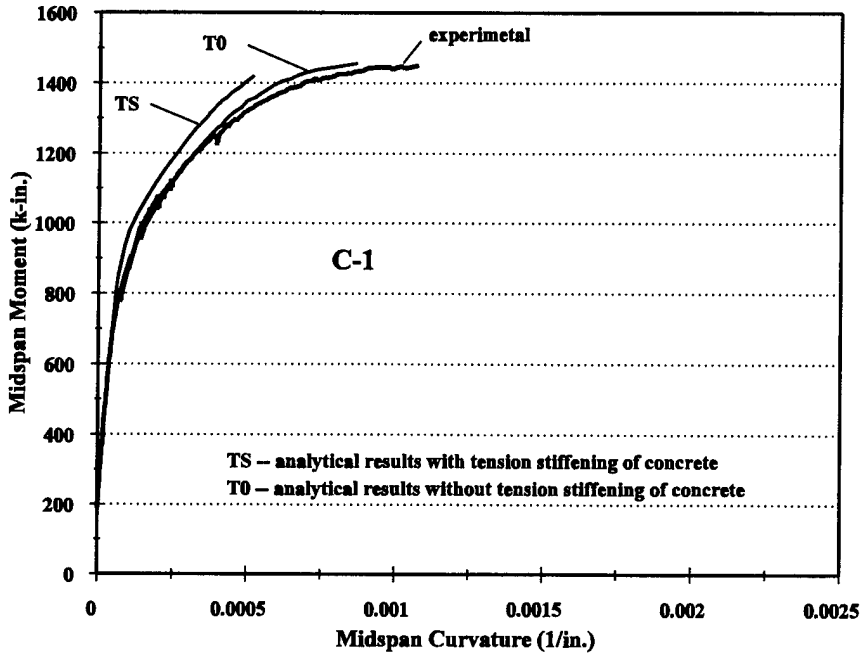

Figure 4.29 Midspan moment-curvature relationship for Beam C-1

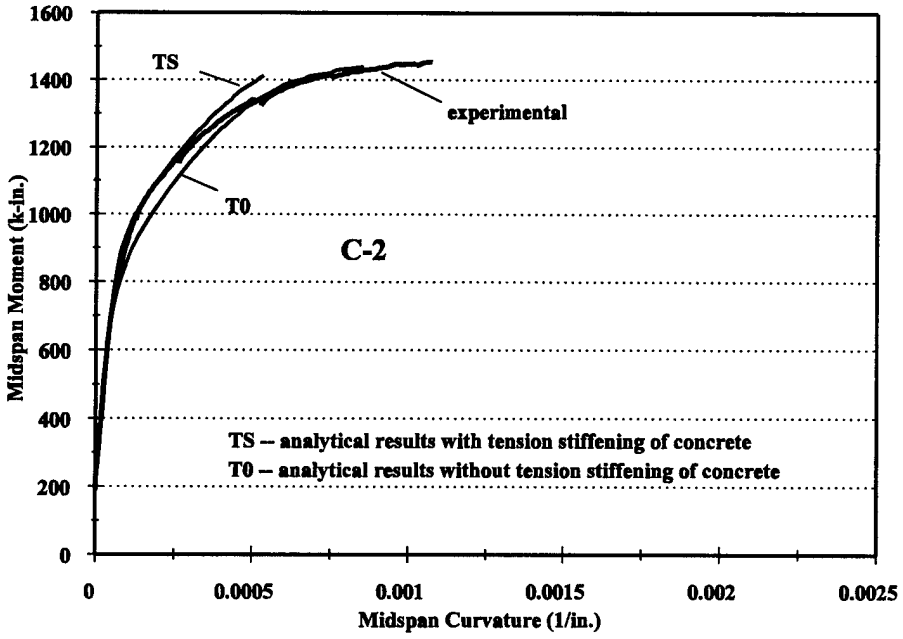

Figure 4.30 Midspan moment-curvature relationship for Beam C-2

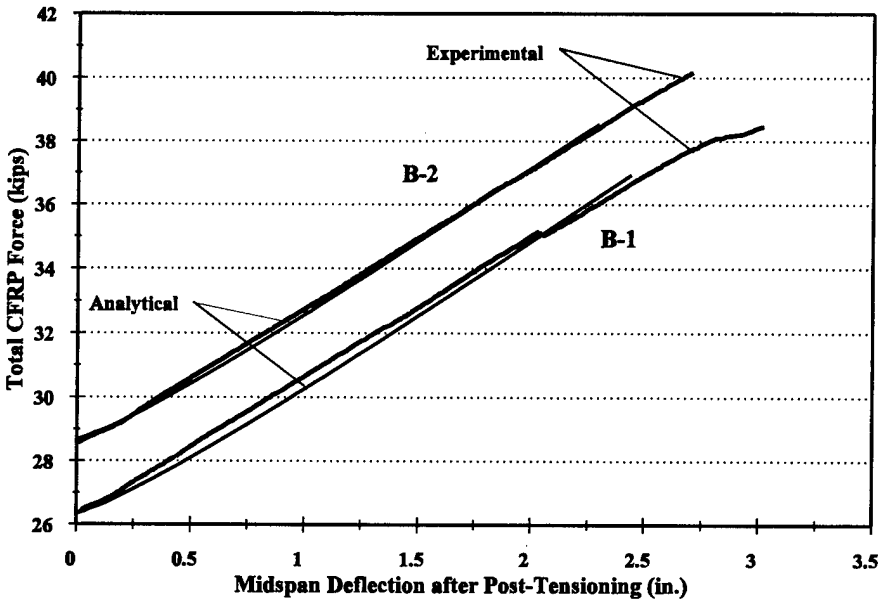

Figure 4.31 Total CFRP tendon force versus midspan deflection after post-tensioning, B-1 and B-2

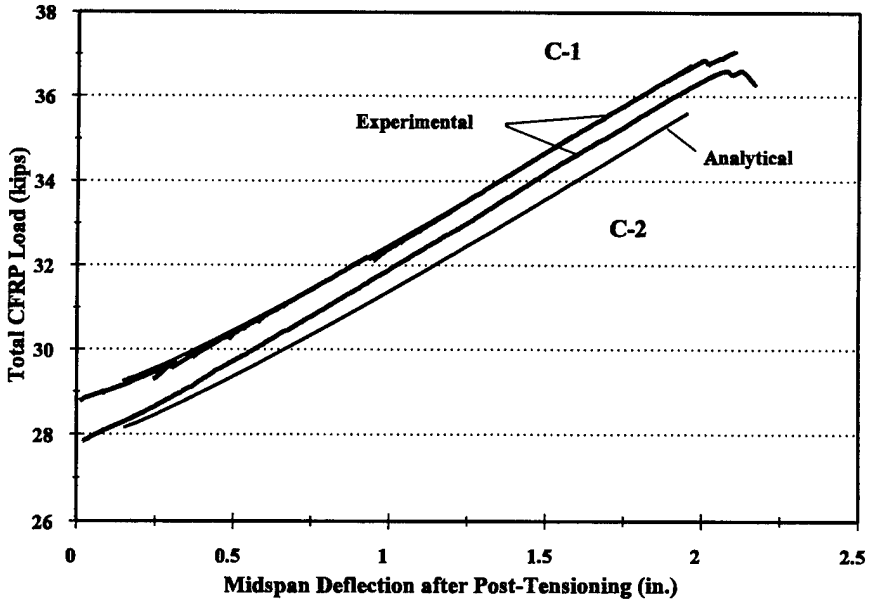

Figure 4.32 Total CFRP tendon force versus midspan deflection after post-tensioning, C-1 and C-2

CHAPTER 5

PARAMETRIC STUDY OF STEEL PRESTRESSED CONCRETE BEAMS STRENTHENED WITH EXTERIOR POST-TENSIONED FRP TENDONS

5.1 INTRODUCTION

To generate information on the effects of external FRP post-tensioning on steel prestressed concrete beams, a limited parametric study was accomplished using computer program EXPOST developed in this study (Appendix B). The intent of the study was to better understand the affect of properties of FRP tendons, tendon profile, and tendon forces on the behavior of the externally post-tensioned beams. The parameters of the study were limited to the initial force of the external FRP tendons, the load-strain relationship of the external FRP tendons, and the location of the external FRP tendon harping points.

Changes in the initial force of the external FRP tendons and the load-strain relationship of the external FRP tendons were accomplished by making appropriate changes in the elastic modulus value, cross-sectional area and initial post-tensioning stress of the FRP tendons. The effects on beam performance resulting from changes in these parameters were studied for four different reference beams. These reference beams included rectangular cross-section and 'T' cross-section (T-beams) beams. For each of these two types of beams, two prestressing steel reinforcement indexes were investigated, for a total of four reference beams. The two reinforcement indexes were designed to obtain results for fully prestressed beams that are externally strengthened by FRP tendons and for prestressed beams that have partially lost prestressing force due to corrosion of steel tendons and therefore need restoration of the design strength. The study investigates the parametric affects on the

ultimate load of the beam, midspan deflection at ultimate, FRP tendon force at ultimate load, and the area under the load-midspan deflection curve.

5.2 MATRIX OF VARIABLES FOR THE PARAMETRIC STUDY

The effects of external post-tensioning was investigated for four different reference beams. **Tables 5.1a** and **5.1b** lists the parameters of the four reference beams. The beams include two beams with a rectangular cross-section and two beams with a T cross-section (**Figure 5.1**). Each of the four beams had different amounts of prestressing steel. The amounts of prestressing steel were chosen to obtain results for fully prestressed beams that are externally strengthened by FRP tendons and for prestressed beams that have partially lost prestressing force due to corrosion of steel tendons and therefore need restoration of the design strength.

Tables 5.2a and **5.2b** show the matrix variables for the parametric study that was conducted for each of the four reference beams. Test variables identified in **Tables 5.2a** and **5.2b** are divided into primary and secondary variables. The primary variables are the parameters that are being studied for determining their influence on the beam behavior. These parameters include the initial post-tensioning force of the external FRP tendons, the location of the harping points of the external FRP tendons, and the axial stiffness of the external FRP tendons. The secondary variables are the FRP material properties that are inputs for computer program EXPOST. These variables were chosen to satisfy the initial force and axial stiffness requirements of the FRP tendons. These secondary variables can be adjusted without affecting the results of computer program EXPOST, provided the primary variables are not changed. The primary variables and parameters of the reference beams are discussed further in this section.

The preload values listed in **Tables 5.2a** and **5.2b** are the point loads, (P), applied to the beam during post-tensioning (**Figure 5.1**). These loads roughly equate to the upward

harping forces due to the exterior post-tensioning. They are applied prior to post-tensioning to avoid failure of the beams due to the application of the external post-tensioning. The reference numbers listed in **Tables 5.2a** and **5.2b** are a 5 character identification used to describe a particular beam with various combinations of parameters. The first character identifies the beam cross-section with R for rectangular and T for T-beam. The second character identifies the relative prestressing steel reinforcement index with L for low reinforcement index and H for high reinforcement index. The remaining 3 characters signify, in order, the initial force of the external FRP tendons (1 for 12 kips (53 MPa), 2 for 24 kips (110 MPa), or 3 for 36 kips (160 MPa)), the external tendon harping points (1 for third-point harping or 2 -- midpoint harping), and the axial stiffness (i.e. load-strain ratio) for the external reinforcement (1 for 1600 kip/in./in. (7100 kN), 2 for 3500 kip/in./in. (16000 kN), or 3 for 5400 kip/in./in. (24000 kN)). A total of 76 cases were analyzed for this study.

Each of the individual parametric beams were subjected to the following three conditions:

1. Behavior of the beam when loaded incrementally from 0 to the preload without external post-tensioning.

2. Effect of post-tensioning with the preload applied to the beam.

3. Behavior of the beam with the external post-tensioning applied and the load incrementally increased until failure of the beam.

Description of the test variables are provided in the following sections.

5.2.1 Cross-Section of the Beams

Figure 5.1 shows the cross-sections investigated in this study. The cross-sections include a rectangular beam and a T-beam. These cross-sections were considered representative of cross-section types used in construction. No non-prestressed tensile or compression reinforcement was included in the analysis.

5.2.2 Prestressing Steel Reinforcing Index

The prestressing steel reinforcing index, ω, was used as an indicator of the amount of prestressing steel for the beams. In general, the prestressing steel reinforcement index is defined as:

$$\omega = \frac{A_{ps} f_{ps}}{b\ d\ f_c} \tag{5.1}$$

where ω = prestressing steel reinforcement index
A_{ps} = cross-sectional area of prestressing steel
f_{ps} = prestressing steel stress at nominal strength
b = width of concrete section
d = depth of prestressing steel reinforcement
f_c = concrete compressive strength

The two values of ω used for the study were $\omega_{max}/4$ and $\omega_{max}/2$ (**Tables 5.1a** and **5.1b**). The value of ω_{max} was the maximum reinforcing index allowed by the ACI 318-95 code [ACI Committee 318, 1995]. Calculations of the limiting values of ω_{max} and the resulting prestressing steel areas used in the study are shown in Appendix C.

5.2.3 Initial Force of the External FRP Tendons

The initial force of the external FRP tendons was varied between 12 and 36 kips (53 and 160 kN) (**Tables 5.2a** and **5.2b**). This force is equivalent to the product of the total cross-sectional area of the external FRP tendons and the initial post-tensioning stress for the tendons. These values were considered representative of the prestress values that may be used in exterior post-tensioning with FRP tendons.

5.2.4 Location of Harping Points for the External FRP Tendons

The location of harping points for the external FRP tendons investigated in this study were at 1/3 and 1/2 of the span length from the end of the beam (**Tables 5.2a** and **5.2b**). The location of harping points for the external FRP tendons were considered to be representative of the harping point locations typically found in construction.

5.2.5 Axial Stiffness of the External FRP Tendons

The values of the external FRP tendon axial stiffness varied between 1600 and 5400 kip/in./in. (7100 and 24000 kN) (**Tables 5.2a** and **5.2b**). The value of the external FRP tendon axial stiffness can be calculated as the product of the total FRP cross-sectional area used in the post-tensioning and the elastic modulus of the FRP tendons. The values of the external FRP tendon axial stiffness were chosen as representative of the FRP tendons currently available.

5.2.6 Other Parameters

Anchorage of the external FRP tendons was located above the beam supports at the center of gravity of the concrete section. This equated to 8 in. (203 mm) from the top of the concrete for the rectangular beams and 5.3 in. (135 mm) from the top of the concrete for the T-beams. At the midspan region of the beams, the location of the FRP tendon was set to 16 in. (406 mm) from the top of the beam. The concrete strength used was 6 ksi (41 MPa). The effective depth of the prestressing steel was set to 13.0 in. (330 mm) (**Tables 5.1a** and **5.1b**). Loading of the beams was from two point loads placed one-third of the span length from the beam supports. All beams were simply supported.

5.3 RESULTS

A wide variety of information is available from the results of computer program EXPOST. Results discussed in this study are, however, limited to the effects of external post-tensioning on the ultimate load, midspan deflections at ultimate load, FRP tendon force at ultimate load, and the area under the load-midspan deflection curve for the beams. The results of the parametric study are shown graphically in **Figures 5.2** through **5.17**. The legend shown in these figures refers to the reference number of the parametric beam as shown in **Tables 5.2a** and **5.2b**. **Tables 5.3a** and **5.3b** provide a summary of the results for the parametric study.

5.3.1 Ultimate Load

Figures 5.2 through **5.5** show the effect of the initial force of the external FRP tendons on the increase in ultimate load of the beams. The increase in ultimate load for the externally post-tensioned beams is expressed as a percent of the companion non-post-tensioned reference beams. Results from all six combinations of harping point location and axial stiffness of FRP tendons are plotted on the same figure for each reference beam.

Average ultimate loads for the externally post-tensioned beams were 11.7, 10.5, 10.0 and 9.3 kips (52.0, 46.7, 44.5 and 41.4 kN) greater than the ultimate load for companion non-post-tensioned beams for the RL, RH, TL and TH beams, respectively (**Tables 5.3a** and **5.3b**). This corresponds to ultimate loads of 231, 156, 172 and 130 percent of the ultimate loads for the companion non-post-tensioned reference beams for the RL, RH, TL and TH beams, respectively.

The results indicate that increases in the initial force of the external FRP tendons resulted in linear increases in the ultimate load of the beams (**Figures 5.2** through **5.5**). Increasing the initial force of the external FRP tendon from 12 to 36 kips (53 to 160 kN) resulted in average ultimate load increases of 6.7, 6.2, 4.1, and 4.2 kips (30, 28, 18, and

19 kN) for the RL, RH, TL and TH beams, respectively (**Tables 5.3a** and **5.3b**). This corresponds to ultimate load increases of 39, 24, 19, and 11 percent of the average ultimate load of beams with initial force in external FRP tendons of 12 kips (53 kN) for the RL, RH, TL and TH beams, respectively.

Beams with tendons harped at third-points showed a larger increase in ultimate load than did beams with tendons harped at midpoint (**Tables 5.3a** and **5.3b**). Additionally, the affects on the ultimate load due to varying the initial external FRP tendon force was more significant for the beams with tendons harped at third-points than for beams with tendons harped at midspan (**Figures 5.2** through **5.5**). The average increases in ultimate load for beams with tendons harped at third-points versus beams with tendons harped at midpoint were 2.9, 2.7, 1.8, and 2.5 kips (12.9, 12.0, 8.0, and 11.1 kN) for the RL, RH, TL and TH beams, respectively (**Tables 5.3a** and **5.3b**). This corresponds to ultimate load increases of 15, 10, 8, and 6 percent of the average ultimate load for the midpoint harped beams for the RL, RH, TL and TH beams, respectively.

Beams post-tensioned with higher axial stiffness of the external tendons resulted in consistently higher ultimate loads than those post-tensioned with lower axial stiffness of the external tendons (**Figures 5.2** through **5.5**). Increasing the external FRP tendon axial stiffness from 1600 to 5400 kips (7100 to 24000 kN) resulted in average ultimate load increases of 3.6, 3.0, 3.9, and 3.7 kips (16, 13, 17, and 16 kN) for the RL, RH, TL and TH beams, respectively (**Tables 5.3a** and **5.3b**). This corresponds to ultimate load increases of 19, 11, 18, and 10 percent of the average ultimate load of beams with external FRP tendon axial stiffness of 1600 kips (7100 kN) for the RL, RH, TL and TH beams, respectively.

5.3.2 Midspan Deflection at Ultimate

Figures 5.6 through **5.9** show the effect of the initial force of the external FRP tendons on the midspan deflection at ultimate. Midspan deflections at ultimate for beams externally post-tensioned reduced an average of 3.7, 1.0, 20.6 and 6.4 in. (94, 25, 523 and 163 mm)

compared to the companion non-post-tensioned beams for the RL, RH, TL and TH beams, respectively (**Tables 5.3a** and **5.3b**). This corresponds to midspan deflections of 47, 77, 34, and 60 percent of the midspan deflection at ultimate for the companion non-post-tensioned reference beam for the RL, RH, TL and TH beams, respectively. The average reduction in midspan deflection for all externally post-tensioned beams was 46% of the midspan deflection of the companion non-post-tensioned beams.

Increasing the initial external FRP tendon force from 12 to 36 kips (53 to 160 kN) resulted in average midspan deflection at ultimate decreases of 0.69, 0.47, 2.20, and 1.74 in. (18, 12, 56, and 44 mm) for the RL, RH, TL and TH beams, respectively (**Tables 5.3a** and **5.3b**). This corresponds to reductions in midspan deflections at ultimate of 19, 14, 19, and 17 percent of the average midspan deflection at ultimate of beams with initial external FRP tendon forces of 12 kips (53 kN) for the RL, RH, TL and TH beams, respectively.

For the rectangular beams, average midspan deflections at ultimate for beams with tendons harped at third-points were larger than average midspan deflections at ultimate for beams with tendons harped at midspan (**Tables 5.3a** and **5.3b**). For the T-beams, average midspan deflections at ultimate for beams with tendons harped at third-points were smaller than average midspan deflections at ultimate for beams with tendons harped at midspan (**Tables 5.3a** and **5.3b**). The variation in average midspan deflection at ultimate for beams with tendons harped at third-points versus beams with tendons harped at midpoint were 0.34, 0.25, -1.32, and -0.15 in. (9, 6, -34, and -4 mm) for the RL, RH, TL and TH beams, respectively (**Tables 5.3a** and **5.3b**). This corresponds to variations in midspan deflections at ultimate of 11, 8, -12, and -2 percent of the average midspan deflection at ultimate for the beams with tendons harped at midpoint for the RL, RH, TL and TH beams, respectively. For the rectangular beams, the affects on the midspan deflection at ultimate due to varying the initial force of the external FRP tendon was more significant for the beams with tendons harped at midpoints than for beams with tendons harped at third-points (**Figures 5.6** and **5.7**). For the T-beams, the affects on the midspan deflection at ultimate due to varying the

initial force of the external FRP tendon was about the same for beams with tendons harped at midpoints and beams with tendons harped at third-points (**Figures 5.8** and **5.9**).

Beams post-tensioned with higher axial stiffness of the external tendons resulted in consistently smaller midspan deflections at ultimate than those post-tensioned with lower axial stiffness of the external tendons (**Tables 5.3a** and **5.3b**). Increasing the external FRP tendon axial stiffness from 1600 to 5400 kips (7100 to 24000 kN) resulted in average midspan deflection at ultimate decreases of 0.25, 0.22, 2.16, and 1.35 in. (6, 6, 55, and 34 mm) for the RL, RH, TL and TH beams, respectively (**Tables 5.3a** and **5.3b**). This corresponds to midspan deflections at ultimate of 93, 93, 81, and 87 percent of the average midspan deflection at ultimate of beams with external FRP tendon axial stiffness of 1600 kips (7100 kN) for the RL, RH, TL and TH beams, respectively.

5.3.3 FRP Tendon Force at Ultimate Load

Figures 5.10 through **5.13** show the effect of the initial force of the external FRP tendons on the force of the external tendons at ultimate. The force of the external tendons at ultimate is expressed as a percentage of the initial force of the external tendons. **Tables 5.3a** and **5.3b** show the average increase in force of the external FRP tendons at ultimate load. The tables also show the average of the percentage increases in force of the external FRP tendons at ultimate load in parentheses.

The forces at ultimate for the external FRP tendons increased over their initial forces an average of 11.3, 10.6, 20.9 and 18.6 kips (50, 47, 93 and 83 kN) for the RL, RH, TL and TH beams, respectively (**Tables 5.3a** and **5.3b**). These increases correspond to average percentage increases of 60, 56, 111 and 99 percent of the associated initial forces of the external FRP tendons for the RL, RH, TL and TH beams, respectively (**Tables 5.3a** and **5.3b**). Forces of the external tendons at ultimate averaged 158% and 205% of the associated initial force of the external tendons for the rectangular and T-beams, respectively.

Increases in the initial force of the external FRP tendon from 12 to 36 kips (53 to

160 kN) resulted in lower average increases of the forces in external FRP tendons at ultimate by 2.9, 2.0, 5.1, and 3.9 kips (13, 9, 23, and 17 kN) for the RL, RH, TL, and TH beams, respectively (**Tables 5.3a** and **5.3b**).

The beams with tendons harped at third-points showed an average increase in the force of the external FRP tendons at ultimate of 2.6, 2.4, -1.9, and 1.8 kips (12, 11, -8.5, and 8.0 kN) higher than did similar beams with tendons harped at midpoint for the RL, RH, TL, and TH beams, respectively (**Tables 5.3a** and **5.3b**). Note that for the TL beams, the increase is negative (i.e. the average increase in force of the external FRP tendons at ultimate was larger for the beams with tendons harped at midspan than for beams with tendons harped at third-points).

Beams post-tensioned with higher axial stiffness of the external FRP tendons resulted in consistently higher increases in forces of the external FRP tendon at ultimate than did lower axial stiffness tendons (**Figures 5.10** through **5.13**). Increasing the external FRP tendon axial stiffness from 1600 to 5400 kips (53 to 160 kN) resulted in average increases in forces of the external FRP tendons at ultimate of 11.2, 10.7, 18.0, and 17.4 kips (49.8, 47.6, 80.1, and 77.4 kN) for the RL, RH, TL and TH beams, respectively (**Tables 5.3a** and **5.3b**). This corresponds to average increases in forces of the external FRP tendons of 300, 306, 255, and 278 percent of the average increases in forces of the external FRP tendons with external FRP tendon axial stiffness of 1600 kips (53 kN) for the RL, RH, TL and TH beams, respectively.

5.3.4 Area Under Load-Midspan Deflection Curve

Figures 5.14 through **5.17** show the effect of the initial force of the external FRP tendons on the energy absorption capacity of the beam which is considered to be the area under the load-midspan deflection curve for the beams. Even though the area is defined based on the midspan deflection instead of the deflection at the point loads, this area will be referred to as the energy absorption capacity at failure. The midspan deflection was chosen

for the relationship instead of the deflection at point load because the midspan deflection is typically used in definition of ductility of beams.

Average energy absorption capacity at failure for the externally post-tensioned beams were 2.5, -8.9, 201, and 132 kip-in. (0.3, -1.0, 22.7, and 14.9 kN-m) less than the energy absorption capacity at failure for companion non-post-tensioned beams for the RL, RH, TL and TH beams, respectively (**Tables 5.3a** and **5.3b**). This corresponds to energy absorption capacity at failure of 95, 114, 49, and 69 percent of the energy absorption capacity at failure for the companion non-post-tensioned reference beams for the RL, RH, TL and TH beams, respectively. The average reduction of the energy absorption capacity at failure for the post-tensioned T-beams was 41% of the energy absorption capacity at failure of the companion non-post-tensioned beams, which is due to reduced deformation capacity of externally post-tensioned beams.

The results indicate that increases in the initial force of the external FRP tendons resulted in no significant change in the energy absorption capacity at failure for most beams (**Figures 5.14** through **5.17**). Only the rectangular beams with tendons harped at midspan showed any significant change in energy absorption capacity at failure resulting from increases in the initial force of the external FRP tendons. For rectangular beams with tendons harped at midspan, increasing the initial force of the external FRP tendons from 12 to 36 kips (53 to 160 kN) resulted in increases in energy absorption capacity at failure of 15 and 10 kip-in. (1.7 and 1.1 kN-m) for the RL and RH beams, respectively (**Figures 5.14** and **5.15**).

For the T-beams, no significant difference was observed in the energy absorption capacity at failure between beams with tendons harped at third-points and beams with tendons harped at midpoint (**Figures 5.16** and **5.17**). For the rectangular beams, the average energy absorption capacity at failure for the beams with tendons harped at third-points was 128 and 119 percent of the average energy absorption capacity at failure for beams with tendons harped at midpoint (**Tables 5.3a** and **5.3b**).

For the T-beams, no significant difference was observed in the energy absorption capacity at failure for beams with various axial stiffness of the external tendons (**Figures 5.16** and **5.17**). For the rectangular beams, increasing the external FRP tendon axial stiffness from 1600 to 5400 kips (7100 to 24000 kN) resulted in average decreases in the energy absorption capacity at failure of 12 and 11 percent compared to beams with external FRP tendon axial stiffness of 1600 kips (7100 kN) (**Tables 5.3a** and **5.3b**).

5.4 SUMMARY AND CONCLUSIONS

A parametric study using the computerized model -- EXPOST (Appendix B) was conducted. The effects of initial force of the external FRP tendons, the location of harping points for external FRP tendons, and the axial stiffness of the external FRP tendons on four reference beams were studied. For the parameters studied, the following conclusions are made:

1. For externally post-tensioned prestressed concrete beams, the ultimate load increases with increases in initial force of the external tendons, harping at third-points as opposed to midpoints of the beam, and with increases in the stiffness of the external tendons. Beams with a lower amount of prestressing steel showed a slightly higher average quantitative increase in ultimate load and a substantially higher average percentage increase in ultimate load versus the companion non-post-tensioned beam. External post-tensioning resulted in average ultimate loads corresponding to 231, 156, 172 and 130 percent of the companion reference beam ultimate load for the RL, RH, TL and TH beams, respectively.

2. The addition of external post-tensioning reduced midspan deflections at ultimate an average of 46%. The magnitude of the reduction was greater for beams with lower amounts of steel prestressing compared to beams with higher amounts of steel

prestressing.

3. Forces of the external tendons at ultimate averaged 158% and 205% of the associated initial forces of the external tendons for the rectangular and T-beams, respectively.

4. For the rectangular beams, the energy absorption capacity at failure, defined as the area under the load-midspan deflection relationship of the beam, was about the same for post-tensioned and companion non-post-tensioned beams. The addition of external post-tensioning for T-beams reduced the energy absorption capacity at failure an average of 41%.

Table 5.1a Parameters of reference beams, US customary units

Parameter	Reference Beams*			
	RL	RH	TL	TH
Concrete cross section	Rectangular	Rectangular	T	T
Dimensions*, in.	b = 6 h = 16 d = 13	b = 6 h = 16 d = 13	$b_w = 4$ $b_f = 24$ h = 16 $h_f = 2$ d = 13	$b_w = 4$ $b_f = 24$ h = 16 $h_f = 2$ d = 13
Beam span, ft.	20	20	30	30
Area of prestressing steel, (A_{ps}), in^2	0.12	0.25	0.27	0.58
Steel reinforcing index, (ω)	0.0675	0.135	0.0385	0.077
Effective prestress of steel, (f_{pe}), ksi	150	150	150	150
Concrete strength, (f'_c), ksi	6	6	6	6
Depth of prestressing steel, (d), in.	13	13	13	13

* Nomenclature

RL = rectangular beam with low prestressing steel reinforcement index
RH = rectangular beam with high prestressing steel reinforcement index
TL = T-beam with low prestressing steel reinforcement index
TH = T-beam with high prestressing steel reinforcement index
b = width of beam
b_w = width of beam web
b_f = width of beam flange
h = total height of beam
h_f = thickness of top flange
d = depth of reinforcement

Table 5.1b Parameters of reference beams, SI units

Parameter	Reference Beams*			
	RL	**RH**	**TL**	**TH**
Concrete cross section	Rectangular	Rectangular	T	T
Dimensions*, mm	b = 152 h = 406 d = 330	b = 152 h = 406 d = 330	b_w = 102 b_f = 610 h = 406 h_f = 51 d = 330	b_w = 102 b_f = 610 h = 406 h_f = 51 d = 330
Beam span, m	6.1	6.1	9.1	9.1
Area of prestressing steel, (A_{ps}), mm^2	77	161	174	374
Steel reinforcing index, (ω)	0.0675	0.135	0.0385	0.077
Effective prestress of steel, (f_{pe}), MPa	1030	1030	1030	1030
Concrete strength, (f'_c), MPa	41	41	41	41
Depth of prestressing steel, (d), mm	330	330	330	330

* Nomenclature

RL = rectangular beam with low prestressing steel reinforcement index
RH = rectangular beam with high prestressing steel reinforcement index
TL = T-beam with low prestressing steel reinforcement index
TH = T-beam with high prestressing steel reinforcement index
b = width of beam
b_w = width of beam web
b_f = width of beam flange
h = total height of beam
h_f = thickness of top flange
d = depth of reinforcement

Table 5.2a Matrix of variables for the parametric study, US customary units

Primary parameters			Secondary parameters			Preload, (P), kips	Reference number*
Initial FRP force, kips	Harping point location	FRP axial stiffness, kip/in./in.	E_{FRP}, ksi	A_{FRP}, in^2	f_{FRP}, ksi		
0	---	0	0	0	0	0	**000
12	0.33L	1600	20000	0.08	150	1.15	**111
		3500	21875	0.16	75	1.15	**112
		5400	22500	0.24	50	1.15	**113
	0.5 L	1600	20000	0.08	150	1.15	**121
		3500	21875	0.16	75	1.15	**122
		5400	22500	0.24	50	1.15	**123
24	0.33L	1600	20000	0.08	300	2.15	**211
		3500	21875	0.16	150	2.15	**212
		5400	22500	0.24	100	2.15	**213
	0.5 L	1600	20000	0.08	300	2.15	**221
		3500	21875	0.16	150	2.15	**222
		5400	22500	0.24	100	2.15	**223
36	0.33L	1600	10000	0.16	225	3.15	**311
		3500	10938	0.32	112.5	3.15	**312
		5400	11250	0.48	75	3.15	**313
	0.5 L	1600	10000	0.16	225	3.15	**321
		3500	10938	0.32	112.5	3.15	**322
		5400	11250	0.48	75	3.15	**323

* Nomenclature: * * 0 0 0

- flag for FRP axial stiffness value -- 0 = no CFRP; 1 = 1600; 2 = 3500; 3 = 5400 kip-in./in.
- flag for harping point location -- 0 = no harping; 1 = 0.33L; 2 = 0.5 L
- flag for initial FRP load -- 0 = no FRP; 1 = 12; 2 = 24; 3 = 36 kip
- flag for relative amount of steel reinforcement -- L = low reinforcement; H = high reinforcement
- flag for beam cross-section -- R = rectangular; T = T-beam

Table 5.2b Matrix of variables for the parametric study, SI units

Primary parameters			Secondary parameters			Preload, (P), kN	Reference number*
Initial FRP force, kN	Harping point location	FRP axial stiffness, kN/m/m	E_{FRP}, GPa	A_{FRP}, mm^2	f_{FRP}, MPa		
0	---	0	0	0	0	0	**000
53	0.33L	7120	138	52	1030	5.11	**111
		15600	151	103	520	5.11	**112
		24000	155	155	345	5.11	**113
	0.5 L	7120	138	52	1030	5.11	**121
		15600	151	103	520	5.11	**122
		24000	155	155	345	5.11	**123
107	0.33L	7120	138	52	2070	9.56	**211
		15600	151	103	1030	9.56	**212
		24000	155	155	690	9.56	**213
	0.5 L	7120	138	52	2070	9.56	**221
		15600	151	103	1030	9.56	**222
		24000	155	155	690	9.56	**223
160	0.33L	7120	69.0	103	1550	14.0	**311
		15600	75.4	206	780	14.0	**312
		24000	77.6	310	520	14.0	**313
	0.5 L	7120	69.0	103	1550	14.0	**321
		15600	75.4	206	780	14.0	**322
		24000	77.6	310	520	14.0	**323

* Nomenclature: **000

- flag for FRP axial stiffness value -- 0 = no CFRP; 1 = 1600; 2 = 3500; 3 = 5400 kip-in./in.
- flag for harping point location -- 0 = no harping; 1 = 0.33L; 2 = 0.5 L
- flag for initial FRP load -- 0 = no FRP; 1 = 12; 2 = 24; 3 = 36 kip
- flag for relative amount of steel reinforcement -- L = low reinforcement; H = high reinforcement
- flag for beam cross-section -- R = rectangular; T = T-beam

Table 5.3a Summary of parametric test results, US customary units

Beams	Ultimate load, kips	Midspan deflection, in.	Increase in FRP load at ultimate, kips (%)	Area under load-midspan deflection curve, kip-in.
RL BEAMS				
RL000	8.9	6.88	--	53.3
Average for beams with initial CFRP load of 12 kips	17.2	3.58	12.8 (107)	45.7
Average for beams with initial CFRP load of 36 kips	23.9	2.89	9.9 (27.4)	55.6
Average for beams harped at ⅓ points	22.0	3.39	12.6 (66.4)	57.0
Average for beams harped at midspan	19.1	3.05	10.0 (54.3)	44.6
Average for beams with FRP stiffness of 1600 kips	18.7	3.34	5.6 (29.9)	50.0
Average for beams with FRP stiffness of 5400 kips	22.3	3.09	16.8 (89.4)	51.3
Average of all post-tensioned RL beams	20.6	3.22	11.3 (60.3)	50.8
RH BEAMS				
RH000	18.9	4.15	--	62.0
Average for beams with initial CFRP load of 12 kips	26.2	3.42	11.6 (96.7)	66.3
Average for beams with initial CFRP load of 36 kips	32.4	2.95	9.6 (26.6)	74.2
Average for beams harped at ⅓ points	30.7	3.32	11.8 (62.1)	77.0
Average for beams harped at midspan	28.0	3.07	9.4 (49.8)	64.8
Average for beams with FRP stiffness of 1600 kips	27.8	3.31	5.2 (27.6)	71.4
Average for beams with FRP stiffness of 5400 kips	30.8	3.09	15.9 (83.2)	70.3
Average of all post-tensioned RH beams	29.4	3.19	10.6 (55.9)	70.9

Table 5.3a (continued)

Beams	Ultimate load, kips	Midspan deflection, in.	Increase in FRP load at ultimate, kips (%)	Area under load-midspan deflection curve, kip-in.
TL BEAMS				
TL000	13.9	31.0	--	394
Average for beams with initial CFRP load of 12 kips	21.9	11.6	23.6 (197)	192
Average for beams with initial CFRP load of 36 kips	26.0	9.40	18.5 (51.3)	195
Average for beams harped at ⅓ points	24.8	9.78	19.9 (106)	187
Average for beams harped at midspan	23.0	11.1	21.8 (117)	198
Average for beams with FRP stiffness of 1600 kips	21.9	11.6	11.6 (63.2)	206
Average for beams with FRP stiffness of 5400 kips	25.8	9.44	29.6 (156)	182
Average of all post-tensioned TL beams	23.9	10.4	20.9 (111)	193
TH BEAMS				
TH000	30.7	16.0	--	425
Average for beams with initial CFRP load of 12 kips	37.9	10.5	20.6 (172)	304
Average for beams with initial CFRP load of 36 kips	42.1	8.76	16.8 (46.6)	284
Average for beams harped at ⅓ points	41.2	9.48	19.5 (102)	298
Average for beams harped at midspan	38.7	9.63	17.7 (94.6)	288
Average for beams with FRP stiffness of 1600 kips	38.1	10.3	9.8 (52.8)	312
Average for beams with FRP stiffness of 5400 kips	41.8	8.95	27.2 (142)	279
Average of all post-tensioned TH beams	40.0	9.56	18.6 (98.5)	293

Table 5.3b Summary of parametric test results, SI units

Beams	Ultimate load, kN	Midspan deflection, mm	Increase in FRP load at ultimate, kN (%)	Area under load-midspan deflection curve, kN-m
RL BEAMS				
RL000	39.6	175	--	6.0
Average for beams with initial CFRP load of 12 kips	76.5	91	56.9 (107)	5.2
Average for beams with initial CFRP load of 36 kips	106	73	44.0 (27.4)	6.3
Average for beams harped at ⅓ points	97.9	86	56.0 (66.4)	6.4
Average for beams harped at midspan	85.0	77	44.5 (54.3)	5.0
Average for beams with FRP stiffness of 1600 kips	83.2	85	24.9 (29.9)	5.7
Average for beams with FRP stiffness of 5400 kips	99.2	78	74.7 (89.4)	5.8
Average of all post-tensioned RL beams	91.6	82	50.3 (60.3)	5.7
RH BEAMS				
RH000	84.1	105	--	7.0
Average for beams with initial CFRP load of 12 kips	117	87	51.6 (96.7)	7.5
Average for beams with initial CFRP load of 36 kips	144	75	42.7 (26.6)	8.4
Average for beams harped at ⅓ points	137	84	52.5 (62.1)	8.7
Average for beams harped at midspan	125	78	41.8 (49.8)	7.3
Average for beams with FRP stiffness of 1600 kips	124	84	23.1 (27.6)	8.1
Average for beams with FRP stiffness of 5400 kips	137	78	70.7 (83.2)	7.9
Average of all post-tensioned RH beams	131	81	47.1 (55.9)	8.0

Table 5.3b (continued)

Beams	Ultimate load, kN	Midspan deflection, mm	Increase in FRP load at ultimate, kN (%)	Area under load-midspan deflection curve, kN-m
TL BEAMS				
TL000	61.8	787	--	44.5
Average for beams with initial CFRP load of 12 kips	97.4	295	105 (197)	21.7
Average for beams with initial CFRP load of 36 kips	116	239	82.3 (51.3)	22.0
Average for beams harped at ⅓ points	110	248	88.5 (106)	21.1
Average for beams harped at midspan	102	282	97.0 (117)	22.4
Average for beams with FRP stiffness of 1600 kips	97.4	295	51.6 (63.2)	23.3
Average for beams with FRP stiffness of 5400 kips	115	240	132 (156)	20.6
Average of all post-tensioned TL beams	106	264	93.0 (111)	21.8
TH BEAMS				
TH000	137	406	--	48.0
Average for beams with initial CFRP load of 12 kips	169	267	92.1 (172)	34.4
Average for beams with initial CFRP load of 36 kips	187	223	74.7 (46.6)	32.1
Average for beams harped at ⅓ points	183	241	86.7 (102)	33.7
Average for beams harped at midspan	172	245	78.7 (94.6)	32.5
Average for beams with FRP stiffness of 1600 kips	170	262	43.6 (52.8)	35.3
Average for beams with FRP stiffness of 5400 kips	186	227	121 (142)	31.5
Average of all post-tensioned TH beams	178	243	82.7 (98.5)	33.1

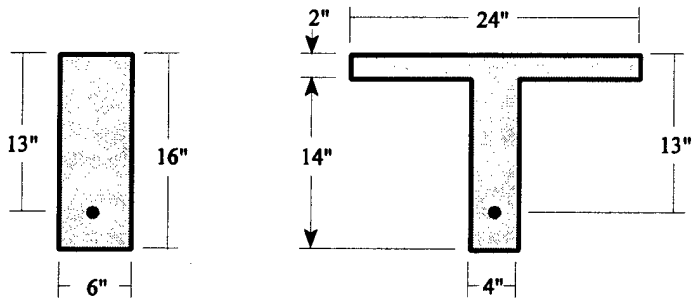

Figure 5.1a Beam cross-sections

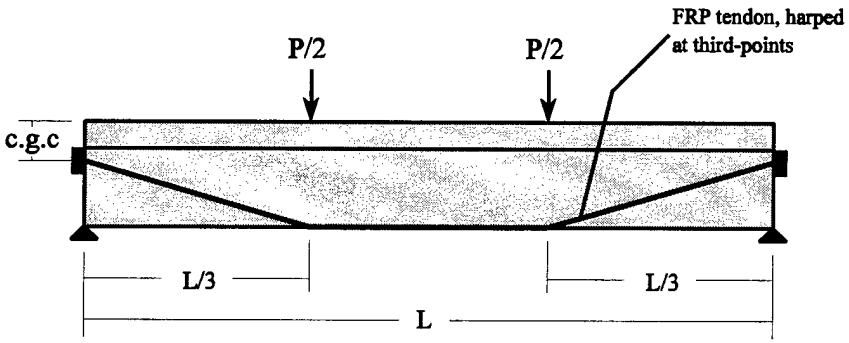

L = 20' for RL and RH beams; L = 30' for TL and TH beams

Figure 5.1b Profile view of beam with tendons harped at third-points

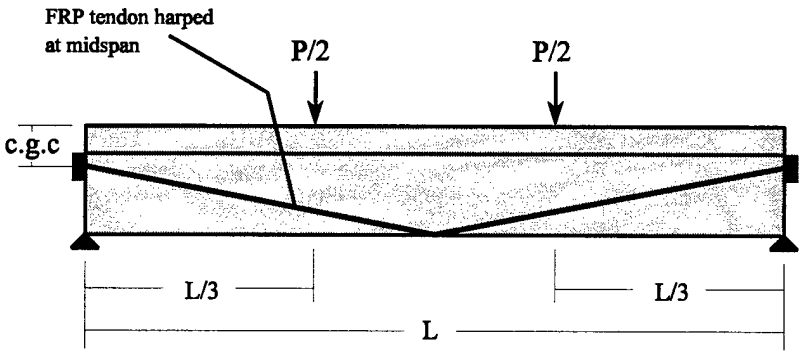

L = 20' for RL and RH beams; L = 30' for TL and TH beams

Figure 5.1c Profile view of beam with tendons harped at midspan

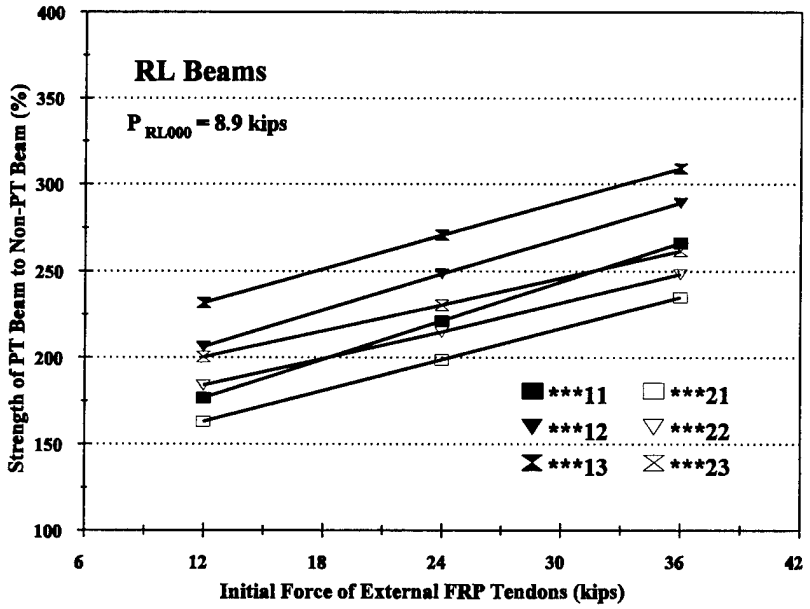

Figure 5.2 Effect of initial force of external FRP tendons on the ultimate load of RL beams

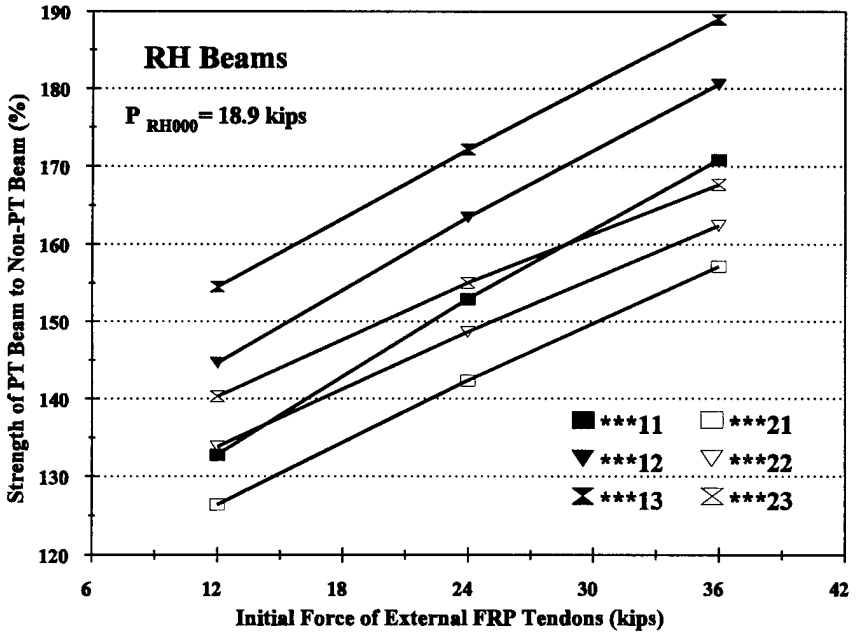

Figure 5.3 Effect of initial force of external FRP tendons on the ultimate load of RH beams

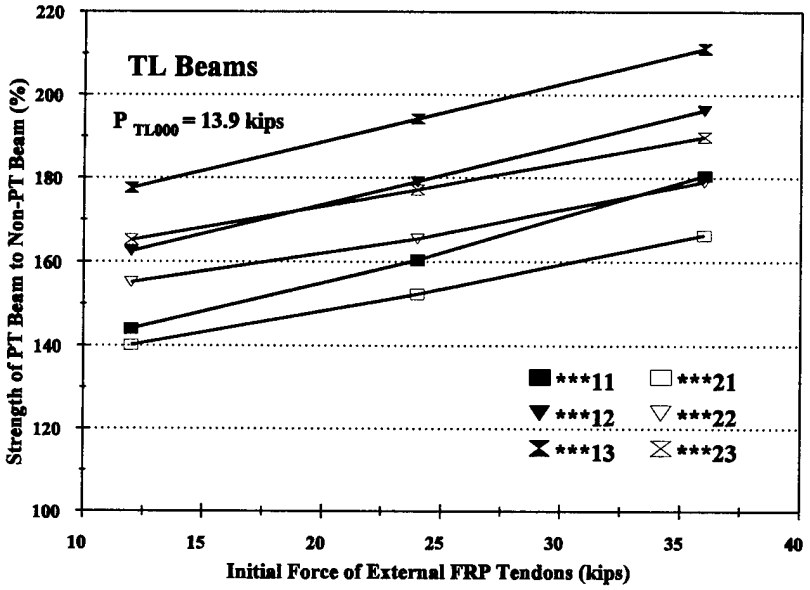

Figure 5.4 Effect of initial force of external FRP tendons on the ultimate load of TL beams

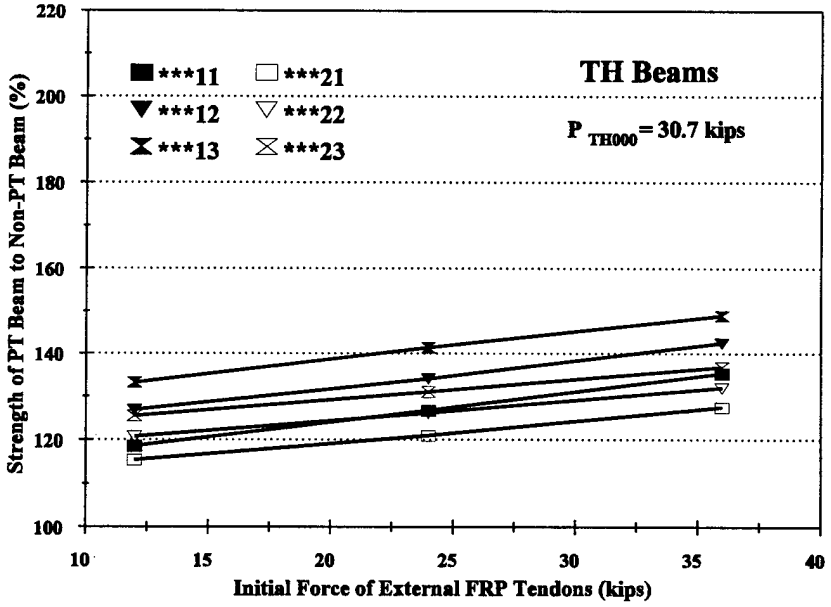

Figure 5.5 Effect of initial force of external FRP tendons on the ultimate load of TH beams

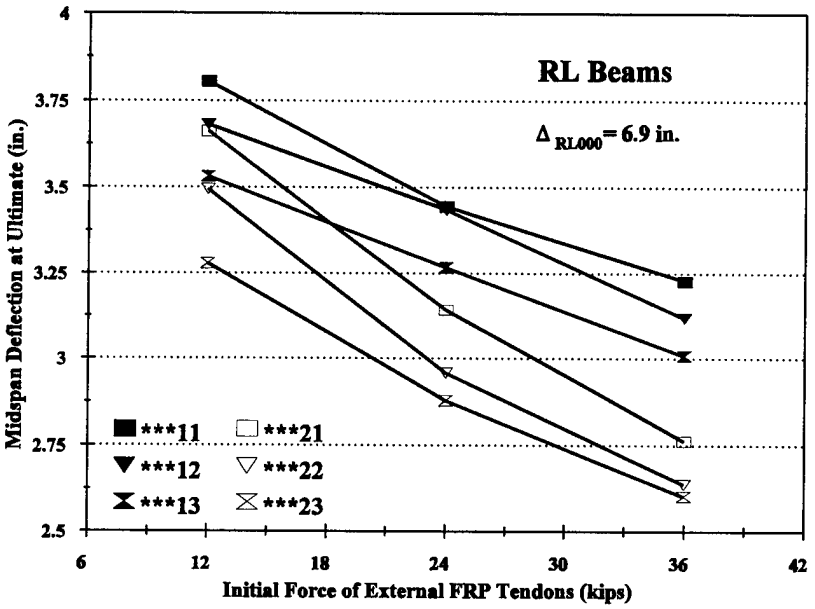

Figure 5.6 Effect of initial force of external FRP tendons on the midspan deflection at ultimate load for RL beams

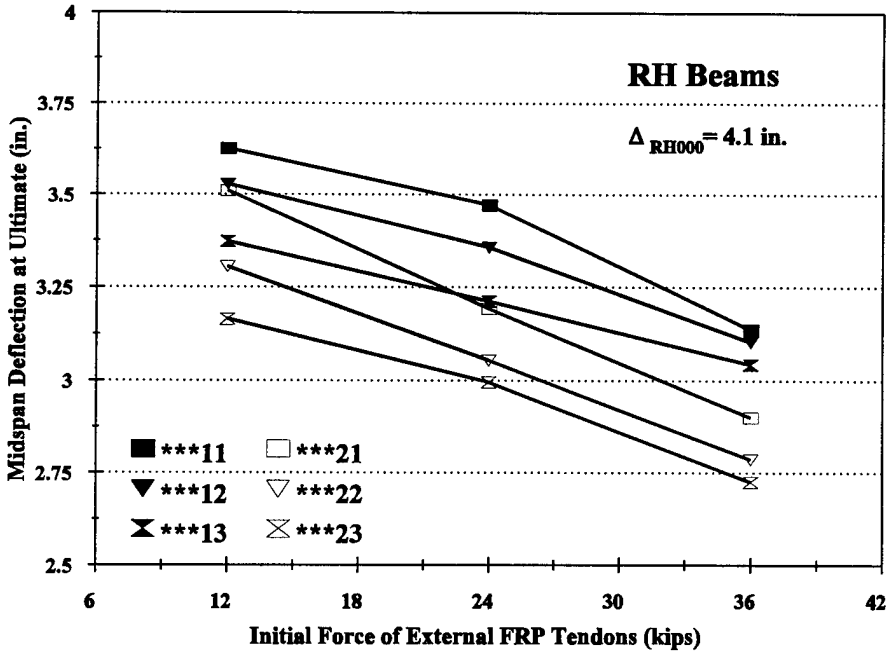

Figure 5.7 Effect of initial force of external FRP tendons on the midspan deflection at ultimate load for RH beams

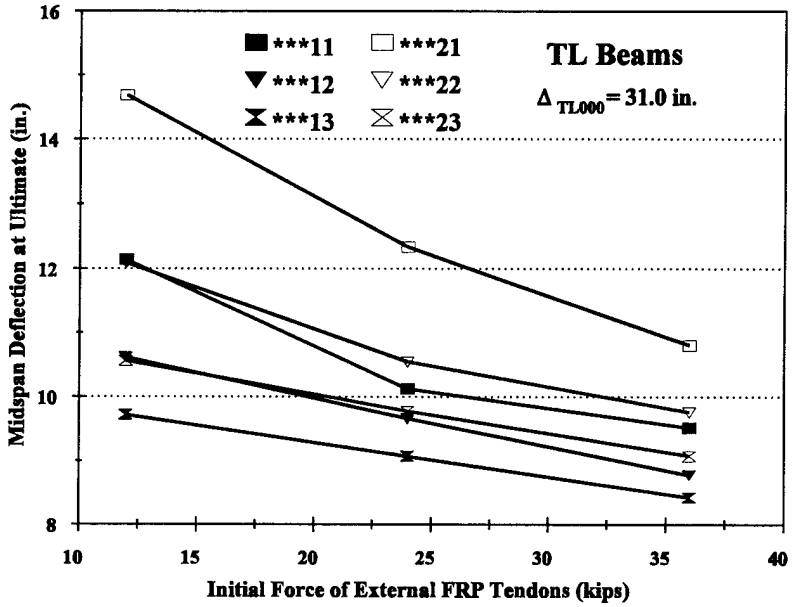

Figure 5.8 Effect of initial force of external FRP tendons on the midspan deflection at ultimate load for TL beams

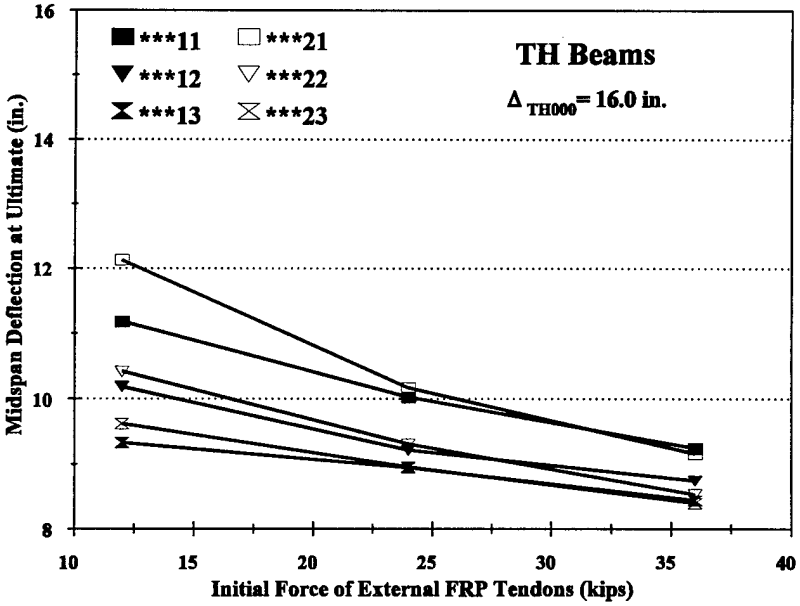

Figure 5.9 Effect of initial force of external FRP tendons on the midspan deflection at ultimate load for TH beams

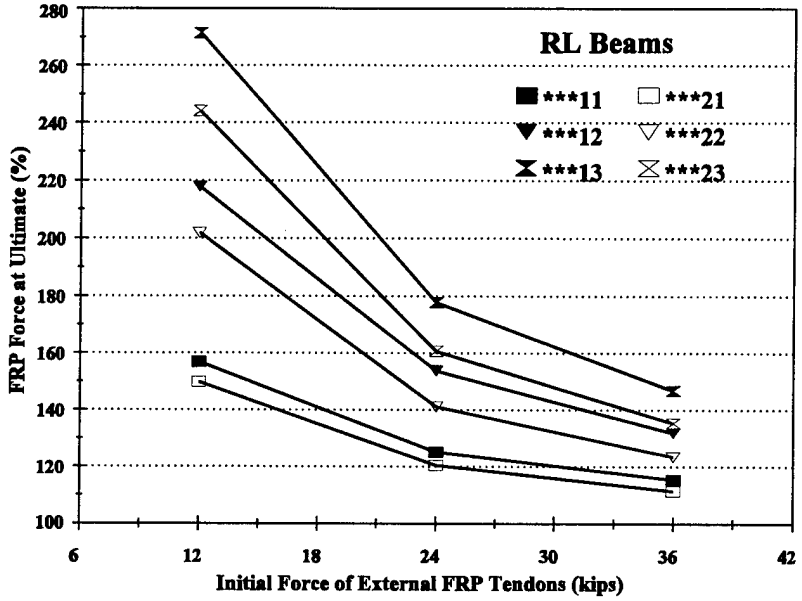

Figure 5.10 Effect of initial force of external FRP tendons on the external FRP force at ultimate load of RL beams

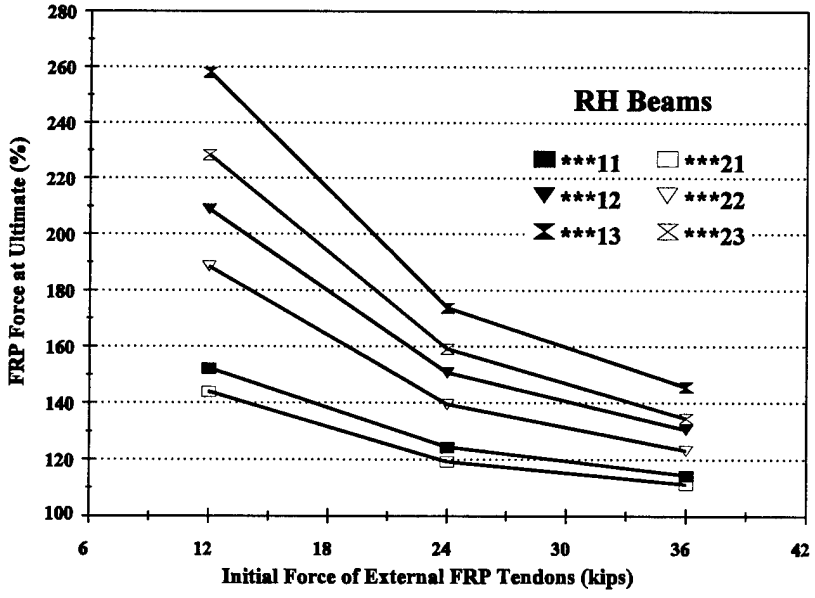

Figure 5.11 Effect of initial force of external FRP tendons on the external FRP force at ultimate load of RH beams

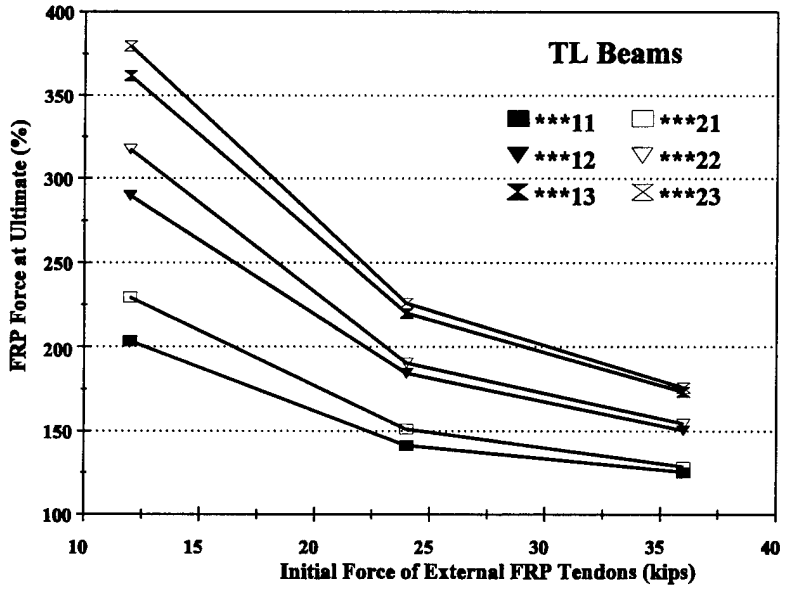

Figure 5.12 Effect of initial force of external FRP tendons on the external FRP force at ultimate load of TL beams

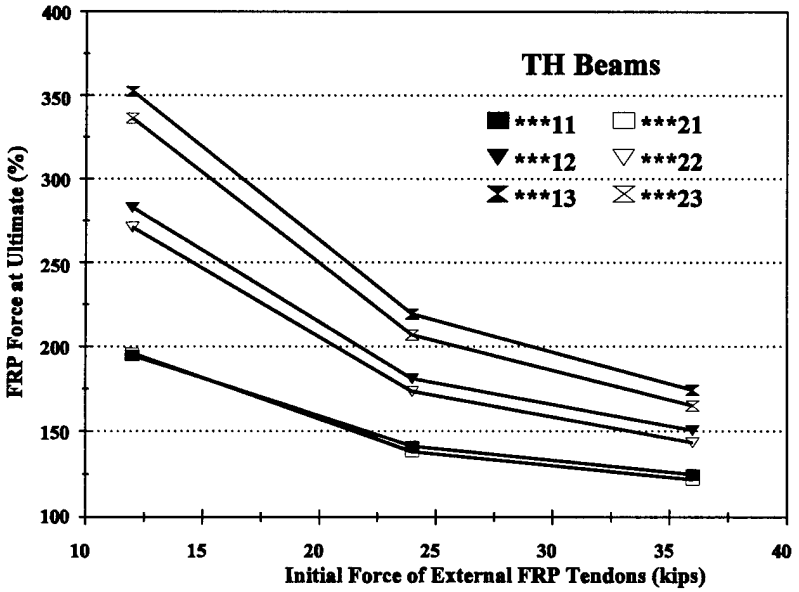

Figure 5.13 Effect of initial force of external FRP tendons on the external FRP force at ultimate load of TH beams

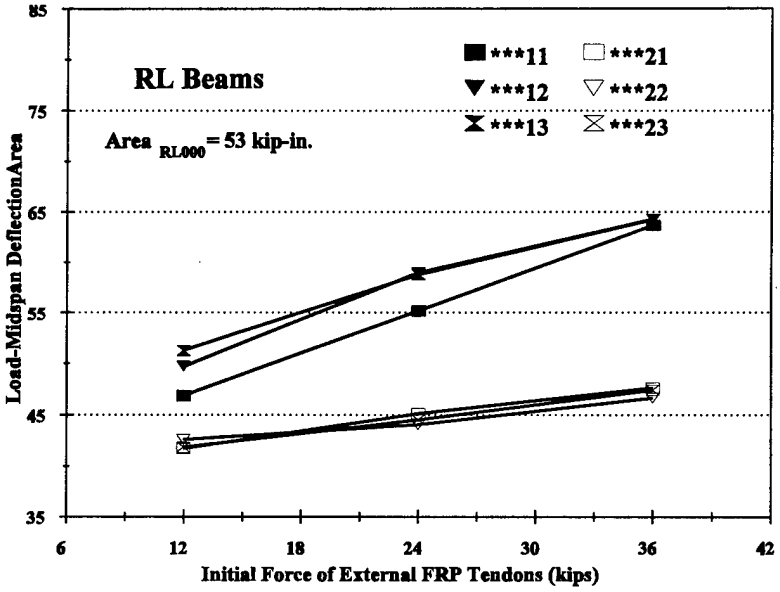

Figure 5.14 Effect of initial force of external FRP tendons on the load-midspan deflection area of RL beams

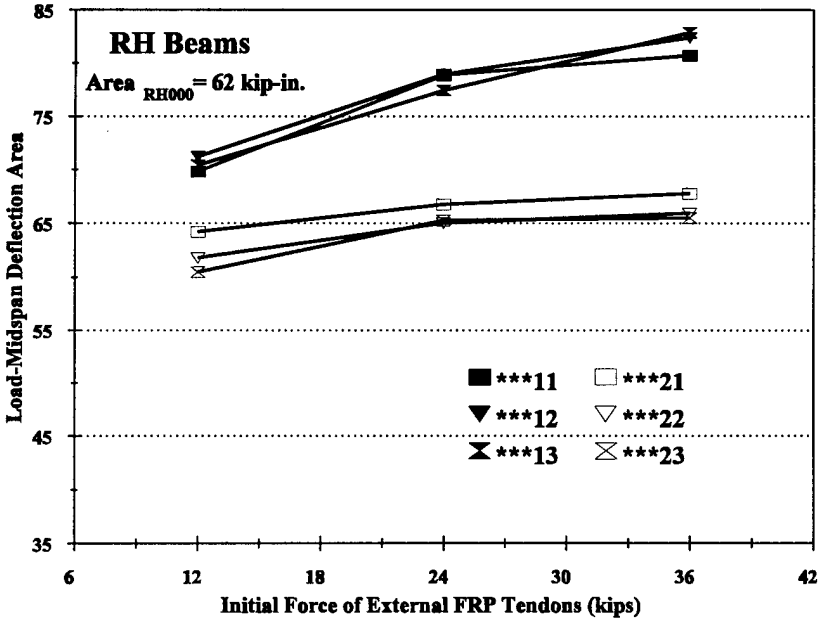

Figure 5.15 Effect of initial force of external FRP tendons on the load-midspan deflection area of RH beams

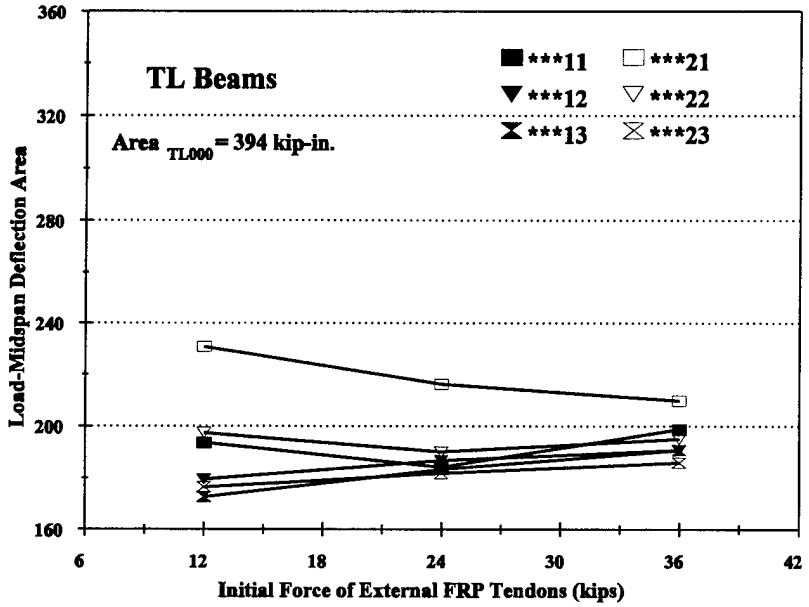

Figure 5.16 Effect of initial force of external FRP tendons on the load-midspan deflection area of TL beams

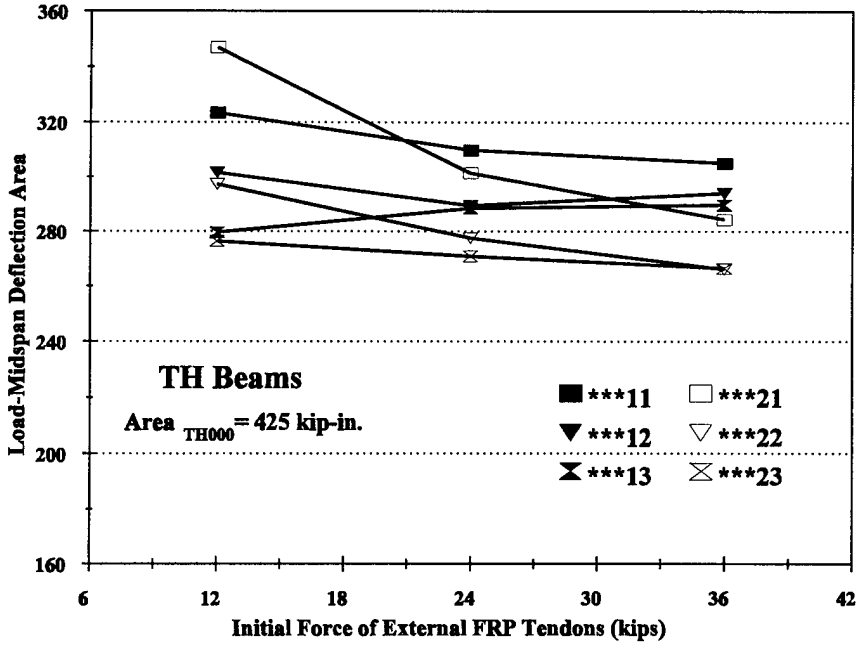

Figure 5.17 Effect of initial force of external FRP tendons on the load-midspan deflection area of TH beams

CHAPTER 6

SUMMARY AND CONCLUSIONS

6.1 SUMMARY

In order to investigate the behavior of prestressed concrete beams externally post-tensioned with carbon fiber reinforced polymer (CFRP) tendons, a two-phase study was undertaken. The first phase of the study investigated the performance of CFRP tendons subjected to combined axial load and harping, which is a common condition placed on the tendons during post-tensioning. The second phase of the study conducted an experimental and analytical investigation of the performance of prestressed concrete beams externally post-tensioned with CFRP tendons.

The investigation of the performance of CFRP tendons subjected to combined axial loading and harping involved the study of a 0.315 in. (8 mm) diameter CFRP tendon. One aspect of the study investigated the strain distribution for the CFRP tendon at the harped point. A second aspect of the study investigated the ultimate behavior of the CFRP tendon while in a harped condition. The loading conditions for which the harped tendons were tested included short-term, fatigue, and sustained loading. Based on the results of the investigation, a failure model for CFRP tendons subjected to combined axial load and harping was developed. The model accurately identifies the CFRP tendon axial load, tendon bend angle, and harping point radius associated with failure of the tendons.

The second phase of the investigation was divided into both experimental and analytical investigations of steel prestressed concrete beams externally post-tensioned with CFRP tendons. For the experimental investigation, four 8 x 16 x 216 in. (203 x 406 x 5490 mm) steel prestressed concrete beams were externally post-tensioned with two CFRP tendons. The beams were simply supported and tested under two-point loading until failure. Failure of the beams was due to crushing of the concrete at midspan. Two control beam

specimens that were not post-tensioned were similarly tested. The beams were equally divided into two types. The only difference in the two types of beams was that one type of beam had twice the prestressing steel area as compared to the other type of beams. The amount of effective prestress in the steel tendons was the same in both types of beams.

The analytical investigation of prestressed concrete beams externally post-tensioned with CFRP tendons involved the development of a computer model that accurately predicts the load-midspan displacement behavior and ultimate load behavior of the beams tested in the laboratory. The analytical model was used to conduct a limited parametric study of prestressed concrete beams externally post-tensioned with FRP tendons.

6.2 CONCLUSIONS OF THE INVESTIGATION OF THE BEHAVIOR OF CFRP TENDONS

The conclusions are limited to the parameters investigated in this study. Based on the results of the experimental and analytical investigation of the behavior of the CFRP tendons studied in this investigation, the following observations can be made:

1. Flexural strains, defined as the difference in extreme fiber strains of a harped tendon and the average axial strain of the tendon, are a maximum at the apex of the tendon bend and are approximately zero beyond 6 in. (152 mm) on either side of the bend point. The maximum value of the flexural strains increase with increases in the tendon bend angle, decreases in the harping plate radius, and increases in the average axial load of the tendon.

2. Failure of CFRP tendons at harping points is generally at an axial load less than the uni-axial rupture strength of the tendon. The failure load of harped tendons decreases with increases in the tendon bend angle and with decreases in the harping plate radius.

3. Failure of tendons at the bend point or harping point appears to be associated with an extreme fiber strain of about 0.0217, which is 145% of the maximum reported uni-axial failure strain of 0.015. Based on a fiber strain of 0.0217 and a modulus of 21,800 ksi (150 GPa), the estimated uni-axial failure stress of the tendon is calculated to be 473 ksi (3260 MPa).

4. For the CFRP tendons tested in this study, failure conditions of the tendons at a harped point can be predicted based on an ultimate fiber strain model. The resulting equations (Equations 3.10, 3.11, 3.12 and 3.13) for predicting the axial load and bend angle at failure are shown to have good predictive capability.

5. CFRP tendons subjected to severe bending-tension fatigue loading show no degradation in performance through 1 million fatigue cycles. Residual strength tests show that bending-tension fatigue does not degrade the strength of the tendons.

6. CFRP tendons subjected to sustained axial loads of 12 kips (53 kN) while harped at an angle of 7 degrees using a 1 in. (25 mm) radius harping plate for a duration of 120 days show no significant relaxation. Residual strength tests show that sustained loading of harped CFRP tendons does not degrade the strength of the tendons.

6.3 CONCLUSIONS OF THE INVESTIGATION OF STEEL PRESTRESSED CONCRETE BEAMS STRENGTHENED WITH EXTERIOR POST-TENSIONED CFRP TENDONS

Based on the results of the experimental and analytical investigation of steel prestressed concrete beams strengthened with exterior post-tensioned CFRP tendons, the following conclusions can be made:

Experimental Investigation:

1. The addition of external post-tensioning can provide significant increases in strength and reductions in ultimate deflection of prestressed concrete beams. Average strength increases of 109% and 49% were observed for the beams tested in this study. Quantitative increases in strength were about the same for beams with different amounts of prestressing steel. Midspan deflections of the externally post-tensioned beams at ultimate averaged 64% of the companion unstrengthened beams.

2. For the CFRP tendons and harping plates used in this study, the average value of the friction coefficient between the tendons and the greased harping plates was 0.33. This value is approximately twice the friction coefficient recommended in the ACI 318-95 code for unbonded steel tendons.

3. Beams strengthened by external post-tensioned CFRP tendons demonstrated a higher tangential stiffness at failure than did the companion unstrengthened beams. This increase in stiffness was equivalent to the stiffness associated with the increased upward forces at the external tendon harping points at failure.

4. Tests conducted in this study verify that CFRP tendons can be effectively used as external post-tensioning tendons under short-term loading conditions.

Analytical Investigation:

1. The computerized model -- EXPOST provides accurate predictions for the response of the prestressed beams strengthened by external post-tensioned CFRP tendons and subjected to short-term loads.

2. Analysis that neglects the contribution of concrete tensile stresses in cracked regions of the externally post-tensioned beams provides accurate predictions of the beam's ultimate load, midspan deflection, and external tendon force at failure.

3. For externally post-tensioned prestressed concrete beams, the ultimate load increases with increases in initial force of the external tendons, harping at third-points as opposed to midpoints of the beam, and with increases in the stiffness of the external tendons. Beams with a lower amount of prestressing steel showed a slightly higher average quantitative increase in ultimate load and a substantially higher average percentage increase in ultimate load versus the companion non-post-tensioned beam. External post-tensioning resulted in average ultimate loads corresponding to 231, 156, 172 and 130 percent of the companion reference beam ultimate load for the RL, RH, TL and TH beams, respectively.

4. The addition of external post-tensioning reduced midspan deflections at ultimate an average of 46%. The magnitude of the reduction was greater for beams with lower amounts of steel prestressing compared to beams with higher amounts of steel prestressing.

5. Forces of the external tendons at ultimate averaged 158% and 205% of the associated initial forces of the external tendons for the rectangular and T-beams, respectively.

6. For the rectangular beams, the energy absorption capacity at failure, defined as the area under the load-midspan deflection relationship of the beam, was about the same for post-tensioned and companion non-post-tensioned beams. The addition of external post-tensioning for T-beams reduced the energy absorption capacity at failure an average of 41%.

REFERENCES

Aalami, B. O. and Swanson, D. T. (1988). "Innovative Rehabilitation of a Parking Structure," *Concrete International*, Vol. 10, No. 2, Feb, pp. 30-35.

Abdelrahman, A. A. and Rizkalla, S. H. (1995). "Serviceability of Concrete Beams Prestressed by Carbon Fibre Plastic Rods," *Proceedings of the Second International RILEM Symposium (FRPRCS-2)*, Ghent, Belgium, pp. 403-412.

ACI Committee 318 (1995). *Building Code Requirements for Reinforced Concrete (ACI 318-95)*, American Concrete Institute, Detroit, Michigan, 347 pp.

Ahmad, S. H. (1986). "Strength and Ductility of Prestressed Concrete Beam-Column Elements Using High Strength Concrete," *Proceedings, International Symposium on Concrete in Developing Countries*, Jan, pp. 707-729.

Alkhairi, F. and Naaman, A. (1993). "Analysis of Beams Prestressed with Unbonded Internal or External Tendons," *Journal of Structural Engineering*, ASCE, Vol. 119, No. 9, Sep, pp. 2680-2700.

Anigol, M. U. (1991). "Testing and Evaluating Fiberglass, Graphite, and Steel Prestressing Cables for Pretensioned Beams," M. S. Thesis, SDSM&T.

Arduini, M., Di Tommaso, A., and Giacani, S. (1996). "Modelling of Concrete Beams Reinforced with External FRP Prestressed Tendons," *Proceedings of the First International Conference on Composites in Infrastructure*, Tucson, Arizona, pp. 481-490.

Burgoyne, C. J. (1992). "Tests on Beams Prestressed with Polyaramid Tendons," In K. W. Neale and P. Labossiere (Ed.), *Advanced Composite Materials in Bridges and Structures*, pp. 231-239.

Chambers, J. J. (1986). "Parallel-lay Aramid Ropes for use as Tendons in Prestressed Concrete," PhD Thesis, University of London.

Collins, M. P. and Mitchell, D. (1991). *Prestressed Concrete Structures*, Prentice Hall, New Jersey, 766 pp.

Erki, M. A. and Rizkalla, S. H. (1993). "Anchorages for FRP Reinforcement," *Concrete International*, Vol. 15, No. 6, Jun, pp. 54-59.

FRP International (1993), Vol 1, Issue 2, 5 pp.

Gerritse, A. and Den Uijl, J. A. (1995). "Long-term Behaviour of Arapree," *Proceedings of the Second International RILEM Symposium (FRPRCS-2)*, Ghent, Belgium, pp. 57-66.

Gorty, S. S. (1994). "Mechanical Properties of Composite Cables," M. S. Thesis, SDSM&T.

Grace N. and Abdel-Sayed, G. (1996). "Double Tee and CFRP/GFRP Bridge System," *Concrete International*, Vol. 18, No. 2, Feb, pp. 39-44.

Holt, L. E., Dolan, C. W. and Schmidt, R. J. (1993). "Epoxy Socketed Anchors for Non-Metallic Prestressing Tendons," *Proceedings of the Fiber-Reinforced-Plastic Reinforcement for Concrete Structures International Symposium, SP-138*, Vancouver, pp. 381-400.

Horiguchi, T., Saeki, N. and Hata, S. (1995). "Fatigue of Reinforced Concrete Beams Externally Prestressed with Aramid Fibre Cables," *Proceedings of the Second International RILEM Symposium (FRPRCS-2)*, Ghent, Belgium, pp. 601-607.

Hoshijima T., Yagi, K., Tanaka, T. and Ando, T. (1996). "Properties of CFRP Composites for Concrete Structures," *Proceedings of the First International Conference on Composites in Infrastructure*, Tucson, Arizona, pp. 227-241.

Iyer, S. L. and Khubchandani, A. (1992). "Evaluation of Graphite Composite Cables for Prestressing Concrete," *Proceedings of the 1st International Conference of Advanced Composite Materials in Bridges and Structures*, Sherbrooke, Canada, pp. 73-82.

Khubchandani, A. (1992). "Evaluation of Graphite Composite Cables for Prestressing Concrete," M. S. Thesis, SDSM&T.

Klaiber, F. W., Dunker, K. F., Wifp, T. J. and Sanders, Jr. W. W. (1987). *Methonds of Strengthening Existing Highway Bridges, NCHRP Report 293*, TRB, National Research Council, Washington, D. C., 114 pp.

Lin, T. Y. and Burns, N. H. (1981). *Design of Prestressed Concrete Structures*, 3rd Ed., John Wiley & Sons, New York, 646 pp.

McKay, K. S. and Erki, M. A. (1993). "Grouted Anchorages for Aramid Fibre Reinforced Plastic Prestressing Tendons," *Canadian Journal of Civil Engineering*, Vol 20, pp. 1065-1069.

Leadline Product Description (1993). Mitsubishi Kasei Corporation.

Model Code 90 (1993). Comité Euro-International du Beton, Lausanne, Switerland.

Mutsuyoshi H. and Machida, A. (1993). "Behavior of Prestressed Concrete Beams Using FRP as External Cable," *Proceedings of the Fiber-Reinforced-Plastic Reinforcement for Concrete Structures International Symposium, SP-138*, Vancouver, Canada, March, pp. 401-417.

Naaman, A. E., and Alkhairi, F. M. (1991). "Stress at Ultimate in Unbonded Post-Tensioing Tendons - Part I: Evaluation of the State-of-the-Art, Part 2: Proposed Methodology," *ACI Structural Journal*, Vol. 88, No. 5, pp. 641-651.

Nanni, A. and Dolan, C. W. (Ed.) (1993). *Fiber-Reinforced-Plastic Reinforcement for Concrete Structures, SP-138*, Technical sessions presented at the American Concrete Institute Conference, Vancouver, Canada, March, 977 pp.

Neale, K. W. and Labossiere, P. (Ed.) (1992). *Advanced Composite Materials in Bridges and Structures*, First International Conference, Sherbrooke, Canada, 705 pp.

Olson, S. A., (1991). "Impact Damage and Repair of AASHTO Type III Girders," PhD Thesis, University of Minnesota.

Olson, S. A., French, C. W., and Leon, R. T. (1992). "Evaluation of Two Repair Schemes for Damaged Prestressed Bridge Girders," *3rd International Workshop on Bridge Rehabilitation*, Darmstadt, pp. 145-157.

Pannell, F. N. (1969). "The Ultimate Moment of Resistance of Unbonded Prestressed Concrete Beams," *Magazine of Concrete Research*, Vol. 21, No. 66, pp. 43-54.

Rao, P. S. and Mathew, G. (1996). "Behavior of Externally Prestressed Concrete Beams with Multiple Deviators," *ACI Structural Journal*, Vol 93, No. 4, Jul-Aug, pp. 387-396.

Saadatmanesh, H. and Ehsani, M. R. (Ed.) (1996). *Fiber Composites in Infrastructure*, Proceedings of the First International Conference on Composites in Infrastructure, Tucson, Arizona, Jan, 1231 pp.

Saeki, N., Horiguchi, T., Inomata, M., Hata, S., and Ikeda, T. (1993). "Strengthening of Damaged Concrete Beams by External Prestressing of Aramid Fiber Cable," *Proceedings of the Fiber-Reinforced-Plastic Reinforcement for Concrete Structures International Symposium, SP-138*, Vancouver, Canada, pp. 913-932.

Saeki, N., Horiguchi, T., and Hata, S. (1995). "Plastic Performance of Reinforced Concrete Beams by Using External Prestressing of Aramid Fibre Cables," *Proceedings of the Second International RILEM Symposium (FRPRCS-2)*, Ghent, Belgium, pp. 608-615.

Schwartz, M. M. (1992). *Composite Materials Handbook*, McGraw-Hill, New York.

Shanafelt, G. O. and Horn, W. B. (1980), *Damage Evaluation and Repair Methods for Prestressed Concrete Bridge Members*, NCHRP 226, TRB, National Research Council, Washington DC, 66 pp.

Shanafelt, G. O. and Horn, W. B., (1985). *Guidelines for Evaluation and Repair of Prestressed Concrete Bridge Members*, NCHRP 280, TRB, National Research Council, Washington DC, 84 pp.

Taerwe, L. (Ed.) (1995). *Non-Metallic (FRP) Reinforcement for Concrete Structures*, Proceedings of the Second International RILEM Symposium (FRPRCS-2), Ghent, Belgium, 714 pp.

University of Virginia Civil Engineering Department, Virginia Highway and Transportation Research Council, and Virginia Department of Highways and Transportation (1980). *Bridges on Secondary Highways and Local Roads -- Rehabilitation and Replacement,* NCHRP 222, TRB, National Research Council, Washington DC, 73 pp.

Uomoto, T., Nishimura, T. and Ohga, H. (1995). "Static and Fatigue Strength of FRP rods for Concrete Reinforcement," *Proceedings of the Second International RILEM Symposium (FRPRCS-2)*, Ghent, Belgium, Aug, pp. 100-107.

Uomoto, T. and Hodhod, H. (1993). "Properties of Fiber Reinforced Plastic Rods for Prestressing Tendons," *Fiber-Reinforced-Plastic Reinforcement for Concrete Structures, SP-138*, Vancouver, Canada, pp. 101-115.

Vernigora, E., Marcil, J. R. M., Slater, W. M. and Aiken, R. V. (1969). "Bridge Rehabilitation and Strengthening by Continuous Post-Tensioning," *Prestressed Concrete Institute Journal*, Vol. 14, No. 2, Apr, pp. 88-104.

Virlogeux, M. P. (1983). "External Prestressing," *IABSE Proceedings*, P63/83, May, pp. 101-108.

Virlogeux, M. P. (1990). "External Prestressing: from Construction History to Modern Technique and Technology," in A. Naaman and J. Breen Editors, External Prestressing in Bridges, ACI SP-120, pp. 1-60.

Walton, J. M. and Yeung, Y. T. C. (1986). "The Fatigue Performance of Structural Strands of Pultruded Composite Rods," *Journal of the Institute of Mechanical Engineers*, London, United Kingdom, C286/86, pp. 315-320.

APPENDIX A

ALGORITHM FOR COMPUTER PROGRAM -- EXPOST

Step 1

Read Input (material properties, beam dimensions, loading history, effective stresses/strengths, etc.)

Step 2

Calculate the following:

a. beam segment lengths and layer dimensions
b. initial concrete stresses and strains
c. steel strain for $f_c = 0$

Step 3

Set P = 0

Step 4

Assume an initial exterior tendon load (TFTRY)

Step 5

Calculate the required moment resisted by the prestressed concrete segment only (i.e. affects of exterior tendons accounted for as negative moment and an axial force). The maximum required beam moment is the maximum required moment of all beam segments.

Step 6

For a given TFTRY and cracked condition, calculate the moment curvature relationship for the beam segment. If concrete strain at top equals ultimate concrete strain, then associated curvature is ϕ_{max}.

(continued on next page)

Step 7	Calculate the appropriate beam curvature for the required segment moment found in Step 5. If segment moment exceeds the maximum segment moment, set segment curvature to ϕ_{max}.
Step 8	Repeat Steps 5 through 7 for all beam segments
Step 9	Integrate segment curvatures across beam to determine beam displacements at midspan and harping points
Step 10	Calculate external tendon load based on tendon axial strains due to vertical displacements at the harping points and horizontal displacements at the anchorage locations (TFDISP)
Step 11	Compare TFTRY and TFDISP. If the two are not equal within a given tolerance, adjust TFTRY and repeat Steps 4 through 10. If TFDISP exceeds allowable value, then stop program
Step 12	Calculate maximum nominal moment of the prestressed concrete beam as done for the segment in Step 6. If maximum beam moment found in Step 5 exceeds this moment, stop program. For analysis, tensile stresses in concrete after cracking is 0.
Step 13	Write output, including beam load, midspan displacement, and external tendon load.
Step 14	Return to Step 4 with P adjusted based on loading history.

APPENDIX B

COMPUTER PROGRAM -- EXPOST

INPUT FILE

```
INB1
OUTB1
```

FILE INB1

```
 TITLE
"BEAM B-1"
 JOB
1
 # LAYERS, # SEGMENTS, TS FLAG
160, 30, 0
 SECTION FLAGE, H, BW, BTF, BBF, HTF, HBF
0, 16, 8, 8, 8, 0, 0
 EFFECTIVE STEEL STRESS
152
 CONCRETE STRENGTH, ULT STRAIN, WEIGHT
6.30, 0.0032, 144
 FRP AREA, MODULUS OF FRP, FRP STRESS FF1, HIGH LL FOR FF1,LOW LL FOR FF2, FF2,
 MAX ALLOWABLE STRESS IN FRP
0.1558, 21800, 0, 4.15, 2.15, 169, 260
 DISTANCE TO FRP BEND, BEAM LENGTH, E AT END, E AT MID SECTION
88, 204, 8, 15.3
 DISTANCE TO POINT LOADS FROM BEAM END
88
NUMBER OF STEEL BARS
1
 IPS, ABAR, YBAR
1, 0.15273, 13.25
```

FILE OUTB1

```
  *****  INPUT  DATA FOR EXPOST.FOR  *****
         "BEAM B-1"
  JOB #  1 INPUT FILE INB1     OUTPUT FILE OUTB1
  NUMBER OF ELEMENTS  = 160  APPROXIMATE MID SEGMENT LENGTH  = 30  TENSION STIFFENING FLAG   = 0
CROSS SECTIONAL DIMENSIONS
  CROSS-SECTION TYPE = 0
  TOTAL HEIGHT OF THE BEAM (IN) =  16.00
  WIDTH OF BEAM WEB (IN) =  8.00
  WIDTH OF BEAM TOP FLANGE (IN) =  8.00
  WIDTH OF BEAM BOTTOM FLANGE (IN) =  8.00
  THICKNESS OF TOP FLANGE (IN) =  .00
  THICKNESS OF BOTTOM FLANGE (IN) =  .00
STEEL STRENGTH
  EFFECTIVE PRESTRESS (KSI) =  152.00
CONCRETE STRENGTH (KSI) =  6.300
FRP REPAIR PROPERTIES
  TOTAL FRP AREA (SQ.IN.) =  .15580E+00
  ELASTIC MODULUS OF FRP (KSI) =  .21800E+05
  FRP INITIAL STRESS (KSI)     =  .00
  MAX LOAD (1/2 LL) BEFORE FRP TENSIONING (KIPS) =  4.2
  LOAD (1/2 LL) AT FRP TENSIONING (KIPS) =  2.2
  FRP SECOND STRESS (KSI)      =  169.00
  MAXIMUM ALLOWABLE FRP STRESS (KSI) = 260.00
  SLOPED SPAN (IN.)      =  88.00
  TOTAL BEAM SPAN (IN.)  =  204.00
  DISTANCE FROM TOP TO FRP AT ENDS (IN.) =  8.00
              AT MIDPOINT (IN.) =  15.30
  DISTANCE FROM BEAM END TO POINT LOAD (IN.) =  88.00
NUMBER OF STEEL REINFORCEMENTS = 1
  STRAND NO.   AREA (SQ.IN.)  Y-CORD.  TYPE R/F
    1        .153        13.250      1
**********  END OF INPUT DATA  **********

CALCULATED PROPERTIES
```

N = 7.4468
MODULUS OF STEEL (KSI) = 28900.
MODULUS OF CONCRETE (KSI) = 3880.9
STRAIN AT TENSILE RUPTURE = -.15242E-03
STRESS AT RUPTURE (KSI) = -.5953
SECTION PROPERTIES (IGNORING FRP)

YT(IN)	YB(IN)	AGC(SQ.IN)	AGT(SQ.IN)	XI(IN**4)
8.040	7.960	128.000	128.985	2757.598

ELEMENT PROPERTIES NEGLECTING FRP
NUMBER OF ELEMENTS = 160
ELEMENT HEIGHT (IN.) = .1000
STRAIN AND STRESS AT TRANSFER (W/O FRP)
AVERAGE CONCRETE STRAIN DUE TO EFFECTIVE PRESTRESS = .46273E-04
AVERAGE CONCRETE STRESS DUE TO EFF PS (KSI) = .17998
STEEL STRAIN DUE TO EFF PS = .52595E-02
EFFECTIVE STEEL STRESS (KSI) = 152.00000
CONCRETE STRESS-TOP (KSI) = -.1727
CONCRETE STRESS-BOTTOM (KSI) = .5291
CONCRETE STRAIN-TOP = -.44393E-04
CONCRETE STRAIN-BOTTOM = .13555E-03

***** RESULTS *****

P	DELTA	DELPB	PHIMID	TFDISP	DCMID	FSTRAIN	YMMAX	XMMAX	XMID
.15	-.32487E-01	-.49895E-03	-.50769E-05	.00000E+00	.47421E-02	.00000E+00	.68659E+02	.54792E+03	-.12554E+01
.65	-.16544E-01	-.97690E-04	-.98243E-06	.00000E+00	.47578E-02	.00000E+00	.11266E+03	.54792E+03	-.39805E+02
1.15	-.57777E-03	.30403E-03	.31167E-05	.00000E+00	.47731E-02	.00000E+00	.15666E+03	.54792E+03	.23093E+02
1.65	.16535E-01	.79062E-03	.80959E-05	.00000E+00	.47510E-02	.00000E+00	.20066E+03	.54792E+03	.13458E+02
2.15	.45789E-01	.18721E-02	.19174E-04	.00000E+00	.42234E-02	.00000E+00	.24466E+03	.54792E+03	.88777E+01
2.65	.11955E+00	.50434E-02	.51625E-04	.00000E+00	.11959E-02	.00000E+00	.28866E+03	.54792E+03	.55934E+01
3.15	.25254E+00	.10081E-01	.10310E-03	.00000E+00	-.60872E-02	.00000E+00	.33266E+03	.54792E+03	.41624E+01
3.65	.44066E+00	.16846E-01	.17216E-03	.00000E+00	-.17897E-01	.00000E+00	.37666E+03	.54792E+03	.33960E+01
4.15	.67259E+00	.24877E-01	.25414E-03	.00000E+00	-.33612E-01	.00000E+00	.42066E+03	.54792E+03	.29379E+01
2.15	.45789E-01	.18721E-02	.19174E-04	.00000E+00	.42234E-02	.00000E+00	.24466E+03	.54792E+03	.88777E+01
2.15	-.37368E-01	-.36741E-01	-.63766E-05	.26330E+02	.10025E-01	.00000E+00	.53106E+02	.71845E+03	-.74992E+01

2.65	-.21579E-01	-.21349E-01	-.23267E-05	.26372E+02	.10047E-01	.12303E-04	.96868E+02	.71925E+03	-.34511E+02
3.15	-.58087E-02	-.59758E-02	.17188E-05	.26412E+02	.10137E-01	.24147E-04	.14056E+03	.71920E+03	.66090E+02
3.65	.99564E-02	.93930E-02	.57637E-05	.26454E+02	.10164E-01	.36446E-04	.18427E+03	.71940E+03	.25376E+02
4.15	.25717E-01	.24757E-01	.98085E-05	.26497E+02	.10154E-01	.49024E-04	.22797E+03	.71904E+03	.18171E+02
4.65	.42191E-01	.40782E-01	.14398E-04	.26541E+02	.10159E-01	.62062E-04	.27166E+03	.72014E+03	.14832E+02
5.15	.61638E-01	.59649E-01	.20334E-04	.26595E+02	.10073E-01	.78077E-04	.31508E+03	.72037E+03	.12564E+02
5.65	.90939E-01	.87895E-01	.31122E-04	.26686E+02	.95682E-02	.10470E-03	.35860E+03	.72100E+03	.10180E+02
6.15	.13543E+00	.13062E+00	.49182E-04	.26835E+02	.83056E-02	.14855E-03	.40142E+03	.72140E+03	.81684E+01
6.65	.20514E+00	.19747E+00	.78425E-04	.27086E+02	.55858E-02	.22266E-03	.44360E+03	.72362E+03	.65548E+01
7.15	.29572E+00	.28460E+00	.11371E-03	.27432E+02	.13948E-02	.32440E-03	.48510E+03	.72489E+03	.55661E+01
7.65	.40950E+00	.39378E+00	.16083E-03	.27883E+02	-.44493E-02	.45712E-03	.52573E+03	.72900E+03	.47929E+01
8.15	.55356E+00	.53236E+00	.21692E-03	.28478E+02	-.12596E-01	.63246E-03	.56553E+03	.73263E+03	.42285E+01
8.65	.71096E+00	.68384E+00	.27743E-03	.29147E+02	-.21928E-01	.82946E-03	.60458E+03	.73637E+03	.38406E+01
9.15	.89034E+00	.85650E+00	.34626E-03	.29931E+02	-.33003E-01	.10601E-02	.64288E+03	.74161E+03	.35336E+01
9.25	.93025E+00	.89492E+00	.36151E-03	.30108E+02	-.35527E-01	.11122E-02	.65052E+03	.74249E+03	.34779E+01
9.35	.96980E+00	.93272E+00	.37963E-03	.30282E+02	-.37988E-01	.11636E-02	.65803E+03	.74376E+03	.34111E+01
9.45	.10083E+01	.96986E+00	.39366E-03	.30455E+02	-.40453E-01	.12145E-02	.66543E+03	.74466E+03	.33707E+01
9.55	.10521E+01	.10118E+01	.41312E-03	.30650E+02	-.43214E-01	.12720E-02	.67289E+03	.74644E+03	.33080E+01
9.65	.10935E+01	.10517E+01	.42815E-03	.30838E+02	-.45890E-01	.13272E-02	.68036E+03	.74661E+03	.32705E+01
9.75	.11397E+01	.10958E+01	.44906E-03	.31046E+02	-.48858E-01	.13886E-02	.68766E+03	.74854E+03	.32113E+01
9.85	.11907E+01	.11446E+01	.47231E-03	.31279E+02	-.52196E-01	.14570E-02	.69477E+03	.74995E+03	.31487E+01
9.95	.12343E+01	.11863E+01	.49252E-03	.31476E+02	-.54964E-01	.15152E-02	.70218E+03	.75120E+03	.31042E+01
10.05	.12876E+01	.12373E+01	.51686E-03	.31721E+02	-.58474E-01	.15873E-02	.70914E+03	.75217E+03	.30489E+01
10.15	.13409E+01	.12879E+01	.54438E-03	.31964E+02	-.61893E-01	.16588E-02	.71615E+03	.75467E+03	.29906E+01
10.25	.13989E+01	.13432E+01	.57162E-03	.32233E+02	-.65722E-01	.17380E-02	.72306E+03	.75604E+03	.29391E+01
10.35	.14491E+01	.13910E+01	.59706E-03	.32464E+02	-.68921E-01	.18058E-02	.73010E+03	.75704E+03	.28983E+01
10.45	.15263E+01	.14629E+01	.67024E-03	.32817E+02	-.73936E-01	.19098E-02	.73638E+03	.75901E+03	.27584E+01
10.55	.16086E+01	.15407E+01	.69865E-03	.33200E+02	-.79332E-01	.20228E-02	.74231E+03	.76122E+03	.27235E+01
10.65	.16796E+01	.16080E+01	.73942E-03	.33534E+02	-.84001E-01	.21209E-02	.74862E+03	.76343E+03	.26727E+01
10.76	.17760E+01	.16969E+01	.84110E-03	.33977E+02	-.90179E-01	.22515E-02	.75519E+03	.76707E+03	.25425E+01
10.86	.18752E+01	.17893E+01	.89879E-03	.34443E+02	-.96676E-01	.23887E-02	.76059E+03	.76852E+03	.24880E+01
11.02	.20476E+01	.19471E+01	.11199E-02	.35243E+02	-.10763E+00	.26241E-02	.76871E+03	.77464E+03	.23085E+01
11.12	.21350E+01	.20306E+01	.11274E-02	.35669E+02	-.11340E+00	.27496E-02	.77444E+03	.77750E+03	.23212E+01
11.22	.22585E+01	.21439E+01	.12254E-02	.36250E+02	-.12119E+00	.29208E-02	.77910E+03	.78001E+03	.22748E+01
11.34	.24022E+01	.22765E+01	.13606E-02	.36935E+02	-.13019E+00	.31222E-02	.78478E+03	.78530E+03	.22331E+01

PROGRAM EXPOST

```
CCC -----------------------------------------------------------------
CCC   EXPOST.FOR
CCC   THIS PROGRAM ANALIZES STEEL PRESTRESSED OR REINFORCED CONCRETE
CCC   RECTANGULAR, T-, OR I-BEAMS THAT ARE EXTERNALLY POST-TENSIONED
CCC   WITH LINEARLY ELASTIC TENDONS. THE PROGRAM CONSIDERS SIMPLY
CCC   SUPPORTED, SYMMETRICALLY HARPED EXTERNAL TENDONS, WITH A UNIFORM
CCC   DEAL LOAD AND TWO SYMMETRICALLY PLACED LIVE LOADS. OUTPUT OF
CCC   THE PROGRAM PROVIDES THE BEAM MIDSPAN DISPLACEMENT AND EXTERNAL
CCC   TENDON LOADS FOR INCREMENTAL INCREASES IN POINT LOADS.
CCC -----------------------------------------------------------------
CCC ***************************************************************
CCC         MAIN VARIABLES OF THE PROGRAM
CCC ***************************************************************
CCC AAB    = DISTANCE FROM END OF BEAM SPAN TO HARPING POINT (IN)
CCC AAT    = DISTANCE FROM END OF BEAM TO LOADING POINT (IN)
CCC ABAR(I) = AREA OF STEEL REINFORCEMENT 'I' (SQ IN)
CCC AF     = TOTAL AREA OF FRP TENDONS (SQ IN)
CCC AGC    = GROSS AREA OF CONCRETE (SQ IN)
CCC AGT    = TRANSFORMED AREA OF CONCRETE (SQ IN)
CCC ALPHA  = ANGLE BETWEEN HORIZONATAL AND FRP AT ENDS (RADIANS)
CCC AS     = TOTAL AREA OF PRESTRESSING STEEL (SQ IN)
CCC ASC    = TOTAL AREA OF COMPRESSION REINFORCEMENT (SQ IN)
CCC AST    = TOTAL AREA OF TENSILE REINFORCEMENT (SQ IN)
CCC BBF    = WIDTH OF BOTTOM FLANGE (IN)
CCC BTF    = WIDTH OF TOP FLANGE (IN)
CCC BW     = WIDTH OF BEAM WEB (IN)
CCC C      = TOTAL CONCRETE SECTION FORCE (KIPS)
CCC CO     = COMPRESSIVE STRENGTH OF THE CONCRETE (KSI)
CCC D      = DISTANCE FROM TOP OF BEAM TO PRESTRESSING STEEL (IN)
CCC DC1    = DISTANCE FROM TOP OF BEAM TO FRP AT END (IN)
CCC DC2    = DISTANCE FROM TOP OF BEAM TO FRP AT CENTER (IN)
CCC DCMID  = 1/2 LONGITUDINAL ELONGATION OF BEAM AT THE HEIGHT
C          OF DC1 (IN)
CCC DCMID0 = DCMID IMMEDIATELY AFTER POST-TENSIONING (IN)
CCC DELDELPB = CHANGE IN DEFLECTION OF HARPING POINT SINCE COMPLETION OF
C          POST-TENSIONING (IN)
CCC DELE   = CROSS-SECTION ELEMENT HEIGHT (IN)
CCC DELF   = RESULTANT FORCE ON CROSS-SECTION (KIPS)
CCC DELPB  = VERTICAL DEFLECTION OF HARPING POINT (IN)
CCC DELPB0 = VERTICAL DEFLECTION OF HARPING POINT IMMEDIATELY AFTER
C          POST-TENSIONING (IN)
CCC DELRAT = RATIO OF DELF AND TENSILE FORCE ACROSS BEAM SECTION
CCC DELTA  = VERTICAL DEFLECTION OF MIDSPAN (IN)
CCC DELTATF = INCREMENTAL STEP CHANGE FOR EXTERIOR TENDON FORCE (KIPS)
CCC DELTF  = PERCENT DIFFERENCE BETWEEN TFTRY AND TFDISP
CCC DPHI   = INCREMENTAL STEP CHANGE FOR PHI (1/IN)
CCC DREFC  = DISTANCE FROM TOP OF BEAM TO COMPRESSIVE STEEL (IN)
CCC DREFT  = DISTANCE FROM TOP OF BEAM TO TENSILE STEEL (IN)
```

```
CCC  EC     = STRAIN IN CONCRETE ELEMENT
CCC  ECBOT   = STRAIN IN CONCRETE BOTTOM WITH NO LIVE LOAD OR EXTERIOR
C           POST-TENSIONING LOAD
CCC  ECMIDP  = STRAIN AT HEIGHT OF DC1 FOUND WITH MOMENT CURVATURE
C           RELATIONSHIP
CCC  ECMIDS  = CONCRETE STRAIN FOR BEAM SEGMENT AT HEIGHT DC1
CCC  ECT     = CONCRETE STRAIN AT TOP OF BEAM
CCC  ECTOP   = STRAIN IN CONCRETE TOP WITH NO LIVE LOAD OR EXTERIOR
C           POST-TENSIONING LOAD
CCC  ECU     = ULTIMATE ALLOWABLE STRAIN IN CONCRETE
CCC  EMC     = ELASTIC MODULUS OF CONCRETE (KSI)
CCC  EMF     = ELASTIC MODULUS OF FRP (KSI)
CCC  EMS     = ELASTIC MODULUS OF STEEL (KSI)
CCC  EO      = CONCRETE STRAIN ASSOCIATED WITH MAX STRENGTH
CCC  ERUPT   = CONCRETE STRAIN ASSOCIATED WITH FRUPT
CCC  ES      = STRAIN IN PRESTRESSING STEEL
CCC  ESEFF   = STEEL STRAIN ASSOCIATED WITH FSEFF
CCC  ESH     = STRAIN IN PRESTRESSING STEEL AT START OF STRAIN HARDENING
CCC  ESO     = PRESTRESSING STEEL STRAIN ASSOCIATED WITH ZERO CONCRETE
C           STRAIN
CCC  ESU     = ULTIMATE ALLOWABLE STRAIN OF STEEL
CCC  ESY     = STRAIN IN STEEL AT ELASTIC LIMIT
CCC  FC      = STRESS IN CONCRETE (KSI)
CCC  FCBOT   = CONCRETE STRESS ASSOCIATED WITH ECBOT (KSI)
CCC  FCEFF   = AVERAGE CONCRETE EFFECTIVE STRESS (KSI)
CCC  FCTOP   = CONCRETE STRESS ASSOCIATED WITH ECTOP (KSI)
CCC  FF1     = FRP STRESS AT FIRST ITERATION -- TYPICALLY ZERO (KSI)
CCC  FF2     = FRP STRESS IMMEDIATELY AFTER POST-TENSIONING (KSI)
CCC  FFMAX   = MAXIMUM ALLOWABLE STRESS/LOAD IN FRP TENDON (KSI/KIPS)
CCC  FIN     = SEQUENTIAL LIST OF INPUT AND OUTPUT FILES FOR ANALYSIS
CCC  FRUPT   = MODULUS OF RUPTUTE OF CONCRETE (KSI)
CCC  FS      = STRESS OF PRESTRESSING STEEL (KSI)
CCC  FSEFF   = EFFECTIVE PRESTRESS OF STEEL STRAND (KSI)
CCC  FSH     = PRESTRESSING STEEL STRESS AT START OF STRAIN HARDENING (KSI)
CCC  FSTRAIN = FRP STRAIN DUE TO BEAM DISPLACEMENTS
CCC  FSU     = ULTIMATE STRESS OF THE STEEL STRAND (KSI)
CCC  H       = OVERALL BEAM HEIGHT (IN)
CCC  HBF     = THICKNESS OF BOTTTOM FLANGE (IN)
CCC  HTF     = THICKNESS OF TOP FLANGE (IN)
CCC  ICRACK  = FLAG FOR SEGMENT CRACKING; 0=BOTTOM NOT CRACKED,
C           1 = BOTTOM CRACKED
CCC  IPB     = SEGMENT NUMBER IDENTIFYING LOCATION OF HARPING POINT
CCC  ISEC    = FLAG FOR CROSS-SECTION (0=RECTANGLE;1=T;2=I)
CCC  ITS     = FLAG FOR TENSION STIFFENING (1=TS;0=NO TS)
CCC  JOB     = NUMBER IDENTIFYING PROGRAM RUN
CCC  KK      = SEGMENT NUMBER
CCC  NBAR    = STEEL REINFORCEMENT NUMBER IDENTIFICATION
CCC  NELE    = NUMBER OF BEAM CROSS-SECTIONAL LAYERS
CCC  NELEDC1 = NUMBER OF BEAM LAYERS BETWEEN TOP AND DC1
```

```
CCC  NSEG    = NUMBER OF BEAM SEGMENTS FOR 1/2 OF BEAM
CCC  P       = LIVE LOAD ON 1/2 OF BEAM (KIPS)
CCC  P2A     = INITIAL HIGH LIVE LOAD ON 1/2 OF BEAM PRIOR TO
C            POST-TENSIONING (KIPS)
CCC  P2B     = INITIAL LOW LIVE LOAD ON 1/2 OF BEAM DURING
C            POST-TENSIONING (KIPS)
CCC  PHI     = AVERAGE SEGMENT CURVATURE (1/IN)
CCC  PHIMID  = AVERAGE SEGMENT CURVATURE FOR MIDSPAN SEGMENT (1/IN)
CCC  PHISEG  = SEGMETN CURVATURE INTERPOLATED IN SPHI SUBROUTINE (1/IN)
CCC  PF      = UPWARD FORCE AT HARPING POINTS (KIPS)
CCC  TFDISP  = FORCE IN FRP FOUND BY DEFLECTIONS (KIPS)
CCC  TFEFF   = EFFECTIVE POST-TENSIONING FORCE IN FRP (KIPS)
CCC  TFTRY   = FORCE IN FRP USED IN ITERATION (KIPS)
CCC  TS      = TOTAL PRESTRESSING STEEL FORCE (KIPS)
CCC  TSEFF   = EFFECTIVE PRESTRESS FORCE IN STEEL (KIPS)
CCC  TITLE   = TITLE OF PROBLEM RUN
CCC  W       = UNIT WEIGHT OF BEAM (PCF)
CCC  X       = DISTANCE FROM BEAM END TO CENTER OF SEGMENT IN SUBROUTINE
C            SPHI (IN)
CCC  XI      = MOMENT OF INERTIA OF TRANSFORMED CONCRETE SECTION (IN^4)
CCC  XL      = TOTAL LENGTH OF BEAM SPAN (IN)
CCC  XM      = MOMENT OF CROSS-SECTION WITH CURVATURE PHI (KIP-IN)
CCC  XMMAX   = MAXIMUM ALLOWABLE MOMENT FOR CROSS-SECTION (KIP-IN)
CCC  XMMAXTS = MAXIMUM MOMENT FOUND IN MOMENT CURVATURE DERIVATION
WHICH
C            MAY INCLUDE TENSION STIFFENING
CCC  XMS     = MOMENT ON SEGMENT DUE TO STEEL FORCE (KIP-IN)
CCC  XN      = MODULUS RATIO (EMS/EMC)
CCC  XXL(I)  = LENGTH OF BEAM SEGMENT 'I' (IN)
CCC  YB      = DISTANCE FROM TOP FIBER TO CENTROID OF TRANSFORMED
C            SECTION (IN)
CCC  YBAR(I) = Y-COORDINATE OF PRESTRESSING BAR FORM TOP OF
C            CROSS-SECTION (IN)
CCC  YELE(I) = COORDINATE FROM THE TOP FIBER OF THE 'I' ELEMENT (IN)
CCC  YM      = REQUIRED MOMENT RESISTED BY STEEL PRESTRESSED CONCRETE
C            SECTION (KIP-IN)
CCC  YMF     = MOMENT ON SEGMENT DUE TO UPWARD LOADS AT HARPING POINT
(KIP-IN)
CCC  YMP     = MOMENT ON SEGMENT DUE TO LIVE LOAD (KIP-IN)
CCC  YMW     = MOMENT ON SEGMENT DUE TO UNIFORM LOAD (KIP-IN)
CCC  YT      = DISTANCE FROM BOTTOM FIBER TO CENTROID OF TRANSFORMED
C            SECTION (IN)
CCC  ----------------------------------------------------------------
CCC     SIGN CONVENTION
CCC  CONCRETE STRESS (KSI) = +....FOR COMPRESSION
CCC  CONCRETE STRAIN       = +....FOR COMPRESSION
CCC  PRESTRESSING STRAIN   = +....FOR TENSION
CCC  PRESTRESSING FORCES(K)= +....FOR TENSION
CCC  ----------------------------------------------------------------
```

```
CCC     SUBROUTINES
CCC  SSTEEL  - DETERMINES PRESTRESSING STEEL STRESS FOR GIVEN STRAIN
CCC  SCONC1  - DETERMINES CONCRETE STRAIN FOR GIVEN STRESS
CCC  SCONC2  - DETERMINES CONCRETE STRESS FOR GIVEN STRAIN, STRAIN AND
C          STRESS IN DOUBLE PRECISION
CCC  SPHI    - MAIN SUBROUTINE, CONDUCTS LOADING ITERATIONS, CALCULATES
C          APPLIED MOMENTS, INTERPOLATES CORRECT SEGMENT CURVATURES,
C          CONVERGENCE OF EXTERNAL TENDON FORCES, PRINTS OUTPUT
CCC  MPHI    - CALCULATES SEGMENT MOMENT-CURVATURE RELATIONSHIP
CCC  ----------------------------------------------------------------
     DIMENSION YELE(300),ABAR(20),YBAR(20),ICRACK(24),IPS(20),XXL(24)
     CHARACTER TITLE*60, IN*8, OUT*8, FIN*8
     WRITE(*,50)
  50 FORMAT(5X,' INPUT FILE?')
     READ(*,'(A)') FIN
     OPEN(2,FILE=FIN,STATUS='OLD')
     DO 1 ICARL=1,20
     READ(2,'(A)') IN, OUT
     OPEN(1,FILE=IN,STATUS='OLD')
     OPEN(3,FILE=OUT,STATUS='NEW')
     REWIND 1
C
CCC  ************************  READ INPUT DATA  ********************
     READ(1,*)
     READ(1,'(A)') TITLE
     READ(1,*)
     READ(1,*) JOB
     READ(1,*)
     READ(1,*) NELE,NSEG,ITS
     READ(1,*)
     READ(1,*) ISEC,H,BW,BTF,BBF,HTF,HBF
     READ(1,*)
     READ(1,*) FSEFF
     READ(1,*)
     READ(1,*) CO,ECU,W
     READ(1,*)
     READ(1,*) AF,EMF,FF1,P2A,P2B,FF2,FFMAX
     READ(1,*)
     READ(1,*) AAB,XL,DC1,DC2
     READ(1,*)
     READ(1,*) AAT
     READ(1,*)
     READ(1,*) NBAR
     READ(1,*)
     DO 110 I=1,NBAR
     READ(1,*) IPS(I),ABAR(I),YBAR(I)
 110 CONTINUE
C
CCC  ***************  WRITE TO OUTPUT THE INPUT DATA  **************
```

```
      WRITE(3,120)
  120 FORMAT(3X,'*****  INPUT  DATA FOR EXPOST.FOR  *****')
      WRITE(3,122) TITLE
  122 FORMAT(16X,A60)
      WRITE(3,124) JOB, IN, OUT
  124 FORMAT('  JOB #',I3, ' INPUT FILE ', A8, ' OUTPUT FILE ', A8)
      WRITE(3,126) NELE,NSEG,ITS
  126 FORMAT('  NUMBER OF ELEMENTS   = ',I3,
     $     '  APPROXIMATE MID SEGMENT LENGTH   = ',I3,
     $     '  TENSION STIFFENING FLAG    = ',I3)
      WRITE(3,128) ISEC,H,BW,BTF,BBF,HTF,HBF
  128 FORMAT('CROSS SECTIONAL DIMENSIONS',/,
     $     '  CROSS-SECTION TYPE = ',I2/,
     $     '  TOTAL HEIGHT OF THE BEAM (IN) = ',F6.2/,
     $     '  WIDTH OF BEAM WEB (IN) = ',F6.2/,
     $     '  WIDTH OF BEAM TOP FLANGE (IN) = ',F6.2/,
     $     '  WIDTH OF BEAM BOTTOM FLANGE (IN) = ',F6.2/,
     $     '  THICKNESS OF TOP FLANGE (IN) = ',F6.2/,
     $     '  THICKNESS OF BOTTOM FLANGE (IN) = ',F6.2)
      WRITE (3,130) FSEFF
  130 FORMAT('STEEL STRENGTH',/,
     $     '  EFFECTIVE PRESTRESS (KSI) = ',F8.2)
      WRITE(3,132) CO
  132 FORMAT('CONCRETE STRENGTH (KSI) = ',F8.3)
      WRITE(3,134) AF,EMF,FF1,P2A,P2B,FF2,FFMAX,AAB,XL,DC1,DC2,AAT
  134 FORMAT('FRP REPAIR PROPERTIES',/,
     $     '  TOTAL FRP AREA (SQ.IN.) = ', E12.5,/,
     $     '  ELASTIC MODULUS OF FRP (KSI) = ', E12.5,/,
     $     '  FRP INITIAL STRESS (KSI)      = ', F8.2,/,
     $  '  MAX LOAD (1/2 LL) BEFORE FRP TENSIONING (KIPS) = ', F6.1,/,
     $  '  LOAD (1/2 LL) AT FRP TENSIONING (KIPS) = ', F6.1,/,
     $     '  FRP SECOND STRESS (KSI)       = ', F8.2,/,
     $     '  MAXIMUM ALLOWABLE FRP STRESS (KSI) = ', F6.1,/,
     $     '  SLOPED SPAN (IN.)       = ', F8.2,/,
     $     '  TOTAL BEAM SPAN (IN.)    = ', F8.2,/,
     $     '  DISTANCE FROM TOP TO FRP AT ENDS (IN.) = ', F8.2,/,
     $     '                  AT MIDPOINT (IN.) = ', F8.2,/,
     $     '  DISTANCE FROM BEAM END TO POINT LOAD (IN.) = ', F8.2)
      WRITE(3,144) NBAR
  144 FORMAT('NUMBER OF STEEL REINFORCEMENTS = ',I2)
      WRITE(3,145)
  145 FORMAT('  STRAND NO.   AREA (SQ.IN.)   Y-CORD.   TYPE R/F')
      DO 150 I=1,NBAR
      WRITE(3,146) I,ABAR(I),YBAR(I),IPS(I)
  146 FORMAT(I8,5X,F10.3,6X,F10.3,6X,I2)
  150 CONTINUE
      WRITE(3,160)
  160 FORMAT('**********  END OF INPUT DATA  **********')
C
```

```
CCC  ********** CALCULATE INITIAL STRESS/STRAIN OF BEAM **********
     FRUPT=-7.5*SQRT(CO*1000)/1000
     CALL SCONC1(ERUPT,EMC,FRUPT,CO)
     EMS=28900
     XN=EMS/EMC
     WRITE(*,174) XN, EMS, EMC, ERUPT, FRUPT
     WRITE(3,174) XN, EMS, EMC, ERUPT, FRUPT
  174 FORMAT(/,'CALCULATED PROPERTIES',/,
    $     ' N = ', F12.4,/,
    $     ' MODULUS OF STEEL (KSI)   = ', F10.0,/,
    $     ' MODULUS OF CONCRETE (KSI) = ', F10.1,/,
    $     ' STRAIN AT TENSILE RUPTURE = ', E12.5,/,
    $     ' STRESS AT RUPTURE (KSI)  = ', F10.4)
     AS=0
     AST=0
     ASC=0
     D=0
     DREFT=0
     DREFC=0
     TSEFF=0
C
CCC  ********** CALCULATE STEEL PROPERTIES **********
     DO 180 I=1,NBAR
     IF(IPS(I).EQ.1) THEN
      TSEFF=TSEFF+FSEFF*ABAR(I)
      AS=AS+ABAR(I)
      D=D+ABAR(I)*YBAR(I)
      ENDIF
     IF(IPS(I).EQ.2) THEN
      AST=AST+ABAR(I)
      DREFT=DREFT+ABAR(I)*YBAR(I)
      ENDIF
     IF(IPS(I).EQ.3) THEN
      ASC=ASC+ABAR(I)
      DREFC=DREFC+ABAR(I)*YBAR(I)
      ENDIF
  180 CONTINUE
     IF(AS.NE.0) THEN
      D=D/AS
      ELSE
      D=1
      ENDIF
     IF(AST.NE.0) THEN
      DREFT=DREFT/AST
      ELSE
      DREFT=1
      ENDIF
     IF(ASC.NE.0) THEN
      DREFC=DREFC/ASC
```

```
      ELSE
      DREFC=1
      ENDIF
     ESEFF=FSEFF/EMS
C
CCC  ***************  CALCULATE SECTION PROPERTIES  **************
     AGC=H*BW+HTF*(BTF-BW)+HBF*(BBF-BW)
     AGT=AGC+(AS+AST+ASC)*(XN-1)
     FCEFF=TSEFF/AGT
     CALL SCONC1(ECEFF,EMC,FCEFF,CO)
CCC
     YB=(H*BW*H/2+HTF*(BTF-BW)*(H-HTF/2)+HBF*(BBF-BW)*HBF/2+
    $   AS*(XN-1)*(H-D)+AST*(XN-1)*(H-DREFT)+ASC*(XN-1)*(H-DREFC))/
    $   AGT
     YT=H-YB
     XI=BW*H**3/12+BW*H*(YB-H/2)**2+
    $    (BTF-BW)*HTF**3/12+(BTF-BW)*HTF*(YT-HTF/2)**2+
    $    (BBF-BW)*HBF**3/12+(BBF-BW)*HBF*(YB-HBF/2)**2
     DO 210 I=1,NBAR
     XI=XI+(XN-1)*ABAR(I)*(YBAR(I)-YT)**2
 210 CONTINUE
     WRITE (3,222)YT,YB,AGC,AGT,XI
 222 FORMAT('  SECTION PROPERTIES (IGNORING FRP)',/,6X,
    $     'YT(IN)  YB(IN)  AGC(SQ.IN)  AGT(SQ.IN)  XI(IN**4)',
    $     /,2X,2F9.3,1X,F9.3,2X,F9.3,2X,F10.3/)
C
CCC  ********  CALCULATE CROSS-SECTIONAL ELEMENT PROPERTIES  *******
     DELE=H/NELE
     DO 260 I=1,NELE
     YELE(I)=(I-0.5)*DELE
 260 CONTINUE
     WRITE(*,262) NELE,DELE
     WRITE(3,262) NELE,DELE
 262 FORMAT('  ELEMENT PROPERTIES NEGLECTING FRP',
    1 /,'     NUMBER OF ELEMENTS = ',I3/,
    2 '     ELEMENT HEIGHT (IN.) = ', F7.4)
     WRITE (3,264) ECEFF,FCEFF,ESEFF,FSEFF
 264 FORMAT('  STRAIN AND STRESS AT TRANSFER (W/O FRP)',/,6X,
    1 'AVERAGE CONCRETE STRAIN DUE TO EFFECTIVE PRESTRESS = ',
    2 E12.5,/,6X,'AVERAGE CONCRETE STRESS DUE TO EFF PS (KSI) = ',
    3 F10.5/,6X,'STEEL STRAIN DUE TO EFF PS = ',E12.5/,
    4 '     EFFECTIVE STEEL STRESS (KSI) = ', F10.5)
C
CCC  *********  CALCULATE LONGITUDINAL ELEMENT PROPERTIES  ********
     DELXL=XL/NSEG
     KK=0
     IF(AAB.LE.AAT) THEN
      NDELXL=(XL/2-AAT)/DELXL+1
      DO 270, K=1,NDELXL
```

```
      KK=KK+1
      ICRACK(KK)=0
      XXL(KK)=(XL/2-AAT)/NDELXL
  270 CONTINUE
      IPT=KK
      IF(AAB.NE.AAT) THEN
       NDELXL=(AAT-AAB)/DELXL+1
       DO 271, K=1,NDELXL
       KK=KK+1
       ICRACK(KK)=0
       XXL(KK)=(AAT-AAB)/NDELXL
  271   CONTINUE
       ENDIF
      IPB=KK
      NDELXL=AAB/(2*DELXL)+1
      DO 272, K=1,NDELXL
      KK=KK+1
      ICRACK(KK)=0
      XXL(KK)=AAB/NDELXL
  272 CONTINUE
C
      ELSE
      NDELXL=(XL/2-AAB)/DELXL+1
      DO 273, K=1,NDELXL
      KK=KK+1
      ICRACK(KK)=0
      XXL(KK)=(XL/2-AAB)/NDELXL
  273 CONTINUE
      IPB=KK
      NDELXL=(AAB-AAT)/DELXL+1
      DO 274, K=1,NDELXL
      KK=KK+1
      ICRACK(KK)=0
      XXL(KK)=(AAB-AAT)/NDELXL
  274 CONTINUE
      IPT=KK
      NDELXL=AAT/(2*DELXL)+1
      DO 275, K=1,NDELXL
      KK=KK+1
      ICRACK(KK)=0
      XXL(KK)=AAT/NDELXL
  275 CONTINUE
     ENDIF
C
CCC  ******  CALCULATE CURVATURE AT PRESTRESSING STEEL TRANSFER  *****
     XMS = TSEFF*(D-YT)
     FCTOP = ((XMS)*(-YT))/XI + FCEFF
     FCBOT = ((XMS)*(YB))/XI + FCEFF
     CALL SCONC1(ECTOP,EMC,FCTOP,CO)
```

```
      CALL SCONC1(ECBOT,EMC,FCBOT,CO)
      IF(ECTOP.LT.ERUPT) THEN
        WRITE (*,282)
        WRITE (3,282)
  282   FORMAT('TOP STRESS AT PRESTRESS RELEASE EXCEEDS RUPTURE STRESS')
        ENDIF
      WRITE(*,281) FCTOP, FCBOT, ECTOP, ECBOT
      WRITE(3,281) FCTOP, FCBOT, ECTOP, ECBOT
  281 FORMAT(6X,'CONCRETE STRESS-TOP (KSI) = ', F10.4,/,
     $     6X,'CONCRETE STRESS-BOTTOM (KSI) = ', F10.4,/,
     $     6X,'CONCRETE STRAIN-TOP = ', E12.5,/,
     $     6X,'CONCRETE STRAIN-BOTTOM = ', E12.5)
      WRITE(*,200)
      WRITE(3,200)
  200 FORMAT(/,3X,'*****  RESULTS  *****')
      ESO = ESEFF+D/H*(ECBOT-ECTOP)+ECTOP
      W=W*AGC/(144*12*1000)
      FFMAX=FFMAX*AF
      CALL SPHI(AAB,AAT,AF,AS,ASC,AST,BBF,BTF,BW,CO,D,DC1,DC2,DELE,
     $   DREFC,DREFT,ECU,EMF,ERUPT,ESO,FF1,FF2,FFMAX,FRUPT,H,HBF,
     $   HTF,ICRACK,IPB,IPT,ITS,KK,NELE,P2A,P2B,TFEFF,TFDISP,XL,XXL,
     $   W,YELE)
    1 CONTINUE
      STOP
      RETURN
      END
CC=====================================================================
      SUBROUTINE SSTEEL(FS,ES)
CCC   STEEL STRESS-STAIN CURVE REPRESENTED BY AN INITIAL STRAIGHT LINE
CCC   A POLYNOMIAL CURVE AND ANOTHER STRAIGHT LINE UP TO ULTIMATE
      EMS=28900
      FSH=272
      ESY=0.006
      ESH=0.014
      ESU=0.065
      FSU=289
      AO=175.92
      A1=267.65
      A2=-39.09
      A3=-440.90
      A4=324.62
C
      X=100.*(ES-ESY)
      Y1=AO+A1*X+A2*X*X+A3*X*X*X+A4*X*X*X*X
      IF(ES.LE.ESY) FS=EMS*ES
      IF (ES.GT.ESY.AND.ES.LT.ESH) FS=Y1
      IF(ES.GE.ESH) FS=FSH+(FSU-FSH)*(ES-ESH)/(ESU-ESH)
      IF(ES.GT.ESU) FS=FSU
  100 CONTINUE
```

```
      RETURN
      END
CC=====================================================================
      SUBROUTINE SCONC1(EC,EMC,FC,CO)
C     DEVELOP CONCRETE STRESS-STRAIN RELATIONSHIP
      IF(CO.LT.4.5) GOTO 4
      IF(CO.LT.5.5) GOTO 5
      IF(CO.LT.6.5) GOTO 6
      IF(CO.LT.8) GOTO 7
      IF(CO.LT.10) GOTO 9
      IF(CO.LT.12) GOTO 11
      IF(CO.LT.14) GOTO 13
CCC
    4 CONTINUE
      A1=1.60026
      B1=0.65510
      A2=1.50450
      B2=0.88006
      GOTO 555
    5 CONTINUE
      A1=1.50886
      B1=0.47080
      A2=0.78813
      B2=0.94970
      GOTO 555
    6 CONTINUE
      A1=1.4576
      B1=0.3855
      A2=0.5804
      B2=0.9655
      GOTO 555
    7 CONTINUE
      A1=1.40631
      B1=0.30016
      A2=0.37260
      B2=0.98141
      GOTO 555
    9 CONTINUE
      A1=1.35586
      B1=0.23024
      A2=0.22156
      B2=0.99041
      GOTO 555
   11 CONTINUE
      A1=1.33099
      B1=0.19919
      A2=0.14246
      B2=0.99487
      GOTO 555
```

```
  13 CONTINUE
     A1=1.32052
     B1=0.18679
     A2=0.09404
     B2=0.99777
     GOTO 555
CCC
  555 CONTINUE
     EO=0.001648+0.000114*CO
     EMC=A1*CO/EO
     ICHECK=1
     IF(FC.LT.0) ICHECK=-1
     FC1=FC*ICHECK
     AA=B1*(1-FC1/CO)-1
     BB=A1*(1-FC1/CO)+2*FC1/CO
     CC=-FC1/CO
     X=(-BB+SQRT(BB*BB-4*AA*CC))/(2*AA)
     EC=(X*EO)*ICHECK
     RETURN
     END
CC=====================================================================
     SUBROUTINE SCONC2(EC,FC,CO)
C    DEVELOP CONCRETE STRESS-STRAIN RELATIONSHIP WITH DOUBLE PRECISION
     DOUBLE PRECISION EC,EC1,Y,FC,X
     IF(CO.LT.4.5) GOTO 4
     IF(CO.LT.5.5) GOTO 5
     IF(CO.LT.6.5) GOTO 6
     IF(CO.LT.8) GOTO 7
     IF(CO.LT.10) GOTO 9
     IF(CO.LT.12) GOTO 11
     IF(CO.LT.14) GOTO 13
CCC
   4 CONTINUE
     A1=1.60026
     B1=0.65510
     A2=1.50450
     B2=0.88006
     GOTO 555
   5 CONTINUE
     A1=1.50886
     B1=0.47080
     A2=0.78813
     B2=0.94970
     GOTO 555
   6 CONTINUE
     A1=1.4576
     B1=0.3855
     A2=0.5804
     B2=0.9655
```

```
      GOTO 555
    7 CONTINUE
      A1=1.40631
      B1=0.30016
      A2=0.37260
      B2=0.98141
      GOTO 555
    9 CONTINUE
      A1=1.35586
      B1=0.23024
      A2=0.22156
      B2=0.99041
      GOTO 555
   11 CONTINUE
      A1=1.33099
      B1=0.19919
      A2=0.14246
      B2=0.99487
      GOTO 555
   13 CONTINUE
      A1=1.32052
      B1=0.18679
      A2=0.09404
      B2=0.99777
      GOTO 555
CCC
  555 CONTINUE
      EO=0.001648+0.000114*CO
      ICHECK=1
      IF(EC.LT.0) ICHECK=-1
      EC1=EC*ICHECK
      X=EC1/EO
      IF(X.LE.1)  Y=(A1*X+(B1-1)*X*X)/(1.+(A1-2)*X+B1*X*X)
      IF(X.GT.1)  Y=(A2*X+(B2-1)*X*X)/(1.+(A2-2)*X+B2*X*X)
      FC=(CO*Y)*ICHECK
  100 CONTINUE
      RETURN
      END
CC=====================================================================
      SUBROUTINE SPHI(AAB,AAT,AF,AS,ASC,AST,BBF,BTF,BW,CO,D,DC1,DC2,
     $   DELE,DREFC,DREFT,ECU,EMF,ERUPT,ESO,FF1,FF2,FFMAX,FRUPT,H,
     $   HBF,HTF,ICRACK,IPB,IPT,ITS,KK,NELE,P2A,P2B,TFEFF,TFDISP,
     $   XL,XXL,W,YELE)
C     CONDUCT LOAD ITERATIONS AND DETERMINE BEAM DISPLACEMENTS
      DIMENSION YELE(300),ICRACK(24),XXL(24),ECMIDS(180),
     $        PHI(180),XM(180),ECT(180),PHIP(24)
      DOUBLE PRECISION PHISEG,PHI,DELDELPB,FSTRAIN,ALPHA
C     INITIAL LOAD IS SET FOR P=0.15 KIPS, WHERE P IS LOAD FROM ONE OF
C     TWO POINT LOADS
```

```
      P=-.35
      P2APLUS=P2A+.5
      P2BPLUS=P2B+.5
      TFEFF=FF1*AF
      TFTRY=TFEFF
      IMMAX=0
      TFDISP=0
      IP2ACHK=0
      IP2BCHK=0
      DCMID0=0.
      XMMAX=10000
      WRITE(3,50)
   50 FORMAT('P,DELTA,DELPB,PHIMID,TFDISP,DCMID,FSTRAIN,YMMAX,XMMAX,
     $XMID,DELPT')
C
CCC  ***************  ITERATE OVER LOAD INCREMENTS  ***************
      DO 3000 K=1,120
      WRITE(*,*) '3000 DO LOOP, K=', K
      IIPCHK=0
      BTFDISP=0
 1000 CONTINUE
      P=P+.5
      IF(IMMAX.NE.0) P=P-.4
      WRITE(*,*) P
      DELTATF=0.1
 1010 CONTINUE
      IICRACK=2
      DELTA=0.0
      DELPT=0
      DELPB=0
      IF(P.EQ.P2BPLUS.AND.IP2ACHK.EQ.1.AND.IP2BCHK.EQ.0) THEN
       IP2BCHK=1
       P=P2B
       TFEFF=FF2*AF
       TFTRY=FF2*AF
       ENDIF
      IF(P.EQ.P2APLUS.AND.IP2ACHK.EQ.0) THEN
       IP2ACHK=1
       P=P2B
       ENDIF
C
CCC  ****************  ITERATE OVER BEAM SEGMENTS  ***************
      DO 2000 I=1,KK
      IF(I.EQ.1) DCMID=0.
      X=XL/2.
      DO 10 JJ=1,I
      X=X-XXL(JJ)
   10 CONTINUE
      X=X+0.5*XXL(I)
```

```
      XX=XL/2.-X
   20 CONTINUE
      IF(X.LT.AAT) THEN
       YMP=P*X
       ELSE
       YMP=P*AAT
       ENDIF
      YMW=W*X*.5*(XL-X)
 1050 CONTINUE
      IF(IP2BCHK.EQ.0) THEN
       ALPHA=ATAN((DC2-DC1)/AAB)
       ELSE
       ALPHA=ATAN((DC2-DC1+DELPB)/AAB)
       ENDIF
      PF=SIN(ALPHA)*TFTRY
      IF(X.LT.AAB) THEN
       YMF=-PF*X
       ELSE
       YMF=-PF*AAB
       ENDIF
      YM=YMP+YMW+YMF
      IF(I.EQ.1) YMMAX=YM
      IF(YM.GT.YMMAX) YMMAX=YM
 2100 CONTINUE
      IF(ICRACK(I).NE.IICRACK) THEN
       IICRACK=ICRACK(I)
       CALL MPHI(AS,ASC,AST,BBF,BTF,BW,CO,D,DC1,DELE,DREFC,DREFT,
     $   ECMIDS,ECT,ECU,ERUPT,ESO,FRUPT,H,HBF,HTF,IICRACK,
     $   IJKMAX,ITS,JCRACK,MAXI,NELE,PHI,TFTRY,XM,XMMAXTS,YELE)
       ENDIF
C     THE FOLLOWING STATEMENT EFFECTIVELY REDUCE THE LOAD INCREMENT WHEN
C     LOADS APPROACH ULTIMATE
      XMMAX9=0.9*XMMAX
      IF(YM.GT.XMMAX9.AND.IMMAX.EQ.0) THEN
       IMMAX=1
       P=P-.5
       GOTO 3000
       ENDIF
C     IDENTIFY SEGMENT CURVATURE
      IF(YM.GT.XMMAXTS) THEN
       PHISEG=PHI(IJKMAX)
       PHIP(I)=PHISEG
       ECMIDP=ECMIDS(IJKMAX)
       ECTT=ECU
       IF(IJKMAX.GE.JCRACK.AND.ICRACK(I).EQ.0) THEN
        ICRACK(I)=1
        GOTO 2100
        ENDIF
       GOTO 2700
```

```
      ENDIF
     DO 2500, JJ=1,IJKMAX
     JJJ=JJ
     IF(YM.LT.XM(JJ)) THEN
      IF(JJ.EQ.1) THEN
       JJJ=2
       ENDIF
      PHISEG=(YM-XM(JJJ-1))*(PHI(JJJ)-PHI(JJJ-1))/(XM(JJJ)-XM(JJJ-1))+
     $       PHI(JJJ-1)
      PHIP(I)=PHISEG
      ECMIDP=(YM-XM(JJJ-1))*(ECMIDS(JJJ)-ECMIDS(JJJ-1))/
     $       (XM(JJJ)-XM(JJJ-1))+ECMIDS(JJJ-1)
      ECTT=(YM-XM(JJJ-1))*(ECT(JJJ)-ECT(JJJ-1))/
     $       (XM(JJJ)-XM(JJJ-1))+ECT(JJJ-1)
      IF(JJ.GE.JCRACK.AND.ICRACK(I).EQ.0) THEN
       ICRACK(I)=1
       GOTO 2100
       ENDIF
      GOTO 2700
      ENDIF
 2500 CONTINUE
 2700 CONTINUE
     IF(I.EQ.1) THEN
      PHIMID=PHISEG
      XMID=ECTT/PHISEG
      ENDIF
C    CALCULATE DEFLECTIONS AT MIDSPAN, HARPING POINTS AND POINT LOADS
     DELTA=DELTA+PHISEG*XXL(I)*X
     IF(I.LE.IPT) DELPT=DELPT+PHISEG*XXL(I)*(X-AAT)
     IF(I.LE.IPB) DELPB=DELPB+PHISEG*XXL(I)*(X-AAB)
     DCMID=DCMID+ECMIDP*XXL(I)
 2000 CONTINUE
C
     IF(TFTRY.EQ.0) GOTO 2991
     DELPT=DELTA-DELPT
     DELPB=DELTA-DELPB
     IF(P.EQ.0) DELPB0=DELPB
     IF(P.EQ.P2B.AND.IP2BCHK.EQ.1) THEN
      DELPB0=DELPB
      DCMID0=DCMID
      ENDIF
     DELDELPB=DELPB-DELPB0
     IF(DELDELPB.LT.0) DELDELPB=0.
C    CALCULATE TFDISP
     FSTRAIN=SQRT((DC2-DC1)**2.+AAB**2.)
     IF(ITS.EQ.1) THEN
      FSTRAIN=(SQRT((DC2-DC1+DELDELPB)**2.+AAB**2.)-FSTRAIN-
     $       (DCMID-DCMID0))/(FSTRAIN+XL/2.-AAB)
      ELSE
```

```
      FSTRAIN=(SQRT((DC2-DC1+DELDELPB)**2.+AAB**2.)-FSTRAIN-
     $       0.7*(DCMID-DCMID0))/(FSTRAIN+XL/2.-AAB)
      ENDIF
     TFDISP=TFEFF+FSTRAIN*EMF*AF
     DELTF=(TFDISP-TFTRY)*2/(TFDISP+TFTRY)
     IF(TFTRY.LT.1) DELTF=0.
C    IF NO CONVERGENCE WITH DELTATF < 0.00001, THEN CHECK XMMAX AND
C    INCREASE P BY 0.010 KIPS
     IF(DELTATF.LT.0.00001) THEN
      P=P-.09
      CALL MPHI(AS,ASC,AST,BBF,BTF,BW,CO,D,DC1,DELE,DREFC,DREFT,
     $   ECMIDS,ECT,ECU,ERUPT,ESO,FRUPT,H,HBF,HTF,1,IJKMAX,
     $   0,JCRACK,MAXI,NELE,PHI,TFTRY,XM,XMMAX,YELE)
      IF(YMMAX.GT.XMMAX) GOTO 3001
      GOTO 1000
      ENDIF
C    IF TFDISP NOT EQUAL TO TFTRY, THEN ADJUST TFTRY AND REDO FROM
C    LINE 1010
     IF(DELTF.GT.0.0005) THEN
      IF(IIPCHK.EQ.1) THEN
       DELTATF=DELTATF*1.05
       ELSE
       DELTATF=DELTATF*0.8
       ENDIF
      TFTRY=TFTRY+DELTATF
      IIPCHK=1
      GOTO 1010
      ENDIF
     IF(DELTF.LT.-0.0005) THEN
      IF(IIPCHK.EQ.-1) THEN
       DELTATF=DELTATF*1.05
       ELSE
       DELTATF=DELTATF*0.8
       ENDIF
      TFTRY=TFTRY-DELTATF
      IIPCHK=-1
      GOTO 1010
      ENDIF
2991 CONTINUE
     CALL MPHI(AS,ASC,AST,BBF,BTF,BW,CO,D,DC1,DELE,DREFC,DREFT,
    $ ECMIDS,ECT,ECU,ERUPT,ESO,FRUPT,H,HBF,HTF,1,IJKMAX,
    $ 0,JCRACK,MAXI,NELE,PHI,TFTRY,XM,XMMAX,YELE)
     IF(YMMAX.GT.XMMAX) GOTO 3001
     IF(TFDISP.GT.FFMAX) THEN
      WRITE(*,*) 'MAXIMUM TENDON STRESS EXCEEDED'
      WRITE(3,*) 'MAXIMUM TENDON STRESS EXCEEDED'
      STOP
      ENDIF
     WRITE(*,301) P,DELTA,DELPB,PHIMID,TFDISP,DCMID,FSTRAIN,
```

```
     $          YMMAX,XMMAX,XMID,DELPT
      WRITE(3,301) P,DELTA,DELPB,PHIMID,TFDISP,DCMID,FSTRAIN,
     $          YMMAX,XMMAX,XMID,DELPT
  301 FORMAT(F6.2,10(2X,E12.5))
      DELTLAST=DELTA
      TFTRY=TFDISP
 3000 CONTINUE
 3001 CONTINUE
      RETURN
      END
CC=====================================================================
      SUBROUTINE MPHI(AS,ASC,AST,BBF,BTF,BW,CO,D,DC1,DELE,DREFC,DREFT,
     $  ECMIDS,ECT,ECU,ERUPT,ESO,FRUPT,H,HBF,HTF,IICRACK,
     $  IJKMAX,ITS,JCRACK,MAXI,NELE,PHI,TFTRY,XM,XMMAXTS,YELE)
C     DETERMINE MAXIMUM MOMENT AND MOMENT-CURVATURE RELATIONSHIP OF
SEGMENT
      DIMENSION YELE(300),PHI(180),XM(180),ECMIDS(180),ECT(180)
      DOUBLE PRECISION X,PHI,EC,FC
      JCRACK=200
      X=H/2.1
      ECTT=ERUPT-5.0E-5
      KCHECK = 0
      IJK=0
      XMMAXTS=0
      NELEDC1=DC1/H*NELE
      NELETF=HTF/H*NELE
      NELEBF=(H-HBF)/H*NELE
C     ITERATE ECTT VALUES TO DETERMINE M-PHI RELATIONSHIP
      DO 4000, JJK = 1,180
      LMN=0
      IJK=IJK+1
      DPHI=1.0E-05
  980 CONTINUE
      ECTT=ECTT+5.0E-5
      IF(ECTT.GT.ECU) ECTT=ECU
  990 CONTINUE
      LMN=LMN+1
      C = 0
      XM(IJK) = 0
      PHI(IJK)=ECTT/X
C     CALCULATE CONCRETE FORCES
      DO 600, J = 1,NELE
      EC=PHI(IJK)*(X-YELE(J))
      IF(J.EQ.NELEDC1) ECMIDS(IJK)=EC
      IF(EC.LT.ERUPT.AND.PHI(IJK).GT.0) THEN
       IF(ITS.EQ.1) THEN
        FC=0.7*0.7*FRUPT/(1+SQRT(500*(-EC)))
        ELSE
        FC=0
```

```
        ENDIF
       IF(IJK.LT.JCRACK) JCRACK=IJK
       IF(YELE(J).LT.10.25) FC=0
       ELSE
       CALL SCONC2(EC,FC,CO)
       IF(IICRACK.EQ.1.AND.EC.LT.0) THEN
        IF(ITS.EQ.1) THEN
         FC=0.7*0.7*FC
         ELSE
         FC=0
         ENDIF
        IF(YELE(J).LT.10.25) FC=0
        ENDIF
       ENDIF
      IF(J.GT.NELETF) THEN
       IF(J.GT.NELEBF) THEN
        C=C+FC*DELE*BBF
        XM(IJK)=XM(IJK)+FC*DELE*BBF*(DC1-YELE(J))
        ELSE
        C=C+FC*DELE*BW
        XM(IJK)=XM(IJK)+FC*DELE*BW*(DC1-YELE(J))
        ENDIF
       ELSE
       C=C+FC*DELE*BTF
       XM(IJK)=XM(IJK)+FC*DELE*BTF*(DC1-YELE(J))
       ENDIF
  600 CONTINUE
C     CALCULATE STEEL FORCES
      ES=ESO+PHI(IJK)*(D-X)
      CALL SSTEEL(FS,ES)
      TS=FS*AS
      ESC=PHI(IJK)*(DREFC-X)
      TSC=ESC*29000
      IF(TSC.LT.-60) THEN
       TSC=-60*ASC
       ELSE
       TSC=TSC*ASC
       ENDIF
      EST=PHI(IJK)*(DREFT-X)
      TST=EST*29000
      IF(TST.GT.60) THEN
       TST=60*AST
       ELSE
       TST=TST*AST
       ENDIF
C     CALCULATE FORCE EQUILIBRIUM CONVERGENCE; IF NOT CONVERGE, ADJUST
C     PHI AND NEUTRAL AXIS, (X), WITH ECTT REMAINING THE SAME
      DELF=C-TS-TSC-TST-TFTRY
      TSF=TS+TST+TFTRY
```

```
      DELRAT=DELF/(TSF)
      IF(LMN.GT.1000) THEN
       LMN=0
       GOTO 980
       ENDIF
      IF(TSF.LT.0) DELRAT=-DELRAT
      IF(DELRAT.GT.0.005) THEN
       IF(KCHECK.EQ.2) THEN
        DPHI=.8*DPHI
        ELSE
        DPHI=1.1*DPHI
        ENDIF
       PHI(IJK)=PHI(IJK)+DPHI
       X=ECTT/PHI(IJK)
       KCHECK=1
       GOTO 990
       ENDIF
      IF(DELRAT.LT.-0.005) THEN
       IF(KCHECK.EQ.1) THEN
        DPHI=.8*DPHI
        ELSE
        DPHI=1.1*DPHI
        ENDIF
       PHI(IJK)=PHI(IJK)-DPHI
       X=ECTT/PHI(IJK)
       KCHECK=2
       GOTO 990
       ENDIF
  999 CONTINUE
C     CALCULATE SECTIONAL MOMENT
      XM(IJK)=XM(IJK)+TS*(D-DC1)+TSC*(DREFC-DC1)+TST*(DREFT-DC1)
      IF(XM(IJK).GT.XMMAXTS) THEN
       XMMAXTS=XM(IJK)
       MAXI=IJK
       ENDIF
      ECT(IJK)=ECTT
      IF(ECTT.EQ.ECU) GOTO 4010
 4000 CONTINUE
 4010 CONTINUE
      IJKMAX=IJK
      RETURN
      END
```

APPENDIX C

CALCULATION OF STEEL REINFORCEMENT AREA FOR PARAMETRIC STUDY

The calculation of steel reinforcement area, A_{ps}, used throughout the parametric study discussed in Chapter 5 was based on the limiting steel reinforcement index. The value of A_{ps} was based on $\omega_{max}/4$ and $\omega_{max}/2$, where ω_{max} is the maximum allowable reinforceing index defined in ACI 318-95 [ACI, 1995]. The reinforcing index is defined as:

$$\omega_p = \frac{A_{ps}\, f_{ps}}{b\, d\, f_c}$$

where ω_p = reinforcing index
A_{ps} = cross-sectional area of prestressing steel
f_{ps} = the stress in prestressing steel at ultimate capacity of the section
b = width of compression face of member
d = depth of prestressing steel
f_c = concrete compressive strength

Diagrams of the parametric specimen cross sections are shown in **Figure 5.1**. The following properties are assumed in the calculation of the area of prestressing steel, A_{ps}.

Assumed: f_c = 6 ksi
f_{pu} = 270 ksi
γ_p = 0.40 (assumed based on ACI, Chapter 18)

Rectangular Beams

From ACI 318-89, the limiting value of the reinforcing index for rectangular beams is:

$$\omega_{max} = 0.36\,\beta_1$$

where $\beta_1 = 0.85 - (6 - 4)(0.05)$
$= 0.75$

Therefore,

$\omega_{max} = 0.36\,(0.75)$
$= 0.27$

Now, the remaining unknowns are A_{ps} and f_{ps}. An approximate expression for f_{ps} is identified in ACI 318-89 [ACI, 1992]. For the parameters studied in this investigation, the approximate expression for f_{ps} is:

$$f_{ps} \approx f_{pu}\left(1 - \frac{\gamma_p}{\beta_1}\left[\rho_p \frac{f_{pu}}{f_c}\right]\right)$$

where f_{pu} = ultimate stress of prestressing steel
γ_p = factor for type of prestressing tendon defined in Chapter 18, ACI 318-89; assumed in this case to be equal to 0.40
β_1 = 0.75 for f_c = 6 ksi (41 MPa)
ρ_p = A_{ps} / (bd)
f_c = concrete compressive strength

For the rectangular beam in this study, the estimated value of f_{ps} is:

$$f_{ps} \approx 270\left(1 - \frac{0.4}{0.75}\left[\frac{A_{ps}\,(270)}{(6)\,(13)\,(6)}\right]\right)$$

$$\approx 270 - 83.1\,A_{ps}$$

Now, for $\omega = \omega_{max}/4$:

$$\frac{0.27}{4} = \frac{A_{ps}\ (270\ -\ 83.1\ A_{ps})}{(6)\ (13)\ (6)}$$

which yields:

$$\mathbf{A_{ps} = 0.12\ in.^2}$$

Similarly, for $\omega = \omega_{max}/2$:

$$\mathbf{A_{ps} = 0.25\ in.^2}$$

T Beams

For T beams, the reinforcing index for the web and flange must be accounted for separately. A suitable equation for ω_{max} can be expressed as [Naaman, 1982]:

$$(\omega_{max})_T = (\omega_{max})_{rect.} \frac{b_w}{b} + \frac{0.85\ (b\ -\ b_w)\ h_f}{b\ d}$$

where $(\omega_{max})_T$ = maximum reinforcing index for T section
$(\omega_{max})_{rect.}$ = maximum reinforcing index for rectangular section
b_w = width of web
b = width of top flange
h_f = thickness of top flange
d = depth of prestressing steel

Therefore,

$$(\omega_{max})_T = 0.27\ \frac{(4)}{(24)} + \frac{0.85\ (24\ -\ 4)\ 2}{(24)\ (13)}$$

$$(\omega_{max})_T = 0.154$$

To verify that the section behaves as a T section, the depth of the concrete compression block, a, is calculated. The value of the compression block is found by equating the compressive and tensile forces across the cross section. This expression is written as:

$$\mathbf{0.85\ (f_c)\ b\ a = A_{ps}\ f_{ps}}$$

Which can be written as:

$$\mathbf{0.85\ (f_c)\ b\ a = \omega\ (b\ d\ f_c)}$$

And solving for the value of 'a':

$$\begin{aligned} a &= (\omega\ d)/0.85 \\ &= (0.154(13))/0.85 \\ &= 2.36 \text{ in.} > 2 \text{ in. (therefore the section behaves as a T section)} \end{aligned}$$

The equation for f_{ps} is found similar to the rectangular section, such that:

$$f_{ps} \approx 270 \left(1 - \frac{0.4}{0.75} \left[\frac{A_{ps}\ (270)}{(24)\ (13)\ (6)} \right] \right)$$

$$f_{ps} \approx 270 - 20.8\ A_{ps}$$

Now, for $\omega = \omega_{max}/4$:

$$\frac{0.154}{4} = \frac{A_{ps}\ (270 - 20.8\ A_{ps})}{(24)\ (13)\ (6)}$$

Which yields:

$$\mathbf{A_{ps} = 0.27 \text{ in.}^2}$$

Similarly, for $\omega = \omega_{max}/2$:

$$\mathbf{A_{ps} = 0.58 \text{ in.}^2}$$